MONASH University

Electrode Kinetics Study by Large Amplitude Fourier Transformed Alternating Current Voltammetry

By:

Jiezhen Li

A thesis submitted to the Faculty of Science, Monash University, in fulfillment of the requirements for the degree of Doctor of Philosophy.

School of Chemistry

Monash University

Australia

June 2017

Copyright notice

Table of Contents

Abstract

The field of polyoxometalates (POMs) has attracted great attention in both academia and industry in the past two decades. Numbers of electrochemical studies of POMs are reported, however, quantitative studies of heterogeneous electron transfer kinetics at an electrode/electrolyte interface are relatively rare. For this reason, the electrode kinetics of POMs has been investigated in both aqueous and organic media.

Firstly, in chapter 2, a new strategy which can improve the reliability of kinetics measurement by Fourier transformed alternating current voltammetry (FTACV) is developed. FTACV is powerful technique for fast electrode kinetics study. Even so, when the heterogeneous electron transfer rate constant (k^0) approaches the reversible limit, any small uncertainties can lead to significant systematic error in the determination of k^0. To improve the accuracy, dual-frequency designer waveform is introduced into FTACV.

In chapter 3, we investigated the influence of electrolyte cation on electron transfer kinetics of POMs. However, in aqueous media, the electron transfer kinetics of [a-$SiW_{12}O_{40}$]$^{4-/5-}$ and [a-$SiW_{12}O_{40}$]$^{5-/6-}$ are so fast and close to the reversible limit at glassy carbon (GC) and metal electrodes even using kinetically sensitive FTACV. In order to study the electrolyte cation effect on the electron transfer kinetics of these two processes, boron doped diamond (BDD) electrode is used as much slower k^0 values are found compared to GC and metal electrodes, and lie well below the reversible limit.

In chapter 4, the electrode kinetics studies of POMs are then expanded to organic media. FTACV has been used to determine the k^0 values associated with the vanadium $[SVW_{11}O_{40}]^{3-/4-}$ ($V^{V/IV}$) and tungsten $[SVW_{11}O_{40}]^{4-/5-}$ processes ($W^{VI/V}$) in dimethylformamide. Both processes are found to be electrode materials and electrolyte

concentration dependent. Density of states of electrode materials, functional groups and double layer effect are taken into consideration.

In chapter 5, we found that by changing the electrolyte cation from hexafluorophosphate to 1-butyl-3-methylimidazolium, a significant difference of the k^0 values associated with the $V^{V/IV}$ and $W^{VI/V}$ processes are found. These findings are discussed in terms of ion-pairing effect, surface functional groups, double layer effect and nature of the processes.

In chapter 6, the work in Chapter 5 is expanded systematically to provide a general account of the influence of electrolyte cations on the rate of POM electron transfer. Seven different electrolyte cations were used in this study, including imidazolium and tetraalkylammonium based cations.

In chapter 7, the heterogeneous electron transfer kinetics, mass transport and thermodynamic properties associated with the $Fe^{3+/2+}$ process have been also studied in aqueous solutions containing 0.1 M HCl, $HClO_4$, bis(trifluoromethanesulfonyl)imide ($HNTf_2$) or 0.05 M silicotungstic acid ($H_4SiW_{12}O_{40}$) supporting electrolytes. Based on the formal potential value, $HNTf_2$ is found to be a more innocent electrolyte than commonly used $HClO_4$ in terms of determining the true k^0 values of the outer-sphere $[Fe(H_2O)_6]^{3+/2+}$ process. FTACV was used to determine k^0 values associated with the $Fe^{3+/2+}$ process in $H_4SiW_{12}O_{40}$ and $HNTf_2$ electrolyte media at GC electrodes and probe the implication of the heterogeneity of the BDD electrode surface on the electrode kinetic determination in $H_4SiW_{12}O_{40}$ electrolyte media.

Declaration

All Students should reproduce this section in their thesis verbatim

This thesis contains no material which has been accepted for the award of any other degree or diploma at any university or equivalent institution and that, to the best of my knowledge and belief, this thesis contains no material previously published or written by another person, except where due reference is made in the text of the thesis.

Signature: [redacted]

Print Name: [redacted]

Date: 08/06/17

General Declaration

Monash University

Declaration for thesis based or partially based on conjointly published or unpublished work

In accordance with Monash University Doctorate Regulation 17.2 Doctor of Philosophy and Research Master's regulations the following declarations are made:

I hereby declare that this thesis contains no material which has been accepted for the award of any other degree or diploma at any university or equivalent institution and that, to the best of my knowledge and belief, this thesis contains no material previously published or written by another person, except where due reference is made in the text of the thesis.

This thesis includes 4 original papers published in peer-reviewed journals and *2* unpublished publications. The core theme of the thesis is electrode kinetics study. The ideas, development and writing up of all the papers in the thesis were the principal responsibility of myself, the student, working within the School of chemistry under the supervision of Dr. Jie Zhang and Prof. Alan M.Bond.

The inclusion of co-authors reflects the fact that the work came from active collaboration between researchers and acknowledges input into team-based research.

In all chapters in the thesis, my contribution to the work involved the following:

Thesis Chapter	**Publication Title**	**Status**	Nature and % of student contribution	Co-author name(s) Nature and % of Co-author's contribution*	Co authors Monash student Y/N*
2	Dual-Frequency Alternating Current Designer Waveform for Reliable Voltammetric Determination of Electrode Kinetics Approaching the Reversible Limit	Published	80% Concept, collecting data and writing first draft	Cameron Bentley 20% Data analysis, Jie Zhang Supervision, Alan Bond Supervision	Y N N
3	Probing Electrolyte Cation Effects on the Electron Transfer Kinetics of the $[a\text{-}SiW_{12}O_{40}]^{4-/5-}$ and $[a\text{-}SiW_{12}O_{40}]^{5-/6-}$ Processes using a Boron-Doped Diamond Electrode.	Published	100% Concept, collecting data and writing first draft	Jie Zhang Supervision, Alan Bond Supervision	N N

4	Electrode Material Dependence of the Electron Transfer Kinetics Associated with the $[SVW_{11}O_{40}]^{3-/4-}$ ($V^{V/VI}$) and $[SVW_{11}O_{40}]^{4-/5-}$ $W^{VI/V}$) Processes in Dimethylformamide.	Published	70% Concept, collecting data and writing first draft	Sixuan Guo 10% Data analysis, Cameron L. Bentley 10% Data analysis, Kiran Bano 5% Data analysis Tadaharu Ueda 5% Data analysis, Jie Zhang Supervision, Alan Bond Supervision	N Y Y N N N
5	Influence of 1-Butyl-3-Methylimidazolium on the Electron Transfer Kinetics Associated with the $[SVW_{11}O_{40}]^{3-/4-}$ ($V^{V/VI}$) and $[SVW_{11}O_{40}]^{4-/5-}$ $W^{VI/V}$) Processes in Dimethylformamide.	Published	80% Concept, collecting data and writing first draft	Cameron L. Bentley 10% Data analysis, Tadaharu Ueda 10% Data analysis, Jie Zhang Supervision, Alan Bond Supervision	Y N N N
6	Electrolyte Cation Dependence of the Electron Transfer Kinetics Associated with the $[SVW_{11}O_{40}]^{3-/4-}$ ($V^{V/IV}$) and $[SVW_{11}O_{40}]^{4-/5-}$ ($W^{VI/V}$) Processes in Propylene Carbonate.	In preparation	80% Concept, collecting data and writing first draft	Cameron Bentley 10% Data analysis, Tadaharu Ueda 10% Data analysis, Jie Zhang Supervision, Alan Bond Supervision	Y N N N
7	A Systematic Study of the Kinetic and Thermodynamic Properties of the Fe^{III}/Fe^{II} Electron Transfer Process at Glassy Carbon and Boron-Doped Diamond Electrodes	In preparation	50% Concept, collecting data and writing first draft	Mingyue Lin 50% Data analysis, Dawei Pan Supervision, Jie Zhang Supervision, Alan Bond Supervision	N N N N

**If no co-authors, leave fields blank*

I have renumbered sections of submitted or published papers in order to generate a consistent presentation within the thesis.

Student signature: [redacted] **Date:** 08/06/17

The undersigned hereby certify that the above declaration correctly reflects the nature and extent of the student's and co-authors' contributions to this work. In instances where I am not the responsible author I have consulted with the responsible author to agree on the respective contributions of the authors.

Main Supervisor signature: [redacted] **ate:** 08/06/17

Publications

1. J. Li, A.M. Bond, J. Zhang, Probing Electrolyte Cation Effects on the Electron Transfer Kinetics of the [*a*-$SiW_{12}O_{40}$]$^{4-/5-}$ and [*a*-$SiW_{12}O_{40}$]$^{5-/6-}$ Processes using a Boron-Doped Diamond Electrode. *Electrochimica Acta*, **2015**, 178, 631-637.
2. J. Li, C.B. Bentley, A.M. Bond, J. Zhang. Dual-Frequency Alternating Current Designer Waveform for Reliable Voltammetric Determination of Electrode Kinetics Approaching the Reversible Limit. *Analytical Chemistry*, **2016**, 88(4), 2367-2374.
3. J. Li, S.-X. Guo, C.B. Bentley, K, Bano, A.M. Bond, J. Zhang, T. Ueda. Electrode Material Dependence of the Electron Transfer Kinetics Associated with the [$SVW_{11}O_{40}$]$^{3-/4-}$ ($V^{V/VI}$) and [$SVW_{11}O_{40}$]$^{4-/5-}$ $W^{VI/V}$) Processes in Dimethylformamide. *Electrochimica Acta*, **2016**, 201, 45-56.
4. J. Li, C.B. Bentley, K, Bano, A.M. Bond, J. Zhang, T, Ueda. Influence of 1-butyl-3-methylimidazolium on the electron transfer kinetics associated with the [$SVW_{11}O_{40}$]$^{3-/4-}$ ($V^{V/VI}$) and [$SVW_{11}O_{40}$]$^{4-/5-}$ $W^{VI/V}$) Processes in dimethylformamide. *Journal of Electroanalytical Chemistry*, **2016**, 779, 67-74.
5. C.B. Bentley, J. Li, A.M. Bond, J. Zhang. Mass-Transport and Heterogeneous Electron-Transfer Kinetics Associated with the Ferrocene/Ferrocenium Process in Ionic Liquids. *The Journal of Physical Chemistry C,* **2016**, 120.30, 16516-16525.
6. J. Li, C.B. Bentley, A.M. Bond, J. Zhang, T, Ueda. Electrolyte Cation Dependence of the Electron Transfer Kinetics Associated with the [$SVW_{11}O_{40}$]$^{3-/4-}$ ($V^{V/IV}$) and [$SVW_{11}O_{40}$]$^{4-/5-}$ ($W^{VI/V}$) Processes in Propylene Carbonate. Accepted by *Journal of Electroanalytical Chemistry*, **2017.**
7. M. Lin, J. Li, D. Pan, A.M. Bond, J. Zhang. A Systematic Study of the Kinetic and Thermodynamic Properties of the Fe^{3+}/Fe^{2+} Electron Transfer Process at Glassy Carbon and Boron-Doped Diamond Electrodes. *Electrochimica Acta*, **2017**, 249, 421-430.

Acknowledgements

I would like to express my sincere gratitude to my supervisors Prof. Alan Bond and Dr. Jie Zhang for the continuous support of my PhD study and related research, for their patience, motivation, and immense knowledge. I extremely thankful to them for the time they spent with me on my projects. Their guidance helped me in all the time of research and writing of this thesis.

I would like to thank my committee members, Prof. Leone Spiccia, Dr.Chenghua Sun, Professor Doug Macfarlane and Dr David Turner, for their insightful comments and encouragement.

I would like to acknowledge the award from Monash University which provides my tuition fees and living allowances. I also want to acknowledge the support of the Monash University Institute of Graduate Research and school of chemistry for providing travel grants to present my research at the 67th annual ISE Meeting (The Hague, Netherlands, 2016)

I would like to thank all the members from our electrochemistry group. Such nice and friendly environment makes my three years PhD study memorable for me. I sincerely thank Dr. Stephen Feldberg for his brilliant comments and suggestions.

I deeply thank my parents for their unconditional trust, timely encouragement, and endless patience.

Finally, I would like to thank my parents for the continuous supports and encouragements. At the end I would like express appreciation to my beloved wife Evelyn and my daughter Melody. The encouragement and support from my wife is a powerful source of inspiration and energy.

Symbols

Symbol	Meaning	Usual Units
A	electrode area	cm^2
C	concentration	mol dm^{-3}
C_{dl}	double layer capacitance	F
D	diffusion coefficient	cm^2 s^{-1}
E	potential of an electrode versus a reference	V
ΔE	amplitude in ac voltammetry	mV
E^0	standard potential	V
ΔE^0	difference in standard potential of two couples	V
$E^{0\prime}$	formal potential of an electrode	V
$E_p{}^{ox}$	oxidation peak potential	V
$E_p{}^{red}$	reduction peak potential	V
ΔE	voltametric peak to peak sepearation	V
F	Faraday's constant	96485 C mol^{-1}
f	(a) F/RT	V^{-1}
	(b) frequency	s^{-1}
I	current	A
I_L	steady-state limiting current	A
I_p	voltametric peak current	A
J_j	flux of species *j*	mol s^{-1} cm^{-2}
k^0	standard heterogeneous rate constant	cm s^{-1}
n	number of electrons	
N_A	Avogadro constant	mol^{-1}
Q	charge	C
R	gas constant	J mol^{-1} K^{-1}
R_u	uncompensated resistance	Ω
T	absolute temperature	K
t	time	s
V	volume	cm^3
v	linear potential scan rate	V/s

z_j	valence (charge) of species j	
α	transfer coefficient	
η	medium viscosity	cP

List of Figures

Chapter 1. Introduction

1.1 Polyoxometalates

Polyoxometalates (POMs) are discrete nanometer-sized oxide clusters of molybdenum, tungsten and other transition metals in high oxidation states. They represent an important class of inorganic material.[1] The first preparation of a polyoxometalate was reported by Berzelius in 1826.[2] It is ammonium 12-molybdophosphate $[PMo_{12}O_{40}]^{3-}$, a yellow precipitate and its structure was identified using X-ray diffraction about 100 years later.[3] Polyoxometalates are also known in different names, such as, heteropoly salt,[4-7] polyanions[8-11] or POMs[12-15]. Typically, a polyoxometalate is a polyatomic anion which contains a high proportion of one kind of atom (e.g., W, Mo, V) in positive oxidation state and other kind of atom with much smaller proportion (e.g., Nb, Ta, Re) in positive oxidation state which are linked together by shared oxygen atoms to form nanometer-sized cluster. With the advantage of modern high-resolution instrumentation, POM molecular science (chemistry,[15-23] physics,[1, 24-26] medicine,[27-33] biology and materials science[34-42]) has moved rapidly forward and intensive studies have been reported in the past decades.

1.1.1 Structure

Although a larger number of POMs have been found, they can be broadly divided into three groups.

Isopolyanions. Typically, isopolyanions contain only transition metals, such as V, W, Nb and Mo. Some main group elements may appear but they are considered as ligands only, not involved in the structure of the framework. The structure of

isopolyanions can be changed based on various frameworks with a number of metal centers varying from 2 up to over 150.[43-46] The most symmetrical structure and the most well known of isopolyanions is Lindqvist structure[47-51], $[M_6O_{19}]^{n-}$ (M = Nb, Ta, Mo, V and W), which contains a central oxygen atom about which are arrayed six metal atoms in an octahedral geometry. Each metal bears one terminal oxygen atom, and shares an additional four μ2-oxygen atoms with adjacent metal atoms.[52] The Lindqvist structure is represented in Figure 1.

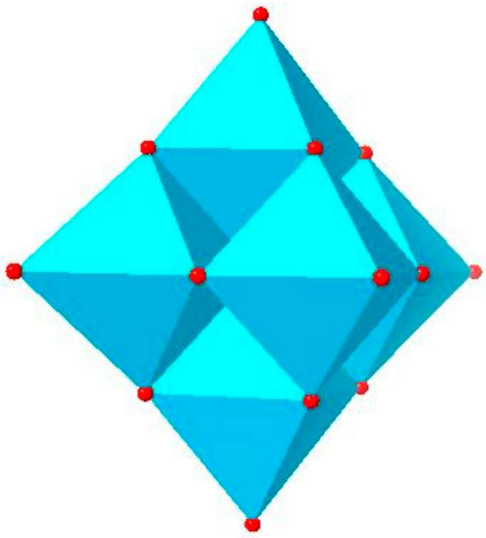

Figure 1. Structure of Lindqvist POMs $[M_6O_{19}]^{n-}$. Color code: M (blue), O (red).

Heteropolyanions. Heteropolyanions are those which made of an assembly of several fused MO_6 octahedrons wrapped around a tetrahedron containing a main group element, more seldom a transition metal.[53] Among those, Keggin[54] $[XM_{12}O_{40}]^{n-}$ (X = Si, P, As, Ge or B; M = W or Mo) and Wells–Dawson[55] $[X_2M_{18}O_{54}]^{n-}$ (where X = Si, P, As, Ge or B; M = W or Mo) are the most widely investigated. The structures are shown in Figure 2. Interestingly, when one or more W or Mo is replaced by other transition metal such as V, a so-called " lacunary POMs" is formed and their property may vary depend on the identity of the substituted metal ions. [56-58]

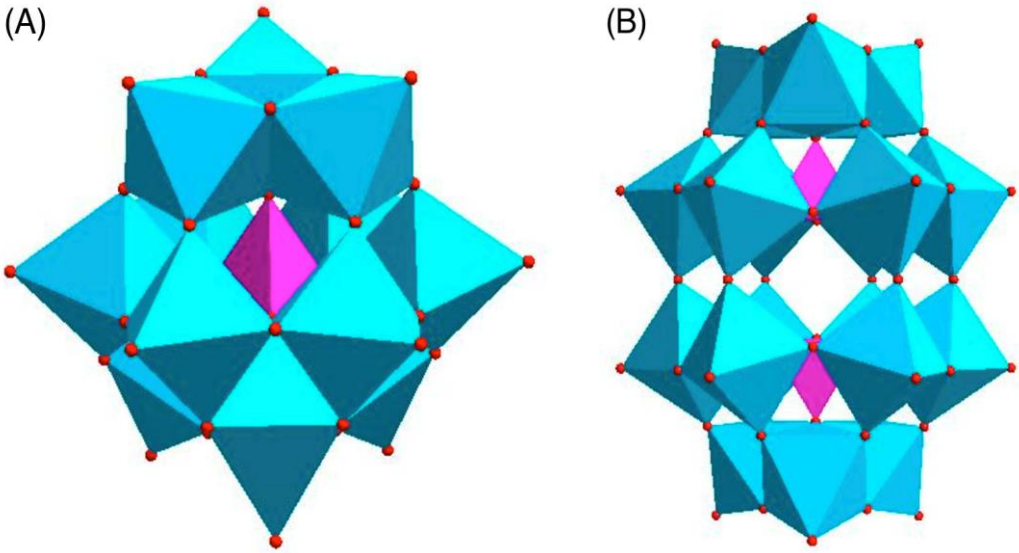

Figure 2. Structure of Keggin $[XM_{12}O_{40}]^{n-}$ (A) and Wells–Dawson $[X_2M_{18}O_{54}]^{n-}$ POMs (B). Color code: M (blue), O (red), purple (X).

Mo-blue and Mo-brown reduced POM clusters: Scheele first reported a new type of species molybdenum blue in 1783.[59] Their structure and composition were unknown until Mu¨ller et al. reported in 1995.[60] They synthesized and crystallised from a solution of Mo-blue and found that the species is a very high nuclearity cluster {Mo154} (shown in Figure 3) which has a ring topology. Other distinct structure types include spherical {Mo132},[61] ring-shaped {Mo176}[62-63] and lemon-shaed {Mo368}[64-65].

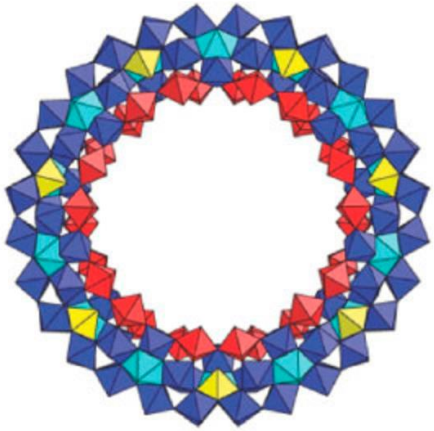

Figure 3. Structure of {Mo154}

1.1.2 Application

The field of polyoxometalate has attracted great attention in both academia and industry in the past two decades. Figure 4 demonstrates the growth of the publication on the topic per year during this period.

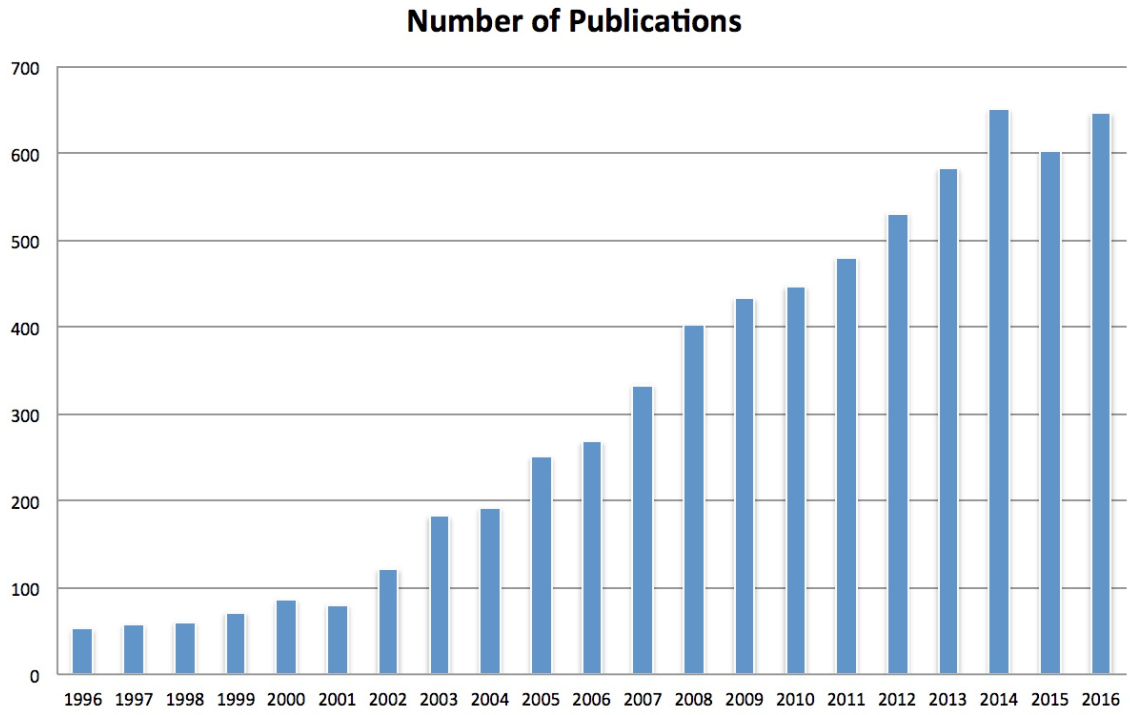

Figure 4. Comparison of the number of publications on the topic "polyoxometalates" from 1996 to 2016. Data obtained from a literature search using the ISI Web database.

Corrosion inhibitors. Corrosion is a global problem and has a detrimental impact on the world's economy. The most widely used methods to avoid corrosion is to isolate metal from corrosive agents and utilize corrosion inhibitor, such as nitrite, dichromate, chromate, phosphate.[66] However, some of them are toxic or non friendly to the environment.[67] POMs are relatively less toxic as compared to those corrosion inhibitors and they are cable to accept electrons without major structure changes and form insoluble salts with cations. All these properties make them suitable as corrosion inhibitors.[65, 68] Lomakina et al.[69] reported that in the present of POMs, the corrosion

rate of aluminium and its alloys in high temperature water decreased by 10 times compared to without addition of POMs. Streb et al.[70] found that using hydrophobic POMs-based ionic liquids (POMs-ILs) as coating, the corrosion resistance of copper metal against acetic acid vapors improved compared with using ionic liquids or POMs solely. Interestingly, mechanical damage (*e.g.* scratches) to the POMs-ILs coating can be self-repaired in a short time.

Capacitor. Due to their high intrinsic electron-storage capacity and high stability, expression in the term "electron reservoir" or "electron sponge" is sometimes applied to them. Combining POMs with carbon materials or polymers as electrical conductors with high surface area is a promising approach for the energy storage application. POMs have been studied widely as capacitor.[71-78] Lian et al. reported that POMs deposited onto multi-walled carbon nanotubes (MWCNT) via layer - by - layer method can increase charge storage capacity by a factor of 5.[79] Kulesza et al.[76] modified the surfaces of MWCNT with ultra-thin monolayer film of POMs ($H_3PMo_{12}O_{40}$) and found that significant increases of the capacitance and energy density compared with using MWCNT only. Combining conducting polymer (polyaniline) and POMs ($H_3PMo_{12}O_{40}$) for energy storage capacitor was clamed by Lira-Cantú et al.[73] As the redox processes of $H_3PMo_{12}O_{40}$ occur mostly in the potential range where the polymer is conductive, the charge-discharge processes are facilitated. The hybrid materials show high current densities and high stability.

Sensor. One of the most intriguing properties of POMs is their capability to undergo reversible multi-electron redox-processes with stable redox states.[80] Moreover, the redox chemistry of POMs can be controlled and finetuned by adding the heteroions and addenda ions into (W(VI), Mo(VI) and V(V)) the structural framework.[81-83] These

properties make them interesting for selective, long-lived sensor applications. In order to get a higher amperometric response, POMs are usually combined with high porous and conductive materials such as CNTs graphene to achieve higher sensitivity.[84-87] Kurth et al.[84] immobilized POMs on an electrode through a polyelectrolyte matrix and utilized this composite for quantitative detection of NO. The reduction current of POMs is proportional to the concentration of NO and gives a linear range from 1 nM to 10 μM. Reported by Sun et al. an amperometic sensor based on a sol-gel film containing $Na_2H_6CoW_{11}Co(H_2O)O_{39}$ and poly(4-vinylpyridine) in titania substrate was developed for detection of hydrogen peroxide, bromate and iodate. The sensor gave a linear range from 2.0×10^{-5} to 4.4×10^{-3} M for bromate and 2.0×10^{-5} to 2.8×10^{-3} M for iodate. Combined with grapheme oxide, POMs also displays resonable electrocatalytic activity for the oxidation of dopamine, which can be use for determination of dopamine.[88]

Electrocatalysts. As previously alluded to, POMs are able to undergo several fast and chemically reversible electron reduction processes without significant structural changes, they can be used as reductive electrocatalysts for reaction. About 30 years ago, it was reported that POMs showed a high activity toward hydrogen evolution reaction in acid media. [89-96] When combining POMs and RGO, a remarkable electrocatalytic hydrogen evolution reaction could be detected.[97] POMs also found to be active for oxygen reduction.[98] A combination of porphyrin complexes and POMs was adopt to form supramolecular network which catalyse a two-electron reduction of oxygen to hydrogen peroxide in pH 1-6 buffer solutions.[99]

When substituted by transition metal, POMs can be also used as oxidative electrocatalysts. As the heteropolyanion are completely oxidized inorganic compounds, they are stable under strong oxidized conditions, which makes them suitable as

oxidative electrocatalysts. A highly robust tetraruthenate cluster $[Ru_4O_4(H_2O)_4(OH)_2(SiW_{10}O_{36})_2]^{10-}$ was found to has oxygen-evolving activity. In the system, the four Ru(IV)-H_2O groups can act as a mediator for the four-electron overall process $2H_2O \rightarrow 2H_2 + O_2$ through a successive electron and proton loss.[100] This Ru-POMs were also found to exhibit high catalytic activity in electrooxidation of ethanol and methanol.[101] In aqueous over a wide pH range and alcohol media, ethanol and methanol were electrocatalytic oxidized to acids and aldehydes through four- and two-electron transfer pathways, respectively. In addition, POMs can also catalyst other oxidation process such as olefins oxidation[102] and NADH oxidation.[103-106]

Other applications in several areas including medicine,[107] magnetism,[108] membranes[109], solar energy[110] and etc. also attract a large amount of researchers' great attention. Among those, the dominant use of POMs is in catalysis.

1.1.3 Electrochemical Properties of Polyoxometalates.

In a homogeneous electrocatalyst reaction, two key steps are involved including the electron transfer between the electrode and a catalyst molecule, and the electron transfer between the catalyst molecule and a substrate. The former is critical as it is more like to transfer and disperse the electrons into a three-dimensional space instead of being confined within a two-dimensional space. The active form is generated by accepting electron from the electrode, and it is selected by the conditions as follows: (1) the standard potential of the catalyst is positive to the reduction potential of the substrate; (2) the electron transfer reaction of the catalyst is fast enough; (3) the catalyst is stable under the catalysis condition applied and can be regenerated chemically by the substrate. Although a wide range of POMs has been prepared and identified, only a

small amount of POMs can be used as electrocatalysts such as Keggin and Dawson POMs. The typical structures are: $[SiW_{12}O_{40}]^{4-}$, $[PW_{12}O_{40}]^{4-}$, $[SiMo_{12}O_{40}]^{4-}$, $[P_2W_{18}O_{62}]^{4-}$, $[S_2W_{18}O_{62}]^{4-}$, etc.

Usually, POMs bear several fast one- or two-electron reversible reduction processes. If more negative potential applied, further irreversible multi-electron reduction may occur accompanied with decomposition. When only one kind of addenda ions are present in the framework, the electrons can be delocalized on the POM framework across the oxygen bridges, which makes the reduced form stable. The reduction process may increase the negative charge density of POMs. In addition, the negative charge also increases the basicity of POMs. Therefore, the reduced POMs couple with proton readily and the electrochemical properties of POMs are pH dependent. [111]

Keggin-Type POMs $[XM_{12}O_{40}]^{n-}$

The voltammetric behaviour of $SiW_{12}O_{40}^{4-}$ in aqueous solution is selected as a representative example to illustrate the electrochemistry of Keggin-type POMs.

The whole cyclic voltammetric pattern of the $SiW_{12}O_{40}^{4-}$ complex in acidic solution consists of five redox processes. The formal potential -0.220, -0.420, - 0.580, -0.740 and -0.850 V vs. SCE which represent five reduction processes. The approximate electron ratios are 1:1:2:8:12.[96] The first three redox processes are reversible and well defined (Figure 5), while the fourth and fifth redox processes are irreversible and accompanied by decomposition.[112]

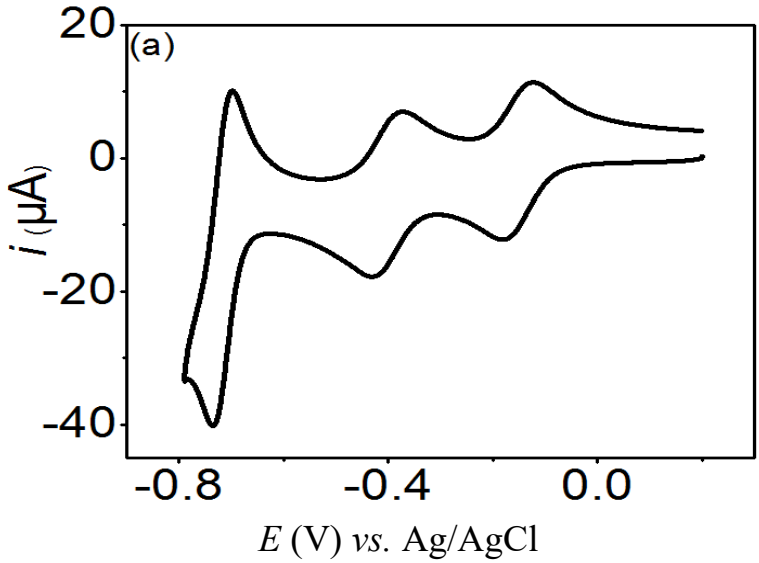

Figure 5. Dc cyclic voltammegrams for reduction of [*a*-$SiW_{12}O_{40}$]$^{4-}$ (1 mM) in aqueous media (1.0 M KNO_3 and 0.010 M HNO_3) at a GC electrode.

The first three processes can be described as follow,

$$[\alpha\text{-}SiW_{12}O_{40}]^{4-} + e^- \rightleftharpoons [\alpha\text{-}SiW_{12}O_{40}]^{5-} \quad \text{(process I)} \quad (1.1)$$

$$[\alpha\text{-}SiW_{12}O_{40}]^{5-} + e^- \rightleftharpoons [\alpha\text{-}SiW_{12}O_{40}]^{6-} \quad \text{(process II)} \quad (1.2)$$

$$[\alpha\text{-}SiW_{12}O_{40}]^{6-} + 2e^- + 4H^+ \rightleftharpoons [\alpha\text{-}H_4SiW_{12}O_{40}]^{4-} \quad \text{(process III)} \quad (1.3)$$

$$1 < pH < 5$$

When the pH is between 1 and 5, no protonation accompanies with the first two reduction processes, while the third process where a more negative charge [*α*-$SiW_{12}O_{40}$]$^{6-}$ involved may couple with proton and its formal potential becomes pH dependent and shifts to more negative potential by about 59 mV per pH unit.[113]

Dawson-Type POMs $[X_2M_{18}O_{62}]^{n-}$

The voltammetric behaviour of $[S_2W_{18}O_{62}]^{4-}$ in acetonitrile containing 0.1 M Bu_4NPF_6 is selected as an example to illustrate the electrochemistry of Daswon-type POMs.

In acetonitrile, six well-defined consecutive reversible one electron-transfer processes can be detected for the $[S_2W_{18}O_{62}]^{4-}$(Figure 6). The reversible potential for

these six waves are located at -0.240, -0.615, -1.180, -1.565, -2.020, and -2.320 V versus Fc^{+}/Fc as shown in Fig. 6. [114] The reaction sequence can be summarized in Eqs. 1.4-1.9.

$$[S_2W_{18}O_{62}]^{4-} + e^- \rightleftharpoons [S_2W_{18}O_{62}]^{5-} \quad \text{(process I)} \quad (1.4)$$

$$[S_2W_{18}O_{62}]^{5-} + e^- \rightleftharpoons [S_2W_{18}O_{62}]^{6-} \quad \text{(process II)} \quad (1.5)$$

$$[S_2W_{18}O_{62}]^{6-} + e^- \rightleftharpoons [S_2W_{18}O_{62}]^{7-} \quad \text{(process III)} \quad (1.6)$$

$$[S_2W_{18}O_{62}]^{7-} + e^- \rightleftharpoons [S_2W_{18}O_{62}]^{8-} \quad \text{(process IV)} \quad (1.7)$$

$$[S_2W_{18}O_{62}]^{8-} + e^- \rightleftharpoons [S_2W_{18}O_{62}]^{9-} \quad \text{(process V)} \quad (1.8)$$

$$[S_2W_{18}O_{62}]^{9-} + e^- \rightleftharpoons [S_2W_{18}O_{62}]^{10-} \quad \text{(process VI)} \quad (1.9)$$

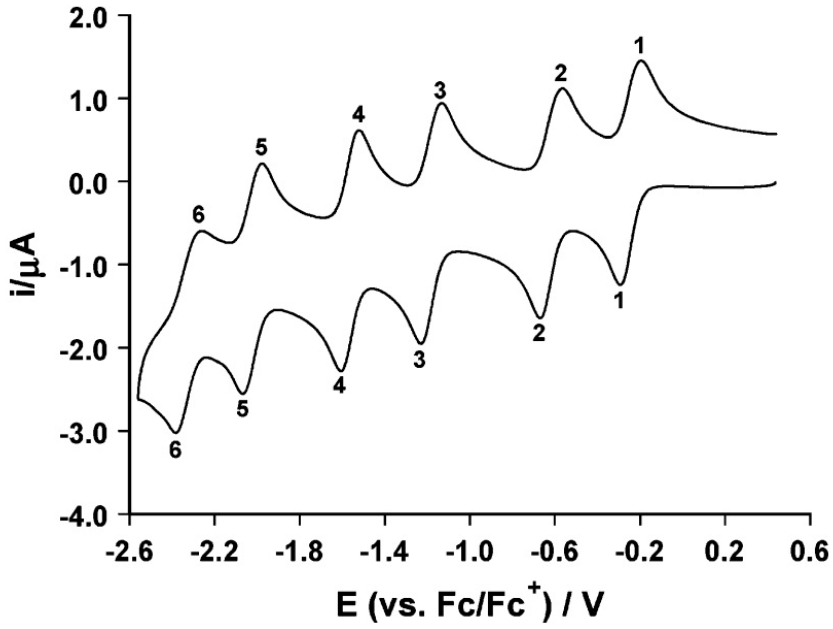

Figure 6. Dc cyclic voltammograms for [*a* -$S_2W_{18}O_{62}]^{4-}$ (0.5 mM) in CH_3CN (0.1 M Bu_4NPF_6) at a GC macrodisc electrode.[114]

1.2 Electrochemistry

Electrochemistry is the branch of chemistry that focuses on the relationship between electricity and chemical change. In an electrochemical system, researchers are

interested in the process that involves the transport of charge across the interface between an ionic conductor (an electrolyte) and electronic conductor (an electrode) and those factors that affect the rate of charge transfer.

1.2.1 Fundamentals of Electrochemistry

Based on different purposes, a two-electrode, three-electrode and four-electrode cell set up can be used for electrochemical measurement. Only the three-electrode cell set up will be introduced since this is the main set up utilized in the thesis. A three-electrode cell set up is made up of three electrodes: the counter electrode (CE), the reference electrode (RE), and the working electrode (WE). The CE is used to close the current circuit in the electrochemical cell. Generally, an inert material (e.g. Pt, Au, graphite) is chosen as a CE which does not participate under the reaction conditions. Because the current is flowing between the WE and the CE, the total active surface area of the CE must be larger than that of the WE so that it is not the limiting factor for the flowing current. The reference electrode is used as a point of reference in the cell for the potential control and measurement of the WE. Therefore, a qualified RE must has a stable and known electrode potential regardless of current flow through the RE. This requires that the reaction at the RE should be reversible, which can be achieved by taking a redox system and maintaining the concentrations of each participant in the redox reaction. A typical RE is silver/silver chloride reference electrode (Ag/AgCl), which is assembled with a high-purity silver wire with AgCl coating, and 1 M KCl solution in a small tube where the system is separated by a vycor frit from the solution outside the tube. The working electrode is where the reaction of interest occurs. Common WE can be made of inert materials such as noble metals (e.g. Au, Pt), carbon (e.g. glassy carbon, carbon paste), liquid metals (mercury), and semiconductors (e.g. Si,

indium-tin oxide). The size (e.g. macro-size, micro-size) and shape (e.g. disk, sphere, semi-sphere) of the WE also varies and it depends on the application.

Three-electrode cell setup. The three-electrode cell setup is the most common electrochemical cell setup used in electrochemistry[115-118] (Figure 7). In the arrangement, the current flows between the CE and the WE. The potential of the WE is measured and controlled relative to the RE. Generally, only the reactions occurring on the WE are of interest. Therefore, those reactions occur on CE are not concerned and the potential between the WE and CE usually is not measured. The advantage of three-electrode cell setup is the potential changes of the WE are measured independent of changes that may occur at the CE. This isolation allows for a specific reaction to be studied with confidence and accuracy.

In a two-electrode cell setup, the major problem is the potential drop (iR_s, where i is the current flowing across the cell, R_s is the solution resistance) as the potential is measure between the WE and the RE. The purpose of diminishing the effect of potential drop can be easily obtained by using the three-electrode cell setup.[119] In this case, the solution resistance can be divided into two parts as shown in Figure 8: compensated resistance (R_c) and the uncompensated resistance (R_u). R_c can be totally eliminated as it is not included in the potential measurement. R_u can be minimized by placing the RE as close as possible to the WE. In some cases, such as in organic solvent where the R_u is high due to the low conductivity, microelectrodes can be used to reduce the current. As a consequence, the iR_u can be greatly reduced.

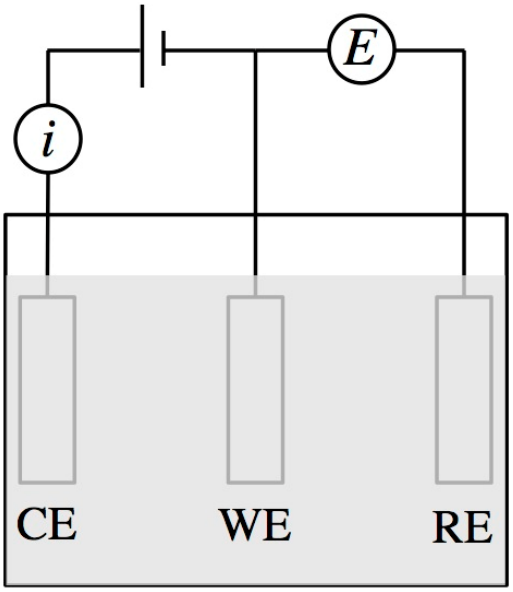

Figure 7. Schematic representation of an three-electrode cell.

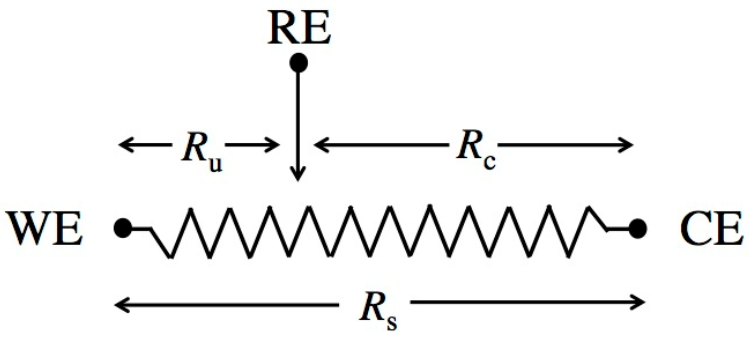

Figure 8. Schematic representation of a three-electrode cell as a potentiostat.

Since the potential of the RE is fixed, the potential of the WE is control with respect to the reference. For an electrode reaction, the potential difference between the WE and RE is varied by a power supply to the cell. This variation in potential can produce a current flow across the cell, because the potential is positive or negative enough to allow the electrode reaction occurs. In other terms, the drive force is high enough to drive the electrons cross the electrode/electrolyte interfaces.[120] Specifically, when applying more negative potential, the energy of the electrons within the WE is raised. They can reach a level where the energy is high enough and then transfer into

vacant electronic states on species in the electrolyte. In this case, the electrons transfer from electrode to solution which represents a flow of reduction current (Figure 9(a)). On the other hand, when applying more positive potential, the energy of the electrons becomes lower. When the energy is low enough, the electrons on species in the electrolyte will keen to a more favorable energy on the electrode and transfer there. In this case, the electrons transfer from solution to electrode which represents a flow of oxidation current (Figure 9(b)). Overall, the direction of the current (i.e. electrons) flow can reverse depending on the applied potential. Therefore, the WE act as anode or cathode alternately.

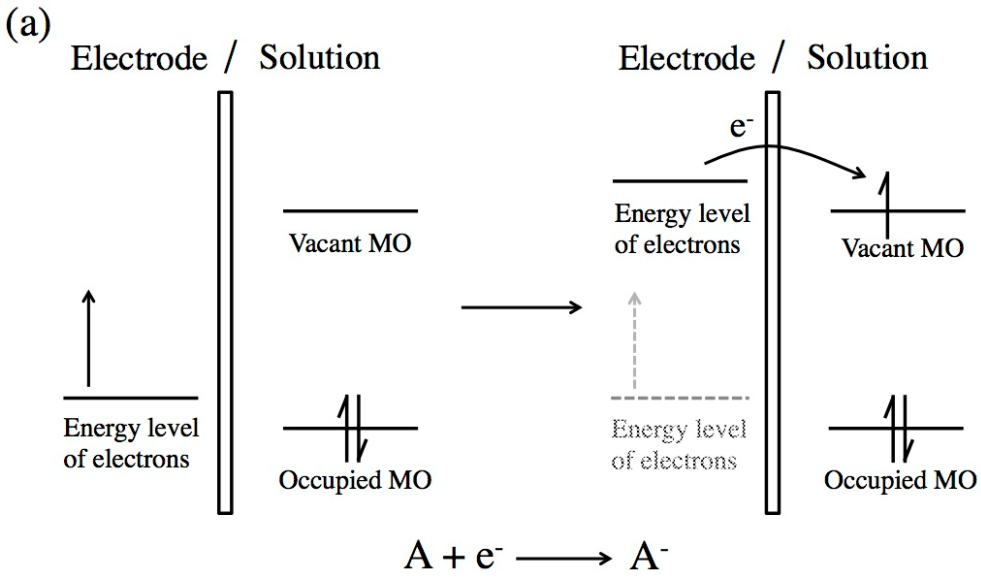

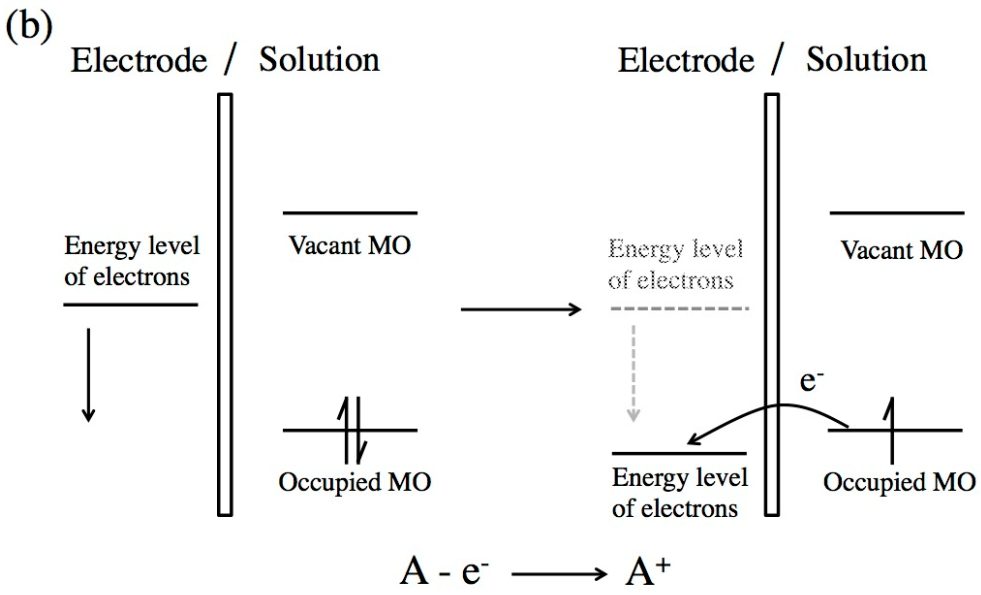

Figure 9. Representation of (a) reduction and (b) oxidation process of a species, A, in solution.

1.2.2 Mass – Transport

For a simplest electrode reaction, where the rate of heterogeneous electron-transfer is very rapid compared to the mass transport rate, we can find that the surface concentration of species is related to the electrode potential govern by the Nernst equation.[120]

$$E = E^0 + \frac{RT}{nF} \ln \frac{C_O(x=0)}{C_R(x=0)} \qquad (1.10)$$

$v_{electrode\ reaction}$ is the net rate of the electrode reaction which is governed by the rate of the species transferred to the surface by mass transport, $v_{mass\ transfer}$, which is proportional to the current (i) flowing across the electrode/electrolyte interface:

$$v_{electrode\ reaction} = v_{mass\ transfer} = \frac{i}{nFA} \qquad (1.11)$$

Mass transport is about the movement of the reactant to the electrode surface and the product to the bulk solution. Mass transport can occur in three ways:[120]

1. Migration. Transport of charged species because of electrical fields.

2. Diffusion. Transport of species because of concentration gradient.

3. Convection. Transport of species because of stirring or density gradient.

In a more quantitative way, when mass transport occurs in one dimensional, it can be express by the Nernst-Planck equation:

$$J_j(x) = -D_j \frac{\partial C_j(x)}{\partial x} - \frac{z_j F}{RT} D_j C_j \frac{\partial \emptyset(x)}{\partial x} + C_j v(x) \qquad (1.12)$$

where $J_j(x)$ with unit of [mol cm^{-2} sec^{-1}] is the flux for species at distance x [cm] away from the electrode; D_j [cm^2 sec^{-1}] is the diffusion coefficient of species, z_j and C_j [mol cm^{-3}] are the charge and concentration of species, respectively, $\partial C_j(x)/\partial x$ is the concentration gradient, $\partial \emptyset(x)/\partial x$ is the potential gradient and $v(x)$ [cm sec^{-1}] is the rate of solution flow. In the Eq.1.12, the first term represents the diffusion, the second term represents the migration of species, and the third term represents the convection of the solution. When all three modes of mass transport are in effect, experiment is very difficult to deal with. Therefore, electrochemical systems are usually designed to reduce the complexity of the equation by minimizing one or more of the contributions to the total flux. For example, electrochemical experiments can be carried out in the presence of large concentrations of supporting electrolyte, making the migration become negligible. The supporting electrolyte should be inert to the system and at a concentration much larger then the species. (e.g. 100 times greater). For the convection, it can be easily avoided by preventing vibrations or stirring in the electrochemical cell. The results discussed in the thesis were carried out under conditions where mass transport is only contributed by diffusion, which is also termed Fick's laws. Fick described two laws of diffusion in solution. The first one relates to the flux of a species,

j, which is proportional to its concentration, C_j, with distance from an electrode x at a time t:

$$-J_j(x) = D_j \frac{\partial C_j(x)}{\partial x} \tag{1.13}$$

The second one describes the change in concentration with time to the change in flux with position:

$$\frac{\partial C_j(x)}{\partial x} = D_j \left(\frac{\partial^2 C_j(x,t)}{\partial x^2}\right) \tag{1.14}$$

One consider the case of a spherical electrode of radius r_s placed in a solution that contains only supporting electrolyte and a redox-active species, j, of concentration C^*. The concentration gradient at the electrode surface is obtained by solving Fick's second law in spherical coordinates:

$$\frac{\partial C_j(r,x)}{\partial x} = D_j \left(\frac{\partial^2 C_j(r,t)}{\partial r^2} + \frac{2}{r}\frac{\partial C(r,t)}{\partial r}\right) \tag{1.15}$$

The boundary conditions for the potential step experiments described above are:

$$\lim_{r\to\infty} C(r,t) = C^* \tag{1.16}$$

$$C(r,0) = C^* \tag{1.17}$$

$$C(o,t) = 0 \text{ for } t > 0 \tag{1.18}$$

where r is the distance from the center of the sphere, D is the diffusion coefficient for the species, j, and C is the concentration as a function of distance r and time t. Using Laplace transform techniques, Eq.1.15 can be transformed to:

$$i(t) = \frac{nFADC^*}{r_s} + \frac{nFAD^{1/2}C^*}{\pi^{1/2}t^{1/2}} \tag{1.19}$$

Obviously, the current response contains two terms, time-independent and time-dependent. This can explain the different response obtained at macroelectrode and microelectrode.

Planar (linear) diffusion. In short time scale, the thickness of the diffusion layer is much smaller than the electrode radius. The electrode behaves like a macroelectrode. Mass transport takes place in one dimension at all points to the electrode surface, which is governed by planar (linear) diffusion. In this condition, the time dependent term in Eq.1.19 becomes more significant than the first one and the transient current response is given by:[119]

$$i(t) = \frac{nFAD^{1/2}C^*}{\pi^{1/2}t^{1/2}} \tag{1.20}$$

which is known as Cottrell equation.

Spherical (radial) diffusion. In long time scale, the contribution of the second term of Eq.1.19 to the total current is negligible while the first term which represents radial (spherical) diffusion becomes important. The steady-state current is given by:

$$i_{ss} = \frac{nFADC^*}{r_s} = 4\pi nFDC^* r_s \tag{1.21}$$

As "short" and "long" time scale are relative terms, in practice, one can distinguish the transient and steady-state limits by comparing r_s and $(Dt)^{1/2}$ which relate the radius of the electrode and the diffusion layer thickness. When $r_s \gg (Dt)^{1/2}$, the diffusion layer is thin compared to r_s and the system is dominated by transient behavior. On the other hand, when $r_s \ll (Dt)^{1/2}$, the thickness of diffusion layer is greater then the r_s and the system is in the steady-state regime. Therefore, one can vary the size of electrode or experiment time scale for probing the electrode reaction to observe transient or steady-state current based on different experiment purpose.[121-124]

1.2.3 Kinetics of Electrode Reactions

Generally speaking, the rate of an electrode reaction is governed by the rates of processes including: (1) Mass transfer; (2) electron transfer across the electrode/electrolyte interface; (3) chemical reactions such as protonation; (4) surface reactions, such as crystallization, adsorption or desorption. The overall rate of charge transfer is often limited by one or more slow reactions, known as rate-determining steps.

Consider a simple electron transfer reaction:

$$O + ne^- \underset{k_b}{\overset{k_f}{\leftrightarrows}} R \ (k^0, a, E^0) \tag{1.22}$$

where O is the oxidized form, R is the reduced form, n is the number of electrons needed in the reaction, k_f and k_b represent the heterogeneous rate constant for forward reduction and backward oxidation electrode reactions, respectively. k^0 is the heterogenous charge transfer rate constant, E^0 is the formal potential and a is charge transfer coefficient. The reversible potential (E_r) (*i.e.*, the reaction is at equilibrium state) is governed by the Nernst equation[119]:

$$E_r = E^0 + \frac{RT}{nF} \ln \frac{C_O^*}{C_R^*} \tag{1.23}$$

where R is the gas constant, T is the temperature, F is the Faraday's constant and C^* is the bulk concentration for the considered species. For the reaction in Eq.1.23, the net current (I_{net}) across the electrode/electrolyte interface can be expressed as the different of the reduction current (I_{red}) and the oxidation current (I_{ox}):

$$I_{net} = I_{red} - I_{ox} = nFA[k_f C_O(0,t) - k_b C_R(0,t)] \tag{1.24}$$

where A is the area of the electrode. In the case of a simple reduction reaction (*i.e.*, n =1), the forward and backward rate constants can be expressed as a function of k^0[120]:

$$k_f = k^0 e^{-af(E-E^{0\prime})} \quad (1.25)$$

$$k_b = k^0 e^{(1-a)f(E-E^{0\prime})} \quad (1.26)$$

where $f = F/(RT)$. We can combine Eqs.1.24-1.26 to get the expression of the net current of the reaction:

$$I_{net} = FAk^0[C_O(0,t)e^{-af(E-E^{0\prime})} - C_R(0,t)e^{(1-a)f(E-E^{0\prime})}] \quad (1.27)$$

This equation is known as the Bulter-Volmer formulation,[120] the fundamental relationship between current and applied potential. It is the basis for all studiess of heterogeneous kinetics.

1.2.3.1 Introduction to Kinetics Measurement

The electron transfer behavior occurred on the electrode/electrolyte interface can be described as a simplified electrical equivalent circuit (Figure 10).[119] R_{ct} represents the charge transfer resistance, Z_W represents the diffusion (Warburg) impedance, C_d represents the capacitance associated with the electrical double layer and R_s represents the solution resistance.

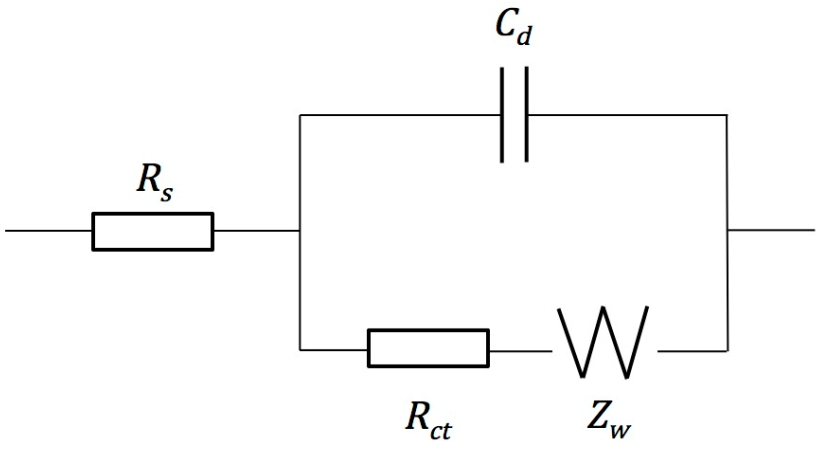

Figure 10. Electrical equivalent circuit of an electrode/electrolyte interface.

In order to measure the kinetics parameter (*i.e.* k^0, which is inversely proportional to the R_{ct} value), first step is to make sure the contribution from the C_d is negligible which is the case in steady-state conditions or subtract the charging current from the total current which is the case in fast-scan voltammetry. Therefore, the electrons across the electrode/electrolyte interface via the bottom pathway and the range of accessible kinetic parameters is determined by the R_s, R_{ct} and Z_W. The determination of k^0 can be straightforward when the R_{ct} value is much larger then the solution resistance (R_s) and the diffusion impedance (Z_W). This is the case when measuring a slow kinetics. However, for measuring fast electrode kinetics (*i.e.* R_{ct} becomes relatively small), both R_s and Z_W should be even smaller, which can be achieved using ultramicroelectrodes under steady-state conditions.

1.2.3.2 Conventional Method for Kinetics Measurement

Transient Methods. Under appropriate conditions when the electrode process optimized to be a quasi-reversible process, the method developed by Nicholson[125] is commonly used to determine the standard rate constants. This method is extremely simple and only requires the difference of the reduction and oxidation peaks, $\Delta E_p = |E_{red} - E_{ox}|$, where E_{red} and E_{ox} are the potentials of the reduction and oxidation peaks, respectively. A corresponding value of ψ can be found in Table 1 based on the obtained ΔE_p value. Then the kinetic parameter can be calculated from the equation X assuming the diffusion coefficient (D) of the oxidized and reduced forms are similar (*i.e.* $(D_O/D_R)^{a/2} \cong 1$):

$$\psi = \frac{(D_O/D_R)^{a/2} k^0}{(\pi D_O v F/RT)^{1/2}} \tag{1.28}$$

Table 1. Variation of ΔE_p with ψ at 25 ℃

ψ	ΔE_p
20	61
7	63
6	64
5	65
4	66
3	68
2	72
1	84
0.75	92
0.5	105
0.35	121
0.25	141
0.10	212

The disadvantages of using Nicholson's method for transient measurement are that it fails to take into account the uncompensated ohmic potential drop in the theories. As pointed out by Nicholson,[126] the uncompensated resistance and slow kinetics give a similar effects on peak shape and other characteristics, which will underestimate the electrode kinetics property (Figure 11). One can overcome the limitation by comparing the entire experimental voltammogram to the theory using computer program (*e.g.*, DigiSim program). [127-128]

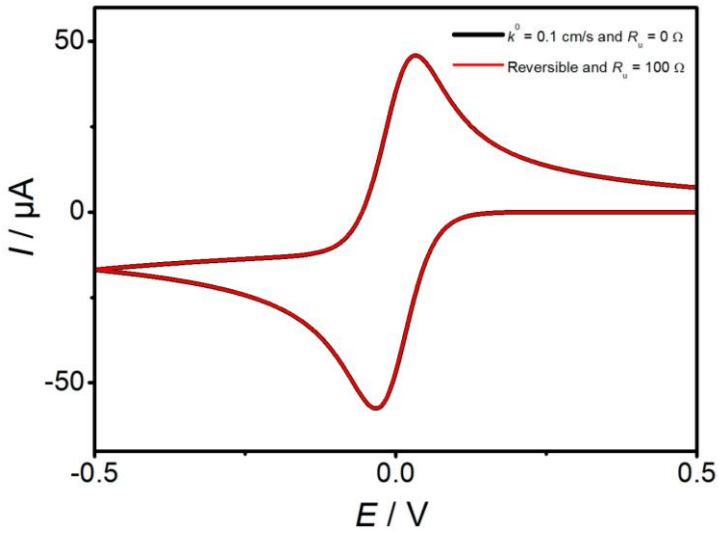

Figure 11. Comparison of the influence of uncompensated resistance and slow kinetics on dc voltammogram.

To investigate fast electrode kinetics at macroscopic planer electrodes, as mentioned above, one should increase the mass transfer rate to render the process to be kinetics controlled but not diffusion controlled.[129-130] By applying high scan rates, a high mass transfer rate can be obtained. However, in such conditions, potential drop and double layer charging current become more significant which may complicate the measurement of electrode kinetics. One can overcome the problems by using ultramicroelectrodes (UMEs),[131-133] due to theirs fast double layer charging and the small magnitude current (*i.e.* minimize the impact of potential drop). The advantages of using microelectrodes include: (1) high mass transport rate; (2) decreased potential drop and (3) decreased double layer charging current. When $v \gg RTD/nFr^2$ (r is the radius of a UMEs), the faradaic response of an UME is equivalent to that of a macro electrode. The approaches discussed above can be also used at UMEs for fast-scan voltammetry.

Steady-state voltammetry. Steady-state voltammetry is one of the best techniques for studying fast electrochemical kinetics. It can be obtained by using a UMEs. The advantages of steady-state voltammetry over the transient voltammetry are the absence

of the double layer charging current and reduced potential drop effects. Similar to transient voltammetry, the kinetics parameter, k^0 is determined from the difference of quartile potentials, $\Delta E_{1/4} = \left|E_{1/2} - E_{1/4}\right|$ and $\Delta E_{3/4} = \left|E_{3/4} - E_{1/2}\right|$ from a steady-state response. Under appropriate conditions, one can obtain steady-state current and measure the quartile potential values. By comparing the experimentally determined $\Delta E_{1/4}$ and $\Delta E_{3/4}$ values with those in the tables available in reference,[134] the k^0 value can be found in the table cell. This approach is simple and fast. However, the potential drop effect cannot be excluded by only comparing $\Delta E_{1/4}$ and $\Delta E_{3/4}$ values. As transient voltammetry, an alternative approach is to fit the entire experimental voltammogram to the theory using computer program (*e.g.*, DigiSim program). Besides, to obtain steady-state conditions one has to fabricate submicrometer-sized electrode, which is not easy to acquire.

1.3 Alternating Current (ac) Voltammetry

AC voltammetry was first invented in the 1950s[135] and developed by Smith and co-worker.[136-141] In a direct current (dc) cyclic voltammetry, the potential is applied over a range at a known scan rate. Then the current is recorded as a function of potential (time). The determination of the kinetics of an electrode process has been introduced briefly above. AC voltammetry is a more powerful approach to probe the electrode kinetics. In the technique, a sinusoidal wave of known frequency and amplitude is superimposed onto the dc ramp, then the ac current is measured as a function of dc potential. The electrode kinetics can be extracted either from the amplitude of ac current or from the phase angle between the ac current and ac voltage (Φ). Normally, the amplitude of the alternating current is usually smaller than 10 mV.

The main reason for that is to ensure the dc potential can be assumed to be constant when ac signal is superimposed on it. The other reason is that the theory for large amplitude has not been well developed. Even some work related to large amplitude ac voltammetry has been reported, [142-143] however, the lack of advanced computer technique for simulation limited the development of ac voltammetry.[144]

1.3.1 Large Amplitude Fourier Transformed Alternating Current Voltammetry.

As the ac signal increases with the amplitude of ac potential, in principle, large amplitude ac voltammetry can relatively improve the sensitivity. Great effects made by Bond and co-worker[145-147] accompanied with the development of fast numerical simulation techniques have given access to data analysis of large amplitude ac voltammetry. Quantitative study of electrode kinetics can be achieved by large amplitude Fourier Transformed Alternating Current voltammetry (FTACV). Briefly, both experimental and simulated data are resolved into the aperiodic and ac harmonic components by application of the FT and inverse FT algorithms. By comparing the dc, fundamental, second, third and higher harmonic components in experimental and simulated data, the thermodynamic and kinetics properties of an electrode process can be estimated quantitatively. The basis of large amplitude FTACV and simulation software used in the thesis are described in detail as below.

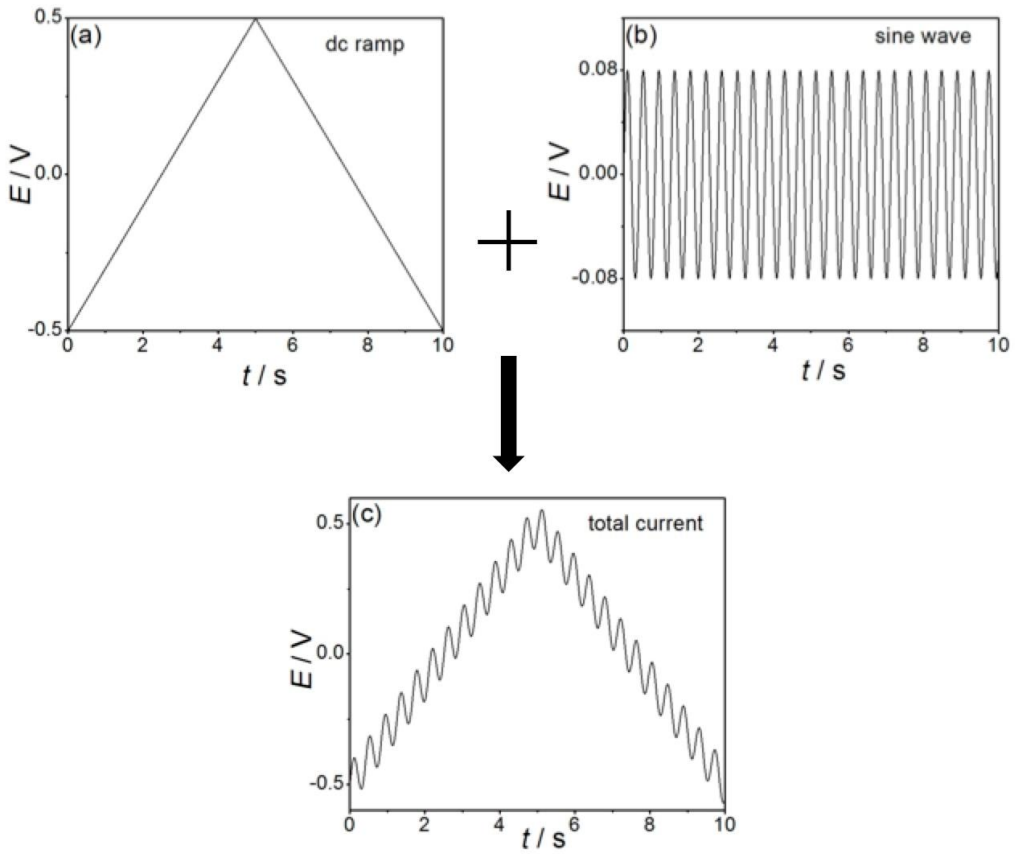

Figure 12. A schematic representation of the FTAC waveform.

As mentioned above, dc potential is applied to the working electrode and the current is recorded as a function of applied potential (or time) (figure 12(a)). At the same time, a sine wave of large amplitude (*e.g.* ΔE= 80 mV) is superimposed onto the dc potential (figure 12(b)). The overall current (Figure 13(a)) data is initially transferred from time domain to frequency domain by FT algorithm (Figure 13(b)). Then dc and a series of higher order harmonics (figure 13(c)) can be obtained by using a FT-band filtering and followed by the inverse FT operation. As the information given in this format is very messy (black area in figure 13(c)), therefore, only the envelope form (red curve) is used for data analysis.

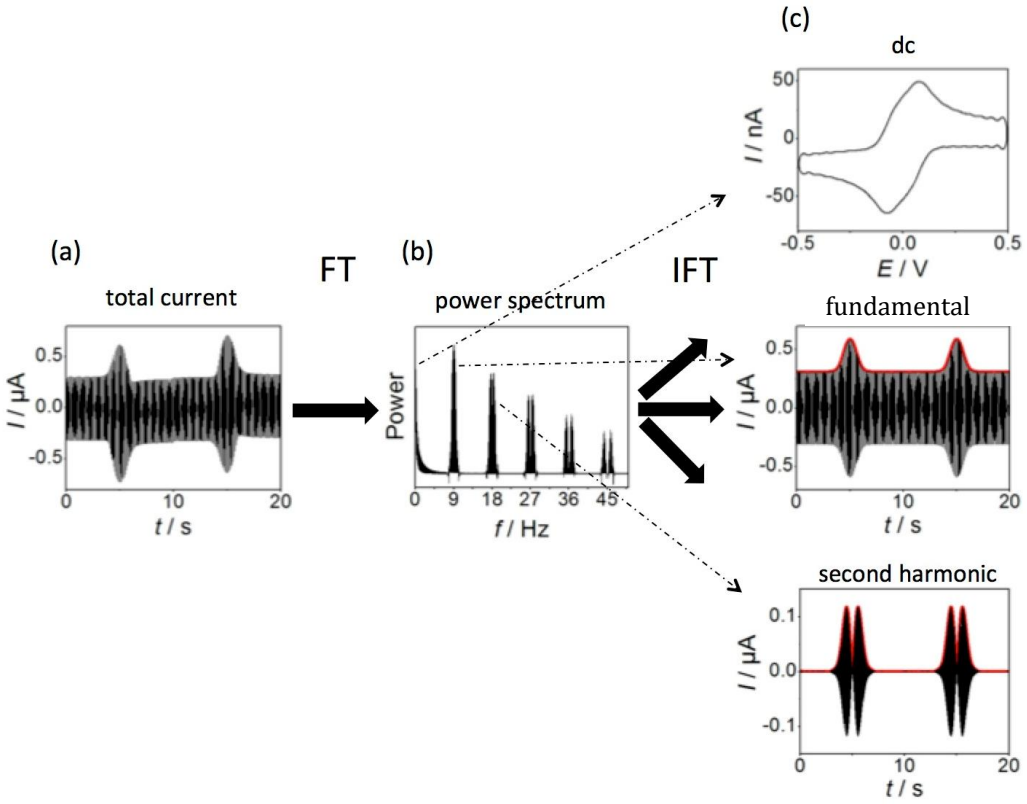

Figure 13. A schematic representation of data analysis for FTAC waveform.

In terms of studying electrode kinetics quantitatively, there are three main advantages of using large amplitude FTACV compared to dc voltammetry. The first advantage is the second and higher harmonic components are very insensitive to the background charging process although the background current is present in the fundamental harmonic, which means excellent signal to noise ratios can be obtained in higher harmonics.[148-149] The second advantage is that differences in effects of potential drop and slow kinetics can be readily distinguished in higher harmonics.[150] The potential drop can be very important in dc voltammetry if the effect of R_u is not carefully taken into account as R_u may lead to a larger ΔE_p same as slow kinetics does. However, in large amplitude FTACV, uncompensated resistance also contributes to all harmonic components but in a different way compared to slow kinetics (Figure 14). In some cases, the presence of uncompensated resistance may lead to peak splitting in

higher harmonics[150] which is substantial different from the peak shape of slow kinetics. The third advantage is that the current magnitude is extremely sensitive to the kinetics parameters.[151-152] The current of each harmonic component decreases as k^0 decreases and the trend becomes more obvious for the higher harmonics, which means the sensitivity increases as the higher order of the harmonic. These advantages demonstrate large amplitude FTACV is a powerful technique for quantifying electrode kinetics. Kiran et al.[153] found that use of large amplitude FTAC voltammetry for determination of electrode kinetics associated with $TCNQ^{0/\bullet-}$ and $TCNQ^{\bullet-/2-}$ in acetonitrile gives k^0 values of about $0.30 \pm 0.05\ cm\ s^{-1}$. Although FTAC voltammetry is kinetically sensitive, uncertainty of the k^0 values arises because the kinetics of these processes is so fast and close to the reversible limit. The authors also point out that in theory higher frequency can be used to expend the upper limit of FTAC voltammetry. However, the accompanied contribution from both R_u and capacitance makes it unlikely to achieve. Later, a slightly higher frequency (233 Hz) was used to probe the kinetics of a similar species F_4TCNQ in acetonitrile and gave a k^0 value of $1\ cm\ s^{-1}$ which was still close to the upper limit.[154] In order to use a much higher frequency (1233 Hz), they decreased the electrode size from macro (1 mm) to micro (123 μm) size as well as changed the solvent from acetonitrile to ionic liquid. High sensitivity was successfully achieved and k^0 value of $0.1\ cm\ s^{-1}$ was determined.

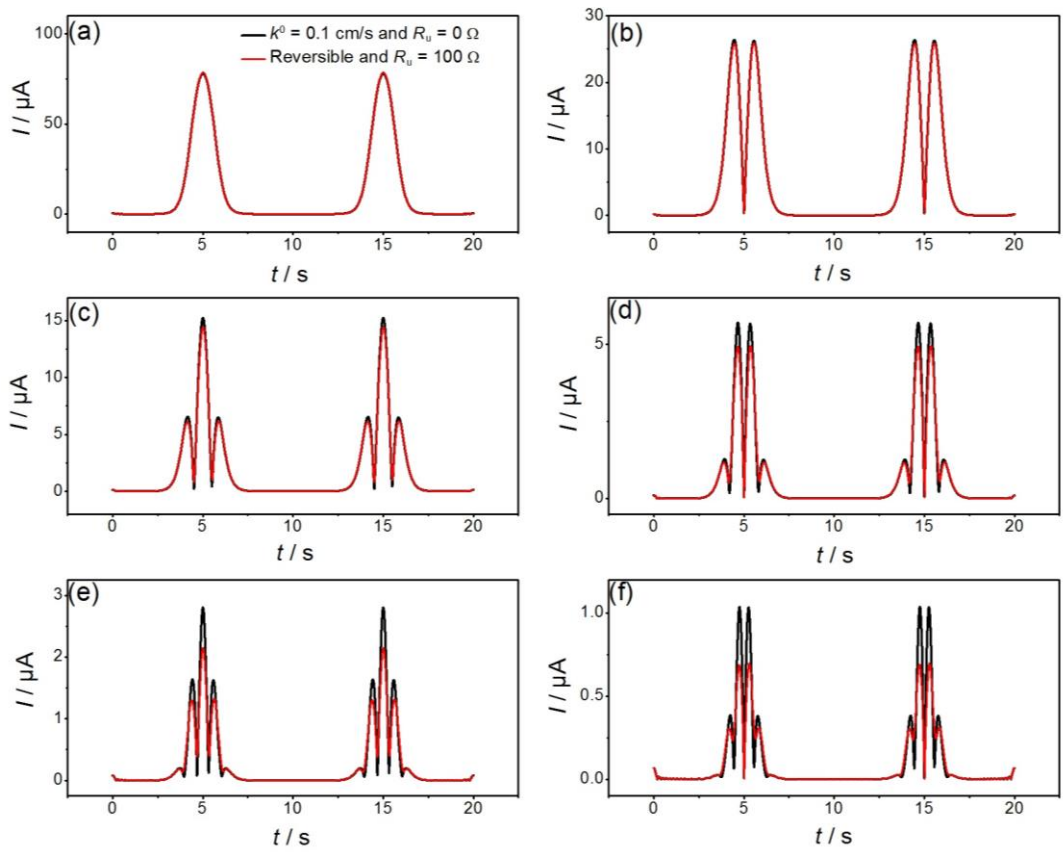

Figure 14. Comparison of simulated FT large-amplitude ac voltammograms for a reversible process with R_u of 100 Ω and a quasi-reversible process with $k^0 = 0.1\ cm\ s^{-1}$ and R_u of 0 Ω.

1.3.2 Kinetics Measurement by FTACV.

Large amplitude FTACV experiments are implemented by a home built instrument which is used to generate ac waveform and process the voltammetric data including Fourier transformation, band selection, inverse Fourier transformation to generate dc and a series of ac harmonic component. In order to acquire kinetics properties of an electrode process, the experimental data is subjected to compare with simulated data which can be obtained by freeware Monash electrochemistry simulator, MECSim. (http://www.garethkennedy.net/MECSim.html)

8 parameters of the system of interested have to be measured.[155] E^0 is the formal potential and can be estimated from the dc cyclic voltammetry. R_u is the resistance of the solution between the working electrode and reference electrode and can be determined experimentally from the RC time constant at potential where no faradaic current is present. For a reaction involving dissolved species, the faradaic current is governed by diffusion transport describe by Fick's law. Therefore, diffusion coefficient (D, which can be estimated by using Randles-Sevcik relationship[120]), concentration (c, which can ben calculated from the known mass of the species and volume of the solution) and electrode area (A, which can be assumed as the geometric area) are required. C_{dl} is capacitance of the double layer, which can be estimated from the background current in the fundamental harmonic.[156] After all, heterogeneous charge transfer rate constant (k^0) and charge transfer coefficient (a) can be determined by comparison of experimental and simulated data.[157-161]

1.3.3 Other Applications of FTACV

Other than probing the kinetics property of an electrode reaction, FTAC voltammetry can be also used in other applications as long as experiments are designed and carried out properly. FTAC voltammetry is sensitive to electrode kinetics but not sensitive to background charging current as well as homogeneous catalysis process. Therefore, many strategies had been developed based on this advantage.[162]

For a surface confined process involved with proteins as redox centers, the faradaic signal to background charging current is usually very low in dc voltammetry due to low concentration mobilized on the electrode surface. The concentration of protein is limited to a full monolayer coverage because the communication between the electrode and the

protein located in further layers is less effective.[163] For this case, FTAC voltammetry is a powerful technique for quantifying the electron kinetics associated with surface confined proteins. High faradaic signal to background charging current is obtained in high order harmonic components allows reliable quantitative evaluation of thermodynamic and kinetics properties of a surface confined proteins.[164-166]

Typically, when an electron transfer reaction is coupled to a chemical reaction (i.e. electrocatalysis process), the dc voltammetry exhibits large catalytic current which makes the studies of the underlying electron transfer reactions hard to obtain under catalytic turnover condition. In FTAC voltammetry, since the higher harmonics are insensitive to the background catalytic reaction and sensitive to fast electrode reaction[151, 167-169], they can be used to study the underlying electron transfer process. Studying two enzymatic reactions by FTAC voltammetry, Fleming and co-workers found that the underlying reversible redox chemistry of the ferrocenemonocarboxylic acid which acted as a mediator in glucose oxidation was totally unaffected under catalytic turnover conditions as detected in the third and higher harmonics. In contrast, slight changes were detected in the cytochrome P450 redox process which acted as catalyst in reduction of oxygen.[151] In catalytic water oxidation, water is both substrate and the solvent. The underlying electron transfer processes are barely visible under dc cyclic voltammetric conditions due to the presence of the large catalytic water oxidation current. However, application of FTAC voltammetry allows the direct detection of the electron transfer process that lead to the formation of the active catalyst and the measurement of the reversible potentials.[170-172]

1.4 Research Object

- To develop a new strategy which can improve the reliability of kinetics measurement by FTAC voltammetry.
- To study those factors that can affect the electron transfer kinetics associated with POMs, such as electrode materials, electrolyte cation, double layer.

References

1. Kortz, U.; Mueller, A.; van Slageren, J.; Schnack, J.; Dalal, N. S.; Dressel, M., Polyoxometalates: Fascinating structures, unique magnetic properties. *Coordination Chemistry Reviews* **2009,** *253* (19), 2315-2327.
2. Berzelius, J. J., Beitrag zur näheren Kenntniss des Molybdäns. *Annalen der Physik* **1826,** *82* (4), 369-392.
3. Keggin, J., Structure of the molecule of 12-phosphotungstic acid. *Nature* **1933,** *131* (3321), 908-909.
4. Alhanash, A.; Kozhevnikova, E. F.; Kozhevnikov, I. V., Hydrogenolysis of glycerol to propanediol over Ru: polyoxometalate bifunctional catalyst. *Catalysis letters* **2008,** *120* (3-4), 307-311.
5. Kaur, J.; Kozhevnikov, I. V., Efficient acylation of toluene and anisole with aliphatic carboxylic acids catalysed by heteropoly salt $Cs_{2.5}H_{0.5}PW_{12}O_{40}$. *Chemical Communications* **2002,** (21), 2508-2509.
6. Santos, J. S.; Dias, J. A.; Dias, S. C.; Garcia, F. A.; Macedo, J. L.; Sousa, F. S.; Almeida, L. S., Mixed salts of cesium and ammonium derivatives of 12-tungstophosphoric acid: Synthesis and structural characterization. *Applied Catalysis A: General* **2011,** *394* (1), 138-148.
7. Musawir, M.; Kozhevnikova, E. F.; Kozhevnikov, I. V., Fries rearrangement of phenyl acetate catalysed by platinum-doped heteropoly salt: Catalyst regeneration and reuse. *Journal of Molecular Catalysis A: Chemical* **2007,** *262* (1), 93-97.
8. Fan, L.; Xu, L.; Gao, G.; Li, F.; Li, Z.; Qiu, Y., A novel polyoxometalate chain constructed from sandwich lanthanide-containing polyanion $[Ce(PW_{11}O_{39})_2]^{10-}$ and sodium ion linker. *Inorganic Chemistry Communications* **2006,** *9* (12), 1308-1311.
9. Lehmann, J.; Gaita-Ari; nmacr, A.; Coronado, E.; Loss, D., Spin qubits with electrically gated polyoxometalate molecules. *Nature Nanotechnology* **2007,** *2* (5), 312-317.
10. Inumaru, K.; Ishihara, T.; Kamiya, Y.; Okuhara, T.; Yamanaka, S., Water‐Tolerant, Highly Active Solid Acid Catalysts Composed of the Keggin‐Type Polyoxometalate $H_3PW_{12}O_{40}$ Immobilized in Hydrophobic Nanospaces of Organomodified Mesoporous Silica. *Angewandte Chemie International Edition* **2007,** *46* (40), 7625-7628.

11. Ritchie, C.; Ferguson, A.; Nojiri, H.; Miras, H. N.; Song, Y. F.; Long, D. L.; Burkholder, E.; Murrie, M.; Kögerler, P.; Brechin, E. K., Polyoxometalate‐Mediated Self‐Assembly of Single‐Molecule Magnets:{[XW_9O_{34}]$_2$[$Mn^{III}_4Mn^{II}_2O_4(H_2O)_4$]}$^{12-}$. *Angewandte Chemie* **2008,** *120* (30), 5691-5694.
12. Guo, Y.; Wang, Y.; Hu, C.; Wang, Y.; Wang, E.; Zhou, Y.; Feng, S., Microporous polyoxometalates POMs/SiO_2: synthesis and photocatalytic degradation of aqueous organocholorine pesticides. *Chemistry of materials* **2000,** *12* (11), 3501-3508.
13. Zheng, X.; Zhang, L.; Li, J.; Luo, S.; Cheng, J.-P., Magnetic nanoparticle supported polyoxometalates (POMs) via non-covalent interaction: reusable acid catalysts and catalyst supports for chiral amines. *Chemical Communications* **2011,** *47* (45), 12325-12327.
14. An, H. Y.; Wang, E. B.; Xiao, D. R.; Li, Y. G.; Su, Z. M.; Xu, L., Chiral 3D architectures with helical channels constructed from polyoxometalate clusters and copper–amino acid complexes. *Angewandte Chemie* **2006,** *118* (6), 918-922.
15. Troupis, A.; Hiskia, A.; Papaconstantinou, E., Synthesis of metal nanoparticles by using polyoxometalates as photocatalysts and stabilizers. *Angewandte Chemie International Edition* **2002,** *41* (11), 1911-1914.
16. Kawasaki, N.; Wang, H.; Nakanishi, R.; Hamanaka, S.; Kitaura, R.; Shinohara, H.; Yokoyama, T.; Yoshikawa, H.; Awaga, K., Nanohybridization of polyoxometalate clusters and single‐wall carbon nanotubes: applications in molecular cluster batteries. *Angewandte Chemie* **2011,** *123* (15), 3533-3536.
17. Zou, C.; Zhang, Z.; Xu, X.; Gong, Q.; Li, J.; Wu, C.-D., A multifunctional organic–inorganic hybrid structure based on MnIII–porphyrin and polyoxometalate as a highly effective dye scavenger and heterogenous catalyst. *Journal of the American Chemical Society* **2011,** *134* (1), 87-90.
18. Song, J.; Luo, Z.; Britt, D. K.; Furukawa, H.; Yaghi, O. M.; Hardcastle, K. I.; Hill, C. L., A multiunit catalyst with synergistic stability and reactivity: A polyoxometalate–metal organic framework for aerobic decontamination. *Journal of the American Chemical Society* **2011,** *133* (42), 16839-16846.
19. Weinstock, I. A.; Atalla, R. H.; Reiner, R. S.; Moen, M. A.; Hammel, K. E.; Houtman, C. J.; Hill, C. L.; Harrup, M. K., A new environmentally benign technology for transforming wood pulp into paper. Engineering polyoxometalates as catalysts for multiple processes. *Journal of Molecular Catalysis A: Chemical* **1997,** *116* (1), 59-84.
20. Sartorel, A.; Carraro, M.; Scorrano, G.; Zorzi, R. D.; Geremia, S.; McDaniel, N. D.; Bernhard, S.; Bonchio, M., Polyoxometalate embedding of a tetraruthenium (IV)-oxo-core by template-directed metalation of [γ-$SiW_{10}O_{36}$]$^{8-}$: a totally inorganic oxygen-evolving catalyst. *Journal of the American Chemical Society* **2008,** *130* (15), 5006-5007.
21. Chen, C.; Zhao, W.; Lei, P.; Zhao, J.; Serpone, N., Photosensitized Degradation of Dyes in Polyoxometalate Solutions Versus TiO_2 Dispersions under Visible‐Light Irradiation: Mechanistic Implications. *Chemistry–A European Journal* **2004,** *10* (8), 1956-1965.

22. Seo, M. H.; Choi, S. M.; Kim, H. J.; Kim, J. H.; Cho, B. K.; Kim, W. B., A polyoxometalate-deposited Pt/CNT electrocatalyst via chemical synthesis for methanol electrooxidation. *Journal of power sources* **2008,** *179* (1), 81-86.
23. Yang, H.; Liu, T.; Cao, M.; Li, H.; Gao, S.; Cao, R., A water-insoluble and visible light induced polyoxometalate-based photocatalyst. *Chemical Communications* **2010,** *46* (14), 2429-2431.
24. Boudreau, D. M., Lubricant compositions containing Lindqvist metalates. Google Patents: 2015.
25. YUAN, K.; CHEN, L.; YAN, Z.-c.; CHEN, Y.-m., Epoxidation of methyl oleate catalyzed by Bronsted acid ionic liquid [HSO_3-(CH_2) 3-mim][HSO_4] for lubricant base oil. *Cereals & Oils* **2014,** *10*, 015.
26. Kozhevnikov, I.; Mulder, G.; Steverink-de Zoete, M.; Oostwal, M., Epoxidation of oleic acid catalyzed by peroxo phosphotungstate in a two-phase system. *Journal of Molecular Catalysis A: Chemical* **1998,** *134* (1), 223-228.
27. Barnard, D. L.; Hill, C.; Gage, T.; Matheson, J.; Huffman, J.; Sidwell, R.; Otto, M.; Schinazi, R., Potent inhibition of respiratory syncytial virus by polyoxometalates of several structural classes. *Antiviral research* **1997,** *34* (1), 27-37.
28. Huffman, J.; Sidwell, R.; Barnard, D. L.; Morrison, A.; Otto, M.; Hill, C.; Schinazi, R., Influenza virus-inhibitory effects of a series of germanium-and silicon-centred polyoxometalates. *Antiviral Chemistry and Chemotherapy* **1997,** *8* (2), 75-83.
29. Sarafianos, S. G.; KORTZ, U.; MODAK, M. J., Mechanism of polyoxometalate-mediated inactivation of DNA polymerases: an analysis with HIV-1 reverse transcriptase indicates specificity for the DNA-binding cleft. *Biochemical Journal* **1996,** *319* (2), 619-626.
30. Bussereau, F.; Picard, M.; Malick, C.; Teze, A.; Blancou, J. In *Efficacy of heteropolyanions against rabies virus infection in mice*, Annales de l'Institut Pasteur/Virologie, Elsevier: 1986; pp 391-400.
31. Kimberlin, R. H.; Walker, C., Suppression of scrapie infection in mice by heteropolyanion 23, dextran sulfate, and some other polyanions. *Antimicrobial agents and chemotherapy* **1986,** *30* (3), 409-413.
32. Jasmin, C.; Chermann, J.-C.; Herve, G.; Teze, A.; Souchay, P.; Boy-Loustau, C.; Raybaud, N.; Sinoussi, F.; Raynaud, M., In vivo inhibition of murine leukemia and sarcoma viruses by the heteropolyanion 5-tungsto-2-antimoniate. *Journal of the National Cancer Institute* **1974,** *53* (2), 469-474.
33. Inouye, Y.; Tokutake, Y.; Yoshida, T.; Seto, Y.; Hujita, H.; Dan, K.; Yamamoto, A.; Nishiya, S.; Yamase, T.; Nakamura, S., In vitro antiviral activity of polyoxomolybdates. Mechanism of inhibitory effect of PM-104 $(NH_4)_{12}H_2(Eu_4(MoO_4(H_2O)_{16}(Mo_7O_{24})_4)\cdot 13H_2O$ on human immunodeficiency virus type 1. *Antiviral research* **1993,** *20* (4), 317-331.
34. Kang, Z.; Tsang, C. H. A.; Zhang, Z.; Zhang, M.; Wong, N.-b.; Zapien, J. A.; Shan, Y.; Lee, S.-T., A polyoxometalate-assisted electrochemical method for silicon nanostructures preparation: from quantum dots to nanowires. *Journal of the American Chemical Society* **2007,** *129* (17), 5326-5327.
35. Pang, H.-j.; Peng, J.; Zhang, C.-j.; Li, Y.-g.; Zhang, P.-p.; Ma, H.-y.; Su, Z.-m., A polyoxometalate-encapsulated 3D porous metal–organic pseudo-rotaxane framework. *Chemical Communications* **2010,** *46* (28), 5097-5099.

36. Ma, F.-J.; Liu, S.-X.; Sun, C.-Y.; Liang, D.-D.; Ren, G.-J.; Wei, F.; Chen, Y.-G.; Su, Z.-M., A sodalite-type porous metal− organic framework with polyoxometalate templates: adsorption and decomposition of dimethyl methylphosphonate. *Journal of the American Chemical Society* **2011,** *133* (12), 4178-4181.
37. Sun, C.-Y.; Liu, S.-X.; Liang, D.-D.; Shao, K.-Z.; Ren, Y.-H.; Su, Z.-M., Highly stable crystalline catalysts based on a microporous metal− organic framework and polyoxometalates. *Journal of the American Chemical Society* **2009,** *131* (5), 1883-1888.
38. Yan, Y.; Wang, H.; Li, B.; Hou, G.; Yin, Z.; Wu, L.; Yam, V. W., Smart Self‐Assemblies Based on a Surfactant‐Encapsulated Photoresponsive Polyoxometalate Complex. *Angewandte Chemie* **2010,** *122* (48), 9419-9422.
39. Pradeep, C. P.; Misdrahi, M. F.; Li, F. Y.; Zhang, J.; Xu, L.; Long, D. L.; Liu, T.; Cronin, L., Synthesis of modular "inorganic–organic–inorganic" polyoxometalates and their assembly into vesicles. *Angewandte Chemie International Edition* **2009,** *48* (44), 8309-8313.
40. Xu, L.; Zhang, H.; Wang, E.; Wu, A.; Li, Z., Preparation and characterization of photoluminescent ultrathin films based on polyoxometalates. *Materials chemistry and physics* **2003,** *77* (2), 484-488.
41. Kang, Z.; Wang, Y.; Wang, E.; Lian, S.; Gao, L.; You, W.; Hu, C.; Xu, L., Polyoxometalates nanoparticles: synthesis, characterization and carbon nanotube modification. *Solid state communications* **2004,** *129* (9), 559-564.
42. Fang, X.; Kögerler, P.; Furukawa, Y.; Speldrich, M.; Luban, M., Molecular growth of a core–shell polyoxometalate. *Angewandte Chemie International Edition* **2011,** *50* (22), 5212-5216.
43. Attanasio, D.; Bonamico, M.; Fares, V.; Suber, L., Organic–inorganic charge-transfer salts based on the β-$[Mo_8O_{26}]^{4-}$ isopolyanion: synthesis, properties and X-ray structure. *Journal of the Chemical Society, Dalton Transactions* **1992,** (16), 2523-2528.
44. Guan, W.; Yan, L. K.; Su, Z. M.; Wang, E. B.; Wang, X. H., Density functional study of protonation sites of α‐Keggin isopolyanions. *International journal of quantum chemistry* **2006,** *106* (8), 1860-1864.
45. Yao, S.; Wu, H.-L.; Lei, Z.-Q.; Yan, J.-H.; Wang, E.-B., "S"-shaped isopolyoxotungstate cluster decorated by calcium ions. *Chinese Chemical Letters* **2013,** *24* (4), 283-286.
46. Bassil, B. S.; Kortz, U., Recent Advances in Lanthanide‐Containing Polyoxotungstates. *Zeitschrift für anorganische und allgemeine Chemie* **2010,** *636* (12), 2222-2231.
47. Lindqvist, I., THE STRUCTURE OF THE HEXANIOBATE ION IN $7Na_2O.6Nb_2O_5.32H_2O$. *Arkiv for Kemi* **1953,** *5* (3), 247-250.
48. Bridgeman, A. J.; Cavigliasso, G., Structure and Bonding in $[M_6O_{19}]^{n-}$ Isopolyanions. *Inorganic chemistry* **2002,** *41* (7), 1761-1770.
49. Yang, X.; Waters, T.; Wang, X.-B.; O'Hair, R. A.; Wedd, A. G.; Li, J.; Dixon, D. A.; Wang, L.-S., Photoelectron spectroscopy of free polyoxoanions $Mo_6O_{19}^{2-}$ and $W_6O_{19}^{2-}$ in the gas phase. *The Journal of Physical Chemistry A* **2004,** *108* (46), 10089-10093.

50. Sloan, J.; Matthewman, G.; Dyer-Smith, C.; Sung, A.-Y.; Liu, Z.; Suenaga, K.; Kirkland, A. I.; Flahaut, E., Direct imaging of the structure, relaxation, and sterically constrained motion of encapsulated tungsten polyoxometalate Lindqvist ions within carbon nanotubes. *ACS nano* **2008,** *2* (5), 966-976.
51. Xia, Y.; Wei, Y.; Wang, Y.; Guo, H., A Kinetically Controlled Trans Bifunctionalized Organoimido Derivative of the Lindqvist-Type Hexamolybdate: Synthesis, Spectroscopic Characterization, and Crystal Structure of $(n\text{-}Bu_4N)_2$ {trans-$[Mo_6O_{17}(NAr)_2]$}(Ar= 2, 6-dimethylphenyl). *Inorganic chemistry* **2005,** *44* (26), 9823-9828.
52. Strong, J. B.; Yap, G. P.; Ostrander, R.; Liable-Sands, L. M.; Rheingold, A. L.; Thouvenot, R.; Gouzerh, P.; Maatta, E. A., A new class of functionalized polyoxometalates: synthetic, structural, spectroscopic, and electrochemical studies of organoimido derivatives of $[Mo_6O_{19}]^{2-}$. *Journal of the American Chemical Society* **2000,** *122* (4), 639-649.
53. Jeannin, Y. P., The nomenclature of polyoxometalates: how to connect a name and a structure. *Chemical reviews* **1998,** *98* (1), 51-76.
54. Li, G.; Ding, Y.; Wang, J.; Wang, X.; Suo, J., New progress of Keggin and Wells–Dawson type polyoxometalates catalyze acid and oxidative reactions. *Journal of Molecular Catalysis A: Chemical* **2007,** *262* (1), 67-76.
55. Briand, L. E.; Baronetti, G. T.; Thomas, H. J., The state of the art on Wells–Dawson heteropoly-compounds: a review of their properties and applications. *Applied Catalysis A: General* **2003,** *256* (1), 37-50.
56. Pathan, S.; Patel, A., Novel heterogeneous catalyst, supported undecamolybdophosphate: synthesis, physico-chemical characterization and solvent-free oxidation of styrene. *Dalton Transactions* **2011,** *40* (2), 348-355.
57. Ritchie, C.; Alley, K. G.; Boskovic, C., Lacunary tungstotellurates (iv):$[Te_2W_{17}O_{61}]^{12-}$, $[Te_2W_{16}O_{58}(OH)_2]^{14-}$ and $[Te_2W_{18}O_{62}(OH)_2]^{10-}$. *Dalton Transactions* **2010,** *39* (38), 8872-8874.
58. Honma, N.; Kusaka, K.; Ozeki, T., Self-assembly of a lacunary α-Keggin undecatungstophosphate into a three-dimensional network linked by s-block cations. *Chemical Communications* **2002,** (23), 2896-2897.
59. Moiras, C.; Cronin, L., Polyoxometalate Nanocapsules: From Structure to Function. *ChemInform* **2010,** *41* (23), i.
60. Müller, A.; Krickemeyer, E.; Meyer, J.; Bögge, H.; Peters, F.; Plass, W.; Diemann, E.; Dillinger, S.; Nonnenbruch, F.; Randerath, M., $[Mo_{154}(NO)_{14}O_{420}(OH)_{28}(H_2O)_{70}]^{(25\pm5)-}$: A Water‐Soluble Big Wheel with More than 700 Atoms and a Relative Molecular Mass of About 24000. *Angewandte Chemie International Edition in English* **1995,** *34* (19), 2122-2124.
61. Müller, A.; Krickemeyer, E.; Bögge, H.; Schmidtmann, M.; Peters, F., Organizational forms of matter: an inorganic super fullerene and keplerate based on molybdenum oxide. *Angewandte Chemie International Edition* **1998,** *37* (24), 3359-3363.
62. Müller, A.; Krickemeyer, E.; Bögge, H.; Schmidtmann, M.; Beugholt, C.; Kögerler, P.; Lu, C., Formation of a Ring‐Shaped Reduced "Metal Oxide" with the Simple Composition $[(MoO_3)_{176}(H_2O)_{80}H_{32}]$. *Angewandte Chemie International Edition* **1998,** *37* (9), 1220-1223.

63. Jiang, C.-C.; Wei, Y.-G.; Liu, Q.; Zhang, S.-W.; Shao, M.-C.; Tang, Y.-Q., Self-assembly of a novel nanoscale giant cluster:[$Mo_{176}O_{496}(OH)_{32}(H_2O)_{80}$]†. *Chemical Communications* **1998,** (18), 1937-1938.
64. Müller, A.; Beckmann, E.; Bögge, H.; Schmidtmann, M.; Dress, A., Inorganic Chemistry Goes Protein Size: A Mo_{368} Nano - Hedgehog Initiating Nanochemistry by Symmetry Breaking. *Angewandte Chemie International Edition* **2002,** *41* (7), 1162-1167.
65. Müller, A.; Botar, B.; Das, S. K.; Bögge, H.; Schmidtmann, M.; Merca, A., On the complex hedgehog-shaped cluster species containing 368 Mo atoms: simple preparation method, new spectral details and information about the unique formation. *Polyhedron* **2004,** *23* (15), 2381-2385.
66. Fontana, M. G., *Corrosion engineering*. Tata McGraw-Hill Education: 2005.
67. Manahan, S. E., *Environmental science and technology*. CRC Press: 1997.
68. PIKEL'NYI, A.; Reznikova, G.; Brynza, A.; Khmelovskaya, S.; Pikel'naya, O., Electrochemical behavior and corrosion of steel in the presence of some heteropolycompounds. *Russian journal of electrochemistry* **1995,** *31* (5), 484-486.
69. Lomakina, S.; Shatova, T.; Kazansky, L., Heteropoly anions as corrosion inhibitors for aluminium in high temperature water. *Corrosion science* **1994,** *36* (9), 1645-1651.
70. Herrmann, S.; Kostrzewa, M.; Wierschem, A.; Streb, C., Polyoxometalate Ionic Liquids as Self - Repairing Acid - Resistant Corrosion Protection. *Angewandte Chemie International Edition* **2014,** *53* (49), 13596-13599.
71. Akter, T.; Hu, K.; Lian, K., Investigations of multilayer polyoxometalates-modified carbon nanotubes for electrochemical capacitors. *Electrochimica Acta* **2011,** *56* (14), 4966-4971.
72. Nishimoto, Y.; Yokogawa, D.; Yoshikawa, H.; Awaga, K.; Irle, S., Super-reduced polyoxometalates: excellent molecular cluster battery components and semipermeable molecular capacitors. *Journal of the American Chemical Society* **2014,** *136* (25), 9042-9052.
73. Gómez-Romero, P.; Chojak, M.; Cuentas-Gallegos, K.; Asensio, J. A.; Kulesza, P. J.; Casañ-Pastor, N.; Lira-Cantú, M., Hybrid organic–inorganic nanocomposite materials for application in solid state electrochemical supercapacitors. *Electrochemistry Communications* **2003,** *5* (2), 149-153.
74. Kume, K.; Kawasaki, N.; Wang, H.; Yamada, T.; Yoshikawa, H.; Awaga, K., Enhanced capacitor effects in polyoxometalate/graphene nanohybrid materials: a synergetic approach to high performance energy storage. *Journal of Materials Chemistry A* **2014,** *2* (11), 3801-3807.
75. Mu, A.; Li, J.; Chen, W.; Sang, X.; Su, Z.; Wang, E., The composite material based on Dawson-type polyoxometalate and activated carbon as the supercapacitor electrode. *Inorganic Chemistry Communications* **2015,** *55*, 149-152.
76. Skunik, M.; Chojak, M.; Rutkowska, I. A.; Kulesza, P. J., Improved capacitance characteristics during electrochemical charging of carbon nanotubes modified with polyoxometallate monolayers. *Electrochimica Acta* **2008,** *53* (11), 3862-3869.
77. Cuentas-Gallegos, A. K.; Martínez-Rosales, R.; Baibarac, M.; Gómez-Romero, P.; Rincón, M. E., Electrochemical supercapacitors based on novel hybrid materials made of carbon nanotubes and polyoxometalates. *Electrochemistry communications* **2007,** *9* (8), 2088-2092.

78. Ruiz, V.; Suárez-Guevara, J.; Gomez-Romero, P., Hybrid electrodes based on polyoxometalate–carbon materials for electrochemical supercapacitors. *Electrochemistry Communications* **2012,** *24*, 35-38.
79. Bajwa, G.; Genovese, M.; Lian, K., Multilayer polyoxometalates-carbon nanotube composites for electrochemical capacitors. *ECS Journal of Solid State Science and Technology* **2013,** *2* (10), M3046-M3050.
80. Pope, M. T., Molybdenum oxygen chemistry: oxides, oxo complexes, and polyoxoanions. *Progress in Inorganic Chemistry, Volume 39* **1991**, 181-257.
81. Neumann, R.; Dahan, M., A ruthenium-substituted polyoxometalate as an inorganic dioxygenase for activation of molecular oxygen. *Nature* **1997,** *388* (6640), 353-355.
82. Weinstock, I. A.; Barbuzzi, E. M.; Wemple, M. W.; Cowan, J. J.; Reiner, R. S.; Sonnen, D. M.; Heintz, R. A.; Bond, J. S.; Hill, C. L., Equilibrating metal-oxide cluster ensembles for oxidation reactions using oxygen in water. *Nature* **2001,** *414* (6860), 191-195.
83. Neiwert, W. A.; Cowan, J. J.; Hardcastle, K. I.; Hill, C. L.; Weinstock, I. A., Stability and Structure in α-and β-Keggin Heteropolytungstates,$[X^{n+}W_{12}O_{40}]^{(8-n)-}$, X= p-Block Cation. *Inorganic chemistry* **2002,** *41* (26), 6950-6952.
84. Liu, S.; Volkmer, D.; Kurth, D. G., Smart polyoxometalate-based nitrogen monoxide sensors. *Analytical chemistry* **2004,** *76* (15), 4579-4582.
85. Li, Z.; Chen, J.; Pan, D.; Tao, W.; Nie, L.; Yao, S., A sensitive amperometric bromate sensor based on multi-walled carbon nanotubes/phosphomolybdic acid composite film. *Electrochimica acta* **2006,** *51* (20), 4255-4261.
86. Manivel, A.; Sivakumar, R.; Anandan, S.; Ashokkumar, M., Ultrasound-Assisted Synthesis of Hybrid Phosphomolybdate–Polybenzidine Containing Silver Nanoparticles for Electrocatalytic Detection of Chlorate, Bromate and Iodate Ions in Aqueous Solutions. *Electrocatalysis* **2012,** *3* (1), 22-29.
87. Liu, R.; Li, S.; Yu, X.; Zhang, G.; Zhang, S.; Yao, J.; Keita, B.; Nadjo, L.; Zhi, L., Facile Synthesis of Au‐Nanoparticle/Polyoxometalate/Graphene Tricomponent Nanohybrids: An Enzyme‐Free Electrochemical Biosensor for Hydrogen Peroxide. *Small* **2012,** *8* (9), 1398-1406.
88. Zhang, H.; Xie, A.; Shen, Y.; Qiu, L.; Tian, X., Layer-by-layer inkjet printing of fabricating reduced graphene-polyoxometalate composite film for chemical sensors. *Physical Chemistry Chemical Physics* **2012,** *14* (37), 12757-12763.
89. Keita, B.; Nadjo, L., Surface modifications with heteropoly and isopoly oxometalates: Influence of metal additions. *Journal of Electroanalytical Chemistry and Interfacial Electrochemistry* **1989,** *269* (2), 447-453.
90. Keita, B.; Nadjo, L., Surface modifications with heteropoly and isopoly oxometalates: Part V. Electrocatalysis of the HER in alkaline solution. *Journal of Electroanalytical Chemistry and Interfacial Electrochemistry* **1990,** *287* (1), 149-157.
91. Keita, B.; Nadjo, L.; Haeussler, J., Activation of electrode surfaces: semiquantitative characterization of electrode surfaces modified with heteropolyanions. *Journal of electroanalytical chemistry and interfacial electrochemistry* **1987,** *230* (1), 85-97.
92. Keita, B.; Nadjo, L., New aspects of the electrochemistry of heteropolyacids: Part III. Further proof of minimal solvation and ion pairing of silicotungstic and

phosphotungstic species in acidic concentrated aqueous solutions of alkali-metal salts. *Journal of electroanalytical chemistry and interfacial electrochemistry* **1987,** *230* (1-2), 267-271.
93. Keita, B.; Nadjo, L., Surface modifications with heteropoly and isopoly oxometalates: part I. Qualitative aspects of the activation of electrode surfaces towards the hydrogen evolution reaction. *Journal of electroanalytical chemistry and interfacial electrochemistry* **1988,** *243* (1), 87-103.
94. Keita, B.; Nadjo, L.; Saveant, J., Surface modifications with heteropoly and isopoly oxometalates: Part II. Electrocatalytic behaviour of glassy carbon surfaces modified with 17-tungsto, 1-molybdo-diphosphate. *Journal of electroanalytical chemistry and interfacial electrochemistry* **1988,** *243* (1), 105-116.
95. Keita, B.; Nadjo, L.; Parsons, R., Surface modifications with heteropoly and isopoly oxometalates: Part IV11For Parts I–III, see refs. 6–8.. Further details and kinetic aspects of the her on the modified electrodes. *Journal of Electroanalytical Chemistry and Interfacial Electrochemistry* **1989,** *258* (1), 207-218.
96. Keita, B.; Nadjo, L., New aspects of the electrochemistry of heteropolyacids: Part II. Coupled electron and proton transfers in the reduction of silicoungstic species. *Journal of electroanalytical chemistry and interfacial electrochemistry* **1987,** *217* (2), 287-304.
97. Jiang, M.; Zhu, D.; Cai, J.; Zhang, H.; Zhao, X., Electrocatalytic hydrogen evolution and oxygen reduction on polyoxotungstates/graphene nanocomposite multilayers. *The Journal of Physical Chemistry C* **2014,** *118* (26), 14371-14378.
98. Wang, P.; Li, Y., Electrochemical and electrocatalytic properties of polypyrrole film doped with heteropolyanions. *Journal of Electroanalytical Chemistry* **1996,** *408* (1), 77-81.
99. Shen, Y.; Liu, J.; Jiang, J.; Liu, B.; Dong, S., Fabrication of a metalloporphyrin-polyoxometalate hybrid film by a layer-by-layer method and its catalysis for hydrogen evolution and dioxygen reduction. *The Journal of Physical Chemistry B* **2003,** *107* (36), 9744-9748.
100. Toma, F. M.; Sartorel, A.; Iurlo, M.; Carraro, M.; Parisse, P.; Maccato, C.; Rapino, S.; Gonzalez, B. R.; Amenitsch, H.; Da Ros, T., Efficient water oxidation at carbon nanotube–polyoxometalate electrocatalytic interfaces. *Nature chemistry* **2010,** *2* (10), 826-831.
101. Liu, Y.; Zhao, S.-F.; Guo, S.-X.; Bond, A. M.; Zhang, J.; Zhu, G.; Hill, C. L.; Geletii, Y. V., Electrooxidation of Ethanol and Methanol Using the Molecular Catalyst $[\{Ru_4O_4(OH)_2(H_2O)_4\}(\gamma\text{-}SiW_{10}O_{36})_2]^{10-}$. *Journal of the American Chemical Society* **2016,** *138* (8), 2617-2628.
102. Steckhan, E.; Kandzia, C., Ruthenium-Catalysed, Electrochemical Cleavage of Aryl Olefins for the Synthesis of Benzaldehydes. *Synlett* **1992,** *1992* (02), 139-140.
103. Keita, B.; Essaadi, K.; Belhouari, A.; Nadjo, L.; Contant, R.; Justum, Y., Catalysis of the oxidation of NADH by heteropolyanions: a kinetic study. *Comptes Rendus de l'Académie des Sciences-Series IIC-Chemistry* **1998,** *1* (5), 343-350.
104. Essaadi, K.; Keita, B.; Nadjo, L.; Contant, R., Oxidation of NADH by oxometalates. *Journal of Electroanalytical Chemistry* **1994,** *367* (1), 275-278.
105. Keita, B.; Essaadi, K.; Nadjo, L.; Desmadril, M., Rate-limiting one-electron transfer in the oxidation of NADH by polyoxometalates. *Chemical physics letters* **1995,** *237* (5), 411-418.

106. Keita, B.; Essaadi, K.; Nadjo, L.; Contant, R.; Justum, Y., Oxidation kinetics of NADH by heteropolyanions. *Journal of Electroanalytical Chemistry* **1996,** *404* (2), 271-279.
107. Hill, C. L.; Weeks, M. S.; Schinazi, R. F., Anti-HIV-1 activity, toxicity, and stability studies of representative structural families of polyoxometalates. *Journal of medicinal chemistry* **1990,** *33* (10), 2767-2772.
108. Speldrich, M.; Schilder, H.; Lueken, H.; Kögerler, P., A computational framework for magnetic polyoxometalates and molecular spin structures: CONDON 2.0. *Israel Journal of Chemistry* **2011,** *51* (2), 215-227.
109. Fontananova, E.; Donato, L.; Drioli, E.; Lopez, L. C.; Favia, P.; d'Agostino, R., Heterogenization of polyoxometalates on the surface of plasma-modified polymeric membranes. *Chemistry of materials* **2006,** *18* (6), 1561-1568.
110. Luo, X.; Li, F.; Xu, B.; Sun, Z.; Xu, L., Enhanced photovoltaic response of the first polyoxometalate-modified zinc oxide photoanode for solar cell application. *Journal of Materials Chemistry* **2012,** *22* (30), 15050-15055.
111. Liu, S.; Volkmer, D.; Kurth, D. G., Functional polyoxometalate thin films via electrostatic layer-by-layer self-assembly. *Journal of Cluster Science* **2003,** *14* (3), 405-419.
112. Keita, B.; Nadjo, L., Activation of electrode surfaces: Application to the lectrocatalysis of the hydrogen evolution reaction. *Journal of electroanalytical chemistry and interfacial electrochemistry* **1985,** *191* (2), 441-448.
113. Pope, M. T.; Varga Jr, G. M., Heteropoly blues. I. Reduction stoichiometries and reduction potentials of some 12-tungstates. *Inorganic Chemistry* **1966,** *5* (7), 1249-1254.
114. Zhang, J.; Bond, A. M.; Richardt, P. J.; Wedd, A. G., Voltammetric reduction of α-and γ*-$[S_2W_{18}O_{62}]^{4-}$ and α-, β-, and γ-$[SiW_{12}O_{40}]^{4-}$: isomeric dependence of reversible potentials of polyoxometalate anions using data obtained by novel dissolution and conventional solution-phase processes. *Inorganic chemistry* **2004,** *43* (26), 8263-8271.
115. Blyr, A.; Sigala, C.; Amatucci, G.; Guyomard, D.; Chabre, Y.; Tarascon, J. M., Self‐Discharge of $LiMn_2O_4$/C Li‐Ion Cells in Their Discharged State Understanding by Means of Three‐Electrode Measurements. *Journal of The Electrochemical Society* **1998,** *145* (1), 194-209.
116. Stoller, M. D.; Ruoff, R. S., Best practice methods for determining an electrode material's performance for ultracapacitors. *Energy & Environmental Science* **2010,** *3* (9), 1294-1301.
117. Dollé, M.; Orsini, F.; Gozdz, A. S.; Tarascon, J.-M., Development of reliable three-electrode impedance measurements in plastic Li-ion batteries. *Journal of The Electrochemical Society* **2001,** *148* (8), A851-A857.
118. Hoshikawa, T.; Yamada, M.; Kikuchi, R.; Eguchi, K., Impedance analysis for dye-sensitized solar cells with a three-electrode system. *Journal of Electroanalytical Chemistry* **2005,** *577* (2), 339-348.
119. Zoski, C. G., *Handbook of electrochemistry*. Elsevier: 2006.
120. Bard, A. J.; Faulkner, L. R., Fundamentals and applications. *Electrochemical Methods, 2nd ed.; Wiley: New York* **2001**.

121. Oldham, K. B., Steady-state microelectrode voltammetry as a route to homogeneous kinetics. *Journal of electroanalytical chemistry and interfacial electrochemistry* **1991,** *313* (1-2), 3-16.
122. Amatore, C.; Fosset, B.; Bartelt, J.; Deakin, M.; Wightman, R., Electrochemical kinetics at microelectrodes: Part V. Migrational effects on steady or quasi-steady-state voltammograms. *Journal of electroanalytical chemistry and interfacial electrochemistry* **1988,** *256* (2), 255-268.
123. Zoski, C. G.; Bond, A. M.; Allinson, E. T.; Oldham, K. B., How long does it take a microelectrode to reach a voltammetric steady state? *Analytical Chemistry* **1990,** *62* (1), 37-45.
124. Daniele, S.; Lavagnini, I.; Baldo, M. A.; Magno, F., Steady state voltammetry at microelectrodes for the hydrogen evolution from strong and weak acids under pseudo-first and second order kinetic conditions. *Journal of electroanalytical chemistry* **1996,** *404* (1), 105-111.
125. Nicholson, R. S., Theory and Application of Cyclic Voltammetry for Measurement of Electrode Reaction Kinetics. *Analytical Chemistry* **1965,** *37* (11), 1351-1355.
126. Nicholson, R. S., Some examples of the numerical solution of nonlinear integral equations. *Analytical Chemistry* **1965,** *37* (6), 667-671.
127. Rudolph, M.; Reddy, D. P.; Feldberg, S. W., A simulator for cyclic voltammetric responses. *Analytical chemistry* **1994,** *66* (10), 589A-600A.
128. Barcena, H. S.; Liu, B.; Mirkin, M. V.; Canary, J. W., An electrochiroptical molecular switch: Mechanistic and kinetic studies. *Inorganic chemistry* **2005,** *44* (21), 7652-7660.
129. Wipf, D. O.; Kristensen, E. W.; Deakin, M. R.; Wightman, R. M., Fast-scan cyclic voltammetry as a method to measure rapid heterogeneous electron-transfer kinetics. *Analytical Chemistry* **1988,** *60* (4), 306-310.
130. Hsueh, C.; Bravo, R.; Jaramillo, A. J.; Brajter-Toth, A., Surface and kinetic enhancement of selectivity and sensitivity in analysis with fast scan voltammetry at scan rates above 1000 V/s. *Analytica chimica acta* **1997,** *349* (1), 67-76.
131. Andrieux, C.; Garreau, D.; Hapiot, P.; Pinson, J.; Savéant, J., Fast sweep cyclic voltammetry at ultra-microelectrodes: Evaluation of the method for fast electron-transfer kinetic measurements. *Journal of electroanalytical chemistry and interfacial electrochemistry* **1988,** *243* (2), 321-335.
132. Beriet, C.; Pletcher, D., A microelectrode study of the mechanism and kinetics of the ferro/ferricyanide couple in aqueous media: The influence of the electrolyte and its concentration. *Journal of Electroanalytical Chemistry* **1993,** *361* (1), 93-101.
133. Garreau, D.; Hapiot, P.; Savéant, J.-M., Instrumentation for fast voltammetry at ultramicroelectrodes: Stability and bandpass limitations. *Journal of electroanalytical chemistry and interfacial electrochemistry* **1989,** *272* (1), 1-16.
134. Mirkin, M. V.; Bard, A. J., Simple analysis of quasi-reversible steady-state voltammograms. *Analytical Chemistry* **1992,** *64* (19), 2293-2302.
135. Grahame, D. C., Fiftieth Anniversary: Mathematical Theory of the Faradaic Admittance Pseudocapacity and Polarization Resistance. *Journal of the Electrochemical Society* **1952,** *99* (12), 370C-385C.

136. Brown, E. R.; Smith, E.; DeFord, D., Instrumentation for Digital Data Acquisition in Voltammetric Techniques. DC And AC Polarography. *Analytical Chemistry* **1966,** *38* (9), 1130-1136.
137. Hayes, J. W.; Ruić, I.; Smith, D. E.; Booman, G. L.; Delmastro, J. R., Fundamental harmonic ac polarography with irreversible dimerization following the charge transfer step: Theory and experimental results with the benzaldehyd system. *Journal of Electroanalytical Chemistry and Interfacial Electrochemistry* **1974,** *51* (2), 269-285.
138. McCord, T.; Brown, E.; Smith, D., Influence of Spherical Diffusion in Second Harmonic AC Polarography and Related Techniques. *Analytical Chemistry* **1966,** *38* (11), 1615-1620.
139. Bond, A.; Waugh, A., AC polarography and its application to overcome the problem of DC polarographic maxima in the study of complex ions. *Electrochimica Acta* **1970,** *15* (9), 1471-1482.
140. Smith, D.; Reinmuth, W., Second Harmonic Alternating Current Polarography with a Reversible Electrode Process. *Analytical Chemistry* **1961,** *33* (4), 482-485.
141. McCord, T. G.; Smith, D. E., Second harmonic alternating current polarography. Some experimental observations with zinc ion-zinc amalgam system in chloride media. *Analytical Chemistry* **1970,** *42* (1), 126-127.
142. Mooring, C.; Kies, H., AC Voltammetry at large amplitudes: A simplified theoretical approach. *Journal of Electroanalytical Chemistry and Interfacial Electrochemistry* **1977,** *78* (2), 219-227.
143. Saur, D.; Neeb, R., Grundlagen der nichtlinearen wechselstrompolarographischen Analysenverfahren. *Fresenius' Zeitschrift für analytische Chemie* **1978,** *290* (5), 374-381.
144. Bond, A. M.; O'Halloran, R. J.; Ruzic, I.; Smith, D. E., AC Cyclic voltammetry: A digital simulation study of the slow scan limit condition for a reversible electrode process. *Journal of Electroanalytical Chemistry and Interfacial Electrochemistry* **1978,** *90* (3), 381-388.
145. Gavaghan, D.; Bond, A., A complete numerical simulation of the techniques of alternating current linear sweep and cyclic voltammetry: analysis of a reversible process by conventional and fast Fourier transform methods. *Journal of Electroanalytical Chemistry* **2000,** *480* (1), 133-149.
146. Engblom, S. O.; Myland, J. C.; Oldham, K. B., Must ac voltammetry employ small signals? *Journal of Electroanalytical Chemistry* **2000,** *480* (1), 120-132.
147. Engblom, S. O.; Myland, J. C.; Oldham, K. B.; Taylor, A. L., Large Amplitude AC Voltammetry– A Comparison Between Theory and Experiment. *Electroanalysis* **2001,** *13* (8-9), 626-630.
148. O'Mullane, A. P.; Zhang, J.; Brajter-Toth, A.; Bond, A. M., Higher harmonic large-amplitude fourier transformed alternating current voltammetry: analytical attributes derived from studies of the oxidation of ferrocenemethanol and uric acid at a glassy carbon electrode. *Analytical chemistry* **2008,** *80* (12), 4614-4626.
149. Zhang, J.; Guo, S.-X.; Bond, A. M.; Marken, F., Large-amplitude Fourier transformed high-harmonic alternating current cyclic voltammetry: kinetic discrimination of interfering faradaic processes at glassy carbon and at boron-doped diamond electrodes. *Analytical chemistry* **2004,** *76* (13), 3619-3629.

150. Zhang, J.; Guo, S.-X.; Bond, A. M., Discrimination and evaluation of the effects of uncompensated resistance and slow electrode kinetics from the higher harmonic components of a Fourier transformed large-amplitude alternating current voltammogram. *Analytical chemistry* **2007,** *79* (6), 2276-2288.
151. Fleming, B. D.; Zhang, J.; Bond, A. M.; Bell, S. G.; Wong, L.-L., Separation of electron-transfer and coupled chemical reaction components of biocatalytic processes using Fourier transform ac voltammetry. *Analytical chemistry* **2005,** *77* (11), 3502-3510.
152. Zhang, J.; Guo, S.-X.; Bond, A. M.; Honeychurch, M. J.; Oldham, K. B., Novel kinetic and background current selectivity in the even harmonic components of Fourier transformed square-wave voltammograms of surface-confined azurin. *The Journal of Physical Chemistry B* **2005,** *109* (18), 8935-8947.
153. Bano, K.; Nafady, A.; Zhang, J.; Bond, A. M., Electrode Kinetics Associated with Tetracyanoquinodimethane (TCNQ), $TCNQ^{\bullet-}$, and $TCNQ^{2-}$ Redox Chemistry in Acetonitrile As Determined by Analysis of Higher Harmonic Components Derived from Fourier Transformed Large Amplitude ac Voltammetry. *The Journal of Physical Chemistry C* **2011,** *115* (49), 24153-24163.
154. Bano, K.; Zhang, J.; Bond, A. M., Investigations of fast electrode kinetics for reduction of 2, 3, 5, 6-tetrafluoro-7, 7, 8, 8-tetracyanoquinodimethane in conventional solvents and ionic liquids using Fourier transformed large amplitude alternating current voltammetry. *The Journal of Physical Chemistry C* **2014,** *118* (18), 9560-9569.
155. Bond, A. M.; Elton, D.; Guo, S.-X.; Kennedy, G. F.; Mashkina, E.; Simonov, A. N.; Zhang, J., An integrated instrumental and theoretical approach to quantitative electrode kinetic studies based on large amplitude Fourier transformed ac voltammetry: A mini review. *Electrochemistry Communications* **2015,** *57*, 78-83.
156. Bond, A. M.; Duffy, N. W.; Elton, D. M.; Fleming, B. D., Characterization of nonlinear background components in voltammetry by use of large amplitude periodic perturbations and Fourier transform analysis. *Analytical chemistry* **2009,** *81* (21), 8801-8808.
157. Bond, A. M.; Bano, K.; Adeel, S.; Martin, L. L.; Zhang, J., Fourier‐Transformed Large‐Amplitude AC Voltammetric Study of Tetrathiafulvalene (TTF): Electrode Kinetics of the $TTF^{0}/TTF^{\bullet+}$ and $TTF^{\bullet+}/TTF^{2+}$ Processes. *ChemElectroChem* **2014,** *1* (1), 99-107.
158. Bano, K.; Kennedy, G. F.; Zhang, J.; Bond, A. M., Large amplitude Fourier transformed ac voltammetry at a rotating disc electrode: a versatile technique for covering Levich and flow rate insensitive regimes in a single experiment. *Physical Chemistry Chemical Physics* **2012,** *14* (14), 4742-4752.
159. Bano, K.; Zhang, J.; Bond, A. M.; Unwin, P. R.; Macpherson, J. V., Diminished Electron Transfer Kinetics for $[Ru(NH_3)_6]^{3+/2+}$, $[\alpha\text{-}SiW_{12}O_{40}]^{4-/5-}$, and $[\alpha\text{-}SiW_{12}O_{40}]^{5-/6-}$ Processes at Boron-Doped Diamond Electrodes. *The Journal of Physical Chemistry C* **2015,** *119* (22), 12464-12472.
160. Bentley, C. L.; Li, J.; Bond, A. M.; Zhang, J., Mass-Transport and Heterogeneous Electron-Transfer Kinetics Associated with the Ferrocene/Ferrocenium Process in Ionic Liquids. *The Journal of Physical Chemistry C* **2016,** *120* (30), 16516-16525.

161. Bano, K.; Bond, A. M.; Zhang, J., Determination of Fast Electrode Kinetics Facilitated by Use of an Internal Reference. *Analytical chemistry* **2015,** *87* (16), 8387-8393.
162. Si-Xuan, G.; Alan M, B.; Jie, Z., Fourier Transformed Large Amplitude Alternating Current Voltammetry: Principles and Applications. *Review of Polarography* **2015,** *61* (1), 21-32.
163. ONG-DISTANCE, I., Free energy and temperature dependence of electron transfer at the metal-electrolyte interface. **1991**.
164. Simonov, A. N.; Grosse, W.; Mashkina, E. A.; Bethwaite, B.; Tan, J.; Abramson, D.; Wallace, G. G.; Moulton, S. E.; Bond, A. M., New insights into the analysis of the electrode kinetics of flavin adenine dinucleotide redox center of glucose oxidase immobilized on carbon electrodes. *Langmuir* **2014,** *30* (11), 3264-3273.
165. Guo, S.; Zhang, J.; Elton, D. M.; Bond, A. M., Fourier transform large-amplitude alternating current cyclic voltammetry of surface-bound azurin. *Analytical chemistry* **2004,** *76* (1), 166-177.
166. Lee, C.-Y.; Fleming, B. D.; Zhang, J.; Guo, S.-X.; Elton, D. M.; Bond, A. M., Systematic evaluation of electrode kinetics and impact of surface heterogeneity for surface-confined proteins using analysis of harmonic components available in sinusoidal large-amplitude Fourier transformed ac voltammetry. *Analytica chimica acta* **2009,** *652* (1), 205-214.
167. Zhang, J.; Bond, A. M., Theoretical studies of large amplitude alternating current voltammetry for a reversible surface-confined electron transfer process coupled to a pseudo first-order electrocatalytic process. *Journal of Electroanalytical Chemistry* **2007,** *600* (1), 23-34.
168. Shiddiky, M. J.; O'Mullane, A. P.; Zhang, J.; Burke, L. D.; Bond, A. M., Large amplitude Fourier transformed AC voltammetric investigation of the active state electrochemistry of a copper/aqueous base interface and implications for electrocatalysis. *Langmuir* **2011,** *27* (16), 10302-10311.
169. Lertanantawong, B.; O'Mullane, A. P.; Zhang, J.; Surareungchai, W.; Somasundrum, M.; Bond, A. M., Investigation of mediated oxidation of ascorbic acid by ferrocenemethanol using large-amplitude fourier transformed ac voltammetry under quasi-reversible electron-transfer conditions at an indium tin oxide electrode. *Analytical chemistry* **2008,** *80* (17), 6515-6525.
170. Lee, C.-Y.; Guo, S.-X.; Murphy, A. F.; McCormac, T.; Zhang, J.; Bond, A. M.; Zhu, G.; Hill, C. L.; Geletii, Y. V., Detailed electrochemical studies of the tetraruthenium polyoxometalate water oxidation catalyst in acidic media: identification of an extended oxidation series using fourier transformed alternating current voltammetry. *Inorganic chemistry* **2012,** *51* (21), 11521-11532.
171. Liu, Y.; Guo, S.-X.; Bond, A. M.; Zhang, J.; Geletii, Y. V.; Hill, C. L., Voltammetric Determination of the Reversible Potentials for $[\{Ru_4O_4(OH)_2(H_2O)_4\}(\gamma\text{-}SiW_{10}O_{36})_2]^{10-}$ over the pH Range of 2–12: Electrolyte Dependence and Implications for Water Oxidation Catalysis. *Inorganic chemistry* **2013,** *52* (20), 11986-11996.
172. Guo, S.-X.; Liu, Y.; Bond, A. M.; Zhang, J.; Karthik, P. E.; Maheshwaran, I.; Kumar, S. S.; Phani, K., Facile electrochemical co-deposition of a graphene–cobalt nanocomposite for highly efficient water oxidation in alkaline media: direct detection of underlying electron transfer reactions under catalytic turnover conditions. *Physical Chemistry Chemical Physics* **2014,** *16* (35), 19035-19045.

Chapter 2

Dual-Frequency Alternating Current Designer Waveform for Reliable Voltammetric Determination of Electrode Kinetics Approaching the Reversible Limit

analytical chemistry

Article

pubs.acs.org/ac

Dual-Frequency Alternating Current Designer Waveform for Reliable Voltammetric Determination of Electrode Kinetics Approaching the Reversible Limit

Jiezhen Li, Cameron L. Bentley, Alan M. Bond,* and Jie Zhang*

School of Chemistry and Australian Research Council Centre of Excellence for Electromaterials Science, Monash University, Clayton, Victoria 3800, Australia

Supporting Information

ABSTRACT: Alternating current (ac) voltammetry provides access to faster electrode kinetics than direct current (dc) methods. However, difficulties in ac and other methods arise when the heterogeneous electron-transfer rate constant (k^0) approaches the reversible limit, because the voltammetric characteristics become insensitive to electrode kinetics. Thus, in this near-reversible regime, even small uncertainties associated with bulk concentration (C), diffusion coefficient (D), electrode area (A), and uncompensated resistance (R_u) can lead to significant systematic error in the determination of k^0. In this study, we have introduced a kinetically sensitive dual-frequency designer waveform into the Fourier-transformed large-amplitude alternating current (FTAC) voltammetric method that is made up of two sine waves having the same amplitude but with different frequencies (e.g., 37 and 615 Hz) superimposed onto a dc ramp to quantify the close-to-reversible $Fc^{0/+}$ process (Fc = ferrocene) in two nonhaloaluminate ionic liquids. The concept is that from a single experiment the lower-frequency data set, collected on a time scale where the target process is reversible, can be used as an internal reference to calibrate A, D, C, and R_u. These calibrated values are then used to calculate k^0 from analysis of the harmonics of the higher-frequency data set, where the target process is quasi-reversible. With this approach, k^0 values of 0.28 and 0.11 cm·s^{-1} have been obtained at a 50 μm diameter platinum microdisk electrode for the close-to-diffusion-controlled $Fc^{0/+}$ process in two ionic liquids, 1-ethyl-3-methylimidazolium bis(trifluoromethanesulfonyl)imide and 1-butyl-3-methylimidazolium bis(trifluoromethanesulfonyl)imide, respectively.

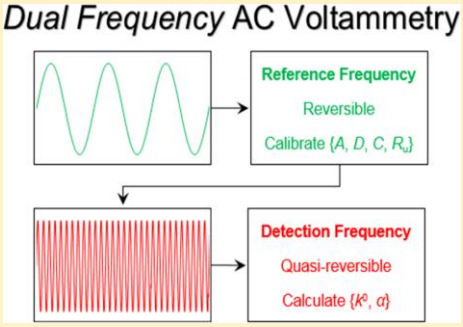

Implementation of strategies to quantify the electrode kinetics of increasingly fast reactions at electrode/electrolyte interfaces has generated considerable long-standing interest, with the ultimate goal being to gain a greater understanding of electron transfer.[1−7] Direct current (dc) cyclic voltammetry is undoubtedly the most widely used method to study electrode kinetics. In a commonly employed transient cyclic voltammetric experiment, the separation in reduction and oxidation peak potentials is measured as a function of scan rate, and kinetic information is extracted by the Nicholson method.[8] In more sophisticated approaches, kinetic information is obtained by comparing the experimental data over a wide range of potentials directly with theory generated by numerical simulation.[9]

Unfortunately, ohmic distortion due to uncompensated resistance (iR_u effect) and nonfaradaic current arising from double layer charging complicate relatively straightforward dc cyclic voltammetric methods of analysis, particularly at the high scan rates required to probe the kinetics of rapid electron-transfer processes.[10] For this reason, accurate kinetic information by dc methods is nowadays often obtained from micro- or even nanoelectrodes, which, relative to macroelectrodes, feature rapid double layer charging, enhanced faradaic-to-nonfaradaic (i.e., signal-to-background) ratios, and minimized iR_u drop.[11,12] It follows that electrochemical methods such as fast-scan voltammetry,[13−15] steady-state voltammetry,[11,16−19] scanning electrochemical microscopy,[20−22] and hydrodynamic voltammetry,[23,24] which utilize micro- or more advantageously nanoelectrodes as the working electrode, are now advocated for the purpose of quantifying kinetic parameters. In addition to the difficulty in fabricating electrodes with well-defined geometry (especially in the case of nanoelectrodes), the main disadvantage associated with these methods under transient conditions is that multiple measurements over a wide range of scan rates are required, which can make maintaining a reproducible electrode surface for the duration of the experiment problematic, introducing extra uncertainty into the determined kinetic parameters. Under steady-state conditions, a series of micro- or nanoelectrodes

Received: November 16, 2015
Accepted: January 15, 2016

DOI: 10.1021/acs.analchem.5b04354
Anal. Chem. XXXX, XXX, XXX−XXX

covering a wide range of radii are needed, and this also can be problematic.

Alternative waveforms to the dc one can also facilitate quantification of fast electron-transfer kinetics. For example, Fourier-transformed large-amplitude alternating current voltammetry (FTACV), in which a sinusoidal or another periodic waveform with frequency, f, and amplitude, ΔE, is superimposed onto the dc ramp, shows significant advantages,[25−28] including (a) minimal charging current contribution in the higher-order harmonic components, (b) the ability to distinguish between the effects of electrode kinetics and uncompensated resistance, and (c) the need for only a single experiment, so the electrode surface is invariant with respect to its impact on data analysis. Thus, heterogeneous electron transfer rate constants (k^0) of up to at least 1.0 cm s^{-1} can be measured at moderate frequencies using the FTACV technique in organic solvents with macrodisk electrodes.[25−28]

As is the case with all voltammetric methods described above, the voltammetric characteristics of a reversible process obey the Nernst equation and hence are insensitive to the Butler−Volmer[10] kinetic parameters, k^0 and α (the charge-transfer coefficient). Furthermore, this also implies that the current magnitude and other characteristics of an FTAC voltammogram become less sensitive to the k^0 and α kinetic parameters associated with a quasi-reversible process as the reversible limit is approached. As a result, it follows that in the near-reversible regime, even small uncertainties associated with the parameters of bulk concentration (C), diffusion coefficient (D), active electrode area (A), and uncompensated resistance (R_u) that also impact on the current magnitude will introduce significant systematic error into the measured k^0 and/or α values.

In order to improve the reliability of electrode kinetic determinations near the reversible limit, we have introduced a reversible process as an internal or external reference to calibrate C, D, A, and R_u.[29] This method was applied to the quasi-reversible $Cc^{+/0}$ (Cc^+ = cobaltocenium) and $TTF^{\bullet+/2+}$ (TTF = tetrathiafulvalene) processes by use of the reversible $Fc^{0/+}$ (Fc = ferrocene) and $TTF^{0/\bullet+}$ processes as external and internal references, respectively. It is now proposed and shown that for a very fast process, application of a dual-frequency method in FTAC voltammetry allows C, D, A, and R_u to be calibrated. The assumption is that at the low "reference" frequency (f_1) the target process can be treated as reversible, thus allowing C, D, A, and R_u to be calibrated and subsequently used to measure k^0 and α by analysis of the high "detection" frequency (f_2) data, where the target process can be treated as quasi-reversible. This procedure is advantageous over the external reference method described previously,[29] because it avoids the need to introduce a new electroactive species into the test solution, which can be problematic in some circumstances.[30]

This dual-frequency method can be implemented by superimposing two sine waves of the same or different amplitude, but with different frequencies, f_1 and f_2, onto the potential-time waveform used in dc cyclic voltammetry and resolving the high- and low-frequency data sets by Fourier transform (FT) methods. In this study, a dual-frequency FTACV designer waveform has been developed by simultaneous application of a low (f_1 = 9 or 37 Hz) and high (f_2 = 182 or 615 Hz) frequency and has been used to quantify the kinetic parameters for the close-to-diffusion-controlled $Fc^{0/+}$ (Fc = ferrocene) process in two ionic liquids, 1-ethyl-3-methylimidazolium bis(trifluoromethanesulfonyl)imide and 1-butyl-3-methylimidazolium bis(trifluoromethanesulfonyl)imide. k^0 values for the $Fc^{0/+}$ process have been of considerable interest in the past few years,[31−33] and as is the case in molecular solvents, it is inevitably near the reversible limit in ionic liquid media. A simulated power spectrum obtained by applying the dual-frequency method under conditions relevant to ionic liquids is shown in Figure 1. Significantly, the dual-frequency method

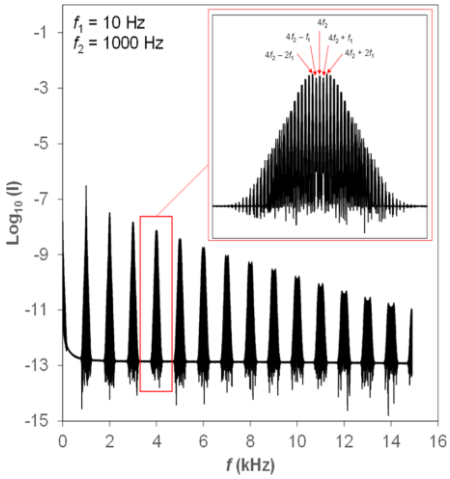

Figure 1. Simulated power spectrum obtained for a simple reversible electron transfer process under conditions relevant to ionic liquids (see below) at frequencies of f_1 = 10 Hz and f_2 = 1000 Hz by the dual-frequency method. (Inset) Power spectrum of all components near the fourth harmonic of f_2. Simulation parameters are as follows: ΔE = 160 mV, R_u = 12 kΩ, D = 4.2 × 10^{-7} $cm^2 \cdot s^{-1}$, C_{dl} = 10.0 $\mu F \cdot cm^{-2}$, A = 1.96 × 10^{-5} cm^2, C = 10 mM, v = 0.25 $V \cdot s^{-1}$, T = 296 K, and E^0 = 0 V.

utilizes the harmonic components of the base frequencies (e.g., f_1, $2f_1$, $3f_1$, ... and f_2, $2f_2$, $3f_2$, ...) that cover voltammetric responses over a wide timescale range and not the sum and difference of the base frequency terms (e.g., $f_2 - f_1$, $f_2 + f_1$) as in small amplitude intermodular alternating current methods developed under polarographic conditions several decades ago.[34]

EXPERIMENTAL SECTION

Chemicals. Ferrocene (Fc, Sigma−Aldrich, ≥98%), 1-ethyl-3-methylimidazolium bis(trifluoromethanesulfonyl)imide ($[C_2mim][NTf_2]$, Io-li-tec, >98%), 1-butyl-3-methylimidazolium bis(trifluoromethanesulfonyl)imide ($[C_4mim][NTf_2]$, Sigma−Aldrich, >98%), potassium ferricyanide ($K_3[Fe(CN)_6]$, Sigma−Aldrich), and potassium chloride (KCl, Merck) were used as received from the manufacturer.

Electrochemical Instrumentation and Procedures. Direct current cyclic voltammetric experiments were carried out on a CHI 760E electrochemical workstation (CH Instruments), while FTAC voltammetric experiments were undertaken with home-built instrumentation.[35] All voltammetric experiments were carried out at 23 ± 1 °C using a standard three-electrode arrangement with a platinum microdisk (nominal diameter = 50 μm) as a working electrode, the appropriate reference electrode, and a Pt wire auxiliary electrode. The platinum microdisk was fabricated in-house by heat-sealing a 0.05 mm diameter microwire (annealed, 99.99%,

DOI: 10.1021/acs.analchem.5b04354
Anal. Chem. XXXX, XXX, XXX−XXX

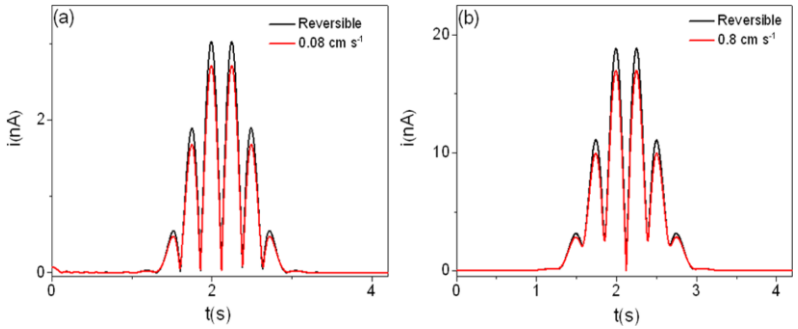

Figure 2. Simulated eighth harmonic FTAC voltammograms, obtained from the $A^{0/+}$ electrode process (eq 1) at frequencies of (a) 10 Hz and (b) 1000 Hz by the single-frequency method. Simulation parameters are ΔE = 160 mV, R_u = 12 kΩ, $D = 4.2 \times 10^{-7}$ cm^2·s^{-1}, C_{dl} = 10.0 μF·cm^{-2}, $A = 1.96 \times 10^{-5}$ cm^2, C = 10 mM, ν = 0.25 V·s^{-1}, T = 296 K, E^0 = 0 V, and α = 0.50.

Goodfellow) in a borosilicate glass capillary under vacuum, as reported elsewhere.[36,37] The quasi-reference electrode in ionic liquid media was a Pt wire, and the reference electrode in aqueous media was Ag/AgCl (3 M NaCl). The quasi-reference electrode potential was calibrated against the recommended $Fc^{0/+}$ process. Prior to voltammetric experimentation, the working electrode was activated by polishing with an aqueous slurry of 1 μm alumina and rinsing thoroughly with deionized water. The electrochemically active area (A) of the Pt microdisk was calibrated with convolution voltammetry,[38−40] using the reduction of a $[Fe(CN)_6]^{3-}$ solution of known concentration (4.0 mM in aqueous medium containing 1.0 M KCl) and adopting a diffusion coefficient of 7.6×10^{-6} cm^2·s^{-1}, as published under these conditions.[25]

Simulations and Data Analysis. FTACV simulations were carried out with the Monash Electrochemistry Simulator (MECSim) software package (http://www.garethkennedy.net/MECSim.html). This Fortran software uses the expanding spatial grid formulation[41] and is based on the mathematical approach derived by Rudolph[42] with minor variations to solve one-dimensional linear diffusion problems. Simulations of the electrode kinetics were based on Butler−Volmer theory[10] and the use of electron-transfer reaction:

$$A \rightleftharpoons A^+ + e^- \qquad (E^0, k^0, \alpha) \tag{1}$$

where E^0 is the reversible potential. FTACV data obtained from either experiment or simulation in the time domain were converted to the frequency domain to generate the power spectrum. Alternating current harmonics derived from low- and high-frequency signals and the corresponding aperiodic dc component were selected from the power spectrum. Band filtering and inverse Fourier transform were then used to obtain the required resolved dc and ac components as a function of either time or potential.[43,44] The sum and difference frequency terms (see Figure 1) were not used.

Scan rate (ν), ac frequencies (f_1 and f_2), ac amplitude (ΔE), and temperature (T) were assumed to be accurately known and R_u, A, E^0, C, D, and C_{dl} (double layer capacitance) were measured experimentally, prior to quantification of k^0, with α assumed to be 0.50 elsewhere. R_u was estimated in a potential region where no faradaic process occurs by electrochemical impedance spectroscopy (amplitude = 5 mV, frequency range = 100 Hz−100 kHz) by fitting the data with a resistor−capacitor (RC) equivalent circuit. Since $Fc^{0/+}$ was the process under investigation, E^0 was defined as 0 V (vs $Fc^{0/+}$) in all simulations. C was calculated from the known mass of the electroactive species and volume of the solution. D was estimated from dc cyclic voltammetric data by convolution, as described elsewhere.[39] C_{dl} was quantified from the background current in the fundamental harmonic at potentials where ac faradaic current is absent. In order to define the potential dependence of C_{dl}, a nonlinear capacitor model was used, as described elsewhere:[45]

$$C_{dl}(t) = c_0 + c_1 E(t) + c_2 E^2(t) + c_3 E^3(t) + c_4 E^4(t) \tag{2}$$

Finally, using the assumption that α is 0.50, k^0 was determined by comparison of experimental and simulated higher-order ac harmonics from resolved low- and high-frequency signals, as described under Results and Discussion.

RESULTS AND DISCUSSION

Theoretical Estimation of Upper Limit for k^0 Determination. A detailed theoretical analysis initially was undertaken to establish and compare the upper (reversible) limit of detection of k^0 by FTACV with the conventional single-frequency and the new dual-frequency methods, with diffusivity and resistance values relevant to ionic liquids. The parameters chosen for this exercise are ΔE = 160 mV, α = 0.50, R_u = 12 kΩ, C = 10 mM, $D = 4.2 \times 10^{-7}$ cm^2·s^{-1}, C_{dl} = 10.0 μF·cm^{-2}, and $A = 1.96 \times 10^{-5}$ cm^2.

The eighth harmonic components of FTAC voltammograms, simulated as a function of k^0 value, are shown in Figure 2 for a single-frequency experiment. In the discussion that follows, we arbitrarily define the k^0 value at which the peak current in the eighth harmonic is 90% of that predicted for a reversible process as the upper limit of detection. As shown in Figure 2, k^0 values up to about 0.08 and 0.8 cm·s^{-1} can be determined with single frequencies of 10 Hz (Figure 2a) and 1000 Hz (Figure 2b), respectively. Increased kinetic sensitivity is achieved at the higher frequency due to the shorter time scale of the (ac) sinusoidal perturbation. It follows that other harmonic components will have different limits of detection (see below).

From Figure 2, and if it is assumed that 0.08 cm·s^{-1} < k^0 < 0.8 cm·s^{-1} (see Figure 2b), it follows that eighth harmonic data collected at 10 Hz (f_1), where the $A^{0/+}$ electrode process is reversible, can be used as an internal reference to calculate k^0 from data collected at 1000 Hz (f_2), where the process is quasi-reversible. We refer to this as the single-frequency method, because two individual, single-frequency experiments must be undertaken, at the reference (f_1) and detection (f_2) frequencies, respectively.

DOI: 10.1021/acs.analchem.5b04354
Anal. Chem. XXXX, XXX, XXX−XXX

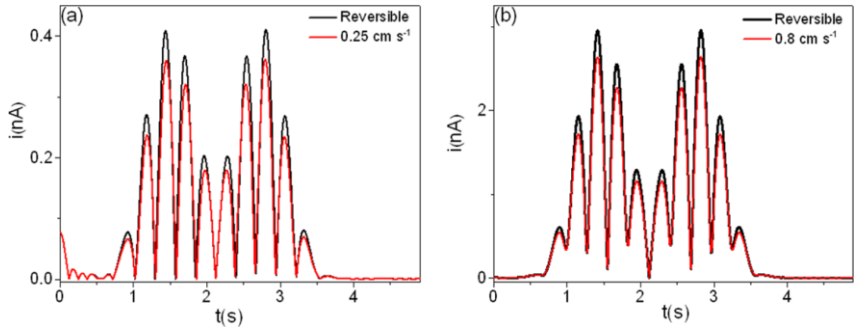

Figure 3. Simulated eighth harmonic FTAC voltammograms, obtained from the $A^{0/+}$ electrode process (eq 1) at frequencies of (a) f_1 = 10 Hz and (b) f_2 = 1000 Hz by the dual-frequency method. Simulation parameters are ΔE = 160 mV, R_u = 12 kΩ, $D = 4.2 \times 10^{-7}$ cm^2·s^{-1}, C_{dl} = 10.0 μF·cm^{-2}, $A = 1.96 \times 10^{-5}$ cm^2, C = 10 mM, ν = 0.25 V·s^{-1}, T = 296 K, E^0 = 0 V, and α = 0.50.

Scheme 1. Protocol for Measurement of k^0 by Dual-Frequency Fourier-Transformed Large-Amplitude Alternating Current Voltammetry

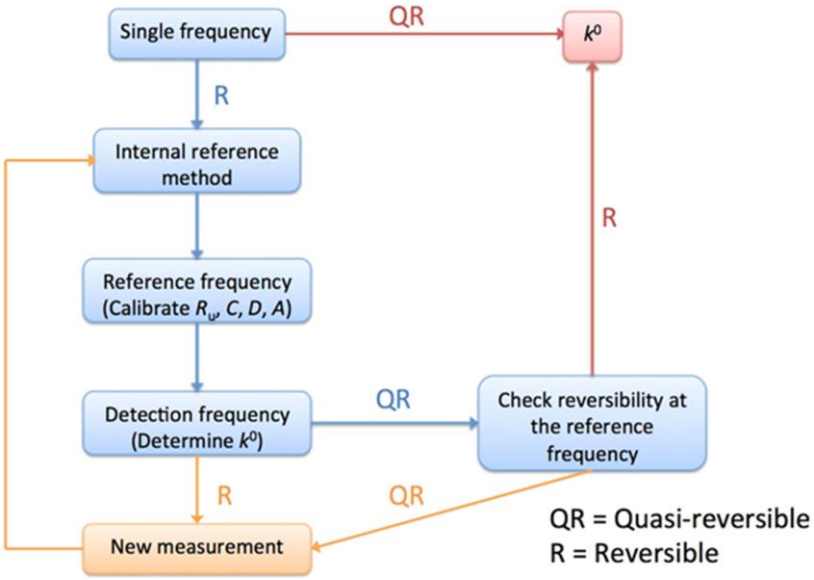

However, performing two separate experiments is not necessary and may introduce uncertainties in the values of R_u, C, and A. Variations between experiments may arise in R_u, due to a change in the distance between the working and reference electrodes; in C, due to solvent evaporation or volatilization of the target species; or in A, due to surface blocking/roughening. Fortunately, a dual frequency (f_1 and f_2) can be applied in a single FTACV experiment to provide the reference (f_1) and detection (f_2) frequency data.

The eighth harmonic components of FTAC voltammograms, simulated as a function of k^0 under the same conditions outlined in Figure 2 except that the two frequencies (f_1 = 10 Hz and f_2 = 1000 Hz) are applied simultaneously, are shown in Figure 3. The voltammetric characteristics of the eighth harmonic under dual-frequency conditions differ from the single-frequency case. Notably, the current magnitude is smaller and peak splitting is evident. Although R_u can cause peak splitting when only a single frequency is applied,[25] this effect is observed under dual-frequency conditions in the absence of R_u and in all harmonics higher than the second (see below). Peak splitting under dual-frequency conditions outlined in Figure 3 is due to coupling between the applied frequencies and the sum and difference frequency terms, as evident in the power spectrum shown in Figure 1. Furthermore, under dual-frequency conditions, the upper limit of k^0 measurement at 10 Hz increases from 0.08 to 0.25 cm·s^{-1}, while the upper limit of k^0 measurement at 1000 Hz remains at 0.8 cm·s^{-1}. This increase in kinetic sensitivity occurs because the thickness of the diffusion layer probed on the low-frequency time scale is perturbed by the presence of the high frequency, but not vice versa. Nonetheless, A, D, C, and R_u values calibrated at the reference frequency (f_1 = 10 Hz) can still be subsequently used in a theory−experiment comparison at the detection frequency (f_2 = 1000 Hz) in order to estimate k^0 for a fast, quasi-reversible process, although the internal reference method becomes narrower under dual-frequency conditions. Of course the sensitivity is harmonic-dependent, as shown in Figure 3 and Figure S1; for example, when the 10th harmonic is considered (see Figure S1), k^0 values in the region of 0.25−1.3 cm s^{-1} can be determined by the dual-frequency method.

DOI: 10.1021/acs.analchem.5b04354
Anal. Chem. XXXX, XXX, XXX−XXX

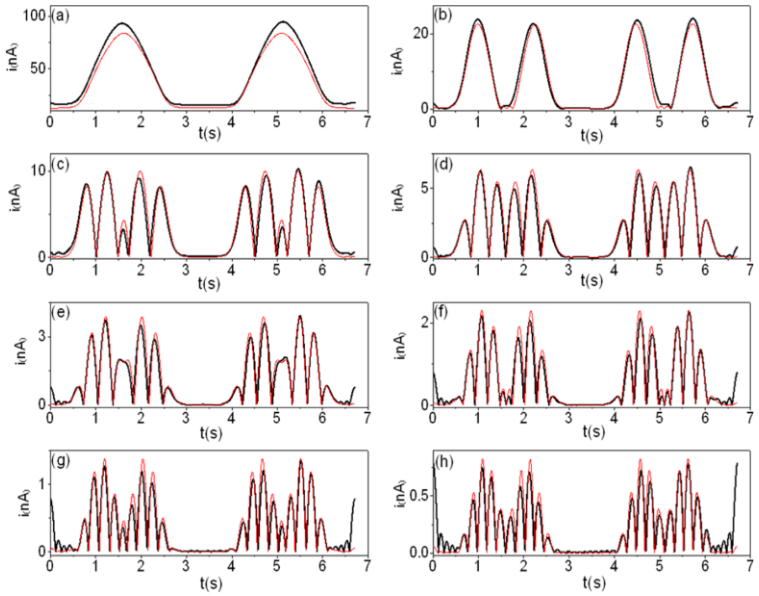

Figure 4. Comparison of (black) experimental FTAC voltammograms, obtained from 10.0 mM Fc in $[C_2mim][NTf_2]$ with a 50 μm diameter Pt microdisk electrode at a (reference) frequency of 37 Hz, and (red) simulated FTAC voltammograms for a reversible one-electron-transfer process. During voltammetric perturbation, two frequencies, f_1 = 37 Hz and f_2 = 615 Hz, were applied simultaneously, superimposed on a dc linear ramp with a scan rate of 0.3278 V·s^{-1}. Panels a–h correspond to the first through eighth harmonics. The simulation parameters are $A = 1.96 \times 10^{-5}$ cm^2, f_1 = 37 Hz and f_2 = 615 Hz, ΔE = 160 mV, calibrated $D = 4.2 \times 10^{-7}$ cm^2·s^{-1}, R_u = 12 kΩ, C_{dl} (c_0 = 18, c_1 = 0.96, c_2 = −0.039, c_3 = 0.44, c_4 = 0.075) μF·cm^{-2} (see eq 2), E^0 = 0 V vs. Fc$^{0/+}$, and T = 296 K.

The upper limit of detection for k^0 is lower under the conditions relevant to ionic liquids than that previously reported for FTACV in conventional molecular solvents, such as acetonitrile.[29] The upper limit of detection for k^0 is governed by the rate of mass transport, which, under the transient conditions of FTACV, is proportional to $D^{1/2}$. Given that D_{Fc} lies in the 10^{-5} and 10^{-7} cm^2·s^{-1} range in acetonitrile and ionic liquids (ILs), respectively, it would be expected that the upper limit of k^0 that can be detected would be ∼10-fold lower in the latter compared to the former. This implies that k^0 for the Fc$^{0/+}$ process in acetonitrile, determined to be ∼10 cm·s^{-1} by Sun and Mirkin[20] using scanning electrochemical microscopy (SECM) with nanosized electrodes, should be measurable with the dual-frequency method at a 50 μm diameter electrode. Significantly, Marcus theory predicts that k^0 is proportional to the viscosity of the medium,[33] and on this basis that k^0 would be ∼100-fold lower in a typical IL compared to acetonitrile. As a result, processes normally assigned as being reversible under FTACV conditions in a molecular solvent (e.g., the Fc$^{0/+}$ process in acetontrile[29]) may possess k^0 values below the upper limit of detection when the dual-frequency method is used in viscous ILs.

Finally, if we take the relevant experimental parameters outlined in Figures 2 and 3 ($D = 4.2 \times 10^{-7}$ cm^2·s^{-1} and T = 296 K) and assume k^0 = 0.5 cm·s^{-1} (i.e., measurable by the dual-frequency method), it is instructive to note that a scan rate of ≥70 V·s^{-1} would be required to achieve departure from reversibility under dc cyclic voltammetric conditions.[46] Thus, as demonstrated in simulations shown in Figure S2, when ν = 70 V·s^{-1}, C = 10 mM, $A = 1.96 \times 10^{-5}$ cm^2, and k^0 = 0.5 cm·s^{-1}, the peak-to-peak separation (ΔE_p) is 60.2 mV when R_u = 0 and and 68.7 mV when R_u = 12 kΩ. This highlights the most common source of error when the Nicholson method is utilized to measure k^0, as the majority of the deviation in ΔE_p from the reversible value of 56.5 mV is due to IR_u drop. Consequently, if the effect of IR_u is not considered, a significantly underestimated k^0 value of ∼0.13 cm·s^{-1} could be reported from the Nicholson method under these conditions.

Protocol for Applying the Dual-Frequency Method in Measurement of k^0. The protocol summarized in Scheme 1 can be adopted when the dual-frequency method is used to measure electrode kinetics near the reversible limit.

Step 1: Measure parameters A, D, C, and R_u experimentally by the methods outlined. Depending on the dimensions, the electrode area A can be calculated under conditions where D is known (e.g., for $[Fe(CN)_6]^{3-}$ or Fc) by cyclic voltammetry, steady-state voltammetry, semiintegration, or convolution.[10,39,47] Concentration C can be determined from known mass of the pure electroactive species and known volume of the solution. Again depending on the electrode dimensions, the diffusion coefficient D can be calculated when A is known via cyclic voltammetry, steady-state voltammetry, semiintegration, or convolution. Uncompensated resistance R_u can be estimated from the R_uC_{dl} time constant obtained from a potential step chronoamperometric or chronocoulometric measurement or from RC equivalent circuit fitting with electrochemical impedance spectroscopy.[10]

Step 2: Use experimentally derived A, D, C, and R_u values to estimate k^0 and α values of target redox process at a single, medium frequency (e.g., 200 Hz). Through theory–experiment comparison, if the redox process is determined to be quasi-reversible on this time scale in a region where FTACV is extremely sensitive to electrode kinetics, only a single "unique" combination of k^0, α, R_u, C^*, D, and A will fit the data; therefore k^0 has been determined and an internal reference is not required. If the redox process is determined to be reversible

DOI: 10.1021/acs.analchem.5b04354
Anal. Chem. XXXX, XXX, XXX−XXX

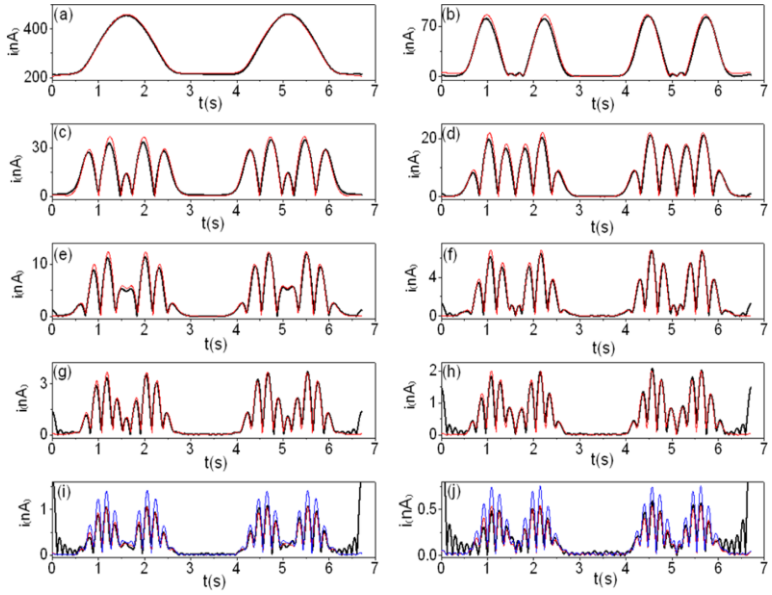

Figure 5. Comparison of (red) simulated and (black) experimental FTAC voltammograms obtained from 10.0 mM Fc in $[C_2mim][NTf_2]$ with a 50 μm diameter Pt microdisk electrode at a (detection) frequency of 615 Hz. During the voltammetric perturbation, two frequencies, f_1 = 37 Hz and f_2 = 615 Hz, were applied simultaneously, superimposed on a dc linear ramp with a scan rate of 0.3278 V·s^{-1}. Panels a–j correspond to the first through 10th harmonics. The simulation parameters are $A = 1.96 \times 10^{-5}$ cm^2, f_1 = 37 Hz and f_2 = 615 Hz, ΔE = 160 mV, calibrated $D = 4.2 \times 10^{-7}$ cm^2·s^{-1}, R_u = 12 kΩ, k^0 = 0.28 cm·s^{-1}, α = 0.50, C_{dl} (c_0 = 18, c_1 = 0.96, c_2 = −0.039, c_3 = 0.44, c_4 = 0.075) μF·cm^{-2} (see eq 2), E^0 = 0 V vs. $Fc^{0/+}$, and T = 296 K. The ninth and 10th harmonic for the reversible case (blue) are also shown for comparison.

within experimental uncertainty on this time scale, then proceed to step 3.

Step 3: Apply the dual-frequency method and confirm the accuracy of experimentally determined A, D, C, and R_u values by theory–experiment comparison at the reference frequency (f_1). Where necessary, use newly calibrated values in subsequent theory–experiment comparisons.

Step 4: Use the original (if confirmed to be accurate) or calibrated A, D, C, and R_u values to determine k^0 and α at the detection frequency (f_2) through a theory–experiment comparison exercise. If the electrode process is determined to be reversible at the detection frequency, repeat steps 3 and 4 with an increased detection frequency. Once the process is deemed to be quasi-reversible on the detection frequency time scale, proceed to step 5.

Step 5: Confirm that a process with k^0 and α values obtained at the detection frequency is reversible at the reference frequency. If not reversible, then start a new measurement series with a lower reference frequency, repeat calibration of original A, D, C, and R_u values in step 3, adjust k^0 and α values in step 4, and repeat step 5 until the theory is consistent with the experimental data.

Application of Dual-Frequency Method. To demonstrate the practical utility of the dual-frequency method, the kinetics of the $Fc^{0/+}$ process were determined in two ionic liquids, $[C_2mim][NTf_2]$ and $[C_4mim][NTf_2]$.

Electrode Kinetics of $Fc^{0/+}$ Process in $[C_2mim][NTf_2]$. Ferrocene oxidation is a frequently studied, reversible or close-to-reversible process. A k^0 value of 0.21 ± 0.06 cm·s^{-1} has been determined in $[C_2mim][NTf_2]$ by use of a high-speed Pt channel electrode:[31]

$$Fc \rightleftharpoons Fc^+ + e^- \qquad (E^0, k^0, \alpha) \tag{3}$$

By the methodology outlined previously, D_{Fc}, R_u, and A were determined to be 4.5×10^{-7} cm^2·s^{-1}, 12 kΩ, and 1.96×10^{-5} cm^2, respectively (step 1). The dual-frequency method was then employed to evaluate k^0 for the $Fc^{0/+}$ process at a platinum microdisk electrode, with a reference frequency (f_1) of 37 Hz, a detection frequency (f_2) of 615 Hz, and an amplitude of 160 mV for both frequencies with a dc scan rate of 0.3278 V·s^{-1}. As shown in Figures 4 and 5, excellent signal-to-noise ratios are obtained for at least the first eight ac harmonic components under these conditions. The aperiodic dc data were not included in the theory–experiment comparison, since these are affected by a contribution from radial diffusion, which is not accounted for in the theory.

Excellent theory–experiment agreement (Figure 4) was obtained for the first through eighth harmonics at the reference frequency of 37 Hz with parameters $D_{Fc} = 4.2 \times 10^{-7}$ cm^2·s^{-1}, C = 10.0 mM, $A = 1.96 \times 10^{-5}$ cm^2, and R_u = 12 kΩ, when the process is assumed to be reversible (step 2). This result provides reassurance that the concentration, electrode area, and R_u are correct, with the only change resulting from calibration (step 3) being made in the value of diffusion coefficient (from 4.5×10^{-7} to 4.2×10^{-7} cm^2·s^{-1}). The known C, A, and R_u values, along with the calibrated D_{Fc} value, were subsequently used to model the $Fc^{0/+}$ process at the detection frequency (step 4), with α and k^0 treated as unknowns. When the process under investigation is close to reversible (k^0 near the upper detection limit), the simulated data were found to be relatively insensitive to α in the range 0.5 ± 0.1, so its value was assumed to be equal to 0.50 in all subsequent simulations. As shown in Figure 5, excellent agreement between theory and experiment is obtained when k^0 is 0.28 cm·s^{-1}. Finally, the validity of using the dual-frequency method to estimate the k^0 value was

DOI: 10.1021/acs.analchem.5b04354
Anal. Chem. XXXX, XXX, XXX−XXX

confirmed, since a process with this k^0 value can be considered reversible at the reference frequency (step 5).

The validity of the measured k^0 value was checked by repeating the experiments described above with an Fc concentration of 3.0 mM, which lowers the effect of uncompensated resistance. Theory–experiment comparisons are shown in Figures S3 and S4 in Supporting Information and, as required, are consistent with a k^0 value of 0.27 cm·s^{-1} for the $Fc^{0/+}$ process in $[C_2mim][NTf_2]$. The value of 0.28 cm·s^{-1} agrees well with the published value[31] of 0.21 ± 0.06 cm·s^{-1} at a Pt channel electrode.

Electrode Kinetics of $Fc^{0/+}$ Process in $[C_4mim][NTf_2]$. By the same procedure described above, except with reference and detection frequencies of 9 and 182 Hz, respectively, the k^0 value for the $Fc^{0/+}$ process was quantified in $[C_4mim][NTf_2]$. Again, the predetermined values of A, D, C, and R_u (A = 1.96 × 10^{-5} cm^2, C = 10.2 mM, D = 3.0 × 10^{-7} cm^2·s^{-1}, and R_u = 26 kΩ) were calibrated via theory–experiment comparison at the reference frequency (9 Hz), as shown in Figure S5. Calibration resulted in R_u being changed to 28 kΩ and D to 2.9 × 10^{-7} cm^2·s^{-1}, while A and C remained the same. From the calibrated parameters and the assumption that α is equal to 0.50 (see above), k^0 was estimated to be 0.11 cm·s^{-1} from theory–experiment comparison at the detection frequency (182 Hz), as shown in Figure S6. The validity of using the dual-frequency method to estimate the k^0 value was again confirmed, since a process with this k^0 value can be considered reversible at the selected reference frequency.

Again, the validity of the measured k^0 value was supported by repeating the experiments described above with an Fc concentration of 2.9 mM, which lowers the effect of uncompensated resistance. The theory–experiment comparisons are shown in Figures S7 and S8 in Supporting Information and are again are consistent with a k^0 value of 0.11 cm s^{-1} for the $Fc^{0/+}$ process in $[C_4mim][NTf_2]$. The larger k^0 value in $[C_2mim][NTf_2]$ than in $[C_4mim][NTf_2]$ is in qualitative agreement with what is predicted by Marcus theory,[33] as the viscosities of these ILs at 296 K are 35 and 55 mPa·s, respectively.[48]

CONCLUSION

An FTACV method has been developed that increases the reliability of determination of k^0 values near the reversible limit. This dual-frequency method involves applying two frequencies simultaneously and obtaining two sets of data, one on a time scale where the target process is reversible (i.e., the reference frequency), which is used as an internal standard to calculate k^0 from the other data set, collected on a time scale where the target process is quasi-reversible (i.e., the detection frequency). This heuristic method reduces the systematic error in k^0 that results from uncertainties in the parameters C, D, A, and R_u without introducing a new electroactive species (internal reference) into the test solution. By this approach, k^0 values of 0.28 and 0.11 cm·s^{-1} were calculated for the $Fc^{0/+}$ process in the ionic liquids 1-ethyl-3-methylimidazolium bis(trifluoromethanesulfonyl)imide and 1-butyl-3-methylimidazolium bis(trifluoromethanesulfonyl)imide, respectively. In principle, an electron-transfer process with a kinetic value as high as ~1 cm·s^{-1} (D ~ 10^{-7} cm^2·s^{-1}) can be determined at a 50 μm diameter electrode by the dual-frequency method under conditions relevant to ionic liquids. In principle, a designer waveform with any combination of sine waves can be generated and employed to achieve the best possible outcome for a specific mechanism. The dual-frequency approach is sufficiently simple to allow heuristic forms of data analysis to be implemented for the particular problem addressed in this paper. Adding more sine waves will in principle be statistically advantageous but will almost certainly increase the complexity to a level where sophisticated computer-aided forms of data analysis will be required.

ASSOCIATED CONTENT

Supporting Information

The Supporting Information is available free of charge on the ACS Publications website at DOI: 10.1021/acs.analchem.5b04354.

Eight figures showing 10th harmonic obtained from simulated dual-frequency data, simulated dc cyclic voltammograms obtained with parameters typically encountered in ILs, and additional theory–experiment comparisons obtained from $Fc^{0/+}$ process in $[C_2mim][NTf_2]$ and $[C_4mim][NTf_2]$ (PDF)

AUTHOR INFORMATION

Corresponding Authors

*E-mail alan.bond@monash.edu (A.M.B).
*E-mail jie.zhang@monash.edu (J.Z.).

Notes

The authors declare no competing financial interest.

REFERENCES

(1) Marcus, R. A. *Annu. Rev. Phys. Chem.* **1964**, *15*, 155–196.
(2) McCreery, R. L. In *Electroanalytical Chemistry*, Vol. *17*; Bard, A. J., Ed.; Marcel Dekker: New York, 1991; pp 221–374.
(3) Chidsey, C. E. D. *Science* **1991**, *251*, 919–922.
(4) Miller, C. J. In *Physical Electrochemistry: Principles, Methods and Applications*, Rubinstein, I., Ed.; Marcel Dekker: New York, 1995; p 595.
(5) Henstridge, M. C.; Laborda, E.; Rees, N. V.; Compton, R. G. *Electrochim. Acta* **2012**, *84*, 12–20.
(6) Bond, A. M.; Elton, D.; Guo, S. X.; Kennedy, G. F.; Mashkina, E.; Simonov, A. N.; Zhang, J. *Electrochem. Commun.* **2015**, *57*, 78–83.
(7) Weaver, M. J. In *Electrode Kinetics: Reactions*; Comprehensive Chemical Kinetics, Vol. *27*; Compton, R. G., Ed.; Elsevier: New York, 1987; Chapt. 1, pp 1–60; DOI: 10.1016/S0069-8040(08)70015-3.
(8) Nicholson, R. S. *Anal. Chem.* **1965**, *37*, 1351–1355.
(9) Rudolph, M.; Reddy, D. P.; Feldberg, S. W. *Anal. Chem.* **1994**, *66*, 589A–600A.
(10) Bard, A. J.; Faulkner, L. R. *Electrochemical Methods: Fundamentals and Applications*, 2nd ed.; Wiley: New York, 2001.
(11) Russell, A.; Repka, K.; Dibble, T.; Ghoroghchian, J.; Smith, J. J.; Fleischmann, M.; Pons, S. *Anal. Chem.* **1986**, *58*, 2961–2964.
(12) Mirkin, M. V.; Bard, A. J. *Anal. Chem.* **1992**, *64*, 2293–2302.
(13) Wipf, D. O.; Kristensen, E. W.; Deakin, M. R.; Wightman, R. M. *Anal. Chem.* **1988**, *60*, 306–310.
(14) Howell, J. O.; Wightman, R. M. *Anal. Chem.* **1984**, *56*, 524–529.
(15) Montenegro, M.; Pletcher, D. *J. Electroanal. Chem. Interfacial Electrochem.* **1986**, *200*, 371–374.
(16) Bond, A. M.; Oldham, K. B.; Zoski, C. G. *Anal. Chim. Acta* **1989**, *216*, 177–230.
(17) Wightman, R. M. *Anal. Chem.* **1981**, *53*, 1125A–1134A.
(18) Bond, A.; Henderson, T.; Mann, D.; Mann, T.; Thormann, W.; Zoski, C. *Anal. Chem.* **1988**, *60*, 1878–1882.
(19) Penner, R. M.; Heben, M. J.; Longin, T. L.; Lewis, N. *Science* **1990**, *250*, 1118–1121.
(20) Sun, P.; Mirkin, M. V. *Anal. Chem.* **2006**, *78*, 6526–6534.
(21) Slevin, C. J.; Gray, N. J.; Macpherson, J. V.; Webb, M. A.; Unwin, P. R. *Electrochem. Commun.* **1999**, *1*, 282–288.

DOI: 10.1021/acs.analchem.5b04354
Anal. Chem. XXXX, XXX, XXX–XXX

(22) Dumitrescu, I.; Dudin, P. V.; Edgeworth, J. P.; Macpherson, J. V.; Unwin, P. R. *J. Phys. Chem. C* **2010**, *114*, 2633−2639.
(23) Rees, N. V.; Alden, J. A.; Dryfe, R. A.; Coles, B. A.; Compton, R. G. *J. Phys. Chem.* **1995**, *99*, 14813−14818.
(24) Rees, N. V.; Klymenko, O. V.; Coles, B. A.; Compton, R. G. *J. Electroanal. Chem.* **2002**, *534*, 151−161.
(25) Zhang, J.; Guo, S.-X.; Bond, A. M. *Anal. Chem.* **2007**, *79*, 2276−2288.
(26) Bano, K.; Nafady, A.; Zhang, J.; Bond, A. M. *J. Phys. Chem. C* **2011**, *115*, 24153−24163.
(27) Bano, K.; Kennedy, G. F.; Zhang, J.; Bond, A. M. *Phys. Chem. Chem. Phys.* **2012**, *14*, 4742−4752.
(28) Bond, A. M.; Bano, K.; Adeel, S.; Martin, L. L.; Zhang, J. *ChemElectroChem* **2014**, *1*, 99−107.
(29) Bano, K.; Bond, A. M.; Zhang, J. *Anal. Chem.* **2015**, *87*, 8387−8393.
(30) Shiddiky, M. J.; Torriero, A. A.; Reyna-González, J. M.; Bond, A. M. *Anal. Chem.* **2010**, *82*, 1680−1691.
(31) Fietkau, N.; Clegg, A. D.; Evans, R. G.; Villagrán, C.; Hardacre, C.; Compton, R. G. *ChemPhysChem* **2006**, *7*, 1041−1045.
(32) Pan, Y. F.; Cleland, W. E.; Hussey, C. L. *J. Electrochem. Soc.* **2012**, *159*, F125−F133.
(33) Fawcett, W. R.; Gaal, A.; Misicak, D. *J. Electroanal. Chem.* **2011**, *660*, 230−233.
(34) Bond, A. M. *Modern Polarographic Methods in Analytical Chemistry*; Marcel Dekker: New York, 1980.
(35) Bond, A. M.; Duffy, N. W.; Guo, S.-X.; Zhang, J.; Elton, D. *Anal. Chem.* **2005**, *77*, 186A−195A.
(36) Wightman, R. M.; Wipf, D. O. In *Electroanalytical Chemistry*, Vol. *15*; Marcel Dekker: New York, 1989; pp 267−354.
(37) Baer, C. D.; Stone, N. J.; Sweigart, D. A. *Anal. Chem.* **1988**, *60*, 188−191.
(38) Mahon, P. J.; Oldham, K. B. *J. Electroanal. Chem.* **1999**, *464*, 1−13.
(39) Bentley, C. L.; Bond, A. M.; Hollenkamp, A. F.; Mahon, P. J.; Zhang, J. *Anal. Chem.* **2014**, *86*, 2073−2081.
(40) Bentley, C. L.; Bond, A. M.; Hollenkamp, A. F.; Mahon, P. J.; Zhang, J. *J. Phys. Chem. C* **2014**, *118*, 29663−29673.
(41) Feldberg, S. W. *J. Electroanal. Chem. Interfacial Electrochem.* **1981**, *127*, 1−10.
(42) Rudolph, M. *J. Electroanal. Chem. Interfacial Electrochem.* **1991**, *314*, 13−22.
(43) Zhang, J.; Guo, S.-X.; Bond, A. M.; Marken, F. *Anal. Chem.* **2004**, *76*, 3619−3629.
(44) Sher, A. A.; Bond, A. M.; Gavaghan, D. J.; Harriman, K.; Feldberg, S. W.; Duffy, N. W.; Guo, S.-X.; Zhang, J. *Anal. Chem.* **2004**, *76*, 6214−6228.
(45) Bond, A. M.; Duffy, N. W.; Elton, D. M.; Fleming, B. D. *Anal. Chem.* **2009**, *81*, 8801−8808.
(46) Mirkin, M. V. *Handbook of Electrochemistry* **2007**, 639−660.
(47) Bentley, C. L.; Bond, A. M.; Hollenkamp, A. F.; Mahon, P. J.; Zhang, J. *Anal. Chem.* **2013**, *85*, 2239−2245.
(48) Tokuda, H.; Hayamizu, K.; Ishii, K.; Susan, M. A. B. H.; Watanabe, M. *J. Phys. Chem. B* **2005**, *109*, 6103−6110.

DOI: 10.1021/acs.analchem.5b04354
Anal. Chem. XXXX, XXX, XXX−XXX

Supporting Information for

A Dual Frequency AC Designer Waveform for the Reliable Voltammetric Determination of Electrode Kinetics Approaching the Reversible Limit

Jiezhen Li, Cameron L. Bentley, Alan M. Bond and Jie Zhang**

School of Chemistry and Australian Research Council Centre of Excellence for Electromaterials Science, Monash University, Clayton, Vic 3800, Australia

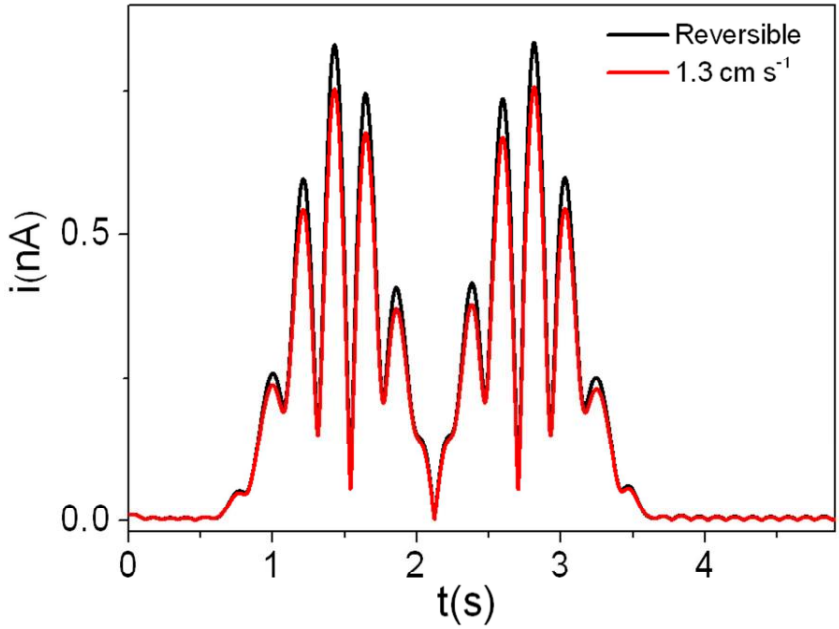

Figure S1. 10th harmonic of simulated FTAC voltammogram obtained using the same set of parameters as given in the caption to Figure 3.

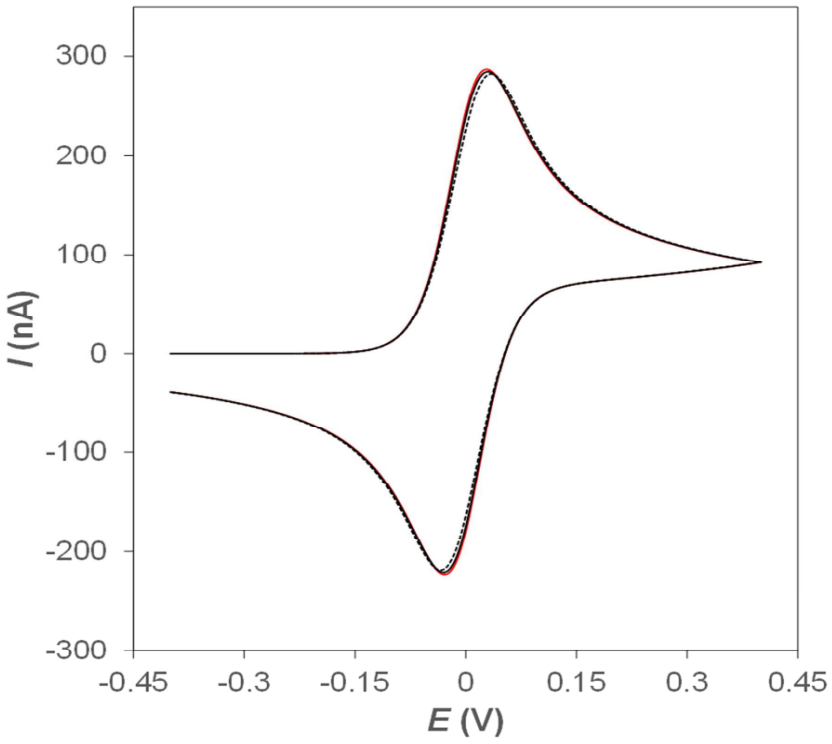

Figure S2. Simulated DC cyclic voltammograms, obtained from the $A^{0/+}$ electrode process (see Eq. 1) with the following parameters: v = 70 V s^{-1}, D = 4.2 × 10^{-7} cm^2 s^{-1}, A = 1.96 × 10^{-5} cm^2, C = 10 mM, T = 296 K, $E^{0'}$ = 0 V and α = 0.50. k^0 and R_u are equal to 10000 cm s^{-1} and 0 Ω (—), (b) 0.5 cm s^{-1} and 0 Ω (—) and (c) 0.5 cm s^{-1} and 12 kΩ (---).

S3

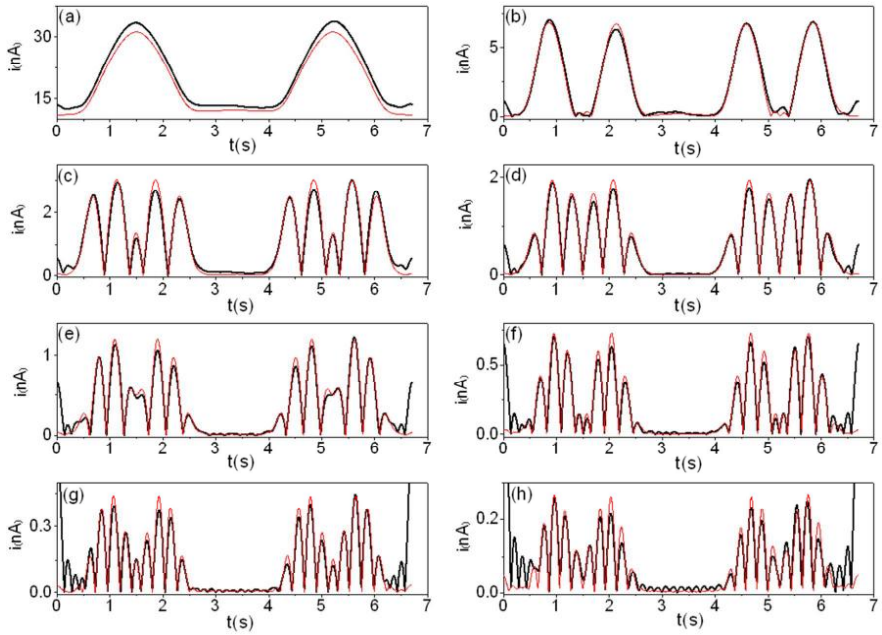

Figure S3. Comparison of the experimental (—) FTAC voltammograms obtained from 3.0 mM Fc in $[C_2mim][NTf_2]$ with a 50 μm dia. Pt microdisk electrode at a (reference) frequency of 37 Hz and the simulated ones for a reversible one-electron transfer process (—). During the voltammetric perturbation, two frequencies, f_1 = 37 Hz and f_2 = 615 Hz, were applied simultaneously, superimposed on a DC linear ramp with a scan rate of 0.3278 V s^{-1}. (a) to (h) correspond to the 1st to 8th harmonics. The simulation parameters are: $A = 1.96 \times 10^{-5}$ cm^2, f_1 = 37 Hz and f_2 = 615 Hz, $\Delta E = 160$ mV, calibrated $D = 4.2 \times 10^{-7}$ cm^2 s^{-1}, R_u = 12 kΩ, C_{dl} (c_0 = 16, c_1 = 0.71, c_2 = -0.43, c_3 = -0.28, c_4 = 0.85) μF cm^{-2} (see Eq. 2) and T = 296 K.

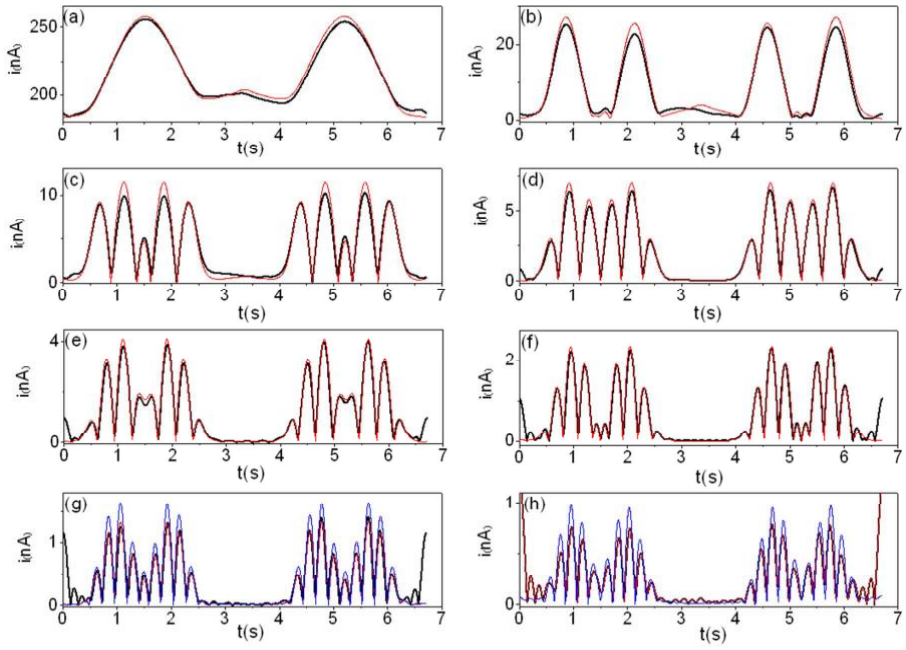

Figure S4. Comparison of the simulated (—) and experimental (—) FTAC voltammograms obtained from 3.0 mM Fc in $[C_2mim][NTf_2]$ with a 50 μm dia. Pt microdisk electrode at a (detection) frequency of 615 Hz. During the voltammetric perturbation, two frequencies, f_1 = 37 Hz and f_2 = 615 Hz, were applied simultaneously, superimposed on a DC linear ramp with a scan rate of 0.3278 V s^{-1}. (a) to (h) correspond to the 1st to 8th harmonics. The simulation parameters are: $A = 1.96 \times 10^{-5}$ cm^2, f_1 = 37 Hz and f_2 = 615 Hz, $\Delta E = 160$ mV, calibrated $D = 4.2 \times 10^{-7}$ cm^2 s^{-1}, R_u = 12 kΩ, k^0 = 0.27 cm s^{-1}, α = 0.50, C_{dl} (c_0 = 16, c_1 = 0.71, c_2 = -0.43, c_3 = -0.28, c_4 = 0.85) μF cm^{-2} (see Eq. 2) and T = 296 K. The 7th and 8th harmonic for a reversible case (—) are also shown for comparison.

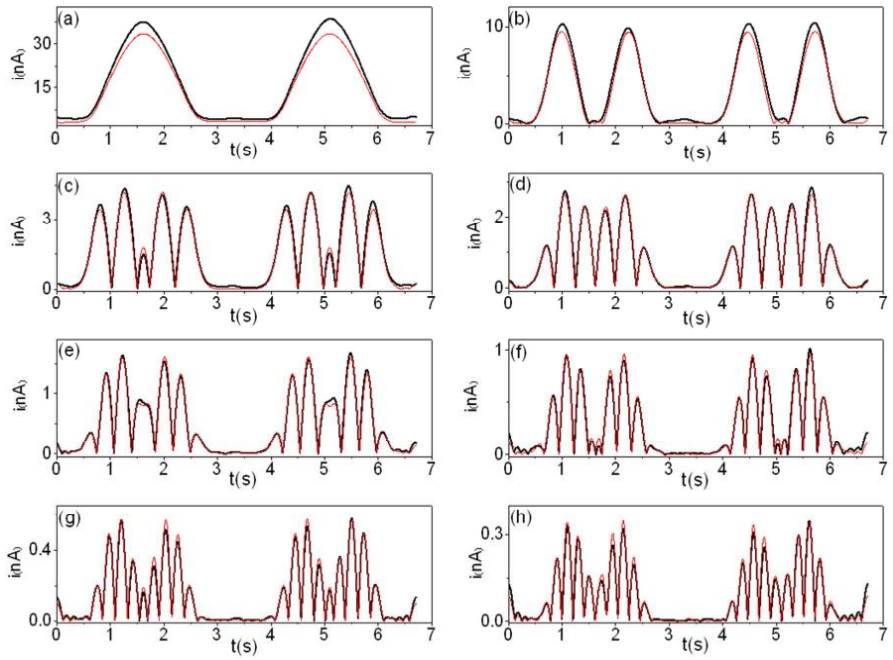

Figure S5. Comparison of the experimental (—) FTAC voltammograms obtained from 10.2 mM Fc in $[C_4mim][NTf_2]$ with a 50 μm dia. Pt microdisk electrode at a (reference) frequency of 9 Hz and the simulated ones for a reversible one-electron transfer process (—). During the voltammetric perturbation, two frequencies, f_1 = 9 Hz and f_2 = 182 Hz, were applied simultaneously, superimposed on a DC linear ramp with a scan rate of 0.3278 V s^{-1}. (a) to (h) correspond to the 1st to 8th harmonics. The simulation parameters are: $A = 1.96 \times 10^{-5}$ cm^2, f_1 = 9 Hz and f_2 = 182 Hz, $\Delta E = 160$ mV, calibrated $D = 2.9 \times 10^{-7}$ cm^2 s^{-1}, calibrated R_u = 28 kΩ, C_{dl} (c_0 = 18, c_1 = 1.3, c_2 = -0.065, c_3 = -1.2, c_4 = 1.2) μF cm^{-2} (see Eq. 2) and T = 296 K.

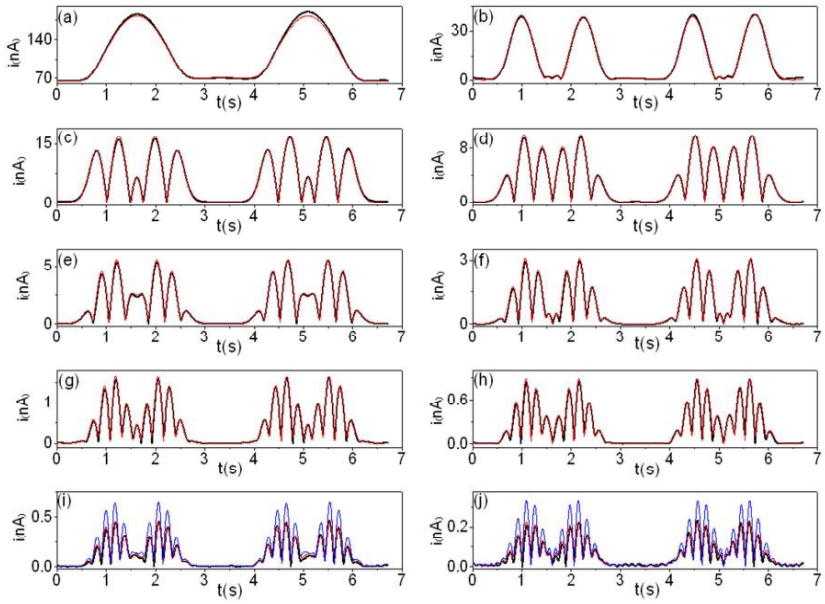

Figure S6. Comparison of the simulated (—) and experimental (—) FTAC voltammograms obtained from 10.2 mM Fc in $[C_4mim][NTf_2]$ with a 50 μm dia. Pt microdisk electrode at a (detection) frequency of 182 Hz. During the voltammetric perturbation, two frequencies, f_1 = 9 Hz and f_2 = 182 Hz, were applied simultaneously, superimposed on a DC linear ramp with a scan rate of 0.3278 V s^{-1}. (a) to (j) correspond to the 1st to 10th harmonics. The simulation parameters are: $A = 1.96 \times 10^{-5}$ cm^2, f_1 = 9 Hz and f_2 = 182 Hz, $\Delta E = 160$ mV, calibrated D = 2.9×10^{-7} cm^2 s^{-1}, calibrated R_u = 28 kΩ, k^0 = 0.11 cm s^{-1}, α = 0.50, C_{dl} (c_0 = 18, c_1 = 1.3, c_2 = -0.065, c_3 = -1.2, c_4 = 1.2) μF cm^{-2} (see Eq. 2) and T = 296 K. The 9th and 10th harmonic for a reversible case (—) are also shown for comparison.

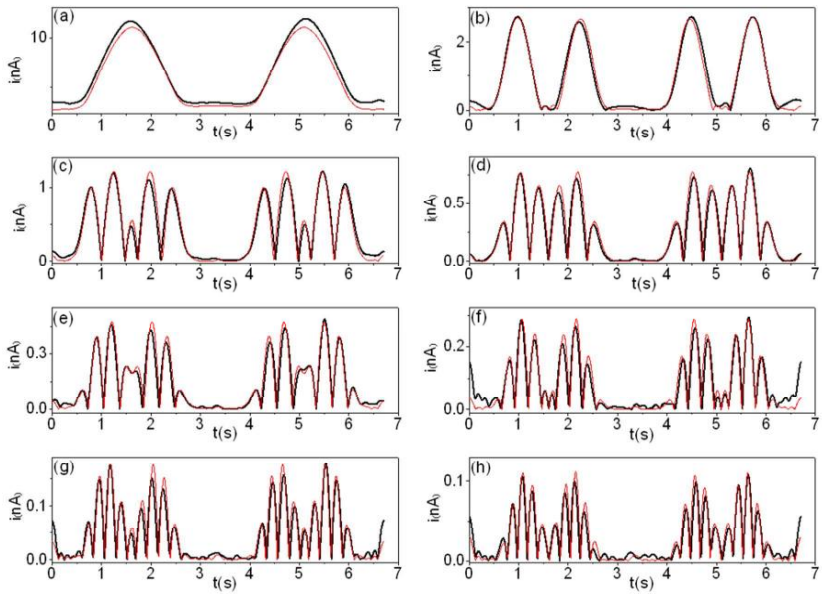

Figure S7. Comparison of the experimental (—) FTAC voltammograms obtained from 2.9 mM Fc in $[C_4mim][NTf_2]$ with a 50 μm dia. Pt microdisk electrode at a (reference) frequency of 9 Hz and the simulated ones for a reversible one-electron transfer process (—). During the voltammetric perturbation, two frequencies, f_1 = 9 Hz and f_2 = 182 Hz, were applied simultaneously, superimposed on a DC linear ramp with a scan rate of 0.3278 V s^{-1}. (a) to (h) correspond to the 1st to 8th harmonics. The simulation parameters are: $A = 1.96 \times 10^{-5}$ cm^2, f_1 = 9 Hz and f_2 = 182 Hz, $\Delta E = 160$ mV, calibrated $D = 2.9 \times 10^{-7}$ cm^2 s^{-1}, R_u = 26 kΩ, C_{dl} (c_0 = 16, c_1 = 0.93, c_2 = 0.084, c_3 = -0.28, c_4 = 0.38) μF cm^{-2} (see Eq. 2) and T = 296 K.

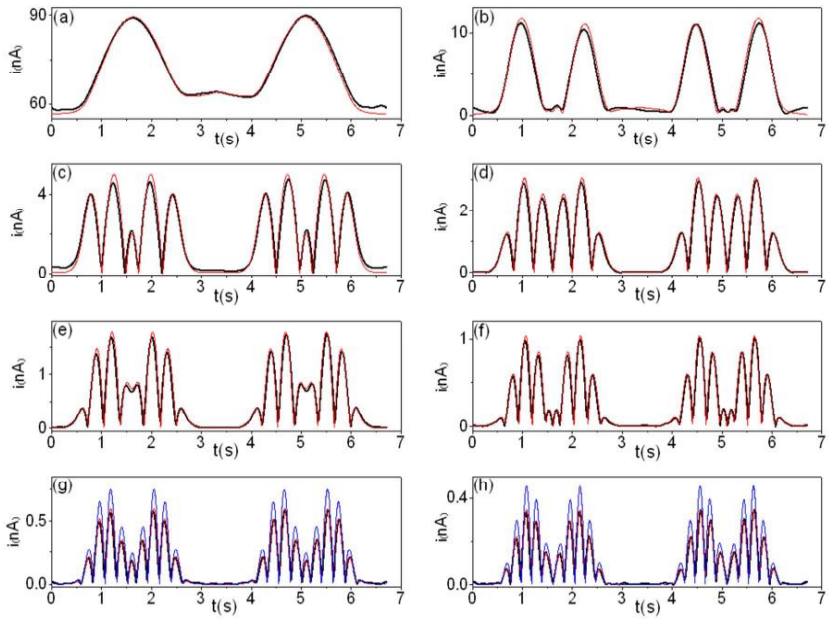

Figure S8. Comparison of the simulated (—) and experimental (—) FTAC voltammograms obtained from 2.9 mM Fc in $[C_4mim][NTf_2]$ with a 50 μm dia. Pt microdisk electrode at a (detection) frequency of 182 Hz. During the voltammetric perturbation, two frequencies, f_1 = 9 Hz and f_2 = 182 Hz, were applied simultaneously, superimposed on a DC linear ramp with a scan rate of 0.3278 V s^{-1}. (a) to (h) correspond to the 1st to 8th harmonics. The simulation parameters are: $A = 1.96 \times 10^{-5}$ cm^2, f_1 = 9 Hz and f_2 = 182 Hz, $\Delta E = 160$ mV, calibrated $D = 2.9 \times 10^{-7}$ cm^2 s^{-1}, R_u = 26 kΩ, k^0 = 0.11 cm s^{-1}, α = 0.50, C_{dl} (c_0 = 16, c_1 = 0.93, c_2 = 0.084, c_3 = -0.28, c_4 = 0.38) μF cm^{-2} (see Eq. 2) and T = 296 K. The 9th and 10th harmonic for a reversible case (—) are also shown for comparison.

Chapter 3

Probing Electrolyte Cation Effects on the Electron Transfer Kinetics of the [*a*-$SiW_{12}O_{40}$]$^{4-/5-}$ and [*a*-$SiW_{12}O_{40}$]$^{5-/6-}$ Processes Using a Boron-Doped Diamond Electrode

Electrochimica Acta 178 (2015) 631–637

Contents lists available at ScienceDirect

Electrochimica Acta

journal homepage: www.elsevier.com/locate/electacta

Probing Electrolyte Cation Effects on the Electron Transfer Kinetics of the $[\alpha\text{-}SiW_{12}O_{40}]^{4-/5-}$ and $[\alpha\text{-}SiW_{12}O_{40}]^{5-/6-}$ Processes using a Boron-Doped Diamond Electrode

Jiezhen Li, Alan M. Bond*, Jie Zhang*

School of Chemistry and Australian Research Council Centre of Excellence for Electromaterials Science, Monash University, Clayton, Victoria 3800, Australia

ARTICLE INFO

Article history:
Received 27 April 2015
Received in revised form 31 July 2015
Accepted 11 August 2015
Available online 14 August 2015

Keywords:
Electron transfer kinetics
Polyoxometalates
Fourier transformed alternation current voltammetry
Boron doped diamond electrode
Cation effect

ABSTRACT

Fourier transformed large amplitude alternating current (FTAC) voltammetry has been used to investigate the electrolyte cation dependence in aqueous media on the electron transfer kinetics (k^0 values) of the $[\alpha\text{-}SiW_{12}O_{40}]^{4-/5-}$ and $[\alpha\text{-}SiW_{12}O_{40}]^{5-/6-}$ one-electron reduction processes of the highly negatively charged Keggin type silicon tungstate $[\alpha\text{-}SiW_{12}O_{40}]^{4-}$ at a boron-doped diamond (BDD) electrode. In the presence of alkali metal nitrate electrolytes, k^0 values for both processes were reliably determined by FTAC voltammetry at a BDD electrode. This proved possible because much smaller rate constants were found relative to those at the more commonly used glassy carbon electrode where the processes are reversible. Similar k^0 values were found for both reduction processes at the BDD electrode and lie in the range of 0.045–0.10 cm s^{-1}, but show a clear electrolyte cation dependence, increasing in the order of $LiNO_3 < NaNO_3 < KNO_3 \approx NH_4NO_3$.

1. Introduction

Transition metal polyoxometalates (POMs) represent a well-known class of negatively charged clusters that vary widely in size, metal-oxygen framework topology and composition [1,2]. They have attracted much interest over many decades in areas ranging from catalysis [3,4], medicine [5], electrochemistry [6], photochromism [7] and magnetism [8]. It is well known that variation of electrolyte can result in substantial changes in the rates of both heterogeneous charge-transfer processes that take place under electrochemical conditions at electrode-solution (electrolyte) interfaces and homogeneous charge transfer processes [9]. In the case of POMs, the cation is known to affect the homogeneous electron transfer process [10]. Additionally, the identity of the cation can substantially influence the structure of POMs [11], as well as the nanoscale architecture and chemical properties [12,13].

In the solution phase, the cation effect is generally attributed to ion pair formation with the POM anion. Whilst the thermodynamic impact of the electrolyte is well-known and many electrochemical studies related to the influence of the cation on the kinetics of electron transfer processes, such as the $[Fe(CN)_6]^{3-/4-}$ reaction, have been reported [14–16], quantitative studies of the influence of the cation on heterogeneous electron transfer for the reduction of POMs have not been reported. This is at least partially due to the fact that these processes are very fast at commonly used metallic and glassy carbon (GC) electrodes [17]. Consequently, it is difficult to determine their kinetics reliably using conventional direct current (dc) cyclic voltammetry. In this study, reduction of $[\alpha\text{-}SiW_{12}O_{40}]^{4-}$ in aqueous electrolyte media is now used to establish the cation effect on the electrode kinetics at a boron doped electrode where recent work [17] has shown that the processes are quasi-reversible and well removed from the reversible limit.

When the electrode kinetics are sufficiently slow, the rate constants can be determined by dc cyclic voltammetry [18–21] and use of the early theoretical results of Nicholson [22]. However, Nicholson showed that uncompensated resistance (R_u) may exhibit a very similar effect to slow electrode kinetics (k^0) on the characteristics of dc cyclic voltammograms [23]. Thus, unless the contribution from R_u is included in the modeling, significant uncertainty may be present. In contrast, Fourier transformed large amplitude alternating current (FTAC) voltammetry [24] is a more sophisticated technique for quantitative investigations of fast electrode kinetics [25]. However, a problem in determining the cation effect in POM redox chemistry, even when using kinetically sensitive FTAC voltammetry, is that the $[\alpha\text{-}SiW_{12}O_{40}]^{4-}$ reduction processes are so fast that k^0 values may lie too close to the reversible limit at GC and metal electrodes to be reliably determined [17]. Ideally, the k^0 value needs to lie in a readily measurable regime.

* Corresponding authors.
E-mail addresses: alan.bond@monash.edu (A.M. Bond), jie.zhang@monash.edu (J. Zhang).

http://dx.doi.org/10.1016/j.electacta.2015.08.049
0013-4686/

In a recent study, it was shown that much slower electrode kinetics are found at a boron doped diamond (BDD) electrode compared to GC and metal electrodes for the $[\alpha\text{-}SiW_{12}O_{40}]^{4-/5-}$ and $[\alpha\text{-}SiW_{12}O_{40}]^{5-/6-}$ processes [17]. BDD electrodes are well suited to quantitative electroanalytical applications due to their low background current, wide potential window and high electrochemical stability [26–29]. For these reasons, BDD has attracted considerable current research interest [30–34]. Diminished electron transfer kinetics would normally be undesirable, but as shown in this paper can be an advantage to enable measurement of cation dependent k^0 values. On the basis that the electrode kinetics of $[\alpha\text{-}SiW_{12}O_{40}]^{4-/5-}$ and $[\alpha\text{-}SiW_{12}O_{40}]^{5-/6-}$ processes would lie well within the detection range of FTAC voltammetry when using BDD as the working electrode [17], this kinetically sensitive technique has now been used for the measurement of k^0 values at this electrode surface for the $[\alpha\text{-}SiW_{12}O_{40}]^{4-/5-}$ and $[\alpha\text{-}SiW_{12}O_{40}]^{5-/6-}$ processes in aqueous 1.0 M $LiNO_3$, $NaNO_3$, KNO_3 or NH_4NO_3 electrolyte, in order to establish the influence of the alkali metal cation on this parameter.

2. Experimental section

2.1. Materials and Reagents

Silicotungstic acid ($H_4[\alpha\text{-}SiW_{12}O_{40}]$) (Sigma-Aldrich, 98%), lithium nitrate ($LiNO_3$, 99%, Sigma-Aldrich), sodium nitrate ($NaNO_3$, 99%, Sigm-Aldrich), potassium nitrate (KNO_3, 99%, Sigma-Aldrich), ammonium nitrate (NH_4NO_3, 99%, Sigma-Aldrich), nitric acid (HNO_3, 99%, Sigma-Aldrich), ferrocene (Fc, ≥98%, Sigma-Aldrich) and acetonitrile (CH_3CN, 99.9%, Sigma-Aldrich) were used as received from the manufacturer. *n*–tetrabutylammonium hexaflurophosphate (Bu_4NPF_6, 98%, Wako) was recrystallised twice from ethanol before use. Deionized water was used for the preparation of all aqueous solutions.

2.2. Instrumentation and procedures

Viscosity of solutions was measured using the falling ball method with an Anton Paar automated microviscometer (AMVn). Dc cyclic voltammetric experiments were carried out using a CHI 760E electrochemical workstation. Large amplitude FTAC voltammetric experiments were undertaken with a home built instrument [35] using an applied sine wave perturbation having an amplitude (ΔE) = 80 mV and a frequency of 9.02 Hz, superimposed onto the dc ramp.

All electrochemical studies were carried out at 23 ± 2 °C. A standard electrochemical cell with a three electrode configuration was used. The working electrodes were GC (CH Instruments, USA) or BDD (Windsor Scientific, UK) macrodisks (all of nominal diameter = 3.0 mm). The electrochemically effective areas (A) of the working electrodes were calculated from analysis of a plot of dc peak current versus square root of scan rate for oxidation of 1.0 mM Fc in CH_3CN (0.10 M Bu_4NPF_6) using the Randles-Sevcik relationship (Eq. (1)) and the known diffusion coefficient of 2.4×10^{-5}

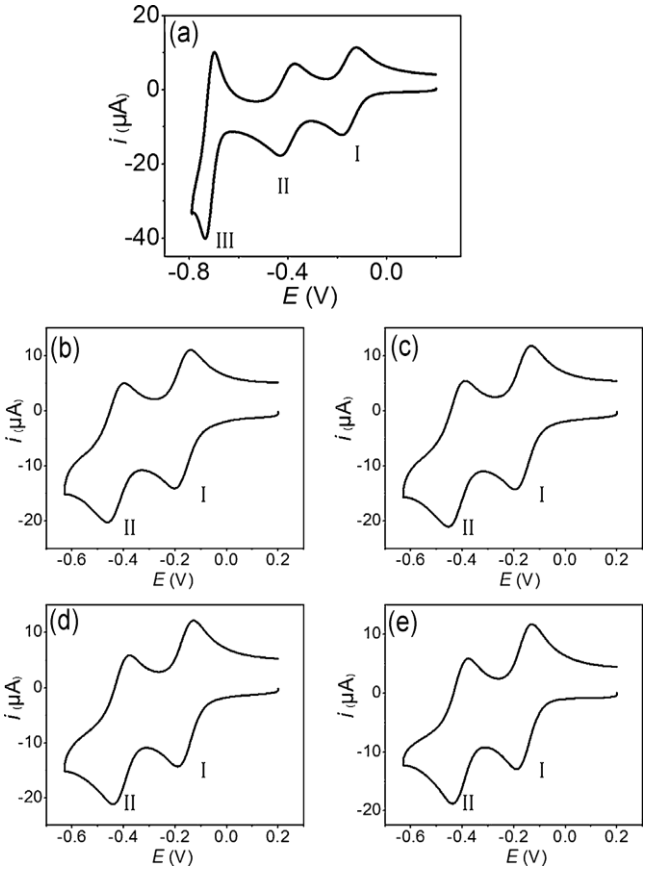

Fig. 1. Dc cyclic voltammegrams for reduction of $[\alpha\text{-}SiW_{12}O_{40}]^{4-}$ in (a) aqueous electrolyte media containing 1.0 M KNO_3 and 0.010 M HNO_3 at a GC electrode with a scan rate of 100 mV s^{-1} over a wide potential range showing three well-defined chemically reversible processes, and in (b-e) aqueous electrolyte media containing 1.0 M $LiNO_3$, 1.0 M $NaNO_3$, 1.0 M KNO_3, 1.0 M NH_4NO_3, respectively, along with 0.010 M HNO_3 over the potential range for the first two processes.

$cm^2\,s^{-1}$ for Fc in this medium [18].

$$i_p = 0.4463\,nFA\left(\frac{nFDv}{RT}\right)^{1/2}C \quad (1)$$

In Eq. (1),i_p is the oxidation peak current, n is the number of electrons transerred ($n = 1$), C is the bulk concentration, D is the diffusion coefficient of Fc, T is the absolute temperature, R is the universal gas constant and F is Faraday's constant. This method gave areas of $6.65 \times 10^{-2}\,cm^2$ and $7.02 \times 10^{-2}\,cm^2$ for the GC and BDD electrodes, respectively. Ag/AgCl (3 M NaCl) and platinum wire were employed as the reference and auxiliary electrodes, respectively, for the measurements in aqueous solutions. For the measurements in CH_3CN, a Ag wire was used as a quasi-reference electrode.

3. Simulations and data analysis

Simulations of FTAC voltammograms were carried out with MECSim (Monash Electrochemistry Simulator) software. This Fortran software package uses the expanding spatial grid formulation [36] and is based on the mathematical approach derived by Rudolph [37] with minor variations. Previous studies [17,38] suggest that the simple Butler-Volmer formalism [18] can be used to describe the electron transfer kinetics at BDD electrodes. Therefore, Butler-Volmer theory was used to model the simple one-electron transfer reaction given in Eq. (2).

$$O + e^- \rightleftharpoons R\ (E^0, k^0, \alpha) \quad (2)$$

where k^0 is the heterogeneous charge transfer rate constant at the reversible potential E^0 and α is the charge transfer coefficient.

FTAC voltammetric data obtained from either experiment or simulation in the time domain were converted to the frequency domain to generate the power spectrum [39,40]. Frequencies corresponding to the ac harmonics and the corresponding dc component were selected from the power spectrum and then subjected to band filtering and inverse Fourier transform to obtain resolved dc and ac components as a function of time. Five parameters, R_u, E^0, k^0, α and C_{dl}, need to be determined in order to obtain the electrode kinetics. R_u was determined experimentally from the R_uC time constant at a potential where no faradaic current was present, E^0 was estimated from the potential of the current minima in the 2nd harmonic and C_{dl} was determined as in Eq. (3) from background current modelled in terms of a non-linear capacitor as suggested by Tokuda and Matsuda [41],

$$i_C = \left(E\frac{dC_{dl}(E)}{dE} + C_{dl}(E)\right)\frac{dE}{dt} \quad (3)$$

In this study, $C_{dl}(E)$ (E vs. Ag/AgCl) is described by a fourth order polynomial

$$C_{dl}(E) = \sum_{i=0}^{4} a_i(E)^i \quad (4)$$

Values of i_C in the potential region where the Faradaic current is not present in the fundamental ac harmonic are calculated using Eq. (4) with coefficients, a_i, being derived from a fit to the background current. Finally k^0 was determined by comparison of experimental and simulated higher order ac harmonics by assuming α is 0.50.

4. Results and discussion

4.1. DC Cyclic voltammetry of $[\alpha\text{-}SiW_{12}O_{40}]^{4-}$

$[\alpha\text{-}SiW_{12}O_{40}]^{4-}$ undergoes three well defined chemically reversible reduction processes (Eqs. (5)–(7)) in 0.010 M HNO_3 and 1.0 M KNO_3 (Fig. 1(a)). High electrolyte concentration was used so that ideally the large $[\alpha\text{-}SiW_{12}O_{40}]^{4-}$ anions underwent electron transfer outside the diffuse double layer. Consequently, the effect of the double layer on k^0 was suppressed.[18] 0.010 M HNO_3 was added so that $[\alpha\text{-}SiW_{12}O_{40}]^{4-}$ was soluble in the aqueous 1.0 M NH_4NO_3 electrolyte medium used to confirm the size effect of the electrolyte cation on the electron transfer kinetics (*vide infra*). The first and the second processes correspond to the $[\alpha\text{-}SiW_{12}O_{40}]^{4-/5-}$ (Eq. (5)) and $[\alpha\text{-}SiW_{12}O_{40}]^{5-/6-}$ (Eq. (6)) one-electron transfer reactions, whereas the third one corresponds to a coupled two-electron four-proton reaction (Eq. (7)). [42] Only the first and second processes are of interest in this study.

$$[\alpha\text{-}SiW_{12}O_{40}]^{4-} + e^- \rightleftharpoons [\alpha\text{-}SiW_{12}O_{40}]^{5-}\ (\text{process I}) \quad (5)$$

$$[\alpha\text{-}SiW_{12}O_{40}]^{5-} + e^- \rightleftharpoons [\alpha\text{-}SiW_{12}O_{40}]^{6-}\ (\text{process II}) \quad (6)$$

$$[\alpha\text{-}SiW_{12}O_{40}]^{6-} + 2e^- + 4H^+ \rightleftharpoons [\alpha\text{-}H_4SiW_{12}O_{40}]^{4-}\ (\text{process III}) \quad (7)$$

Parts b-e of Fig. 1 show cyclic voltammograms obtained at a GC electrode at a scan rate of $0.10\,V\,s^{-1}$ for reduction of 1.0 mM $[\alpha\text{-}SiW_{12}O_{40}]^{4-}$ in 1.0 M $LiNO_3$, $NaNO_3$, KNO_3 and NH_4NO_3, respectively, all containing 0.010 M HNO_3. In the acidic aqueous 1.0 M $LiNO_3$ medium, analysis of dc cyclic voltammetric data for the $[\alpha\text{-}SiW_{12}O_{40}]^{4-/5-}$ and $[\alpha\text{-}SiW_{12}O_{40}]^{5-/6-}$ processes at a GC electrode give formal reversible potentials, E^0 (taken as the average of oxidation and reduction peak potentials), of −0.172 and −0.430 V, respectively. The peak-to-peak separation (ΔE_p) for the oxidation and reduction peak potentials were ca. 60 mV for both processes which is close to the theoretically predicted value of 57 mV for a reversible one-electron transfer process, indicating that they are essentially reversible on the dc voltametric time scale ($v = 0.10\,V\,s^{-1}$). Full details of E^0 and ΔE_p values for both the $[\alpha\text{-}SiW_{12}O_{40}]^{4-/5-}$ and $[\alpha\text{-}SiW_{12}O_{40}]^{5-/6-}$ processes in the different aqueous electrolyte media at GC and BDD electrodes, in addition to the separation in E^0 between the two process (ΔE^0) are provided in Table 1. D values of $[\alpha\text{-}SiW_{12}O_{40}]^{4-}$ calculated from the Randles-Sevcik relationship [43] vary from $3.5 \times 10^{-6}\,cm^2\,s^{-1}$ to $4.1 \times 10^{-6}\,cm^2\,s^{-1}$ (Table 2). It is shown in Table 1 that the E^0 values for both the $[\alpha\text{-}SiW_{12}O_{40}]^{4-/5-}$ and $[\alpha\text{-}SiW_{12}O_{40}]^{5-/6-}$ processes increase in the order of $LiNO_3 < NaNO_3 < KNO_3 \approx NH_4NO_3$. This cation dependence of E^0 is not due to the variation in junction potentials in different medium as confirmed in our previous study [44].

4.2. Determination of electron transfer kinetics using FTAC voltammetry

As in literature data obtained in aqueous media containing 0.10 M H_2SO_4 and 1.0 M Na_2SO_4 [17], the k^0 values ($\geq 0.2\,cm\,s^{-1}$) for both the $[\alpha\text{-}SiW_{12}O_{40}]^{4-/5-}$ and $[\alpha\text{-}SiW_{12}O_{40}]^{5-/6-}$ processes were too fast to be reliably determined in acidified alkali metal and NH_4^+

Table 1
Dc Cyclic Voltammetirc Data Derived from the Reduction of 1.0 mM $[\alpha\text{-}SiW_{12}O_{40}]^{4-}$ in 1.0 M $LiNO_3$, $NaNO_3$, KNO_3 or NH_4NO_3 Media together with 0.010 M HNO_3.

Electrolyte	Process	GC			BDD		
		E^0 (V)	ΔE_p (mV)	ΔE^0 (V)	E^0 (V)	ΔE_p (mV)	ΔE^0 (V)
$LiNO_3$	I	-0.172	63	0.258	-0.172	63	0.259
	II	-0.430	64		-0.431	65	
$NaNO_3$	I	-0.164	64	0.257	-0.166	61	0.257
	II	-0.421	66		-0.423	63	
KNO_3	I	-0.160	61	0.250	-0.159	59	0.251
	II	-0.409	64		-0.410	61	
NH_4NO_3	I	-0.161	61	0.247	-0.161	58	0.247
	II	-0.408	61		-0.408	60	

Table 2
Summary of k^0 and D values obtained from reduction of 1.0 mM $[\alpha\text{-}SiW_{12}O_{40}]^{4-}$ in acidified 1.0 M $LiNO_3$, $NaNO_3$, KNO_3 or NH_4NO_3 Media at a BDD electrode. α was assumbed to be 0.50 in simulation versus experiment comparisons.

Electrolyte	Process	k^0 at GC ($cm\,s^{-1}$)[a]	k^0 at BDD ($cm\,s^{-1}$)[a]	D ($cm^2\,s^{-1}$)[b]
$LiNO_3$	I	≥ 0.2	0.045 ± 0.004	3.5×10^{-6}
	II	≥ 0.2	0.045 ± 0.004	
$NaNO_3$	I	≥ 0.2	0.060 ± 0.005	3.8×10^{-6}
	II	≥ 0.2	0.065 ± 0.007	
KNO_3	I	≥ 0.2	0.090 ± 0.011	4.1×10^{-6}
	II	≥ 0.2	0.100 ± 0.015	
NH_4NO_3	I	≥ 0.2	0.090 ± 0.011	4.1×10^{-6}
	II	≥ 0.2	0.100 ± 0.015	

[a] Determined by FTAC voltammetry.
[b] Determined by dc voltammetry and use of the Randles-Sevcik relationship.

nitrate electrolytes at a GC electrode (Fig. 2) using FTACV with a frequency of 9.02 Hz (the estimated lower limit of $k^0 = 0.2\,cm\,s^{-1}$ produces simulated peak currents that are 90% of that predicted for a reversible process).

The FTAC voltammetry of 1.0 mM $[\alpha\text{-}SiW_{12}O_{40}]^{4-}$ in aqueous media containing 1.0 M KNO_3 and 0.010 M HNO_3 at a BDD electrode ($f = 9.02$ Hz and $\Delta E = 80$ mV) over the potential range from 0.20 V to −0.63 V is shown in Fig. 3. The aperiodic dc and ac harmonics were then subjected to a simulation-experiment comparison in order to extract the k^0 values. Simulations used to mimic experimental data at a BDD electrode at a frequency of 9.02 Hz employed $R_u = 20\,\Omega$, E^0 for the first process = −0.159 V, E^0 for the second process = −0.410 V and a non-liner capacitance modelled as a function of potential using a polynomial of the form of $C_{dl} = c_0 + c_1E + c_2E^2 + c_3E^3 + c_4E^4$ with $c_0 = 5.0$, $c_1 = 0.6$, $c_2 = 9.9$, $c_3 = -69.2$, $c_4 = -95.0$. The k^0 values for the first and second processes were determined to be $0.09\,cm\,s^{-1}$ and $0.10\,cm\,s^{-1}$ respectively and hence gave k^0 values (or current) well below the predicted reversible detection limit of $0.2\,cm\,s^{-1}$ at 9.02 Hz. α was assumed to be 0.50 in all simulations in accordance with the highly symmetrical shapes of all ac harmonics. A comparison of experimental and simulated data at a BDD electrode is provided in Fig. 3. Electron transfer kinetic measurements were also undertaken in aqueous media containing 0.010 M HNO_3 and 1.0 M MNO_3 ($M^+ = Li^+$, Na^+ and NH_4^+) at a BDD electrode with results shown in Figs. S1-S3. k^0 values obtained from all measurements using the same procedure are summarized in Table 2. Excellent theory/experiment agreement was obtained for all electrolytes.

Despite the lack of a strong physical chemistry basis, simple Butler-Volmer theory is fully adequate for the current study, which is in agreement with previous findings [17,38]. The k^0 values obtained in aqueous media containing 1.0 M $NaNO_3$ and 0.010 M HNO_3 are of the same order of magnitude compared to the previously reported [17] values of 0.050 and $0.055\,cm\,s^{-1}$ for the $[\alpha\text{-}SiW_{12}O_{40}]^{4-/5-}$ and $[\alpha\text{-}SiW_{12}O_{40}]^{5-/6-}$ processes respectively in aqueous media containing 1.0 M Na_2SO_4 and 0.10 M H_2SO_4 using BDD electrodes constructed at Warwick University. Unwin and co-workers [38] found that the k^0 value for the $[Ru(NH_3)_6]^{3+/2+}$ process was dependent on the boron doping level. The doping level of the commerically available electrode used in this study is unknown, but certainly lies within the cases conisidered in reference [30]. Therefore, in addition to the differrence in the supporting electrolytes employed and the ionic strength in this and the earlier studies, variations in reported k^0 values may arise from differneces in the boron doping levels.

The results in Table 2 reveal that both the D values of $[\alpha\text{-}SiW_{12}O_{40}]^{4-}$ and the electrode kinetics for the $[\alpha\text{-}SiW_{12}O_{40}]^{4-/5-}$ and $[\alpha\text{-}SiW_{12}O_{40}]^{5-/6-}$ processes are electrolyte cation dependent. The values of D for $[\alpha\text{-}SiW_{12}O_{40}]^{4-}$ increase in the order of $LiNO_3 < NaNO_3 < KNO_3 \approx NH_4NO_3$. The diffusion coefficient is governed by the Stokes-Einstein relationship [45],

$$D = \frac{k_B T}{6\pi\eta a} \tag{8}$$

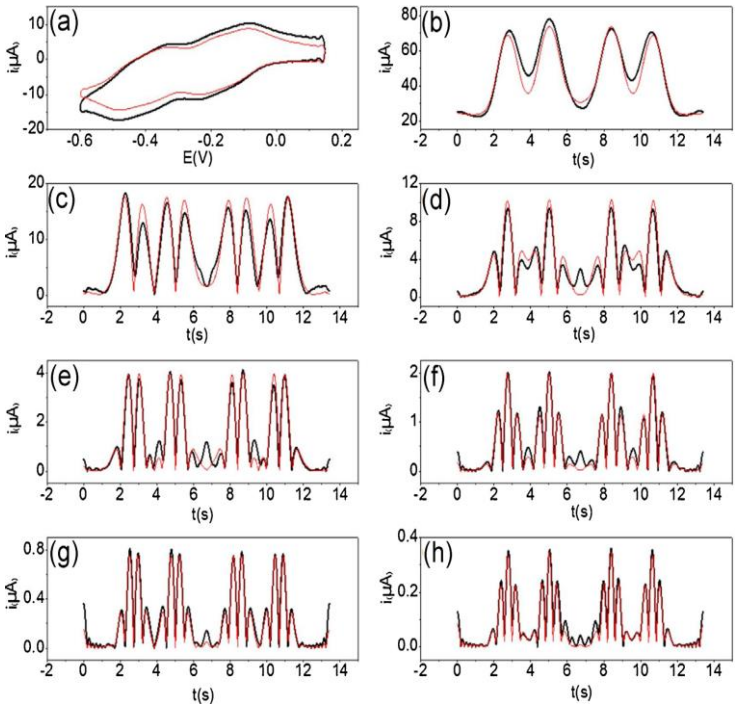

Fig. 2. Comparison of the simulated (—) and experimental (–) FTAC voltammograms obtained from the reduction of 1.0 mM $[\alpha\text{-}SiW_{12}O_{40}]^{4-}$ at a GC electrode in aqueous electrolyte media containing 1.0 M KNO_3 and 0.010 M HNO_3. (a) aperiodic dc component (b-h) 1st-7th ac harmonic components. Both processes are assumed to be reversible in simulation. Other parameters are as defined in the text.

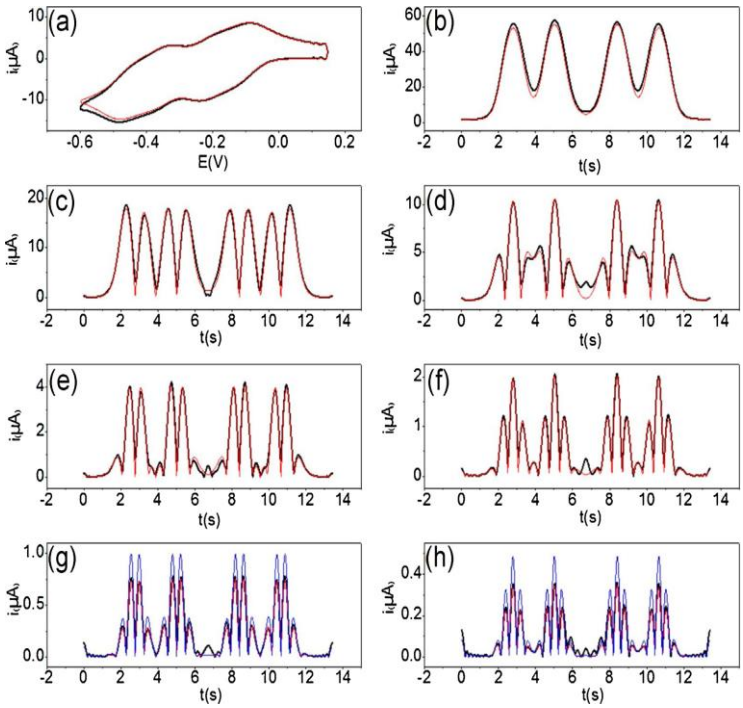

Fig. 3. Comparison of the simulated (—) and experimental (–) FTAC voltammograms obtained from the reduction of 1.0 mM $[\alpha\text{-}SiW_{12}O_{40}]^{4-}$ at a BDD electrode in aqueous electrolyte media containing 1.0 M KNO_3 and 0.010 M HNO_3. (a) aperiodic dc component (b-h) 1st -7th ac harmonic components, 6th and 7th harmonics for a reversible process (—) are also shown for comparison. Other parameters are as defined in the text.

where k_B is the Boltzmann constant, η is the viscosity of the medium and a is the hydrodynamic radius of the diffusing particle. The size term (a) for the ion paired $[\alpha\text{-}SiW_{12}O_{40}]^{4-}$ is not expected to be strongly electrolyte cation dependent as this parameter is dominated by the large size of $[\alpha\text{-}SiW_{12}O_{40}]^{4-}$. However, the viscosity of an aqueous electrolyte can be influenced by the idendity of the electrolyte cation and its concentration [46]. This hypothesis can be tested by comparing the $[D{\cdot}\eta]$ values for each electrolyte medium. The η values of aqueous solution containing 1.0 M $LiNO_3$, $NaNO_3$, KNO_3, NH_4NO_3 with 0.010 M HNO_3 are 0.987, 0.951, 0.870 and 0.868 mpa·s, respectively. Based on the D values in Table 2, $[D{\cdot}\eta]$ values for the corresponding media are 3.46, 3.61, 3.59, 3.56 ($\times 10^{-13}$ m kg s^{-2}), which are almost constant. On this basis, viscosity is believed to be the major factor giving rise to differences in D values, which is consistent with the previous finding [47].

Interestingly, k^0 increases in the order of $LiNO_3 < NaNO_3 < KNO_3 \approx NH_4NO_3$, which is the same order as for D values (Table 2) with 1.0 M electrolyte concentration. This order is in agreement with reports of electrolyte cation effects on electrode kinetics of the $[Fe(CN)_6]^{4-/3-}$ process, although k^0 for the latter process exhibits a much stronger cation dependence.[14,15,48,49] To explain the influence of the electrolyte cation on k^0, the following reaction scheme, which takes into account the contribution from ion-pairing, is introduced,

$$\begin{array}{ccc} A + e^- & \rightleftharpoons & B \quad (E_1^0, k_1^0, \alpha_1) \\ K_1 \Big\| \; X^+ & & X^+ \; \Big\| K_2 \\ XA^+ + e^- & \rightleftharpoons & XB^+ \quad (E_2^0, k_2^0, \alpha_2) \end{array} \tag{9}$$

In Eq. (9), E_1^0 and E_2^0 are the reversible potentials for the designated electron transfer processes, k_1^0, α_1 and k_2^0, α_2 represent the formal rate constants and transfer coefficients for the relevant electron transfer steps at E_1^0 and E_2^0, $K_1 = \frac{[X^+][A]}{[XA^+]}$ and $K_2 = \frac{[X^+][B]}{[XB^+]}$. Parallel protonation reactions are omitted in this reaction scheme since a literature report suggests that the contribution from these reactions is minimal [42], although plausibly, the protonation states of $[\alpha\text{-}SiW_{12}O_{40}]^{4-}$ and its reduced forms are the same in the presence of 0.010 M HNO_3. Under the conditions where the homogeneous ion-pairing reactions are reversible and the depletion of X^+ is negligible, this reaction scheme can be described by an equivalent one-electron transfer reaction, with an apparent electron transfer rate constant ($k_{app}{}^0$) and an apparent charge transfer coefficient (α_{app}) [44,50].

$$A' + e^- \rightleftharpoons B' \left(k_{aap}{}^0, \alpha_{app}\right) \tag{10}$$

where

$$k_{app}{}^0 = \frac{k_1{}^0 (K_2/K_1)^{\alpha_{app}} + k_2{}^0 ([X^+]/K_1)}{[1 + ([X^+]/K_1)]^{1-\alpha_{app}} [(K_2/K_1) + ([X^+]/K_1)]^{\alpha_{app}}} \tag{11}$$

Since higher charge density is associated with species B, K_2 is expected to be smaller than K_1. It is also reasonable to assume both K_1 and K_2 are smaller than unity due to relatively strong association between highly charged POMs and electrolyte cations. Consequently, the relationships $K_2/K_1 \ll [X^+]/K_1$ and $k_1{}^0 (K_2/K_1)^{1/2} \ll k_2{}^0 ([X^+]/K_1)$ are expected to be valid under our experimental conditions and as noted in other studies [44,50]. On this basis,

Eq. (11) can be simplified to give Eq. (12) with α_{app} taken to be 0.50,

$$k_{app}{}^{0} = \frac{k_1{}^{0}(K_2/K_1)^{1/2} + k_2{}^{0}([X^+]/K_1)}{[1+([X^+]/K_1)]^{1/2}[(K_2/k_1)+([X^+]/K_1)]^{1/2}} \approx \frac{k_2{}^{0}([X^+]/K_1)^{1/2}}{[1+([X^+]K_1)]^{1/2}} = \frac{k_2{}^{0}}{[1+(K_1/[X^+])]^{1/2}} \quad (12)$$

As the magnitude of the hydrated radius of the cation decreases [51], the ion pairs become stronger and K_1 is expected to decrease [10] in the order $Li^+ > Na^+ > K^+ \approx NH_4^+$. From Eq. (12), we can deduce that $k_{app}{}^{0}$ increases with a decrease in K_1 assuming $k_2{}^{0}$ is insensitive to the identity of the electrolyte cation. $k_{app}{}^{0}$ is therefore predicted to increase in the order of $LiNO_3 < NaNO_3 < KNO_3 \approx NH_4NO_3$. Eq. (12) also predicts an increase of $k_{app}{}^{0}$ upon an increase of the hydrated radius of $[X^+]$, which is in qualitative agreement with the finding reported in the previous study [14]. Although not the focus of this study, the apparent cation dependence of the reversible potentials for both $[\alpha\text{-}SiW_{12}O_{40}]^{4-/5-}$ and $[\alpha\text{-}SiW_{12}O_{40}]^{5-/6-}$ processes (Table 1) also is consistent with the prediction based on the reaction scheme proposed above [44,50]. Finally, it should be noted that our observation of a cation dependent k^0 value is unlikely to be explained simply by distant dependent electron transfer kinetics resulting from the differences in the sizes of the electrolyte cations. Even if the cations are the major constituent ion of the inner double layer, the variation in the sizes of cations ranging from 90 to 152 pm in radii for the smallest Li^+ and largest K^+ [52], respectively, has minimal effect on the distance of closest approach for $[\alpha\text{-}SiW_{12}O_{40}]^{4-}$ since the size of the latter ion (~1 nm) is much larger [17].

5. Conclusion

The influence of the electrolyte cation on the electron transfer kinetics for $[\alpha\text{-}SiW_{12}O_{40}]^{4-/5-}$ and $[\alpha\text{-}SiW_{12}O_{40}]^{5-/6-}$ processes at a BDD electrode has been established using FTAC voltammetry. The k^0 value is dependent on the electrolyte cation identity, increasing in the order of $LiNO_3 < NaNO_3 < KNO_3 \approx NH_4NO_3$. This order is attributed to a decrease in the strength of ion-pairing between electrolyte cations and POMs, which follows the order $NH_4^+ \approx K^+ < Na^+ < Li^+$, due to an increase in the hydration sphere of the electrolyte cations.

6. Supporting Information

Comparison of simulated and experimental FTAC voltammograms obtained for $[\alpha\text{-}SiW_{12}O_{40}]^{4-/5-}$ and $[\alpha\text{-}SiW_{12}O_{40}]^{5-/6-}$ processes in aqueous electrolyte media containing 1.0 M MNO_3 ($M^+ = Li^+$, Na^+ and NH_4^+) and 0.010 M HNO_3 at a BDD electrode (Figs. S1-S3).

Acknowledgements

The authors gratefully acknowledge Cameron Bentley for his assistance with the viscosity measurements, and Prof. Julie Macpherson (University of Warwick, UK) and Dr Si-Xuan Guo for helpful discussions. AMB and JZ would like to thank the Australian Research Council for financial support.

Appendix A. Supplementary data

Supplementary data associated with this article can be found, in the online version, at http://dx.doi.org/10.1016/j.electacta.2015.08.049.

References

[1] M.T. Pope, Y. Jeannin, M. Fournier, Heteropoly and isopoly oxometalates, Springer Berlin, 1983.
[2] M. Pope, Polyoxometalates: From Platonic Solids to Anti-Retroviral Activity: Kluwer Academic Publishers: Dordrecht, The Netherlands, 1994.
[3] N. Mizuno, K. Yamaguchi, K. Kamata, Epoxidation of olefins with hydrogen peroxide catalyzed by polyoxometalates, Coord. Chem. Rev. 249 (2005) 1944–1956.
[4] C.L. Hill, Foreword: Polyoxometalates in catalysis, J. Mol. Catal 114 (1996) 1.
[5] J.T. Rhule, C.L. Hill, D.A. Judd, R.F. Schinazi, Polyoxometalates in medicine, Chem. Rev. 98 (1998) 327–358.
[6] B. Keita, L. Nadjo, Electrochemistry of isopoly and heteropoly oxometalates, Encyclopedia of electrochemistry (2006) .
[7] T. He, J. Yao, Photochromism in composite and hybrid materials based on transition-metal oxides and polyoxometalates, Prog. Mater. Sci. 51 (2006) 810–879.
[8] J.M. Clemente-Juan, E. Coronado, Magnetic clusters from polyoxometalate complexes, Coord. Chem. Rev. 193 (1999) 361–394.
[9] P. Chen, T.J. Meyer, Medium effects on charge transfer in metal complexes, Chem. Rev. 98 (1998) 1439–1478.
[10] V.A. Grigoriev, D. Cheng, C.L. Hill, I.A. Weinstock, Role of alkali metal cation size in the energy and rate of electron transfer to solvent-separated 1: 1 [(M^+) (acceptor)]($M^+ = Li^+ Na^+, K^+$) ion pairs, J. Am. Chem. Soc. 123 (2001) 5292–5307.
[11] J.F. Kirby, L.C. Baker, Effects of counterions in heteropoly electrolyte chemistry. 1. Evaluations of relative interactions by NMR on Kozik salts, Inorg. Chem. 37 (1998) 5537–5543.
[12] M. Misono, Heterogeneous catalysis by heteropoly compounds of molybdenum and tungsten, Catal. Rev. Sci. Eng. 29 (1987) 269–321.
[13] N. Mizuno, M. Misono, Heterogeneous catalysis, Chem. Rev. 98 (1998) 199–218.
[14] L. Peter, W. Dürr, P. Bindra, H. Gerischer, The influence of alkali metal cations on the rate of the $Fe(CN)_6^{4-}/Fe(CN)_6^{3-}$ electrode process, J. Electroanal. Chem. 71 (1976) 31–50.
[15] J. Kúta, E. Yeager, The influence of cations on the electrode kinetics of ferricyanide-ferrocyanide system on the rotating gold electrode, J. Electroanal. Chem. 59 (1975) 110–112.
[16] D.Y. Kim, J. Wang, J. Yang, H.W. Kim, G.M. Swain, Electrolyte and Temperature Effects on the Electron Transfer Kinetics of $Fe(CN)_6^{4-/3-}$ at Boron-Doped Diamond Thin Film Electrodes, J. Phys. Chem. C 115 (2011) 10026–10032.
[17] K. Bano, A.M. Bond, J. Zhang, P.R. Unwin, J.V. Macpherson, J. Phys. Chem. C 119 (2015) 12464–12472.
[18] A.J. Bard, L.R. Faulkner, Electrochemical methods: fundamentals and applications, 2nd, Hoboken: Wiley and Sons, 2001.
[19] D.K. Gosser, Cyclic voltammetry: simulation and analysis of reaction mechanisms, John Wiley & Sons, New York, 1993.
[20] K. Oldham, J. Myland, Fundamentals of electrochemical science, Elsevier, 1993.
[21] R.S. Nicholson, I. Shain, Theory of stationary electrode polarography. Single scan and cyclic methods applied to reversible, irreversible, and kinetic systems, Anal. Chem. 36 (1964) 706–723.
[22] R.S. Nicholson, Theory and Application of Cyclic Voltammetry for Measurement of Electrode Reaction Kinetics, Anal. Chem. 37 (1965) 1351–1355.
[23] R.S. Nicholson, Some examples of the numerical solution of nonlinear integral equations, Anal. Chem. 37 (1965) 667–671.
[24] S.-X. Guo, A.M. Bond, J. Zhang, Fourier Transformed Large Amplitude Alternating Current Voltammetry: Principles and Applications, Rev. Polarogr. 61 (2015) 21–32.
[25] J. Zhang, S.-X. Guo, A.M. Bond, Discrimination and evaluation of the effects of uncompensated resistance and slow electrode kinetics from the higher harmonic components of a fourier transformed large-amplitude alternating current voltammogram, Anal. Chem. 79 (2007) 2276–2288.
[26] R.G. Compton, J.S. Foord, F. Marken, Electroanalysis at diamond-like and doped-diamond electrodes, Electroanal. 15 (2003) 1349–1363.
[27] A.L. Colley, C.G. Williams, U. D'Haenens Johansson, M.E. Newton, P.R. Unwin, N. R. Wilson, J.V. Macpherson, Examination of the spatially heterogeneous electroactivity of boron-doped diamond microarray electrodes, Anal. Chem. 78 (2006) 2539–2548.
[28] L. Hutton, M.E. Newton, P.R. Unwin, J.V. Macpherson, Amperometric oxygen sensor based on a platinum nanoparticle-modified polycrystalline boron doped diamond disk electrode, Anal. Chem. 81 (2008) 1023–1032.
[29] J. Zhang, S.-X. Guo, A.M. Bond, F. Marken, Large-amplitude Fourier transformed high-harmonic alternating current cyclic voltammetry: kinetic discrimination of interfering Faradaic processes at glassy carbon and at boron-doped diamond electrodes, Anal. Chem. 76 (2004) 3619–3629.
[30] J.V. Macpherson, A practical guide to using boron doped diamond in electrochemical research, Phys. Chem. Chem. Phys. 17 (2015) 2935–2949.
[31] G.M. Swain, Electrically conducting diamond thin films: advanced electrode materials for electrochemical technologies, Electroanal. Chem. 22 (2004) 181–277.
[32] K. Peckova, J. Musilova, J. Barek, Boron-Doped Diamond Film Electrodes-New Tool for Voltammetric Determination of Organic Substances, Crit. Rev. Anal. Chem. 39 (2009) 148–172.
[33] R.L. McCreery, Advanced carbon electrode materials for molecular electrochemistry, Chem. Rev. 108 (2008) 2646–2687.

[34] R.G. Compton, J.S. Foord, F. Marken, Electroanalysis at diamond-like and doped-diamond electrodes, Electroanal 15 (2003) 1349–1363.
[35] A.M. Bond, N.W. Duffy, S.-X. Guo, J. Zhang, D. Elton, Changing the look of voltammetry, Anal. Chem. 77 (2005) 186 A–195 A.
[36] S.W. Feldberg, Optimization of explicit finite-difference simulation of electrochemical phenomena utilizing an exponentially expanded space grid Refinement of the Joslin-Pletcher algorithm, J. Electroanal. Chem. 127 (1981) 1–10.
[37] M. Rudolph, A fast implicit finite difference algorithm for the digital simulation of electrochemical processes, J. Electroanal. Chem 314 (1991) 13–22.
[38] H.V. Patten, K.E. Meadows, L.A. Hutton, J.G. Iacobini, D. Battistel, K. McKelvey, A.W. Colburn, M.E. Newton, J.V. Macpherson, P.R. Unwin, Electrochemical Mapping Reveals Direct Correlation between Heterogeneous Electron-Transfer Kinetics and Local Density of States in Diamond Electrodes, Angew. Chem. Int. Edit. 51 (2012) 7002–7006.
[39] J. Zhang, S.-X. Guo, A.M. Bond, F. Marken, Large-amplitude Fourier transformed high-harmonic alternating current cyclic voltammetry: kinetic discrimination of interfering faradaic processes at glassy carbon and at boron-doped diamond electrodes, Anal. Chem. 76 (2004) 3619–3629.
[40] A.A. Sher, A.M. Bond, D.J. Gavaghan, K. Harriman, S.W. Feldberg, N.W. Duffy, S.-X. Guo, J. Zhang, Resistance, capacitance, and electrode kinetic effects in fourier-transformed large-amplitude sinusoidal voltammetry: Emergence of powerful and intuitively obvious tools for recognition of patterns of behavior, Anal. Chem. 76 (2004) 6214–6228.
[41] Koichi Tokuda, H. Matsuda, Theory of a. c. voltammetry at a rotating disk electrode: Part I. A reversible electrode process, J. Electroanal. Chem. 82 (1977) 157–171.
[42] J. Zhang, J.K. Goh, W.T. Tan, A.M. Bond, Mechanistic analysis of the electrocatalytic properties of dissolved alpha and beta isomers of $[SiW^{12}O^{40}]^{4-}$ and solid $[Ru(bipy)_3]_2[\alpha\text{-}SiW_{12}O_{40}]$ on the reduction of nitrite in acidic aqueous media, Inorg. Chem. 45 (2006) 3732–3740.
[43] A.M. Bond, K. Bano, S. Adeel, L.L. Martin, J. Zhang, Fourier-Transformed Large-Amplitude AC Voltammetric Study of Tetrathiafulvalene (TTF): Electrode Kinetics of the TTF^0/TTF^+ and TTF^+/TTF^{2+} Processes, ChemElectroChem 1 (2014) 99–107.
[44] Y. Liu, S.-X. Guo, A.M. Bond, J. Zhang, Y.V. Geletii, C.L. Hill, Voltammetric Determination of the Reversible Potentials for $[\{Ru_4O_4(OH)_2(H_2O)_4\}(\gamma\text{-}SiW_{10}O_{36})_2]^{10-}$10–over the pH Range of 2–12: Electrolyte Dependence and Implications for Water Oxidation Catalysis, Inorg. Chem. 52 (2013) 11986–11996.
[45] C.C. Miller, Proceedings of the Royal Society of London. Series A, The Stokes-Einstein law for diffusion in solution, 106, 1924, 724–749.
[46] M. Afzal, M. Saleem, M.T. Mahmood, Temperature and concentration dependence of viscosity of aqueous electrolytes from 20. degree.C to 50. degree.C chlorides of Na^+, K^+, Mg^{2+}, Ca^{2+}, Ba^{2+}, Sr^{2+}, Co^{2+}, Ni^{2+}, Cu^{2+}, and Cr^{3+}, J. Chem. Eng. Data 34 (1989) 339–346.
[47] B. Keita, T. Lucas, L. Nadjo, New aspects of the electrochemistry of heteropolyacids Reduction currents as a probe of solvent-electrolyte interactions, J. Electroanal. Chem. 208 (1986) 343–356.
[48] M. Noel, P. Anantharaman, Voltammetric studies on a glassy carbon electrode. Part II. Factors influencing the simple electron-transfer reactions—the $K_3[Fe(CN)_6]$-$K_4[Fe(CN)_6]$ system, Analyst 110 (1985) 1095–1103.
[49] J. Kawiak, T. Jędral, Z. Galus, A reconsideration of the kinetic data for the $Fe(CN)_6^{4-}/Fe(CN)_6^{3-}$ system, J. Electroanal. Chem. 145 (1983) 163–171.
[50] S.-X. Guo, S.W. Feldberg, A.M. Bond, D.L. Callahan, P.J. Richardt, A.G. Wedd, Systematic Approach to the Quantitative Voltammetric Analysis of the Fe^{III}/Fe^{II} Component of the $[\alpha_2\text{-}Fe(OH_2)P_2W_{17}O_{61}]^{7-/8-}$ Reduction Process in Buffered and Unbuffered Aqueous Media, J. Phys. Chem. B 109 (2005) 20641–20651.
[51] P.H. Rieger, Electrochemistry, Springer Science & Business Media, 2012.
[52] J.E. Huheey, Inorganic Chemistry, 3rd ed., Harper and Row, New York, 1983.

Supporting Information

Probing Electrolyte Cation Effect on the Electron Transfer Kinetics of the $[\alpha\text{-}SiW_{12}O_{40}]^{4-/5-}$ and $[\alpha\text{-}SiW_{12}O_{40}]^{5-/6-}$ Processes using a Boron-Doped Diamond Electrode

Jiezhen Li, Alan M. Bond* and Jie Zhang*

School of Chemistry and Australian Research Council Centre of Excellence for Electromaterials Science, Monash University, Clayton, Victoria 3800, Australia

Corresponding authors: jie.zhang@monash.edu, alan.bond@monash.edu

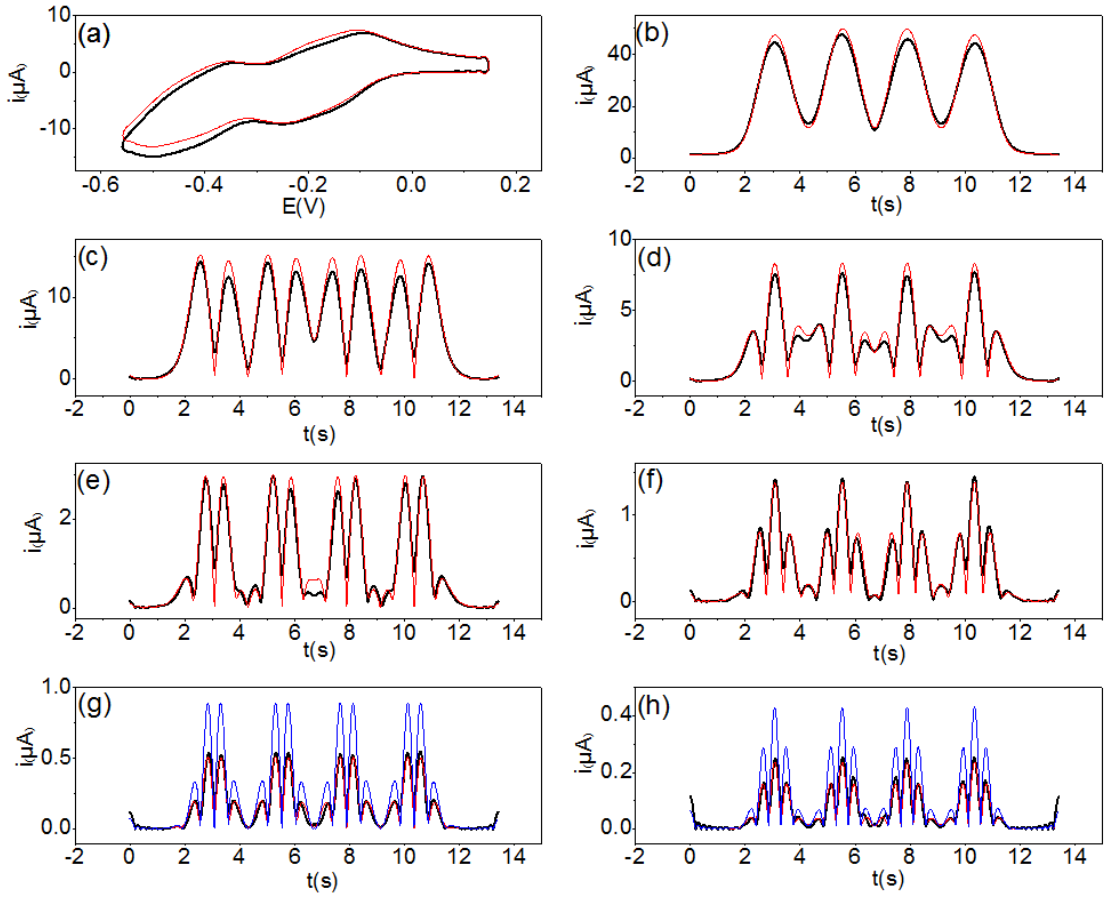

Figure S1. Comparison of the simulated (—) and experimental (—) FTAC voltammograms obtained from the reduction of 1 mM $[\alpha\text{-}SiW_{12}O_{40}]^{4-}$ at a BDD electrode in aqueous electrolyte media containing 1.0 M $LiNO_3$ and 0.01 M HNO_3. (a) aperiodic dc component (b-h) 1^{st} -7^{th} ac harmonic components, 6^{th} and 7^{th} harmonics for a reversible process (—) are also shown for comparison. Other parameters are as defined in the text.

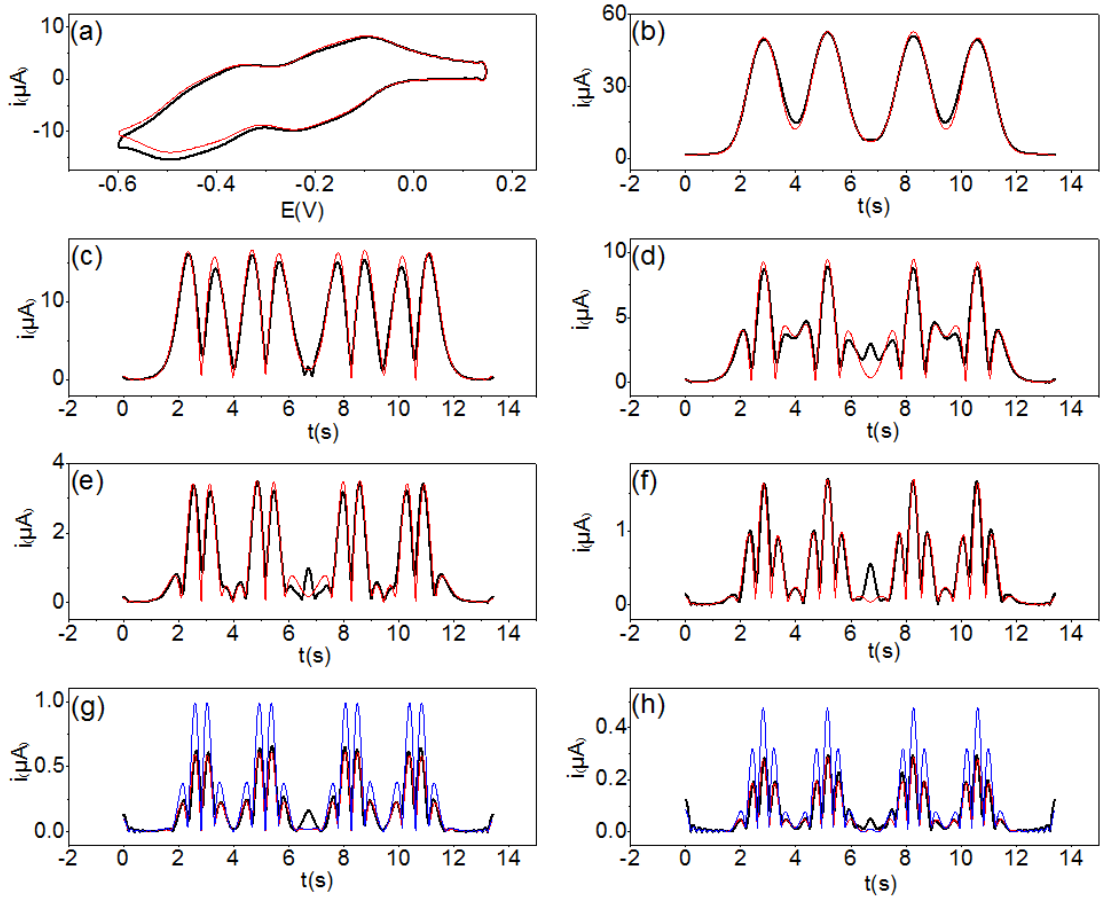

Figure S2. Comparison of the simulated (—) and experimental (—) FTAC voltammograms obtained from the reduction of 1 mM $[\alpha\text{-}SiW_{12}O_{40}]^{4-}$ at a BDD electrode in aqueous electrolyte media containing 1.0 M $NaNO_3$ and 0.01 M HNO_3. (a) aperiodic dc component (b-h) 1^{st} -7^{th} ac harmonic components, 6^{th} and 7^{th} harmonics for a reversible process (—) are also shown for comparison. Other parameters are as defined in the text.

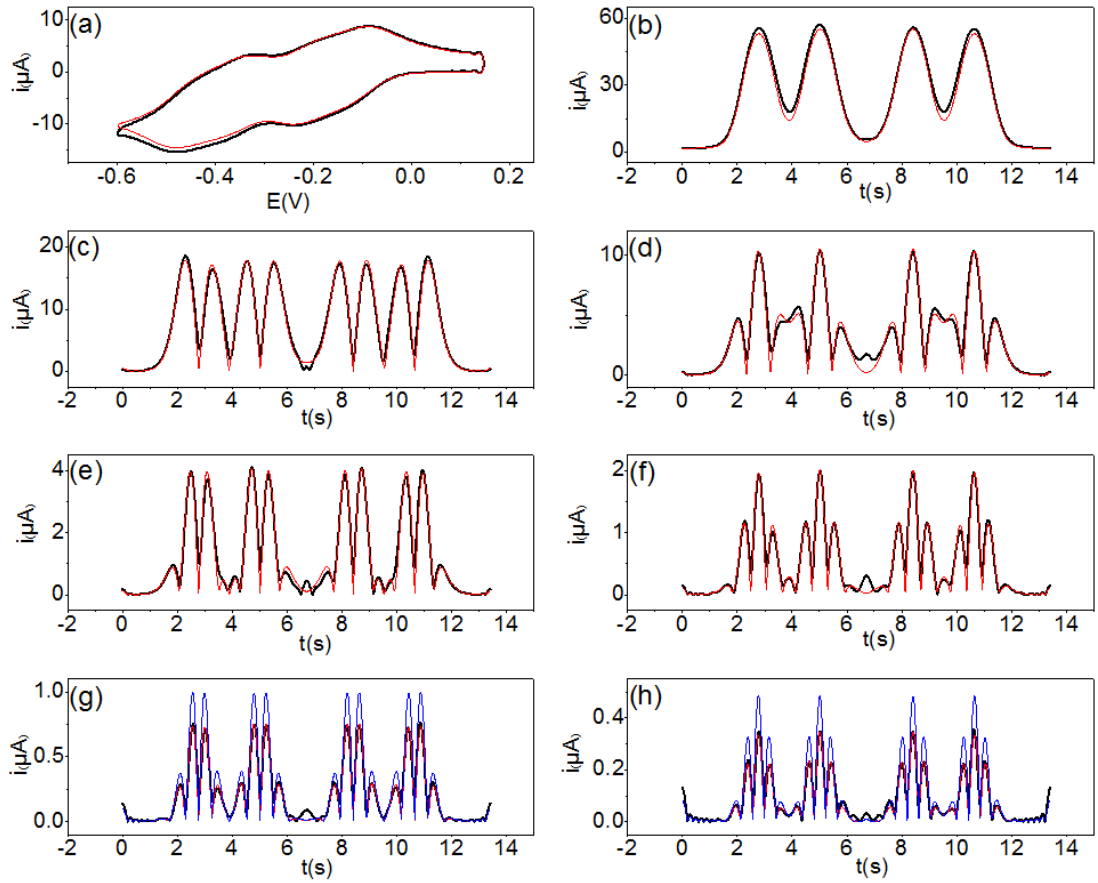

Figure S3. Comparison of the simulated (—) and experimental (—) FTAC voltammograms obtained from the reduction of 1 mM $[\alpha\text{-}SiW_{12}O_{40}]^{4-}$ at a BDD electrode in aqueous electrolyte media containing 1.0 M NH_4NO_3 and 0.01 M HNO_3. (a) aperiodic dc component (b-h) 1st -7th ac harmonic components, 6th and 7th harmonics for a reversible process (—) are also shown for comparison. Other parameters are as defined in the text.

Chapter 4

Electrode Material Dependence of the Electron Transfer Kinetics Associated with the $[SVW_{11}O_{40}]^{3-/4-}$ ($V^{V/IV}$) and $[SVW_{11}O_{40}]^{4-/5-}$ ($W^{VI/V}$) Processes in Dimethylformamide

Electrochimica Acta 201 (2016) 45–56

Contents lists available at ScienceDirect

Electrochimica Acta

journal homepage: www.elsevier.com/locate/electacta

Electrode Material Dependence of the Electron Transfer Kinetics Associated with the $[SVW_{11}O_{40}]^{3-/4-}$ ($V^{V/IV}$) and $[SVW_{11}O_{40}]^{4-/5-}$ ($W^{VI/V}$) Processes in Dimethylformamide

Jiezhen Li[a], Si-Xuan Guo[a], Cameron L. Bentley[a], Kiran Bano[a], Alan M. Bond[a,*], Jie Zhang[a,*], Tadaharu Ueda[b]

[a] School of Chemistry and ARC Centre of Excellence for Electromaterials Science, Monash University, Clayton, Victoria 3800, Australia
[b] Department of Applied Science, Faculty of Science, Kochi University, Kochi 780-8520, Japan

ARTICLE INFO

Article history:
Received 10 January 2016
Received in revised form 14 March 2016
Accepted 18 March 2016
Available online 19 March 2016

Keywords:
Polyoxometalates
Electron transfer kinetics
Fourier transformed alternating current voltammetry
Electrode material dependence

ABSTRACT

In this study, large amplitude Fourier transformed alternating current (FTAC) voltammetry has been used to determine the heterogeneous electron-transfer kinetics (k° and α values) associated with the vanadium $[SVW_{11}O_{40}]^{3-/4-}$ ($V^{V/IV}$, $E^\circ = 0.050$ V vs. Fc/Fc^+, where Fc = ferrocene) and tungsten $[SVW_{11}O_{40}]^{4-/5-}$ ($W^{VI/V}$, $E^\circ = -1.530$ V vs. Fc/Fc^+) processes in dimethylformamide containing tetrabutylammonium hexafluorophosphate as the supporting electrolyte. At glassy carbon (GC), platinum (Pt), gold (Au) and boron-doped diamond (BDD), the $V^{V/IV}$ process is kinetically more facile than the $W^{VI/V}$ one. Excellent simulation-experiment fits were achieved for the $V^{V/IV}$ process at all electrode materials, and at a supporting electrolyte concentration of 0.1 M, the k° value associated with this process increases in the order BDD < Pt ≈ Au < GC. By contrast, at all electrode materials except GC, generally poor simulation-experiment fits were achieved for the $W^{VI/V}$ process, preventing the data from being analysed quantitatively by FTAC voltammetry. Changing the concentration of supporting electrolyte from 0.1 to 0.5 M has a significant influence on the kinetics, with the k° value increasing at GC and decreasing at Pt, Au and BDD. Overall, the findings indicate that differences in density of states do not fully explain the electrode material dependence of the k° values and that other factors such as surface functional groups (on GC) and the double layer effect need to be taken into consideration.

1. Introduction

Polyoxometalates (POMs) are discrete nanometer-sized oxide clusters of molybdenum, tungsten and other transition metals in high oxidation states. They represent an important class of inorganic material [1] and have been studied extensively for many decades [2–7]. POMs are stable, highly negatively charged clusters with rich structural and compositional variety and as a result of their chemical, structural and electronic versatility, have attracted much attention in medicine, catalysis, bioanalysis and materials science [8–10]. One of the most important properties of POM anions is their ability to reversibly undergo an extensive series of electron transfer reactions under relatively mild conditions [11]. Keggin heteropolyanions $[X^{n+}M_{12}O_{40}]^{(8-n)-}$ (M = W(VI) or Mo(VI)) are among the most widely investigated POMs. By varying the metal composition and structure, the electrochemical characteristics of Keggin polyoxometalates can be finely tuned [12]. In particular, when one or more of the W(VI) or Mo(VI) centers are replaced by a transition metal such as V(V), wide variations in electrochemical and catalytic behaviors can emerge [13–15].

Although electrochemical studies of POMs are extensive and the thermodynamic effects of cations and solvents have been widely reported [15–21], quantitative studies of heterogeneous electron transfer kinetics at an electrode/electrolyte interface are relatively rare [22,23]. As POMs typically exhibit fast electrode kinetics, traditional electrochemical techniques such as direct current (DC) cyclic voltammetry are often difficult to apply quantitatively at macrodisk electrodes [24–27]. We have shown that large amplitude Fourier transformed alternating current

* Corresponding authors.
E-mail addresses: alan.bond@monash.edu (A.M. Bond), jie.zhang@monash.edu (J. Zhang).

http://dx.doi.org/10.1016/j.electacta.2016.03.107
0013-4686/

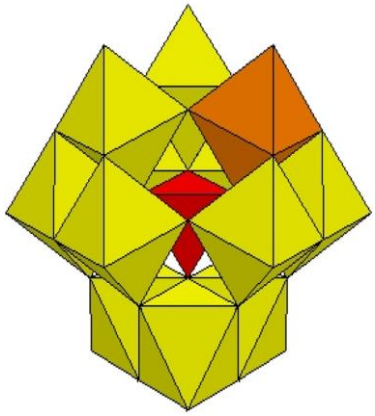

Fig. 1. The structure of $[SVW_{11}O_{40}]^{3-}$. Color code: S (red), V (orange), W (yellow) [34]. (For interpretation of the references to colour in this figure legend, the reader is referred to the web version of this article.)

(FTAC) voltammetry is a more sensitive and generally advantageous method for quantitative investigations of fast electrode kinetics at macrodisk electrodes [28–30]. In this version of AC voltammetry, a sinusoidal perturbation of a known frequency and amplitude of about 100 mV is superimposed onto the DC waveform. Since the amplitude of the AC perturbation is large, the higher harmonic components, which are generally devoid of background capacitive current and are highly sensitive to the electrode kinetics [31–33], are enhanced. Moreover, the effects of slow electrode kinetics and uncompensated resistance (R_u) can be resolved, while the information provided by DC voltammetry is retained, since the aperiodic DC component can be separated from the AC harmonic components. Using FTAC voltammetry, our group have shown that the electrode kinetics of the POM $[\alpha\text{-}SiW_{12}O_{40}]^{4-}$ are fast and strongly dependent on the identity of the electrode material in aqueous media [22,23].

In this study, large amplitude FTAC voltammetry has been employed to investigate the electrode material dependence of the heterogeneous electron-transfer rate constants (k°) and charge transfer coefficients (α) associated with the $[SVW_{11}O_{40}]^{3-/4-/5-}$ processes in dimethylformamide (DMF). The electrode materials used in this study are glassy carbon (GC), boron doped diamond (BDD), platinum (Pt) and gold (Au). The structure of the POM anion [34], as in $[Bu_4N]_3[SVW_{11}O_{40}]$, is shown in Fig. 1. Evidently, one V^V and multiple W^{VI} sites are available for reduction. Indeed, $[SVW_{11}O_{40}]^{3-}$ is known to exhibit three well-defined one-electron reduction processes in conventional organic solvent/electrolyte media [34]. The two initial processes correspond to the reduction

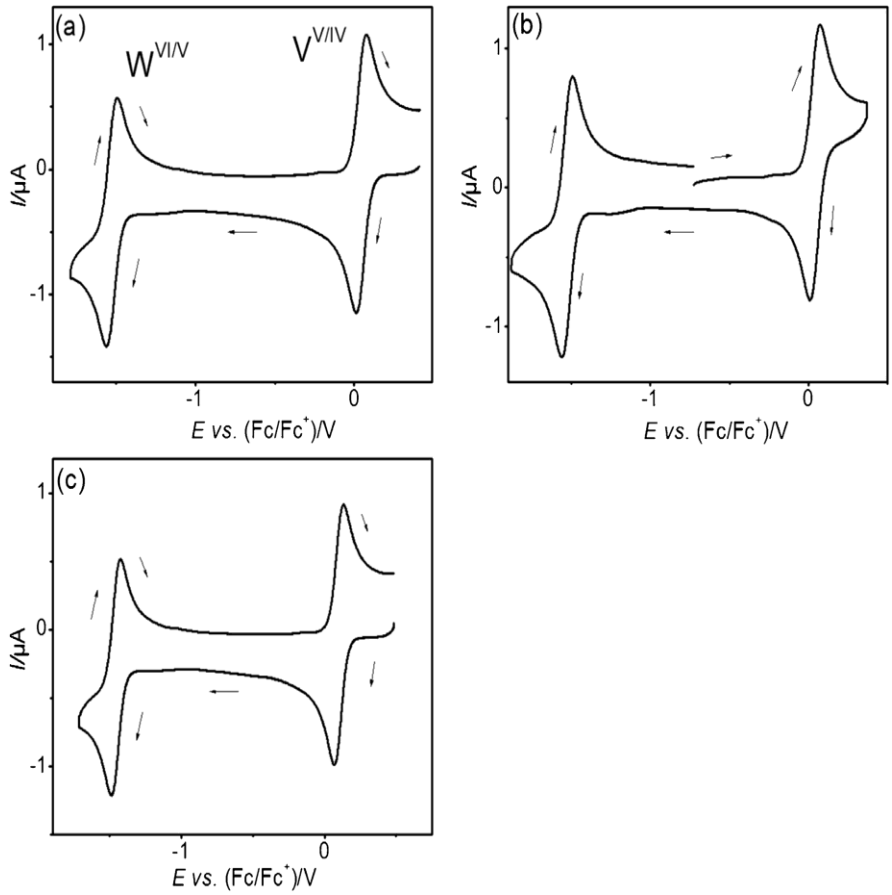

Fig. 2. DC cyclic voltammograms obtained at a GC macrodisk electrode with a scan rate of 0.1 V s^{-1} in DMF containing (a) 1.0 mM $[SVW_{11}O_{40}]^{3-}$ and 0.1 M $[Bu_4N][PF_6]$; (b) 1.0 mM $[SVW_{11}O_{40}]^{4-}$ and 0.1 M $[Bu_4N][PF_6]$ and; (c) 1.0 mM $[SVW_{11}O_{40}]^{3-}$ and 0.5 M $[Bu_4N][PF_6]$. The initial potentials were 0.42 V, −0.74 V and 0.48 V (vs. Fc/Fc^+) in (a), (b) and (c), respectively.

Table 1
DC cyclic voltammetric data derived from the reduction of 1.0 mM $[SVW_{11}O_{40}]^{3-}$ in DMF (0.1 M $[Bu_4N][PF_6]$) at a scan rate of 0.1 V s^{-1}.

Electrode	DMF (0.1 M $[Bu_4N][PF_6]$)				
	E^0_V/V[a]	$(\Delta E_p)_V$/V[b]	E^0_W/V	$(\Delta E_p)_W$/V	ΔE°/V[c]
BDD	0.050	0.076	−1.530	0.239	1.580
Pt	0.050	0.066	−1.540	0.314	1.590
GC	0.050	0.062	−1.525	0.066	1.575
Au	0.050	0.073	−1.530	0.125	1.580

[a] vs. Fc/Fc^+.
[b] ΔE_p is the peak-to-peak separation of the designated process.
[c] ΔE° is the difference in E^0_V and E^0_W.

of V^V to V^{IV} (Eq. (1)) and W^{VI} to W^V (Eq. (2)), respectively, and are the focus of this paper:

$$\left[SV^{V}W^{VI}_{11}O_{40}\right]^{3-} + e^- \rightleftharpoons \left[SV^{IV}W^{VI}_{11}O_{40}\right]^{4-} \quad (1)$$

$$\left[SV^{IV}W^{VI}_{11}O_{40}\right]^{4-} + e^- \rightleftharpoons \left[SV^{IV}W^{V}W^{VI}_{10}O_{40}\right]^{5-} \quad (2)$$

This POM is an excellent model compound for probing the effects of the density of states (DOS) of the electrode materials and double layer for the following reasons: (i) the $V^{V/IV}$ and $W^{VI/V}$ processes occur at very different potentials under voltammetric conditions (they are separated by about 1.58 V) and are associated with different charges; (ii) the DOS values of the electrode materials differ, and are strongly potential dependent for BDD and GC [35] and; (iii) since the double layer is also potential dependent [24], its influence on the $V^{V/IV}$ and $W^{VI/V}$ processes is expected to be different. It should be noted that the electrode processes under consideration (eqs. 1 and 2) involve ion-pairing reactions and hence are not strictly elementary reactions [22] and k° should be more appropriately considered as $k^0_{apparent}$. However, discussion of the electrode material dependence of k° values using Marcus theory remains relevant since coupled homogenous ion pairing reactions are not rate limiting steps and their thermodynamic properties are independent of the electrode material. Finally, the solvent chosen for this study was DMF, in which $[SVW_{11}O_{40}]^{3-}$ and $[SVW_{11}O_{40}]^{4-}$ are very soluble, and tetrabutylammonium hexafluorophosphate ($[Bu_4N][PF_6]$), which is also very soluble in DMF, was used as the supporting electrolyte.

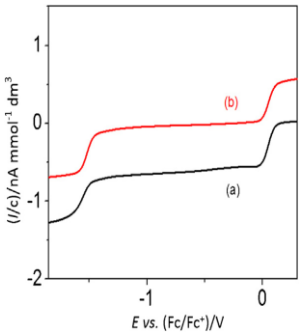

Fig. 3. Concentration-normalised near-steady-state voltammograms obtained at a carbon fiber microdisk electrode (r = 5 μm) in DMF (0.1 M $[Bu_4N][PF_6]$) containing (a) 1.2 mM $[SVW_{11}O_{40}]^{3-}$ and (b) 1.0 mM $[SVW_{11}O_{40}]^{4-}$ with a scan rate of 10 mV s^{-1}.

2. Experimental section

2.1. Chemicals

Dimethylformamide (DMF, 99.8%, Merck), acetonitrile (CH_3CN, 97%, Sigma-Aldrich), ethanol (96%, Merck), ferrocene (Fc, ≥98%, Sigma-Aldrich) and tetrabutylammonium borohydride ($[Bu_4N][BH_4]$, 98%, Sigma-Aldrich) were used as supplied by the manufacturer. Tetrabutylammonium hexafluorophosphate ($[Bu_4N][PF_6]$, 98%, Wako) was recrystallized twice from ethanol before use as the supporting electrolyte in electrochemical experiments. $[Bu_4N]_3[SVW_{11}O_{40}]$ was synthesized and purified according to literature procedures [34].

2.2. Synthesis of the one-electron reduced form, $[SVW_{11}O_{40}]^{4-}$

2.5 mM $[Bu_4N]_3[SVW_{11}O_{40}]$ was dissolved in 10 mL acetonitrile, followed by addition of 100 uL of 0.5 M $[Bu_4N][BH_4]$ (dissolved in acetonitrile). After vigorous shaking, followed by standing at room temperature for ca. 10 min, the yellow colour of the solution became deep blue, which indicates the formation of $[SVW_{11}O_{40}]^{4-}$. The solution was condensed to ~0.3 mL under nitrogen flow to give a deep blue precipitate ($[Bu_4N]_4[SVW_{11}O_{40}]$), which was collected by filtering, and then washed with ethanol, recrystallized from acetonitrile and dried at 55 °C for 2 hours. The $[SVW_{11}O_{40}]^{4-}$ anion has been spectroscopically, electrochemically and structurally characterized as a tetrathiafulvalene (TTF^+) salt [36].

Table 2
Electrode kinetic parameters derived for the $[SVW_{11}O_{40}]^{3-/4-/5-}$ processes in DMF containing $[SVW_{11}O_{40}]^{3-}$ and 0.1 M $[Bu_4N][PF_6]$.[a]

Electrode	c (mM)	E^0_V (V)[b]	E^0_W (V)[b]	R_u (Ω)	C_{dl} (c_0,c_1, c_2, c_3, c_4) (μF cm^{-2})	k^0_V (cm s^{-1})	α_V	k^0_W (cm s^{-1})	α_W
BDD	1.0	0.050	−1.530	900	11.6, 0.21, −7.4, −6.0, 1.3	0.026	0.55[c]	0.0008[e]	0.53[e]
	0.20	0.050	−1.520	880	9.8, 0.7, −5.6, −4.7, −1.0	0.028	0.60[c]	0.0006[e]	0.53[e]
Pt	1.0	0.050	−1.540	1070	26.6, 2.4, −5.7, −4.4, −0.8	0.08	0.50[d]	0.0001[e]	0.56[e]
	0.20	0.050	[f]	1100	21.1, 4.2, −3.6, −5.2, −1.3	0.08	0.50[d]	[f]	[f]
GC	1.0	0.050	−1.525	1120	42.3, 0.5, 10.6, 10.8, 2.8	0.20	0.50[d]	0.050	0.54[c]
	0.20	0.050	−1.525	1060	39.4, 15.6, 4.8, −4.3, −1.7	0.20	0.50[d]	0.045	0.54[c]
Au	1.0	0.050	−1.530	870	34.1, −3.2, −13.5, −6.2, −0.8	0.10	0.50[d]	[g]	[g]
	0.20	0.050	−1.530	850	35.6, 7.6, −20.9, −19.5, −4.5	0.10	0.50[d]	[g]	[g]

[a] Other parameters used in the simulations are: $A_{BDD} = 8.14 \times 10^{-3}$ cm^2, $A_{Pt} = 7.71 \times 10^{-3}$ cm^2, $A_{GC} = 7.45 \times 10^{-3}$ cm^2, $A_{Au} = 1.81 \times 10^{-2}$ cm^2, $\Delta E = 80$ mV, D ($[SVW_{11}O_{40}]^{3-}$) = 2.8×10^{-6} cm^2 s^{-1}, D ($[SVW_{11}O_{40}]^{4-}$) = D ($[SVW_{11}O_{40}]^{5-}$) = 2.9×10^{-6} cm^2 s^{-1}, T = 295 K, $\nu_{BDD\ and\ GC} = 0.171$ V s^{-1}, $\nu_{Pt} = 0.179$ V s^{-1}, $\nu_{Au} = 0.178$ V s^{-1}, $f_{GC} = 27.01$ Hz and $f_{BDD,\ Pt\ and\ Au} = 9.02$ Hz.
[b] vs. Fc/Fc^+.
[c] Calculated.
[d] Assumed.
[e] Approximate values. Complexities are associated with this process (See text for details).
[f] Process is poorly defined.
[g] Not determined. Complexities are associated with this process (See text for details).

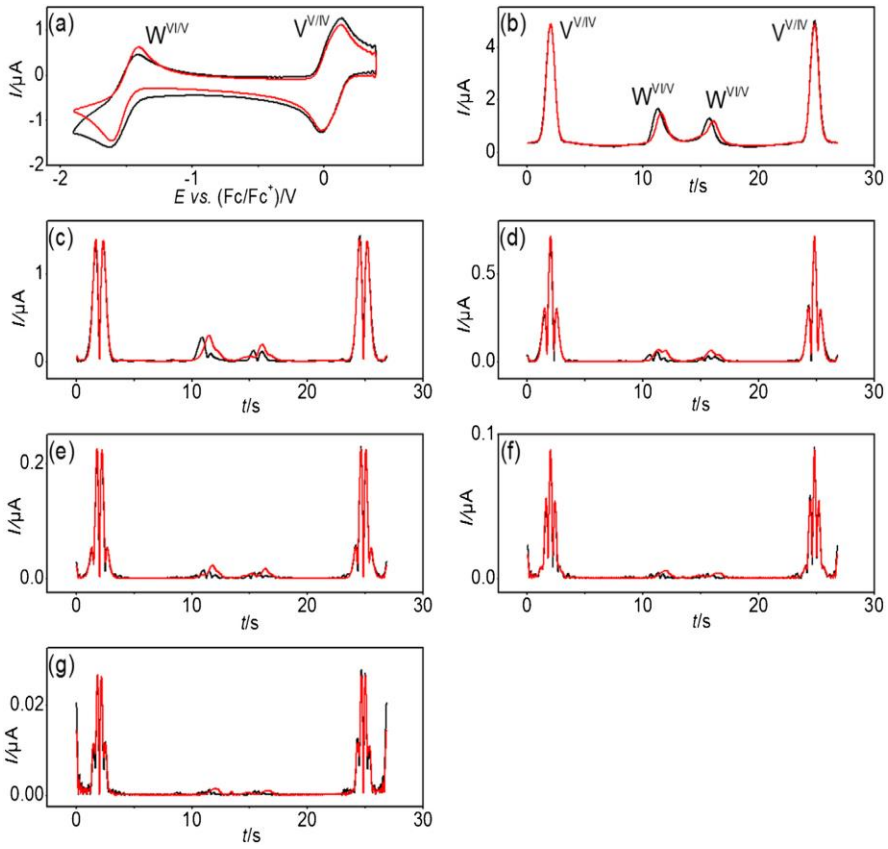

Fig. 4. Comparison of simulated (—) and experimental (—) FTAC voltammetric data obtained for the $[SVW_{11}O_{40}]^{3-/4-/5-}$ processes in DMF containing 1.0 mM $[SVW_{11}O_{40}]^{3-}$ and 0.1 M $[Bu_4N][PF_6]$ at a BDD electrode with $\Delta E = 80$ mV, $f = 9.02$ Hz and $\nu = 0.171$ V s^{-1}. (a) aperiodic DC component, (b-g) 1st to 6th AC harmonic components. To obtain the simulated data, $k^0_V = 0.026$ cm s^{-1}, $\alpha_V = 0.55$, $k^0_W = 0.0008$ cm s^{-1} and $\alpha_W = 0.53$ were used. Other parameters used in the simulations are provided in Table 2.

2.3. Instrumentation and procedures

DC cyclic voltammetric experiments were carried out using a CHI 760E electrochemical workstation (CH Instruments, Texas, USA). Large amplitude FTAC voltammetric experiments were undertaken with a home built instrument [28] using an applied sine wave perturbation with an amplitude (ΔE) of 80 mV and frequency (f) of 9.02 Hz, 27.01 Hz or 68.99 Hz, superimposed onto the DC potential ramp. After data collection, the total DC plus AC current was subjected to Fourier transformation to obtain the power spectrum. After selection of the frequency band of interest, inverse Fourier transformation was used to generate the required DC or AC harmonic components [28–30].

All electrochemical studies were carried out at 22 ± 2 °C using a standard three electrode electrochemical cell. The working electrodes were platinum (Pt, nominal diameter = 1.0 mm), gold (Au, nominal diameter = 1.5 mm), glassy carbon (GC, nominal diameter = 1.0 mm) or BDD (constructed at the University of Warwick, UK, nominal diameter = 1.0 mm) [23]. The BDD electrode was polycrystalline, hydrogen-terminated, degenerately doped above the metallic threshold, lapped to ~ nanometer roughness, and fabricated as described elsewhere [37]. A carbon fiber microdisk electrode (nominal radius = 5 μm) was used for experiments under near-steady-state conditions. The electrochemically effective areas (A) of the macrodisk working electrodes were calculated from analysis of a plot of DC peak current versus the square root of scan rate (v) for the oxidation of 1.0 mM Fc in CH_3CN (0.1 M $[Bu_4N][PF_6]$) using the Randles-Sevcik relationship and the known diffusion coefficient (D) of 2.4×10^{-5} cm^2 s^{-1} for Fc under these conditions [38].

$$I_p = 0.4463nFA\left(\frac{nFDv}{RT}\right)^{1/2} c \quad (3)$$

In Eq. (3), I_p is the oxidation peak current, n is the number of electrons transerred ($n = 1$), c is the bulk concentration, T is the absolute temperature, R is the universal gas constant, F is Faraday's constant and A is the electrode area. The areas of the Pt, Au, GC and BDD macrodisk electrodes determined in this manner were 7.71×10^{-3} cm^2, 1.81×10^{-2} cm^2, 7.45×10^{-3} cm^2 and 8.14×10^{-3} cm^2, respectively. The radius (r) of the carbon fiber microdisk electrode was determined to be 5.0 μm based on the steady-state diffusion limiting current (I_l) for the oxidation of Fc using Eq. (4) and other parameters given above:

$$I_l = 4nFrDc \quad (4)$$

Prior to each voltammetric experiment, the working electrode was polished with an aqueous 0.3 μm alumina slurry on a clean polishing cloth, rinsed with water, sonicated thoroughly in water to remove alumina, rinsed with acetone, and finally dried under nitrogen. Platinum wire was used as the auxiliary and reference

electrodes. The potential of the Pt quasi-reference electrode was calibrated against the IUPAC recommended Fc/Fc^+ process [39]. Before each measurement, the solution was purged with N_2 for at least 5 min to remove O_2 and then the surface of the solution was blanketed with N_2 for the duration of the voltammetric experiment.

2.4. Simulations and AC data analysis

Simulations of FTAC voltammograms were carried out using the MECSim (Monash Electrochemistry Simulator, http://www.garethkennedy.net/MECSim.html) software. This Fortran package uses the expanding spatial grid formulation [40] and is based on the mathematical approach derived by Rudolph [41], with minor variations. The Butler-Volmer theory of electron transfer [24] was used to describe the potential dependence of the electrode kinetics for the simple one-electron transfer reaction given in Eq. (5).

$$O + e^- \rightleftharpoons R\left(E^0, k^0, \alpha\right) \tag{5}$$

where E° is the reversible potential. FTAC voltammetric data obtained from either experiment or simulation in the time domain were converted to the frequency domain to generate the power spectrum [31,32]. Six parameters E°, k°, α, D, R_u and C_{dl} (double layer capacitance) were determined in order to quantitatively define all aspects of the electrode processes. The R_u value was determined experimentally from the *RC* time constant method available with the CHI potentiostat, E° was estimated from the midpoint of the reduction (E_p^{red}) and oxidation (E_p^{ox}) peak potentials in a DC cyclic voltammetric experiment and the D values of $[SVW_{11}O_{40}]^{3-}$ and $[SVW_{11}O_{40}]^{4-}$ were calculated from the reduction peak current of $[SVW_{11}O_{40}]^{3-}$ or the oxidation peak current of $[SVW_{11}O_{40}]^{4-}$ at a GC electrode in DMF using the Randles-Sevcik relationship (see Eq. (3)) [42]. The C_{dl} value was quantified from the background current in the fundamental harmonic component at potentials where faradaic current is absent. In order to define the potential dependence of C_{dl}, a non-linear capacitor model was used, as described elsewhere [43]:

$$C_{dl}(t) = c_0 + c_1E(t) + c_2E^2(t) + c_3E^3(t) + c_4E^4(t) \tag{6}$$

where c_0, c_1, c_2, c_3, and c_4 are the coefficients that determine the degree of nonlinearity of the capacitor and $E(t)$ is time (t) dependent applied potential. The coefficients were determined individually at each frequency. Finally, k° and α values were determined by comparison of the experimental and simulated higher order AC harmonic component data.

In order to simulate the experimental data, a mechanism involving two consecutive one-electron transfer processes (see Eq. (5)) was considered. As it adds considerable complexity to the simulations, the contribution from the thermodynamically

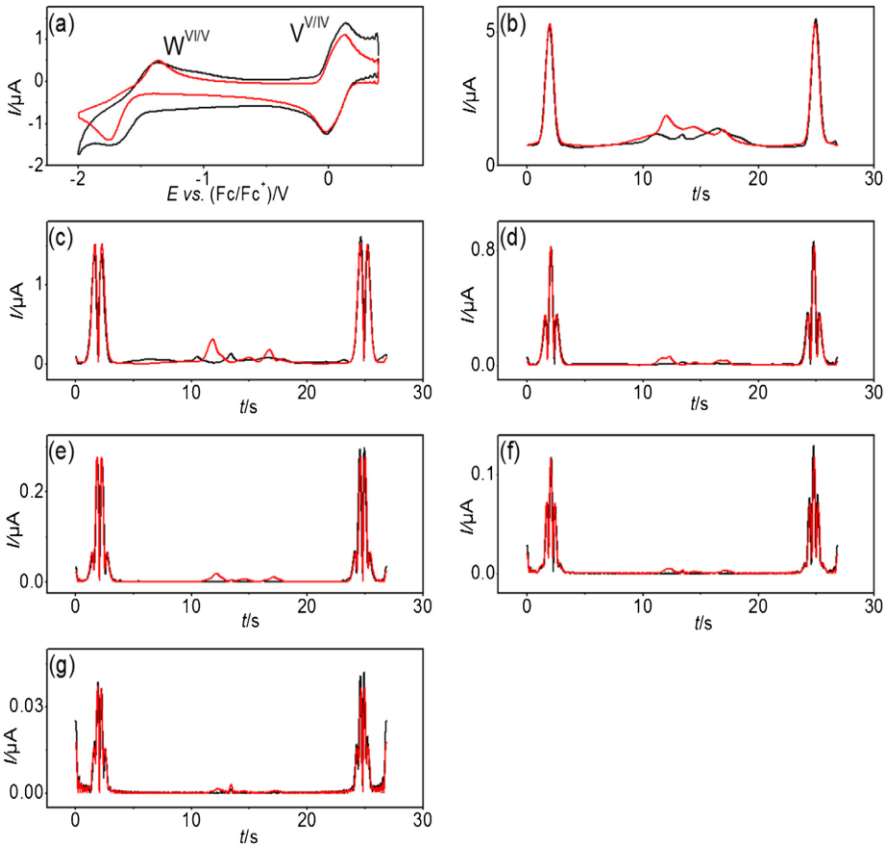

Fig. 5. Comparison of simulated (—) and experimental (—) FTAC voltammetric data obtained for the $[SVW_{11}O_{40}]^{3-/4-/5-}$ processes in DMF containing 1.0 mM $[SVW_{11}O_{40}]^{3-}$ and 0.1 M $[Bu_4N][PF_6]$ at a Pt electrode with $\Delta E = 80$ mV, $f = 9.02$ Hz and $\nu = 0.179$ V s^{-1}. (a) aperiodic DC component, (b-g) 1st to 6th AC harmonic components. To obtain the simulated data, $k_V^0 = 0.08$ cm s^{-1}, $\alpha_V = 0.50$, $k_W^0 = 0.0001$ cm s^{-1} and $\alpha_W = 0.56$ were used. Other parameters used in the simulations are provided in Table 2.

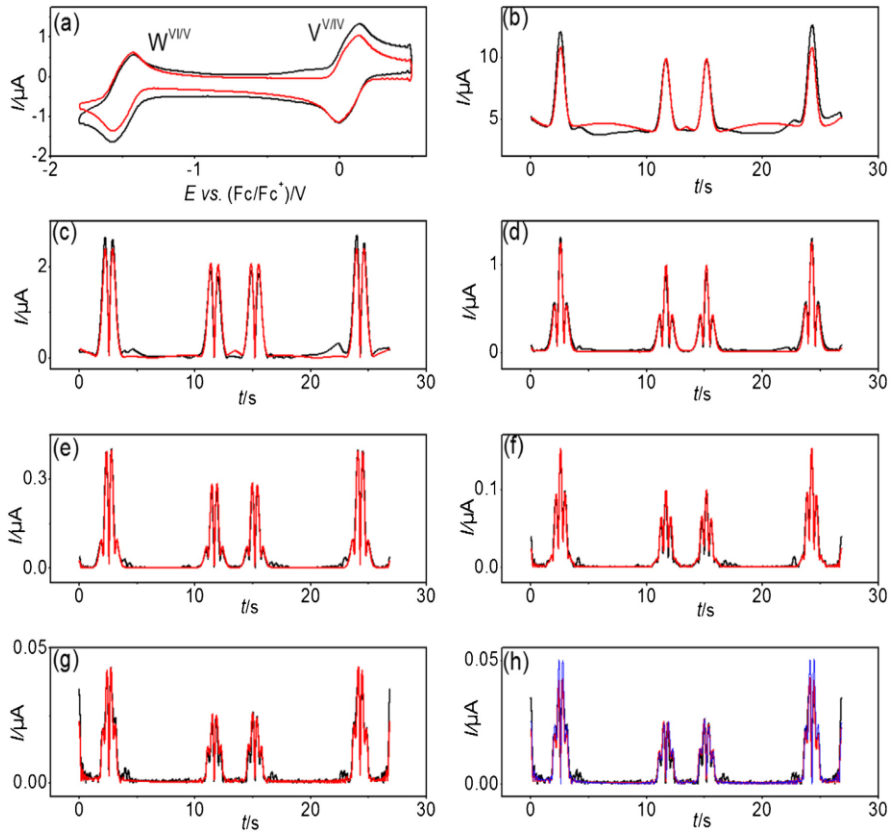

Fig. 6. Comparison of simulated (–) and experimental (–) FTAC voltammetric data obtained for the $[SVW_{11}O_{40}]^{3-/4-/5-}$ processes in DMF containing 1.0 mM $[SVW_{11}O_{40}]^{3-}$ and 0.1 M $[Bu_4N][PF_6]$ at a GC electrode with $\Delta E = 80$ mV, $f = 27.01$ Hz and $\nu = 0.171$ V s^{-1}. (a) aperiodic DC component, (b-g) 1st to 6th AC harmonic components, and (h) simulated 6th harmonic component for the $V^{V/IV}$ process in a reversible case (–). To obtain the simulated data, $k^0_V = 0.20$ cm s^{-1}, $\alpha_V = 0.50$, $k^0_W = 0.050$ cm s^{-1} and $\alpha_W = 0.54$ were used. Other parameters used in the simulations are provided in Table 2.

favourable cross redox reaction between $[SVW_{11}O_{40}]^{3-}$ and $[SVW_{11}O_{40}]^{5-}$ was not considered:

$$[SVW_{11}O_{40}]^{3-} + [SVW_{11}O_{40}]^{5-} \rightleftharpoons 2[SVW_{11}O_{40}]^{4-} (k_f, k_b) \quad (7)$$

where k_f and k_b are the forward and backward rate constants, respectively. In principle, this cross redox reaction could influence the voltammetric data under conditions where both $[SVW_{11}O_{40}]^{3-}$ and $[SVW_{11}O_{40}]^{5-}$ are present in the diffusion layer adjacent to the electrode surface (*e.g.*, during the $W^{VI/V}$ process when $[SVW_{11}O_{40}]^{3-}$ is present in bulk solution). Therefore, in order to avoid complications associated with the redox cross reaction shown in Eq. (7), the oxidation and reduction processes with $[SVW_{11}O_{40}]^{4-}$ (rather than $[SVW_{11}O_{40}]^{3-}$) in the bulk solution (see eqs. 1 and 2) also were investigated.

3. Results and discussion

3.1. DC Cyclic Voltammetric Characterization of the $V^{V/IV}$ and $W^{VI/V}$ processes

Fig. 2a, b and c show DC cyclic voltammetric curves obtained with a scan rate of 0.1 V s^{-1} for $[SVW_{11}O_{40}]^{3-}$ in DMF (0.1 M $[Bu_4N][PF_6]$), $[SVW_{11}O_{40}]^{4-}$ in DMF (0.1 M $[Bu_4N][PF_6]$) and $[SVW_{11}O_{40}]^{3-}$ in DMF (0.5 M $[Bu_4N][PF_6]$) at a GC macrodisk electrode, respectively. In all cases, two well defined, chemically reversible processes separated by approximately 1.58 V are observed. At a supporting electrolyte concentration of 0.1 M, the reversible potentials for the $V^{V/IV}$ and $W^{VI/V}$ processes, E^0_V, and E^0_W, are 0.050 and −1.525 V (vs. Fc/Fc^+), respectively, while at a supporting electrolyte concentration of 0.5 M, E^0_V and E^0_W are 0.100 V and −1.460 V, respectively. The positive E° shift and decreased potential gap between the $V^{V/IV}$ and $W^{VI/V}$ processes (*i.e.*, ΔE°) are in agreement with previous studies [44] and are caused by the stronger interaction of the supporting electrolyte cation with the reduced forms of the POM (*e.g.*, $[SVW_{11}O_{40}]^{5-}$) compared to the oxidized form (*e.g.*, $[SVW_{11}O_{40}]^{3-}$).

A summary of the E° and the peak-to-peak separation ΔE_p ($= E_p^{ox} - E_p^{red}$) values determined by DC cyclic voltammetry at all of the investigated electrode materials with a supporting electrolyte concentration of 0.1 M are provided in Table 1. In general, the ΔE_p values associated with the $V^{V/IV}$ process are much smaller than the $W^{VI/V}$ one, qualitatively indicating that the former process is kinetically faster than the latter (see below), assuming a simple electron transfer mechanism applies. The $(\Delta E_p)_V$ values at all electrodes are slightly larger than what is theoretically predicted for a reversible process (56.4 mV) [24]. However, the $V^{V/IV}$ process at these electrodes is considered reversible at a scan rate of 0.1 V s^{-1} in DC cyclic voltammetry, with the difference between the $(\Delta E_p)_V$ values and the theoretically predicted values predominantly being attributed to uncompensated resistance (IR_u effect). Finally, diffusion coefficients (D) calculated from the Randles-Sevcik relationship (see Eq. (3)) [42] at a GC macrodisk electrode

(Fig. 2) were found to be 2.8×10^{-6} cm^2 s^{-1} for $[SVW_{11}O_{40}]^{3-}$ (0.1 M $[Bu_4N][PF_6]$), 2.9×10^{-6} cm^2 s^{-1} for $[SVW_{11}O_{40}]^{4-}$ (0.1 M $[Bu_4N][PF_6]$) and 2.1×10^{-6} cm^2 s^{-1} for $[SVW_{11}O_{40}]^{3-}$ (0.5 M $[Bu_4N][PF_6]$).

Near steady-state microdisk voltammetry was carried out to demonstrate that the one-electron reduced form of the POM ($[SVW_{11}O_{40}]^{4-}$) had been successfully synthesized (see the Experimental Section). A near steady-state voltammogram obtained from 1.2 mM $[SVW_{11}O_{40}]^{3-}$ (Fig. 3a) at a 5 μm radius carbon fiber microdisk electrode shows a zero-current region at the initial potential of about 0.2 V and contains two reduction processes of equal magnitude. Fig. 3b shows a near steady-state voltammogram obtained from 1.0 mM $[SVW_{11}O_{40}]^{4-}$ with the zero-current region now lying between the two processes, again, both having equal limiting current magnitudes. This observation confirms that $[SV^{V}W_{11}O_{40}]^{3-}$ has been reduced to $[SV^{IV}W_{11}O_{40}]^{4-}$ by $[Bu_4N][BH_4]$. These near steady-state voltammograms give half wave potential ($E_{1/2}$) values of 0.050 V and 1.520 V for the $V^{V/IV}$ and $W^{VI/V}$ processes, respectively, which are in good agreement with the E° values estimated from transient DC cyclic voltammetry (see Table 1).

3.2. Large Amplitude FTAC Voltammetry in DMF (0.1 M $[Bu_4N][PF_6]$)

The k° values associated with the $V^{V/IV}$ (k^0_V) and $W^{VI/V}$ (k^0_W) processes in DMF containing $[SVW_{11}O_{40}]^{3-}$ and 0.1 M $[Bu_4N][PF_6]$ at BDD, Pt, GC and Au electrodes were determined by FTAC voltammetry using a sine wave perturbation with $\Delta E = 80$ mV and $f = 9.02$ Hz or 27.01 Hz. Parameters used in the simulation-experiment comparisons are provided in Table 2. In general, the simulated data is in excellent agreement with the experimental data for the more positive $V^{V/IV}$ process at all electrode materials when the bulk concentration of $[SVW_{11}O_{40}]^{3-}$ is 1.0 mM, as is demonstrated in Figs. 4–7 .

The capacitance model used in the simulations is based on a simple RC circuit, which predicts that the coefficients in Eq. (6) (*i.e.*, c_0, c_1 etc.) are independent of frequency. In practice, the coefficients are slightly frequency-dependent [45], and were determined individually for each frequency examined to achieve the excellent simulation-experiment fits of the background at all frequencies studied (see Fig. 6).

Shown in Fig. 4 is a comparison of the simulated and experimental data obtained at a BDD electrode. Since the kinetics of the $V^{V/IV}$ process are fast, the DC component and the first to sixth AC harmonic components are all well-defined and can be quantitatively analysed to give k^0_V and α_V values of 0.026 cm s^{-1} and 0.55, respectively. However, as also demonstrated in Fig. 4, at BDD, the kinetics of the $W^{VI/V}$ process are much slower than the $V^{V/IV}$ process, and as a result, the signal-to-background ratios associated with the second and higher order harmonics are very poor. Thus, for this process, only the DC and 1st harmonic components were used in the experiment-simulation comparison

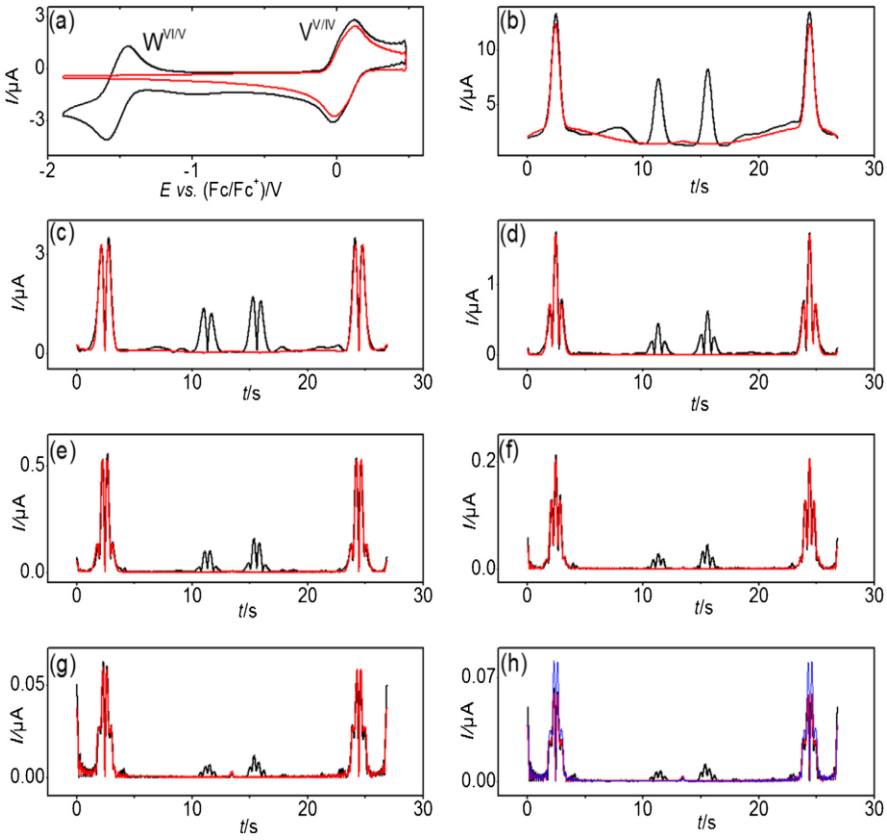

Fig. 7. Comparison of simulated (–) and experimental (–) FTAC voltammetric data obtained for the $[SVW_{11}O_{40}]^{3-/4-}$ process in DMF containing 1.0 mM $[SVW_{11}O_{40}]^{3-}$ and 0.1 M $[Bu_4N][PF_6]$ at an Au electrode with $\Delta E = 80$ mV, $f = 9.02$ Hz and $\nu = 0.178$ V s^{-1}. (a) aperiodic DC component, (b-g) 1st to 6th AC harmonic components, and (h) simulated 6th harmonic component for the $V^{V/IV}$ process in a reversible case (–). To obtain the simulated data, $k^0_V = 0.10$ cm s^{-1}, $\alpha_V = 0.50$. Other parameters used in the simulations are provided in Table 2.

and k^0_W and α_W values were estimated approximately to be 0.0008 cm s^{-1} and 0.53, respectively.

As shown in Fig. 5, similar results were obtained at Pt; the $V^{V/IV}$ process is fast and well-defined, with k^0_V and α_V estimated to be 0.08 cm s^{-1} and 0.50 (this process is close to reversible and hence is relatively insenstive to α_V), respectively, while the $W^{VI/V}$ process is slow and gives rise to poorly defined AC components. For this process, approximate k^0_W and α_W values of 0.0001 cm s^{-1} and 0.56, respectively, were estimated from the DC component data. In general, the agreement between the simulated and experimental data for the AC harmonic components associated with the $W^{VI/V}$ process are poor at BDD and Pt electrodes, which indicates that there are complexities associated with this process at these electrode materials which are not fully accounted for in simulations based on a simple electron transfer mechanism and the application of Butler-Volmer kinetics.

At a GC electrode (see Fig. 6), the k^0_V value is too fast to measure at a frequency of 9.02 Hz (*i.e.*, it is reversible). Therefore, a higher frequency (f = 27.01 Hz) AC perturbation was used to shorten the time scale of the measurement so that a higher kinetic sensitivity could be achieved. k^0_V and k^0_W values were estimated to be 0.20 and 0.050 cm s^{-1}, respectively. α_V was assumed to be 0.50 since the method is not sensitive to this parameter under these conditions (see explanation above) and α_W value was estimated to be 0.54. Finally, at an Au electrode (see Fig. 7), the k^0_V value was found to be 0.10 cm s^{-1} and α_V was assumed to be 0.50, while for the $W^{VI/V}$ process, the AC reduction and oxidation peaks in the harmonic components are highly asymmetric, which is inconsistent with theoretical predictions based on a simple electron transfer mechanism. In light of the complexities observed at BDD, Pt and Au electrodes, all further discussion on the $W^{VI/V}$ process will exclusively relate to the results obtained at the GC electrode.

FTAC voltammetric data were also acquired with a lower bulk concentration of $[SVW_{11}O_{40}]^{3-}$, 0.20 mM, in order to lessen the influence of the iR_u effect. The results obtained at BDD, Pt, GC, Au electrodes in DMF (0.1 M $[Bu_4N][PF_6]$) at the lower concentration are also summarized in Table 2. Comparisons of experimental and simulated data are presented in Figs. S1 to S4 in the Supporting Information. As expected, since the iR_u drop has been correctly accommodated in all simulations, the determined k° values are essentially independent of the $[SVW_{11}O_{40}]^{3-}$ concentration. This concentration independence also implies that contributions from adsorption or non-unity order reactions, such as shown in Eq. (7), are not significant.

In order to assess the influence of the thermodynamically favourable cross reaction (see Eq. (7)) on the voltammetric data, a series of simulations were performed, as is shown in Fig. S5. The forward reaction was assumed to be diffusion-controlled due to the presence of a large driving force. A value of 1×10^{10} M^{-1} s^{-1} was derived for k_f from the steady-state Smoluchowski equation [46], which requires use of a k_b value of 2×10^{-17} M^{-1} s^{-1} as determined from the equilibrium constant for Eq. (7) based on the known ΔE°

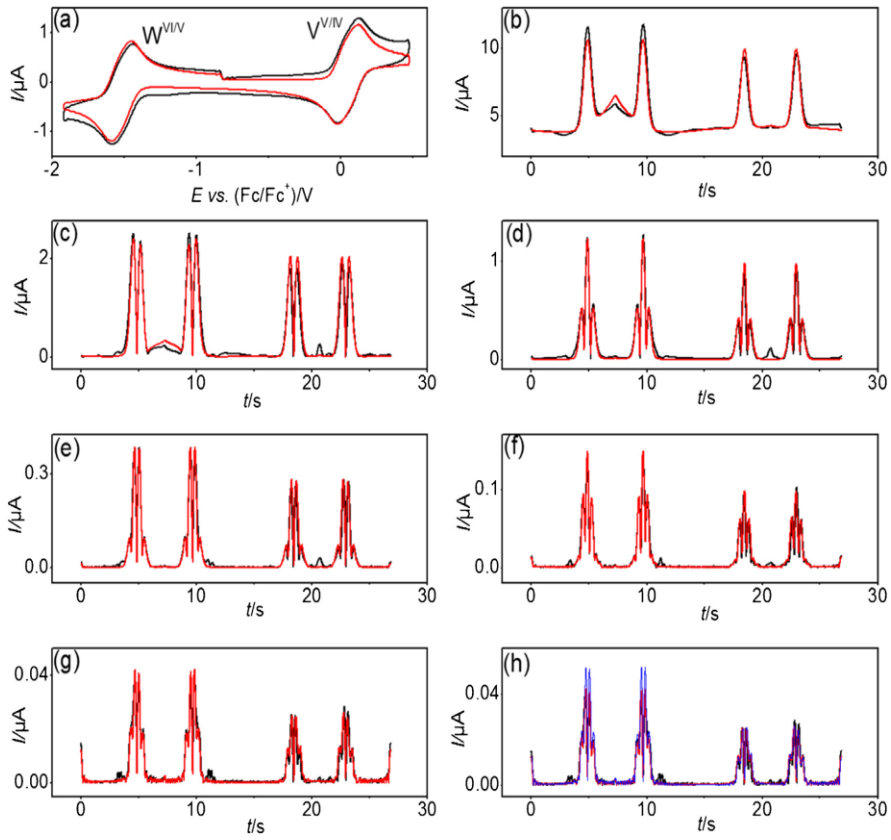

Fig. 8. Comparison of simulated (–) and experimental (–) FTAC voltammetric data obtained for the $V^{IV/V}$ and $W^{VI/V}$ processes processes in DMF containing 1.0 mM $[SVW_{11}O_{40}]^{4-}$ and 0.1 M $[Bu_4N][PF_6]$ at a GC electrode with ΔE = 80 mV, f = 27.01 Hz and ν = 0.179 V s^{-1}. (a) aperiodic DC component, (b-g) 1st to 6th AC harmonic components, and (h) simulated 6th harmonic component for the $V^{V/IV}$ process in a reversible case (–). To obtain the simulated data, k^0_V = 0.18 cm s^{-1}, α_V = 0.50, k^0_W = 0.055 cm s^{-1} and α_W = 0.54 were used. Other parameters used in the simulations are provided in Table 3.

Table 3
Electrode kinetic parameters derived for the $V^{IV/V}$ and $W^{VI/V}$ processes at the GC electrode in DMF containing $[SVW_{11}O_{40}]^{4-}$ and 0.1 M $[Bu_4N][PF_6]$.[a]

c (mM)	E^0_V (V)[b]	E^0_W (V)[b]	R_u (Ω)	C_{dl} (c_0, c_1, c_2, c_3, c_4) (μF cm^{-2})	k^0_V (cm s^{-1})	α_V	k^0_W (cm s^{-1})	α_W
1.0	0.050	−1.525	1250	52.7, −5.0, −3.3, 3.3, 2.5	0.18	0.50[c]	0.055	0.54[d]
0.20	0.050	−1.525	1200	30.0, 4.5, 14.2, 1.0, −1.9	0.20	0.50[c]	0.050	0.54[d]

[a] Other parameters used in the simulations are: $A_{GC} = 7.45 \times 10^{-3}$ cm^2, $\Delta E = 80$ mV, D ($[SVW_{11}O_{40}]^{3-}$) = 2.8×10^{-6} cm^2 s^{-1}, D ($[SVW_{11}O_{40}]^{4-}$) = D ($[SVW_{11}O_{40}]^{5-}$) = 2.9×10^{-6} cm^2 s^{-1}, $T = 295$ K, $v = 0.179$ V s^{-1} and $f = 27.01$ Hz.
[b] vs. Fc/Fc^+.
[c] Assumed.
[d] Calculated.

values. Evidently, only minor differences are predicted in the $W^{VI/V}$ process (with a range of k^0_W values) when the cross redox reaction is considered, suggesting that the impact of this second order reaction on the voltammetric characteristics is insignificant under the conditions given in Fig. S5.

In order to confirm these predictions, the $W^{VI/V}$ reaction was characterized at a GC electrode with $[SVW_{11}O_{40}]^{4-}$ rather than $[SVW_{11}O_{40}]^{3-}$ initially present in bulk solution (Fig. 8). The cross-reaction cannot occur under these conditions. Again, using an AC perturbation frequency of 27.01 Hz, k^0_V, α_V, k^0_W and α_W values were determined to be 0.18 cm s^{-1}, 0.50, 0.055 cm s^{-1} and 0.54, respectively (see Table 3), which are essentially identical to those previously determined with $[SVW_{11}O_{40}]^{3-}$ in the bulk solution (see Table 2). Evidently, the cross redox reaction does not need to be considered in the simulations when determining the electrode kinetics of the $V^{IV/V}$ and $W^{VI/V}$ processes. Finally, FTAC voltammetric data were also acquired using a lower $[SVW_{11}O_{40}]^{4-}$ concentration of 0.20 mM at a GC electrode. Comparisons of experimental and simulated data are presented in Fig. S6 in the Supporting Information. Again, it is verified that the IR_u drop has been correctly accommodated in simulations, since the determined k° values are essentially independent of the $[SVW_{11}O_{40}]^{4-}$ concentration.

The results in Tables 2 and 3 suggest that the k^0_V values are significantly dependent on the identity of the electrode material. For instance, k^0_V was found to be lower at the BDD electrode than at the Pt and Au electrodes. This is consistent with the predictions of Marcus theory [47], where the heterogeneous rate constant of a non-adiabatic electron transfer process is assumed to be proportional to the density of states (DOS) of the electrode material. On this basis, the electron transfer kinetics obtained at BDD (DOS = 6.3×10^{20} cm^{-3} eV^{-1}) [23] are expected to be slower than those obtained at Pt (DOS = 1.46×10^{23} cm^{-3} eV^{-1}) [23] or Au (DOS = 1.7×10^{22} cm^{-3} eV^{-1}) [23,48]. Although the DOS of Pt is an order of magnitude larger than that of Au, comparable k° values were obtained since the extra DOS of Pt is due to the d-shell electrons, which interact very weakly with external fields, and therefore contribute less to the rate constant. However, the predicted dependence on DOS does not apply universally for the $V^{V/IV}$ process in DMF. Notably, even though the DOS value for the highly heterogeneous GC electrode is not well-defined, the DOS of graphitic carbon is of the order of 10^{20} cm^{-3} eV^{-1} [35], which is much lower than that of metal electrodes (of the order of 10^{22} cm^{-3} eV^{-1}) [48,49]. On this basis, it may be assumed that the DOS value of GC is likely to be significantly lower than for metal electrodes, yet higher k^0_V values are found at a GC electrode than at Au or Pt electrodes. Clearly, the DOS value is not the sole origin of the observed electrode material dependent kinetics. Plausibly, surface functional groups on a GC electrode may also play critical roles in electron transfer processes [50] involving highly charged species, such as $[SVW_{11}O_{40}]^{3-}$.

Although k^0_W cannot be determined accurately due to the poor simulation-experiment fits achieved for the $W^{VI/V}$ process at BDD, Pt and Au electrodes, it is still possible to draw the conclusion that the $W^{VI/V}$ process is kinetically much slower than the $V^{IV/V}$ process with all electrode materials. The strong electrode material dependence of k^0_W, which is inconsistent with the predictions based on DOS with an outer sphere process, may be the indication of an inner sphere electron transfer process. This hypothesis is consistent with the larger k^0_W values measured at GC, which, as discussed above is likely to have surface functional groups which facilitate a relatively facile electron-transfer process compared to BDD, Au or Pt. However, further studies are needed to investigate the complexity detected in the $W^{VI/V}$ process before a detailed understanding of the origin of this slow electron transfer for the $W^{VI/V}$ process becomes available.

3.3. Large Amplitude FTAC Voltammetry in DMF (0.5 M $[Bu_4N][PF_6]$)

The influence of supporting electrolyte concentration (ionic strength) on k° values was also investigated. Again, due to the complexities associated with the $W^{VI/V}$ process at BDD, Pt and Au, only the $V^{V/IV}$ process was investigated at all electrode materials, while both processes were investigated at the GC electrode.

Changing the concentration of $[Bu_4N][PF_6]$ from 0.1 M to 0.5 M was found to have a significant influence on k° (see Table 4). At a GC

Table 4
Electrode kinetic parameters derived for the $[SVW_{11}O_{40}]^{3-/4-/5-}$ processes in DMF containing 1.0 mM $[SVW_{11}O_{40}]^{3-}$ and 0.5 M $[Bu_4N][PF_6]$.[a]

Electrode	E^0_V (V)[b]	E^0_W (V)[b]	Ru (Ω)	C_{dl} (c_0, c_1, c_2, c_3, c_4) (μF cm^{-2})	k^0_V (cm s^{-1})	α_V	k^0_W (cm s^{-1})	α_W
GC	0.090	−1.320	370	28.7, 9.3, 3.0, −1.8, −0.8	≥0.50	0.50[c]	0.10	0.54[d]
BDD	0.090	[e]	310	7.4, −1.7, 20.4, 6.0, −80.8	0.009	0.50[d]	[e]	[e]
Pt	0.100	[e]	330	23.2, −12.6, −24.9, 59.2, 112.0	0.035	0.45[d]	[e]	[e]
Au	0.100	[e]	350	19.3, −2.7, −11.7, 7.3, 25.8	0.08	0.45[d]	[e]	[e]

[a] Other parameters used in the simulations are: $A_{BDD} = 8.14 \times 10^{-3}$ cm^2, $A_{Pt} = 7.71 \times 10^{-3}$ cm^2, $A_{GC} = 7.45 \times 10^{-3}$ cm^2, $A_{Au} = 1.81 \times 10^{-2}$ cm^2, $\Delta E = 80$ mV, D ($[SVW_{11}O_{40}]^{3-}$) = 2.8×10^{-6} cm^2 s^{-1}, D ($[SVW_{11}O_{40}]^{4-}$) = D ($[SVW_{11}O_{40}]^{5-}$) = 2.9×10^{-6} cm^2 s^{-1}, $T = 295$ K, $v_{BDD,\ Pt\ and\ Au} = 0.104$ V s^{-1}, $v_{GC} = 0.164$ V s^{-1}, $f_{GC} = 66.98$ Hz and $f_{BDD,\ Pt\ and\ Au} = 9.02$ Hz.
[b] vs. Fc/Fc^+.
[c] Assumed.
[d] Calculated.
[e] Not determined.

electrode, the $V^{V/IV}$ process is very fast, and for this reason a higher frequency of 66.98 Hz was used for electrode kinetics evaluation with 0.5 M $[Bu_4N][PF_6]$ as the supporting electrolyte. As shown in Fig. 9, excellent agreement between theoretical and experimental data is obtained with $k_V^0 = 0.50\,cm\,s^{-1}$ and α_V assumed to be 0.50. However, use of a k_V^0 value of $0.50\,cm\,s^{-1}$ produces simulated data that are indistinguishable from that predicted for a reversible process in the first five harmonic components under these conditions, with a small departure from reversibility only becoming evident in the kinetically more sensitive sixth harmonic component. In order to measure the k_V^0 value reliably, in principle, an even higher frequency AC perturbation is needed to shorten the time-scale of the measurement. Unfortunately, the impact of the iR_u effect becomes very significant under very high frequency conditions and consequently the quality of the higher order AC harmonic data at frequencies greater than 66.98 Hz was diminished. Therefore, $k_V^0 \geq 0.50\,cm\,s^{-1}$ is the preferred form of presentation of the result.

As shown in Table 4, at a GC electrode, the k_V^0 and k_W^0 values increase from $0.20\,cm\,s^{-1}$ and $0.050\,cm\,s^{-1}$ to $\geq 0.5\,cm\,s^{-1}$ and $0.10\,cm\,s^{-1}$, respectively, upon increasing the supporting electrolyte concentration from 0.1 M to 0.5 M. By contrast, at BDD and Pt electrodes (see Figs. S7 and S8, respectively), the k_V^0 value decreases from $0.026\,cm\,s^{-1}$ and $0.08\,cm\,s^{-1}$ to $0.009\,cm\,s^{-1}$ and $0.035\,cm\,s^{-1}$, respectively, when the supporting electrolyte concentration is increased from 0.1 M to 0.5 M. Finally, at an Au electrode (see Fig. S9), the k_V^0 value was found to be relatively insensitive to the supporting electrolyte concentration, with values of $0.10\,cm\,s^{-1}$ and $0.08\,cm\,s^{-1}$ at 0.1 M and 0.5 M $[Bu_4N][PF_6]$, respectively.

When the heterogeneous electron transfer process of a highly charged species is coupled with ion-pairing, the process can be described by a square-scheme mechanism, which can lead to measured k° values apparently increasing with an increase in the supporting electrolyte concentration [22]. However, this explanation alone cannot account for the electrode material dependence of the k° values on $[Bu_4N][PF_6]$ concentration, since the effect of ion pairing is electrode material independent.

Another factor that could contribute to the electrolyte concentration dependence is the double layer, which is a function of electrolyte concentration and potential relative to the point of zero charge (PZC) [24]. At the GC electrode, increasing the concentration of $[Bu_4N][PF_6]$ increases k_V^0, which is what would be expected if the $V^{V/IV}$ process is in the negative potential region with respect to the PZC. At Pt and BDD, increasing the concentration of $[Bu_4N][PF_6]$ decreases k_V^0, which is what would be expected if the $V^{V/IV}$ process is in the positive potential region with respect to the PZC. At an Au electrode, the k_V^0 value is relatively insensitive to the supporting electrolyte concentration in the 0.1 to 0.5 M range, implying that the $V^{V/IV}$ process might be located very close to the PZC. The $W^{VI/V}$ process is in the highly negative

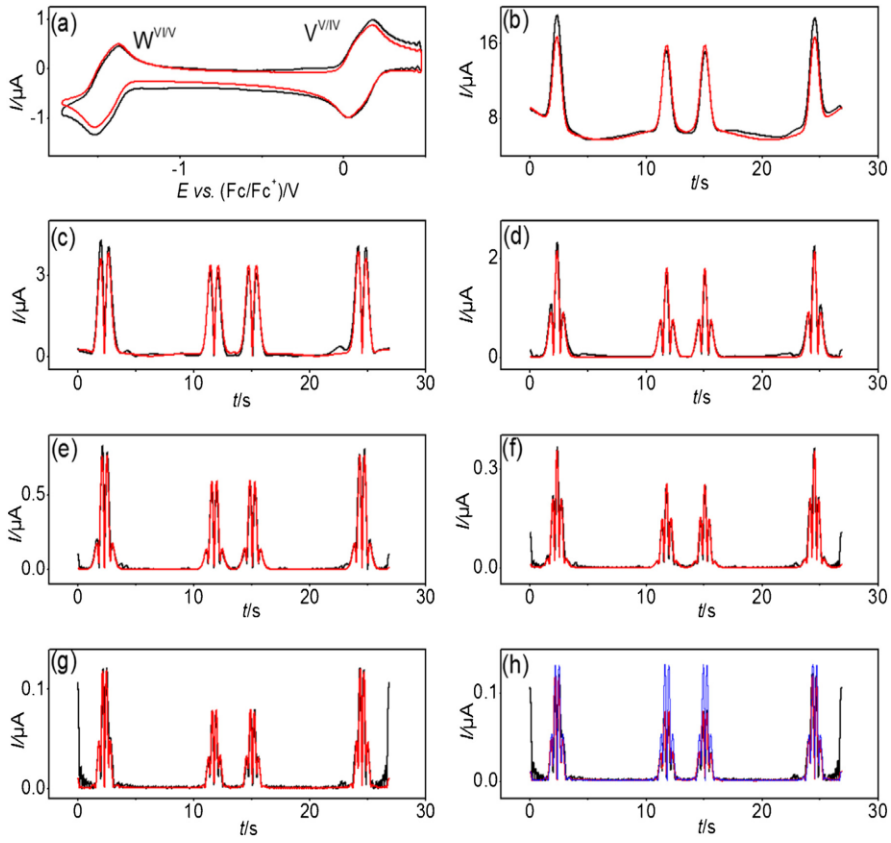

Fig. 9. Comparison of simulated (—) and experimental (▬) FTAC voltammetric data obtained for the $[SVW_{11}O_{40}]^{3-/4-/5-}$ processes in DMF containing 1.0 mM $[SVW_{11}O_{40}]^{3-}$ and 0.5 M $[Bu_4N][PF_6]$ at a GC electrode with $\Delta E = 80$ mV, $f = 66.98$ Hz and $\nu = 0.164\,V\,s^{-1}$. (a) aperiodic DC component, (b-g) 1st to 6th AC harmonic components, and (h) simulated 6th harmonic for the $V^{V/IV}$ and $W^{VI/V}$ processes in a reversible case (▬). To obtain the simulated data, $k_V^0 \geq 0.50\,cm\,s^{-1}$, $\alpha_V = 0.50$, $k_W^0 = 0.10\,cm\,s^{-1}$ and $\alpha_W = 0.54$ were used. Other parameters used in the simulations are provided in Table 4.

potential region, which is almost certainly positioned on the negative side of PZC. The observed enhancement of k^0_W at the GC electrode in the presence of higher concentration of $[Bu_4N][PF_6]$ is therefore consistent with the prediction based on the double layer effect. The apparently sluggish nature of the $W^{VI/V}$ process, which was not observed previously with the un-substituted $[\alpha\text{-}SiW_{12}O_{40}]^{4-}$ in high ionic strength aqueous media [23], could also be attributed to the double layer effect, which could significantly suppress the kinetics. Unfortunately, in the absence of knowledge of the PZC of each electrode material under our experimental conditions, corrections for the double layer effect cannot be made and these explanations suggested are necessarily tentative.

4. Conclusions

The electrode kinetics associated with the $[SVW_{11}O_{40}]^{3-/4-/5-}$ processes in DMF containing $[Bu_4N][PF_6]$ have been quantified at GC, BDD, Pt and Au electrodes using large amplitude FTAC voltammetry. The $V^{V/IV}$ process was found to occur at potentials approximately 1.58 V more positive than the $W^{VI/V}$ process, and the former process was found to be considerably faster than the latter at all electrode materials. Excellent fits between simulated and experimental FTAC voltammetric data were achieved at all electrode materials for the relatively fast $V^{V/IV}$ process, and at a $[Bu_4N][PF_6]$ concentration of 0.1 M, the k^0_V value was found to increase in the order BDD < Pt ≈ Au < GC. By contrast, at all electrode materials except GC, relatively poor simulation-experiment fits based on a quasi-reversible process and Butler-Volmer electron transfer kinetics were found for the considerably slower $W^{VI/V}$ process, indicating that additional complexities are associated with this process at BDD, Pt and Au electrodes. The thermodynamically favourable cross reaction between $[SVW_{11}O_{40}]^{3-}$ and $[SVW_{11}O_{40}]^{5-}$ was shown by simulation to have a negligible influence on the voltammetric characteristics of the $W^{VI/V}$ process. This conclusion was confirmed experimentally by investigating this process at a GC electrode with $[SVW_{11}O_{40}]^{4-}$ present in the bulk solution. Finally, changing the supporting electrolyte ($[Bu_4N][PF_6]$) concentration from 0.1 to 0.5 M resulted in an increase in the electrode kinetics of the $V^{V/IV}$ and $W^{VI/V}$ processes at a GC electrode, while at BDD, Pt and Au, the kinetics of the former process were found to decrease to different degrees. The electrode materials dependence of the k^0_V values were not found to fully correlate with their DOS values, implying that other factors such as potential dependent double layer effects and functional groups on a GC electrode surface may play critical roles. Further investigations will focus on elucidating the influence of the solvent and supporting electrolyte on the k° values in order to gain a better understanding of the kinetics associated with electron transfer reactions involving polyoxometalates.

Appendix A. Supplementary data

Supplementary data associated with this article can be found, in the online version, at http://dx.doi.org/10.1016/j.electacta.2016.03.107.

Figures S1 to S4 provide a comparison of the simulated and experimental FTAC voltammograms obtained from 0.20 mM $[SVW_{11}O_{40}]^{3-}$ in DMF (0.1 M $[Bu_4N][PF_6]$) at BDD, Pt, GC and Au electrodes. Figure S5 is a theoretical study of the influence of the cross redox reaction on the voltammetric characteristics as a function of k^0_W. Figure S6 provides a comparison of the simulated and experimental FTAC voltammograms obtained from 0.20 mM $[SVW_{11}O_{40}]^{4-}$ in DMF (0.1 M $[Bu_4N][PF_6]$) at a GC electrode. Figures S7 to S9 provide a comparison of the simulated and experimental FTAC voltammograms obtained from 1.0 mM $[SVW_{11}O_{40}]^{3-}$ in DMF (0.5 M $[Bu_4N][PF_6]$) at BDD, Pt, and Au electrodes.

References

[1] U. Kortz, A. Mueller, J. van Slageren, J. Schnack, N.S. Dalal, M. Dressel, Polyoxometalates: Fascinating structuresunique magnetic properties, Coord. Chem. Rev. 253 (2009) 2315–2327.
[2] T. Okuhara, A. Kasai, N. Hayakawa, M. Misono, Y. Yoneda, The important role of the bulk of 12-tungustophosphoric acid in the catalytic dehydration of alcohols to olefins, Chem. Lett. (1981) 391–394.
[3] K. Unoura, N. Tanaka, Comparative study of the electrode reactions of 12-molybdosilicate and 12-molybdophosphate, Inorg. Chem. 22 (1983) 2963–2964.
[4] M. Misono, N. Nojiri, Recent progress in catalytic technology in Japan, Appl. catal. 64 (1990) 1–30.
[5] K. Na, T. Okuhara, M. Misono, Catalysis by heteropoly compounds, J. Catal. 170 (1997) 96–107.
[6] C.L. Hill, C.M. Prosser-McCartha, Homogeneous catalysis by transition metal oxygen anion clusters, Coord. Chem. Rev. 143 (1995) 407–455.
[7] J.T. Rhule, C.L. Hill, D.A. Judd, R.F. Schinazi, Polyoxometalates in medicine, Chem. Rev. 98 (1998) 327–358.
[8] M.T. Pope, A. Müller, Polyoxometalate chemistry: an old field with new dimensions in several disciplines, Angew. Chem. Int. Ed. 30 (1991) 34–48.
[9] D.E. Katsoulis, A survey of applications of polyoxometalates, Chem. Rev. 98 (1998) 359–388.
[10] T. Yamase, Photo-and electrochromism of polyoxometalates and related materials, Chem. Rev. 98 (1998) 307–326.
[11] D.L. Long, R. Tsunashima, L. Cronin, Polyoxometalates: building blocks for functional nanoscale systems, Angew. Chem. Int. Ed. 49 (2010) 1736–1758.
[12] N. Anwar, M. Vagin, F. Laffir, G. Armstrong, C. Dickinson, T. McCormac, Transition metal ion-substituted polyoxometalates entrapped in polypyrrole as an electrochemical sensor for hydrogen peroxide, Analyst 137 (2012) 624–630.
[13] C. Li, Y. Zhang, K.P. O'Halloran, J. Zhang, H. Ma, Electrochemical behavior of vanadium-substituted Keggin-type polyoxometalates in aqueous solution, J. Appl. Electrochem. 39 (2009) 421–427.
[14] B.R. Limoges, R.J. Stanis, J.A. Turner, A.M. Herring, Electrocatalyst materials for fuel cells based on the polyoxometalates $[PMo_{(12-n)}V_nO_{40}]^{(3+n)-}$ (n = 0–3), Electrochim. Acta 50 (2005) 1169–1179.
[15] M. Sadakane, E. Steckhan, Electrochemical Properties of Polyoxometalates as Electrocatalysts, Chem. Rev. 98 (1998) 219–238.
[16] C. Baffert, S.W. Feldberg, A.M. Bond, D.-L. Long, L. Cronin, pH-Dependence of the aqueous electrochemistry of the two-electron reduced α-$[Mo_{18}O_{54}(SO_3)]$ sulfite Dawson-like polyoxometalate anion derived from its triethanolammonium salt, Dalton Trans. (2007) 4599–4607.
[17] A.W. Mariotti, J. Xie, B.F. Abrahams, A.M. Bond, A.G. Wedd, Synthesis and voltammetry of $[Bmim]_4[\alpha\text{-}S_2W_{18}O_{62}]$ and related compounds: Rapid precipitation and dissolution of reduced surface films, Inorg. Chem. 46 (2007) 2530–2540.
[18] S. Himeno, M. Takamoto, T. Ueda, Synthesis, characterisation and voltammetric study of a β-Keggin-type $[PW_{12}O_{40}]^{3-}$ complex, J. Electroanal. Chem. 465 (1999) 129–135.
[19] J. Zhang, A.M. Bond, D.R. MacFarlane, S.A. Forsyth, J.M. Pringle, A.W. Mariotti, A. F. Glowinski, A.G. Wedd, Voltammetric studies on the reduction of polyoxometalate anions in ionic liquids, Inorg. Chem. 44 (2005) 5123–5132.
[20] K.K. Kasem, Electrochemical behavior of sodium 12-tungstodicobaltoate in aqueous and mixed solvent electrolytes, Electrochim. Acta 41 (1996) 205–211.
[21] M. Takamoto, T. Ueda, S. Himeno, Solvation effect of Li^+ on the voltammetric properties of $[PMo_{12}O_{40}]^{3-}$ in binary solvent mixtures, J. Electroanal. Chem. 521 (2002) 132–136.
[22] J. Li, A.M. Bond, J. Zhang, Probing electrolyte cation effects on the electron transfer kinetics of the $[\alpha\text{-}SiW_{12}O_{40}]^{4-/5-}$ and $[\alpha\text{-}SiW_{12}O_{40}]^{5-/6-}$ processes using a boron-doped diamond electrode, Electrochim. Acta 178 (2015) 631–637.
[23] K. Bano, J. Zhang, A.M. Bond, P.R. Unwin, J.V. Macpherson, Diminished electron transfer kinetics for $[(Ru(NH_3)_6]^{3+/2+}$, $[\alpha\text{-}SiW_{12}O_{40}]^{4-/5-}$ and $[\alpha\text{-}SiW_{12}O_{40}]^{5-/6-}$ processes at boron doped diamond electrodes, J. Phys. Chem. C 119 (2015) 12464–12472.
[24] A.J. Bard, L.R. Faulkner, Electrochemical methods: Fundamentals and applications, 2nd, Wiley and Sons, Hoboken, 2001.
[25] D.K. Gosser, Cyclic voltammetry: simulation and analysis of reaction mechanisms, VCH, New York, 1993.
[26] K. Oldham, J. Myland, Fundamentals of electrochemical science, Elsevier, Amsterdam, 1993.
[27] R.S. Nicholson, I. Shain, Theory of stationary electrode polarography. Single scan and cyclic methods applied to reversible, irreversible, and kinetic systems, Anal. Chem. 36 (1964) 706–723.
[28] A.M. Bond, N.W. Duffy, S.-X. Guo, J. Zhang, D. Elton, Changing the look of voltammetry, Anal. Chem. 77 (2005) 186A–195A.
[29] S.-X. Guo, A.M. Bond, J. Zhang, Fourier transformed large amplitude alternating current voltammetry: Principles and applications, Rev. Polarogr. 61 (2015) 21–32.

[30] A.M. Bond, D. Elton, S.-X. Guo, G.F. Kennedy, E. Mashkina, A.N. Simonov, J. Zhang, An integrated instrumental and theoretical approach to quantitative electrode kinetic studies based on Large Amplitude Fourier Transformed ac Voltammetry: A mini-review, Electrochem. Commun. 57 (2015) 78–83.
[31] J. Zhang, S.-X. Guo, A.M. Bond, F. Marken, Large-amplitude Fourier transformed high-harmonic alternating current cyclic voltammetry: kinetic discrimination of interfering faradaic processes at glassy carbon and at boron-doped diamond electrodes, Anal. Chem. 76 (2004) 3619–3629.
[32] A.A. Sher, A.M. Bond, D.J. Gavaghan, K. Harriman, S.W. Feldberg, N.W. Duffy, S.-X. Guo, J. Zhang, Resistance, capacitance, and electrode kinetic effects in fourier-transformed large-amplitude sinusoidal voltammetry: Emergence of powerful and intuitively obvious tools for recognition of patterns of behavior, Anal. Chem. 76 (2004) 6214–6228.
[33] S.-X. Guo, J. Zhang, D.M. Elton, A.M. Bond, Fourier transform large-amplitude alternating current cyclic voltammetry of surface-bound azurin, Anal. Chem. 76 (2004) 166–177.
[34] T. Ueda, J.-i. Nambu, J. Lu, S.-X. Guo, Q. Li, J.F. Boas, L.L. Martin, A.M. Bond, Structurally characterised vanadium (v)-substituted Keggin-type heteropolysulfates $[SVM_{11}O_{40}]^{3-}$ (M = Mo, W): voltammetric and spectroscopic studies related to the V (v)/V (iv) redox couple, Dalton Trans. 43 (2014) 5462–5473.
[35] H. Gerischer, An interpretation of the double layer capacity of graphite electrodes in relation to the density of states at the Fermi level, J. Phys. Chem. 89 (1985) 4249–4251.
[36] Q. Li, J. Lu, J.F. Boas, D.A. Traore, M.C. Wilce, L.L. Martin, T. Ueda, A.M. Bond, Spontaneous redox synthesis and characterization of the tetrathiafulvalene–vanadium-substituted polyoxometalate charge-transfer material $TTF_4[SVW_{11}O_{40}]$: Comparison with the Mo analogue, Inorg. Chem. 53 (2014) 10996–11006.
[37] L. Hutton, M.E. Newton, P.R. Unwin, J.V. Macpherson, Amperometric oxygen sensor based on a platinum nanoparticle-modified polycrystalline boron doped diamond disk electrode, Anal. Chem. 81 (2008) 1023–1032.
[38] J. Zhang, S.-X. Guo, A.M. Bond, Discrimination and evaluation of the effects of uncompensated resistance and slow electrode kinetics from the higher harmonic components of a Fourier transformed large-amplitude alternating current voltammogram, Anal. Chem. 79 (2007) 2276–2288.
[39] G. Gritzner, J. Kuta, Recommendations on reporting electrode potentials in nonaqueous solvents (Recommendations 1983), Pure Appl. Chem. 56 (1984) 461–466.
[40] S.W. Feldberg, Optimization of explicit finite-difference simulation of electrochemical phenomena utilizing an exponentially expanded space grid: Refinement of the Joslin-Pletcher algorithm, J . Electroanal. Chem. 127 (1981) 1–10.
[41] M. Rudolph, A fast implicit finite difference algorithm for the digital simulation of electrochemical processes, J. Electroanal. Chem. 314 (1991) 13–22.
[42] A.M. Bond, K. Bano, S. Adeel, L.L. Martin, J. Zhang, Fourier-transformed large-amplitude AC voltammetric study of tetrathiafulvalene (TTF): Electrode kinetics of the TTF°/TTF^{+} and TTF^{+}/TTF^{2+} processes, ChemElectroChem 1 (2014) 99–107.
[43] A.M. Bond, N.W. Duffy, D.M. Elton, B.D. Fleming, Characterization of nonlinear background components in voltammetry by use of large amplitude periodic perturbations and Fourier transform analysis, Anal. Chem. 81 (2009) 8801–8808.
[44] C. Beriet, D. Pletcher, A microelectrode study of the mechanism and kinetics of the ferro/ferricyanide couple in aqueous media: The influence of the electrolyte and its concentration, J. Electroanal. Chem. 361 (1993) 93–101.
[45] K. Aoki, K. Hayashi, A frequency-dependent capacitance model and analysis of the ac impedance of conducting polyaniline films, J. Electroanal. Chem. 384 (1995) 31–37.
[46] C.L. Bentley, A.M. Bond, A.F. Hollenkamp, P.J. Mahon, J. Zhang, Electrode reaction and mass-transport mechanisms associated with the iodide/triiodide couple in the ionic liquid 1-ethyl-3-methylimidazolium bis (trifluoromethanesulfonyl) imide, J. Phys. Chem. C 118 (2014) 22439–22449.
[47] R.A. Marcus, On the theory of oxidation–reduction reactions involving electron transfer. I, J. Phys. Chem. 24 (1956) 966–978.
[48] S. Gosavi, R. Marcus, Nonadiabatic electron transfer at metal surfaces, J. Phys. Chem. B 104 (2000) 2067–2072.
[49] R. Nissim, C. Batchelor-McAuley, M.C. Henstridge, R.G. Compton, Electrode kinetics at carbon electrodes and the density of electronic states, Chem. Commun. 48 (2012) 3294–3296.
[50] R.J. Rice, N.M. Pontikos, R.L. McCreery, Quantitative correlations of heterogeneous electron-transfer kinetics with surface properties of glassy carbon electrodes, J. Am. Chem. Soc. 112 (1990) 4617–4622.

Supporting Information

Electrode Material Dependence of the Electron Transfer Kinetics Associated with the $[SVW_{11}O_{40}]^{3-/4-}$ ($V^{V/IV}$) and $[SVW_{11}O_{40}]^{4-/5-}$ ($W^{VI/V}$) Processes in Dimethylformamide

Jiezhen Li, Si-Xuan Guo, Cameron L. Bentley, Kiran Bano, Alan M. Bond* and Jie Zhang*

School of Chemistry and ARC Centre of Excellence for Electromaterials Science, Monash University, Clayton, Victoria 3800, Australia

Tadaharu Ueda
Department of Applied Science, Faculty of Science, Kochi University, Kochi 780-8520, Japan

Corresponding authors: jie.zhang@monash.edu, alan.bond@monash.edu

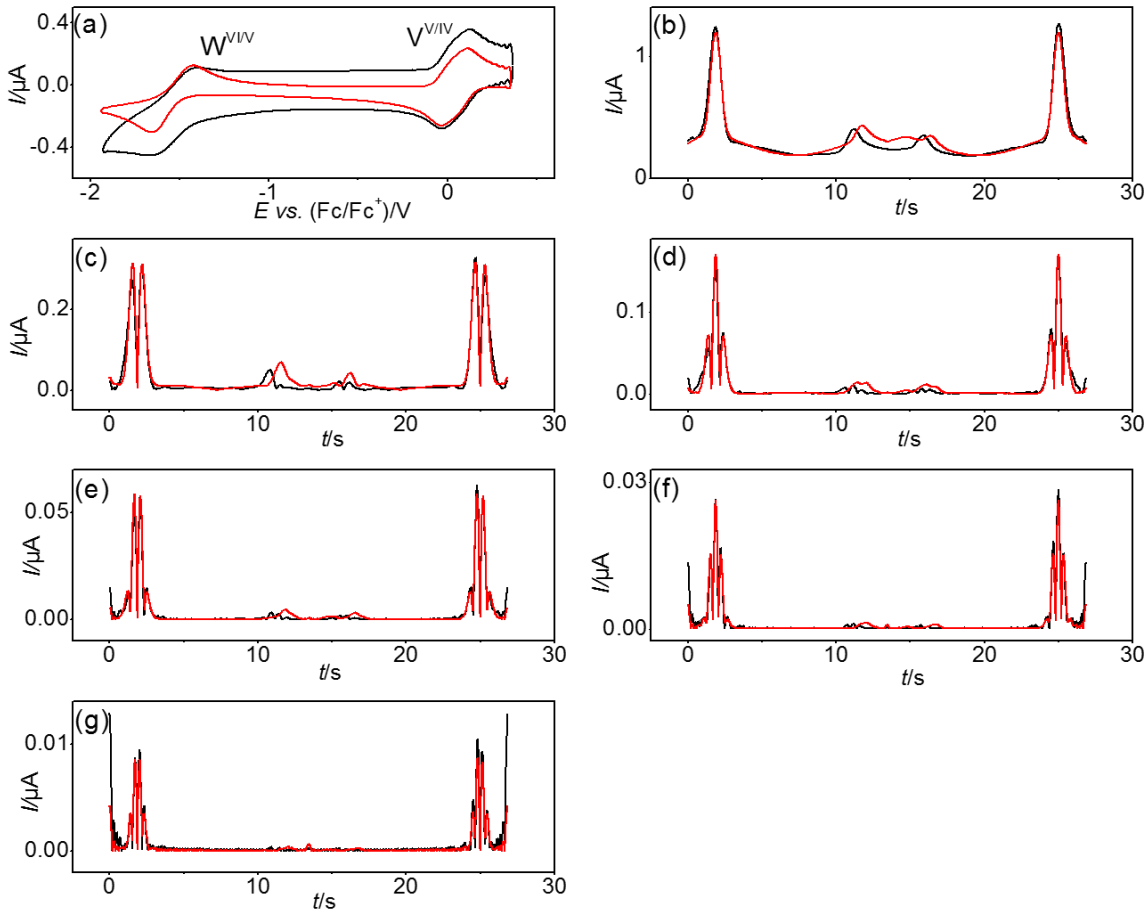

Figure S1. Comparison of simulated (—) and experimental (—) FTAC voltammetric data obtained for the $[SVW_{11}O_{40}]^{3-/4-/5-}$ processes in DMF containing 0.2 mM $[SVW_{11}O_{40}]^{3-}$ and 0.1 M $[Bu_4N][PF_6]$ at a BDD electrode with ΔE = 80 mV, f = 9.02 Hz and ν = 0.171 V s^{-1}. (a) aperiodic DC component, (b-g) 1st to 6th AC harmonic components. To obtain the simulated data, k_V^0 = 0.028 cm s^{-1}, α_V = 0.60, k_W^0 = 0.0006 cm s^{-1} and α_W = 0.53 were used. Other parameters used in the simulations are provided in Table 2 of the main text.

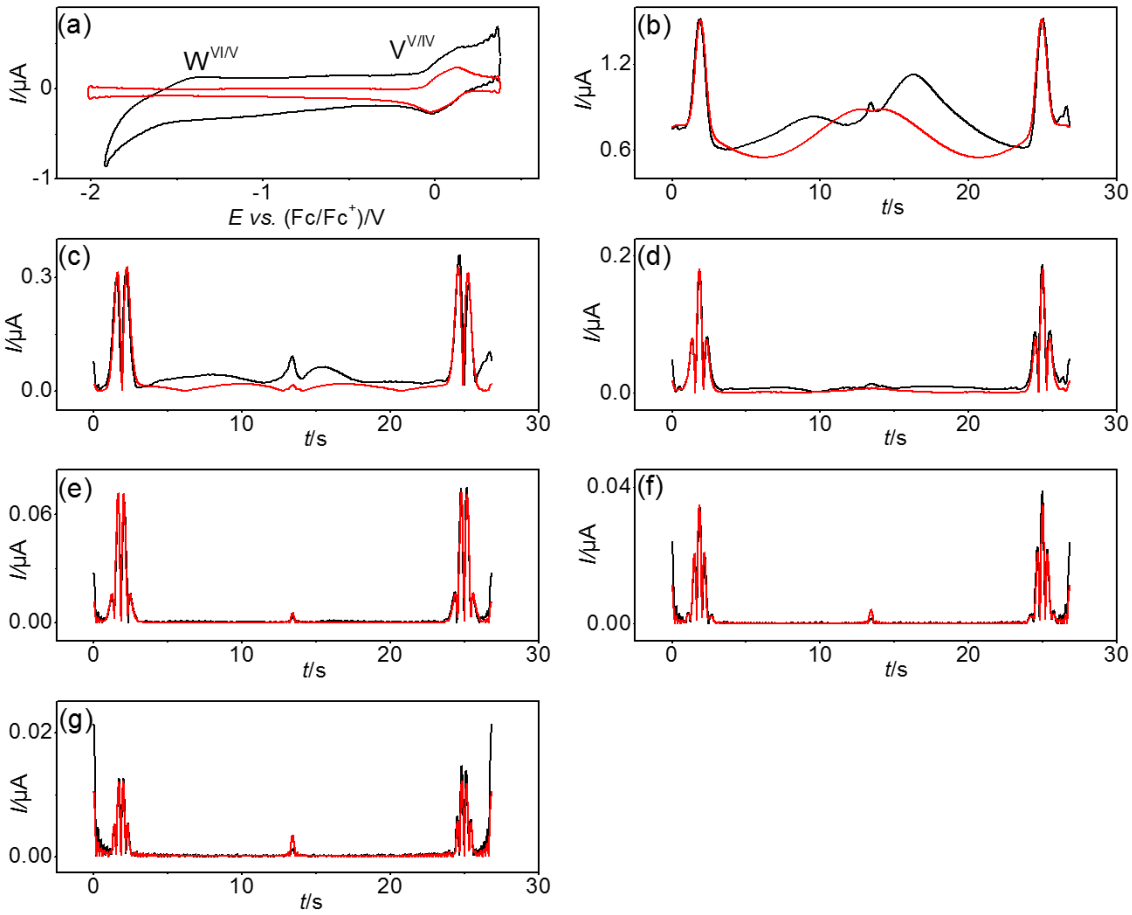

Figure S2. Comparison of simulated (—) and experimental (—) FTAC voltammetric data obtained for the $[SVW_{11}O_{40}]^{3-/4-/5-}$ processes in DMF containing 0.2 mM $[SVW_{11}O_{40}]^{3-}$ and 0.1 M $[Bu_4N][PF_6]$ at a Pt electrode with ΔE = 80 mV, f = 9.02 Hz and ν = 0.171 V s^{-1}. (a) aperiodic DC component, (b-g) 1st to 6th AC harmonic components. To obtain the simulated data, k_V^0 = 0.08 cm s^{-1}, α_V = 0.50 were used. Other parameters used in the simulations are provided in Table 2 of the main text.

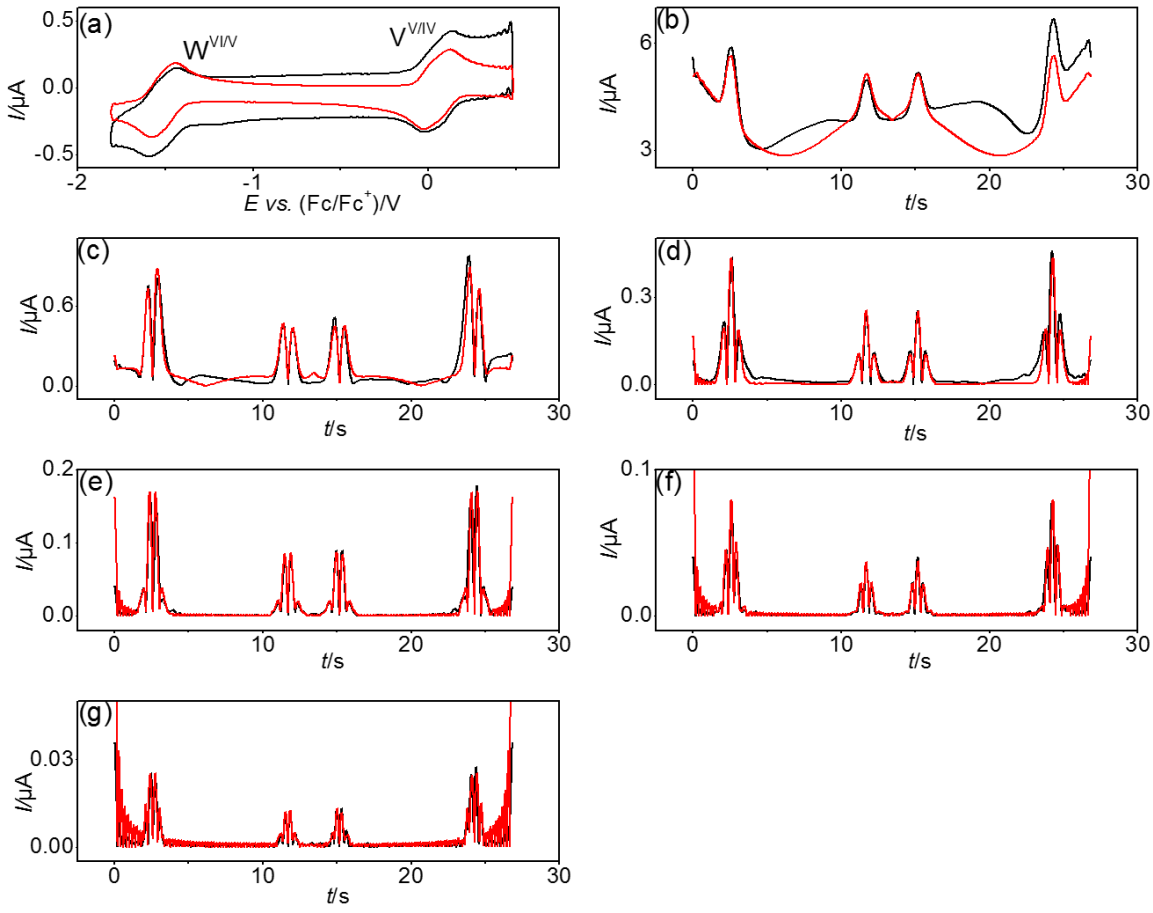

Figure S3. Comparison of simulated (—) and experimental (—) FTAC voltammetric data obtained for the $[SVW_{11}O_{40}]^{3-/4-/5-}$ processes in DMF containing 0.2 mM $[SVW_{11}O_{40}]^{3-}$ and 0.1 M $[Bu_4N][PF_6]$ at a GC electrode with ΔE = 80 mV, f = 27.01 Hz and ν = 0.171 V s^{-1}. (a) aperiodic DC component, (b-g) 1st to 6th AC harmonic components. To obtain the simulated data, k^0_V = 0.20 cm s^{-1}, α_V = 0.50, k^0_W = 0.045 cm s^{-1} and α_W = 0.54 were used. Other parameters used in the simulations are provided in Table 2 of the main text.

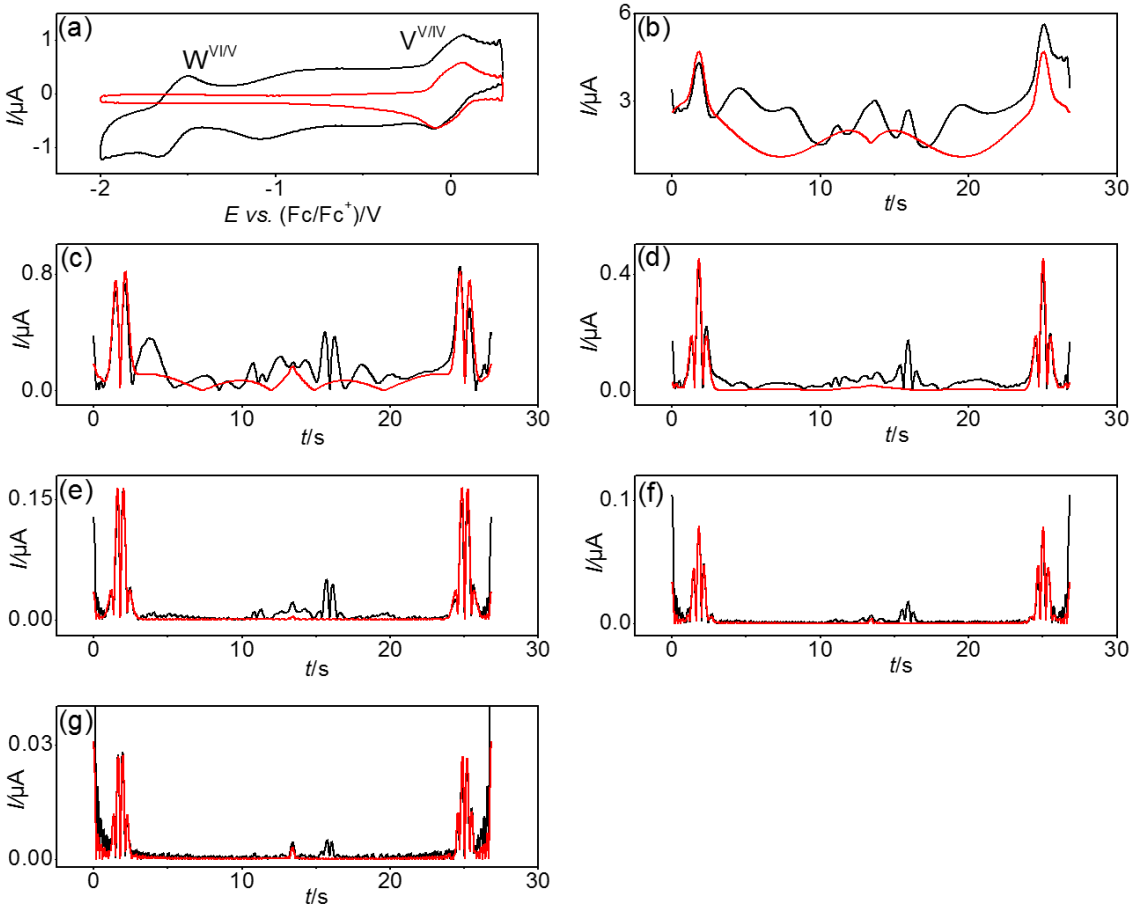

Figure S4. Comparison of simulated (—) and experimental (—) FTAC voltammetric data obtained for the $[SVW_{11}O_{40}]^{3-/4-/5-}$ processes in DMF containing 0.2 mM $[SVW_{11}O_{40}]^{3-}$ and 0.1 M $[Bu_4N][PF_6]$ at an Au electrode with ΔE = 80 mV, f = 9.02 Hz and ν = 0.171 V s^{-1}. (a) aperiodic DC component, (b-g) 1st to 6th AC harmonic components. To obtain the simulated data, k_V^0 = 0.10 cm s^{-1}, α_V = 0.50 were used. Other parameters used in the simulations are provided in Table 2 of the main text.

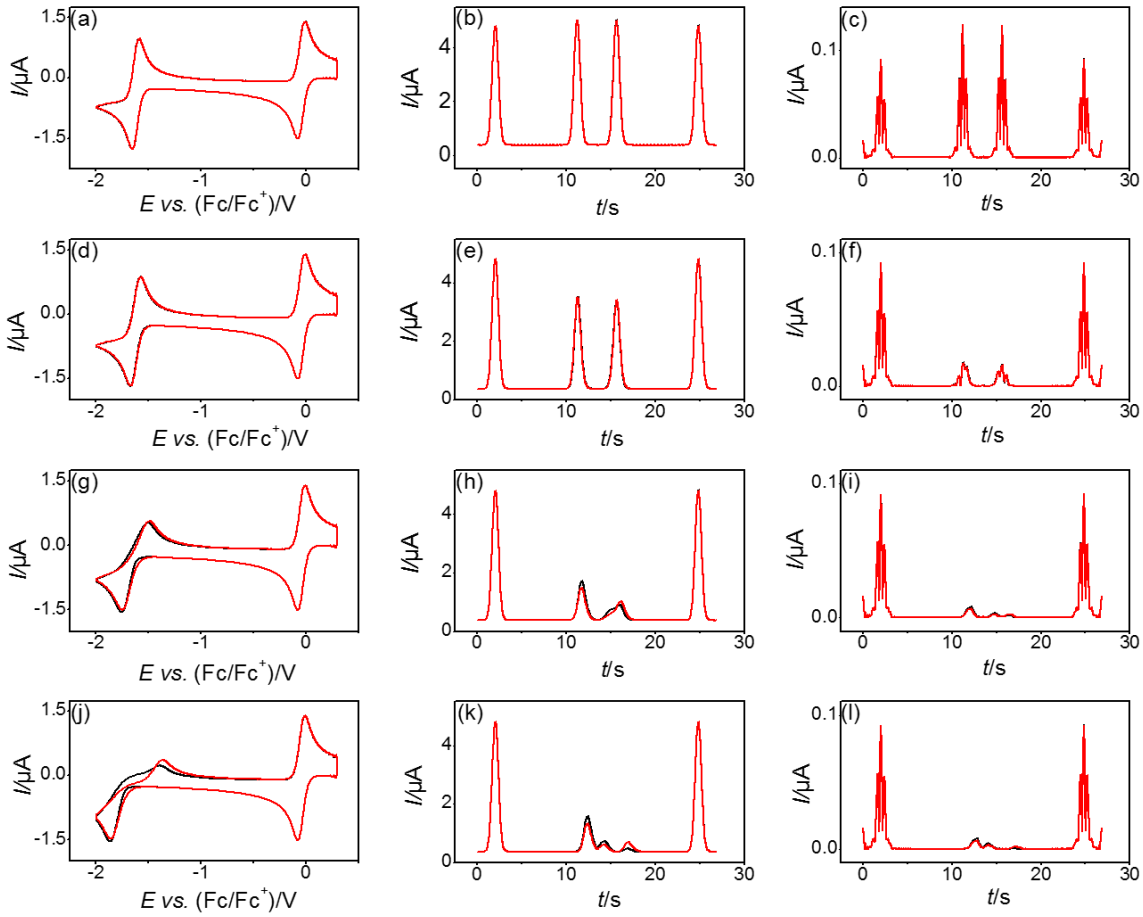

Figure S5. Comparison of simulated DC cyclic voltammograms, first and fifth harmonic (ΔE = 80 mV and f = 9.02 Hz) components obtained with (—) and without (—) considering the cross redox reaction for the $[SVW_{11}O_{40}]^{3-/4-}$ and $[SVW_{11}O_{40}]^{4-/5-}$ processes. The simulation parameters are as follows: E^0_V = 0.050 V, k^0_W = -1.530 V, k^0_V = 0.03 cm s^{-1}, k_f = 1 × 10^{10} M^{-1} s^{-1}, k_b = 2 × 10^{-17} M^{-1} s^{-1}, R_u = 900 Ω, D ($[SVW_{11}O_{40}]^{3-}$) = 2.8 × 10^{-6} cm^2 s^{-1}, D ($[SVW_{11}O_{40}]^{4-}$) = D ($[SVW_{11}O_{40}]^{5-}$) = 2.9 × 10^{-6} cm^2 s^{-1}, A = 8.14 × 10^{-3} cm^2, C = 1.0 mM, υ = 0.1 V s^{-1}, C_{dl} = 10 uF cm^{-2}, T = 295 K, α_V = 0.50, α_W = 0.53 with different k^0_W values of: (a), (b) and (c) 0.05 cm s^{-1}; (d), (e) and (f) 0.005 cm s^{-1}; (g), (h) and (i) 0.0005 cm s^{-1}; (j), (k) and (l) 0.00005 cm s^{-1}.

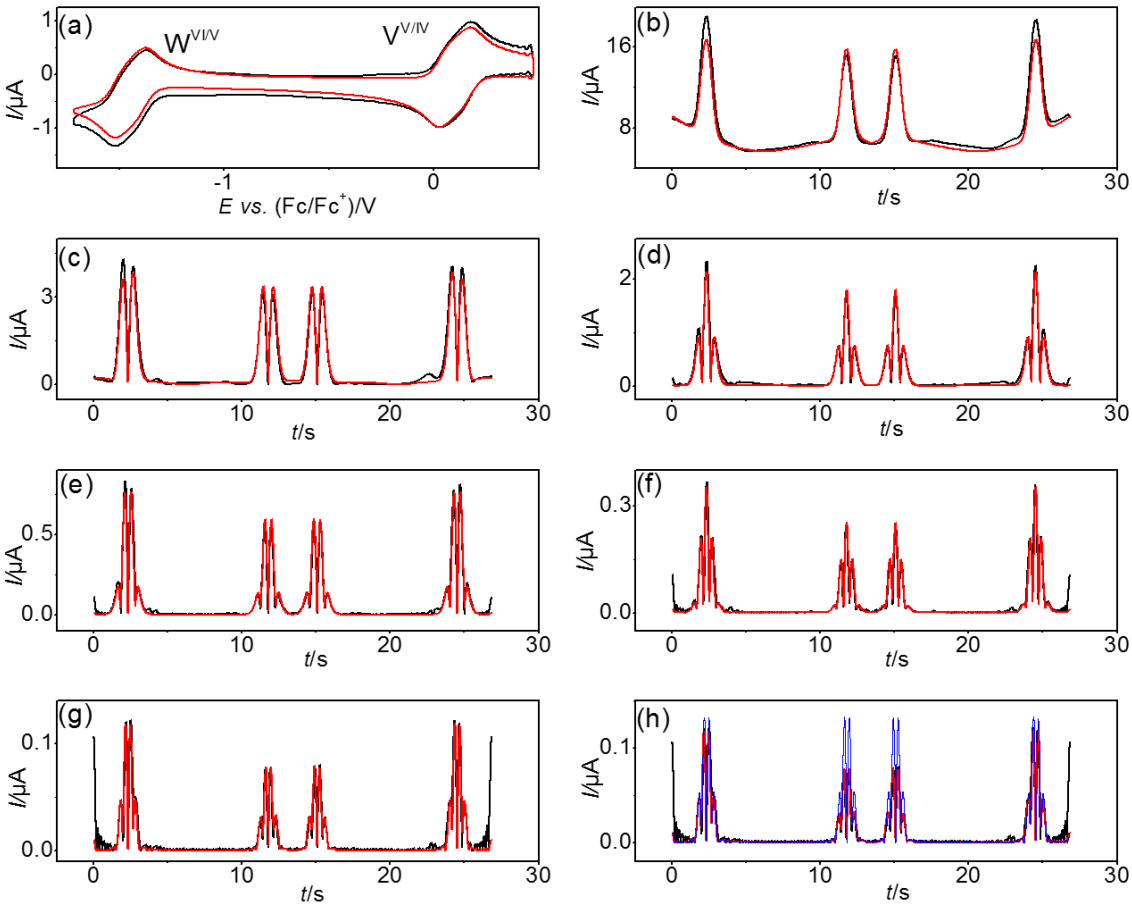

Figure S6. Comparison of simulated (—) and experimental (—) FTAC voltammetric data obtained for the $[SVW_{11}O_{40}]^{3-/4-/5-}$ processes in DMF containing 0.2 mM $[SVW_{11}O_{40}]^{4-}$ and 0.1 M $[Bu_4N][PF_6]$ at a GC electrode with ΔE = 80 mV, f = 66.98 Hz and ν = 0.164 V s^{-1}. (a) aperiodic DC component, (b-g) 1st to 6th AC harmonic components. To obtain the simulated data, k^0_V = 0.18 cm s^{-1}, α_V = 0.50, k^0_W = 0.055 cm s^{-1} and α_W = 0.54 were used. Other parameters used in the simulations are provided in Table 3 of the main text.

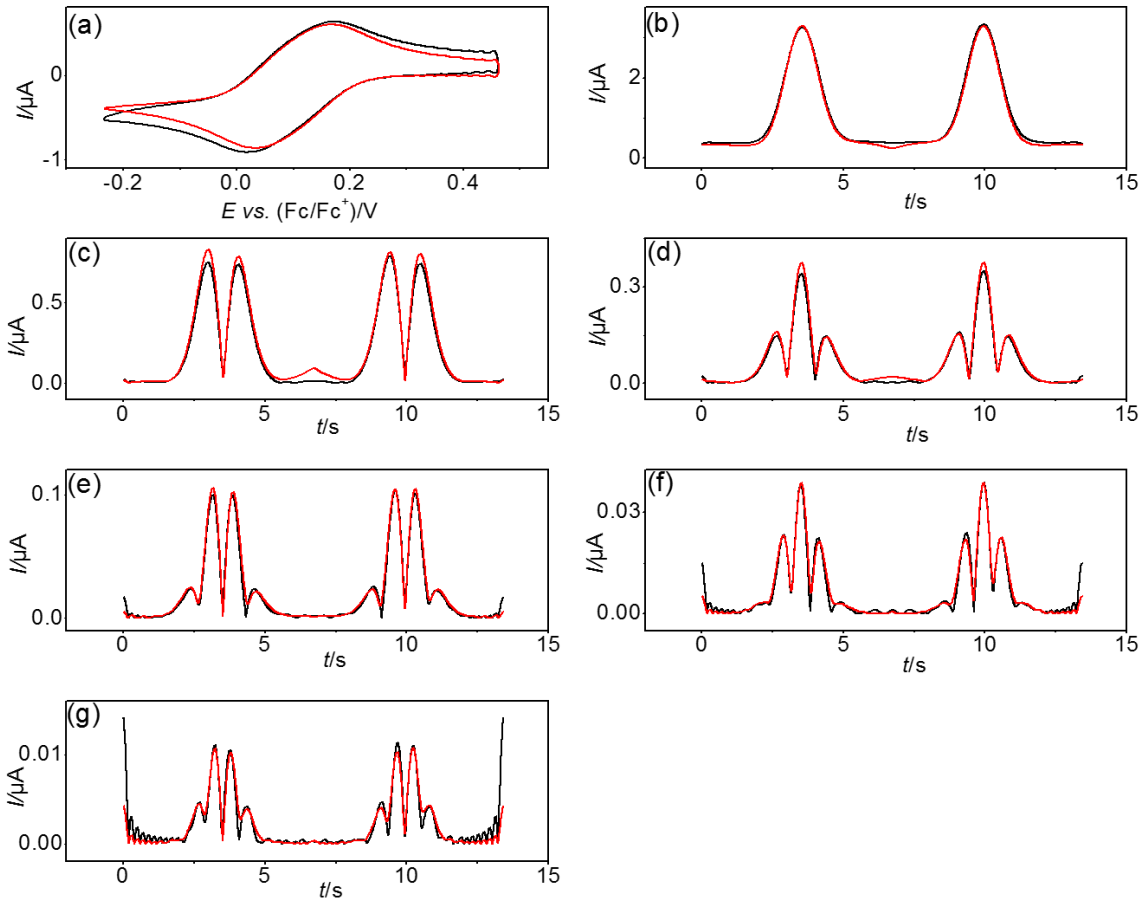

Figure S7. Comparison of simulated (—) and experimental (—) FTAC voltammetric data obtained for the $[SVW_{11}O_{40}]^{3-/4-}$ process in DMF containing 1.0 mM $[SVW_{11}O_{40}]^{3-}$ and 0.5 M $[Bu_4N][PF_6]$ at a BDD electrode with ΔE = 80 mV, f = 9.02 Hz and ν = 0.104 V s^{-1}. (a) aperiodic DC component, (b-g) 1st to 6th AC harmonic components. To obtain the simulated data, k_V^0 = 0.009 cm s^{-1}, α_V = 0.50 were used. Other parameters used in the simulations are provided in Table 4 of the main text.

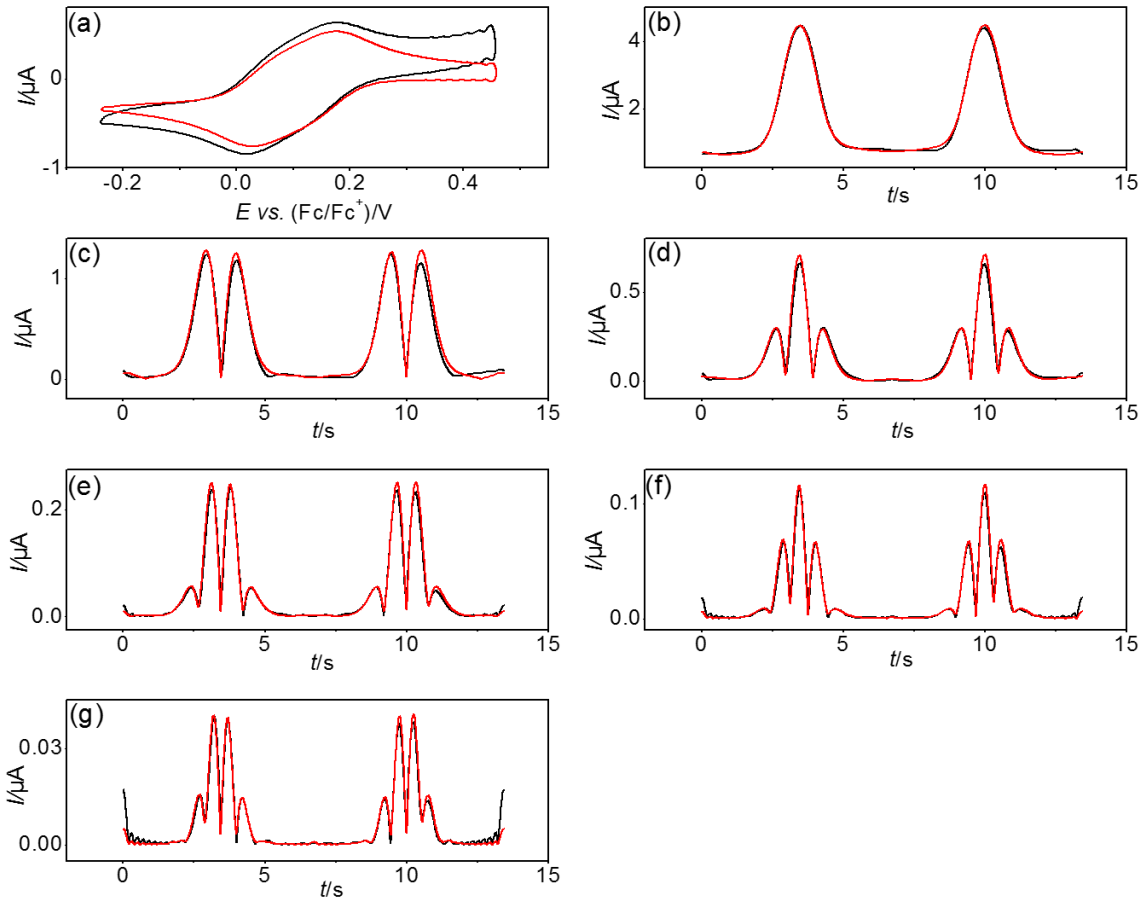

Figure S8. Comparison of simulated (—) and experimental (—) FTAC voltammetric data obtained for the $[SVW_{11}O_{40}]^{3-/4-}$ process in DMF containing 1.0 mM $[SVW_{11}O_{40}]^{3-}$ and 0.5 M $[Bu_4N][PF_6]$ at a Pt electrode with ΔE = 80 mV, f = 9.02 Hz and ν = 0.104 V s^{-1}. (a) aperiodic DC component, (b-g) 1st to 6th AC harmonic components. To obtain the simulated data, k_V^0 = 0.035 cm s^{-1}, α_V = 0.45 were used. Other parameters used in the simulations are provided in Table 4 of the main text.

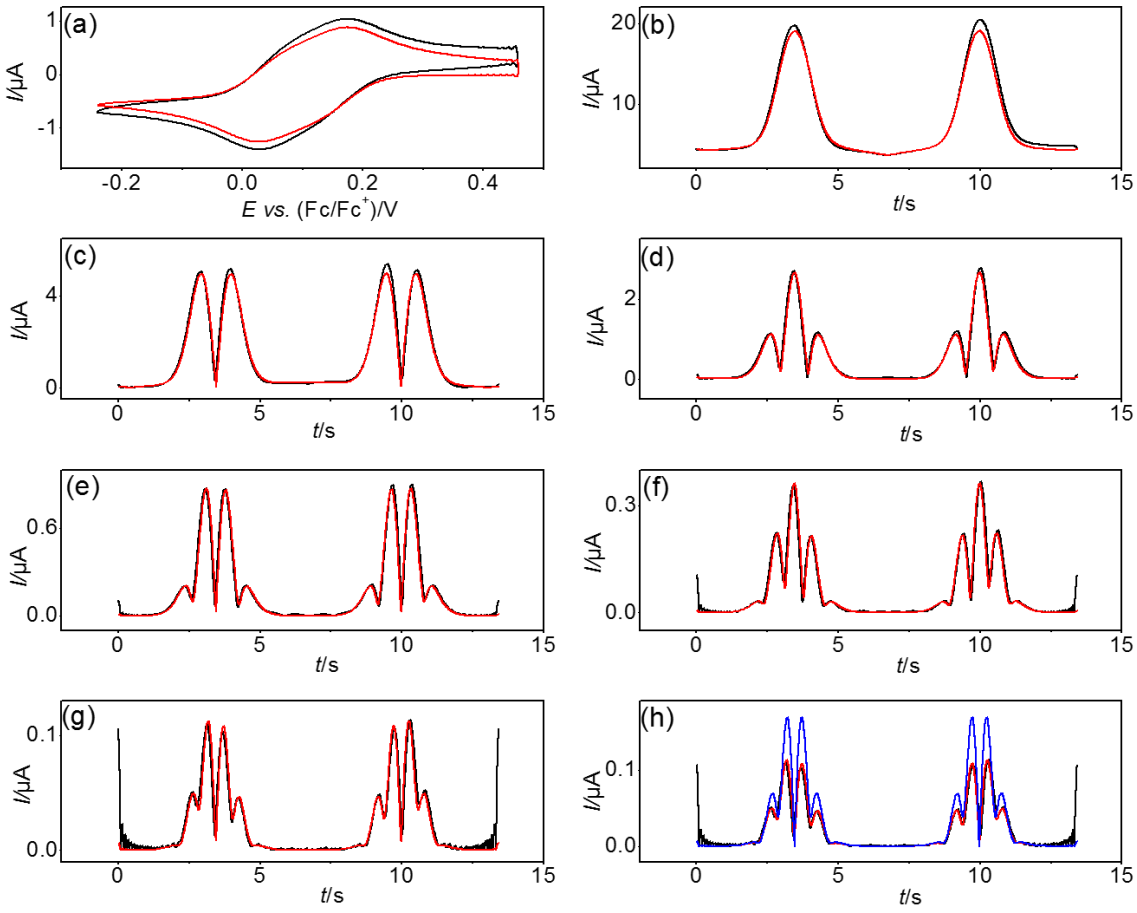

Figure S9. Comparison of simulated (—) and experimental (—) FTAC voltammetric data obtained for the $[SVW_{11}O_{40}]^{3-/4-}$ process in DMF containing 1.0 mM $[SVW_{11}O_{40}]^{3-}$ and 0.5 M $[Bu_4N][PF_6]$ at an Au electrode with ΔE = 80 mV, f = 27.01 Hz and v = 0.104 V s^{-1}. (a) aperiodic DC component, (b-g) 1st to 6th AC harmonic components, and (h) simulated 6th harmonic for the $V^{V/VI}$ process in reversible case (—). To obtain the simulated data, k_V^0 = 0.08 cm s^{-1}, α_V = 0.45 were used. Other parameters used in the simulations are provided in Table 4 of the main text.

Chapter 5

Influence of 1-Butyl-3-Methylimidazolium on the Electron Transfer Kinetics Associated with the $[SVW_{11}O_{40}]^{3-/4-}$ ($V^{V/IV}$) and $[SVW_{11}O_{40}]^{4-/5-}$ ($W^{VI/V}$) Processe in Dimethylformamide

ARTICLE IN PRESS
JEAC-02628; No of Pages 8

Journal of Electroanalytical Chemistry xxx (2016) xxx–xxx

Contents lists available at ScienceDirect

Journal of Electroanalytical Chemistry

journal homepage: www.elsevier.com/locate/jelechem

Influence of 1-butyl-3-methylimidazolium on the electron transfer kinetics associated with the $[SVW_{11}O_{40}]^{3-/4-}$ ($V^{V/IV}$) and $[SVW_{11}O_{40}]^{4-/5-}$ ($W^{VI/V}$) processes in dimethylformamide

Jiezhen Li [a], Cameron L. Bentley [a], Alan M. Bond [a,*], Jie Zhang [a,*], Tadaharu Ueda [b]

[a] School of Chemistry and ARC Centre of Excellence for Electromaterials Science, Monash University, Clayton, Victoria 3800, Australia
[b] Department of Applied Science, Faculty of Science, Kochi University, Kochi 780-8520, Japan

ARTICLE INFO

Article history:
Received 11 March 2016
Received in revised form 25 April 2016
Accepted 28 April 2016
Available online xxxx

Keywords:
Polyoxometalates
Electron transfer kinetics
Fourier transformed alternating current voltammetry
Ionic liquids

ABSTRACT

Fourier transformed large amplitude alternating current voltammetry has been used to determine the heterogeneous electron-transfer kinetics (k^0 and α values) associated with the vanadium $[SVW_{11}O_{40}]^{3-/4-}$ ($V^{V/IV}$) and tungsten $[SVW_{11}O_{40}]^{4-/5-}$ ($W^{VI/V}$) processes at glassy carbon (GC), platinum (Pt), gold (Au) and boron-doped diamond (BDD) electrodes in dimethylformamide (DMF) containing 0.5 M 1-butyl-3-methylimidazolium hexafluorophosphate as the supporting electrolyte. In comparison with data reported previously in DMF containing 0.5 M tetrabutylammonium hexafluorophosphate, the k^0 values at Pt, Au and BDD electrodes, were found to be larger by a factor of 2 to 4 for the $V^{V/IV}$ process and 10 to 100 fold for the $W^{VI/V}$ process. At a GC electrode, the rate of the $V^{V/IV}$ process was too fast to be measured under the experimental conditions used (frequency = 34 Hz) and k^0 for the $W^{VI/V}$ process was found to be insensitive to the identity of the supporting electrolyte cation. The origins of these observations are considered in terms of contributions from ion-pairing, surface functional groups on the GC electrode, the double layer effect, and the inner-sphere nature of the $W^{V/IV}$ process.

1. Introduction

Polyoxometalates, a large class of inorganic transition metal oxygen cluster compounds, have attracted significant interest for many decades due to their vast structural diversity and often-unexpected properties relevant to catalysis, electrochemistry, energy storage and optical materials [1–5].

Electrochemical studies of POMs are extensive and the thermodynamic effects of cations and solvents have been widely reported [5–11]. In contrast, quantitative studies of the heterogeneous electron transfer kinetics (i.e. the electron-transfer rate constant, k^0, and transfer coefficient, α, at an electrode/electrolyte interface are relatively rare. In a recent study [12], we reported that for the Keggin-type silicon tungstate POMs $[\alpha\text{-}SiW_{12}O_{40}]^{4-}$ and $[\alpha\text{-}SiW_{12}O_{40}]^{5-}$, significantly slower electron transfer kinetics are observed with a boron-doped diamond (BDD) electrode compared to a glassy carbon (GC) one. That study was then extended to examine the cation effect on the electrode kinetics associated with the $[\alpha\text{-}SiW_{12}O_{40}]^{4-/5-}$ and $[\alpha\text{-}SiW_{12}O_{40}]^{5-/6-}$ processes in aqueous 1.0 M $LiNO_3$, $NaNO_3$, KNO_3 and NH_4NO_3 electrolyte at a BDD electrode [13]. More recently [14], we showed that the electrode kinetics associated with the $[SVW_{11}O_{40}]^{3-/4-/5-}$ processes in dimethylformamide (DMF) containing tetrabutylammonium hexafluorophosphate ($[Bu_4N][PF_6]$) as the supporting electrolyte are extremely sensitive to the ionic strength (0.1 vs. 0.5 M $[Bu_4N][PF_6]$) and identity of the electrode material (Pt, Au, GC and BDD).

In the above mentioned studies [12–14], it was found that many of the electron-transfer processes exhibit relatively fast electron-transfer kinetics. In such cases and where the effect of uncompensated resistance is significant (e.g. at a macroelectrode in non-aqueous media), it is difficult to quantify the electrode kinetics reliably using direct current (DC) cyclic voltammetry [15,16]. Under these circumstances, large amplitude Fourier transformed alternating current (FTAC) voltammetry is advantageously employed [12–14] as the higher order AC harmonic components generated by the large amplitude periodic perturbation exhibit negligible background (non-faradaic) current, and furthermore the effects of electrode kinetics can be more readily distinguished from uncompensated resistance [17–21].

In the past two decades, rapid developments in the field of ionic liquids (ILs) have resulted in the employment of these neoteric solvents in a range of electrochemical applications [22–25]. In this study, 1-butyl-3-methylimidazolium hexafluorophosphate ($[BMIM][PF_6]$), one of the most commonly used ILs [22–25], was chosen as the supporting electrolyte in dimethylformamide (DMF). The electron transfer kinetics associated with the $[SVW_{11}O_{40}]^{3-/4-/5-}$ processes at BDD, GC, Pt and Au electrodes were determined using Fourier transformed large amplitude ac voltammetry. The structure of $[SVW_{11}O_{40}]^{3-}$

* Corresponding authors.
E-mail addresses: alan.bond@monash.edu (A.M. Bond), jie.zhang@monash.edu (J. Zhang).

http://dx.doi.org/10.1016/j.jelechem.2016.04.050
1572-6657/

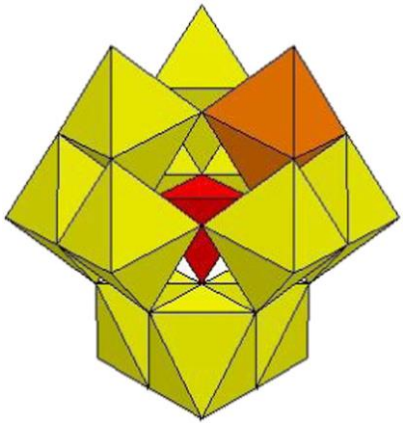

Fig. 1. The structure of $[SVW_{11}O_{40}]^{3-}$. Color code: S (red), V (orange), W (yellow) [26]. (For interpretation of the references to color in this figure legend, the reader is referred to the web version of this article.)

[26], as in $[Bu_4N]_3[SVW_{11}O_{40}]$, is shown in Fig. 1, and provides the location of the V and W metal constituents. $[SVW_{11}O_{40}]^{3-}$ exhibits three well-defined one-electron reduction processes in molecular solvent (electrolyte) media [14,26]. The two initial processes, which are the focus for the current study, correspond to the reduction of V^V to V^{IV} (Eq. (1)) and W^{VI} to W^V (Eq. (2)).

$$\left[SV^{V}W^{VI}_{11}O_{40}\right]^{3-} + e^{-} \rightleftharpoons \left[SV^{IV}W^{VI}_{11}O_{40}\right]^{4-} \quad (1)$$

$$\left[SV^{IV}W^{VI}_{11}O_{40}\right]^{4-} + e^{-} \rightleftharpoons \left[SV^{IV}W^{V}W^{VI}_{10}O_{40}\right]^{5-} \quad (2)$$

While Eqs. (1) and (2) appear to represent simple electron transfer reactions, it should be noted that the electrode processes involve extensive ion-pairing and hence are not strictly elementary reactions [13]. In this context, k^0 should be more appropriately considered as $k^0_{apparent}$. However, since the ion-paring reactions are not rate limiting, $k^0_{apparent}$ should still reflect the nature of the electrochemical electron transfer process. The electrolyte cation, $[BMIM]^+$, used in this study is siginifcantly smaller than $[Bu_4N]^+$ used in our previous study [14] and hence probably exhibits stronger ion-pairing with $[SVW_{11}O_{40}]^{3-}$. This factor is expected to have a significant impact on both the thermodynamics and kinetics associated with initial reduction processes of $[SVW_{11}O_{40}]^{3-}$ (Eqs. (1) and (2)).

2. Experimental section

2.1. Chemicals

Dimethylformamide (DMF, 99.8%, Merck), acetonitrile (CH_3CN, 97%, Sigma-Aldrich), ethanol (96%, Merck), ferrocene (Fc, ≥98%, Sigma-Aldrich) and [BMIM][PF_6] (99%, IoLiTec, Germany) were used as supplied by the manufacturer. [Bu_4N][PF_6] (98%, Wako) was recrystallized twice from ethanol before use as the supporting electrolyte. $[Bu_4N]_3[SVW_{11}O_{40}]$ was synthesized and purified according to a literature procedure [26].

Other experimental details are reported in a previous publication [14] and are summarized in the Supporting information.

3. Results and discussion

3.1. DC cyclic voltammetric characterization of the $V^{V/IV}$ and $W^{VI/V}$ processes

Fig. 2a and b show a comparison of the DC cyclic voltammograms obtained from $[SVW_{11}O_{40}]^{3-}$ in DMF containing 0.5 M [BMIM][PF_6] and 0.5 M [Bu_4N][PF_6], respectively, at BDD, Pt, GC and Au electrodes with a scan rate of 0.1 V s^{-1}. In DMF (0.5 M [BMIM][PF_6]), the reversible potentials for the $V^{V/IV}$ and $W^{VI/V}$ processes, E^0_V, and E^0_W, are 0.170 and

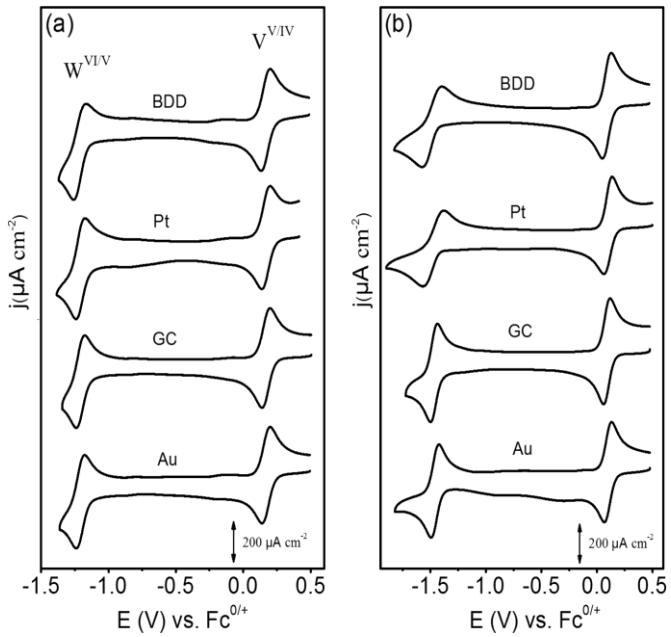

Fig. 2. DC cyclic voltammograms obtained from the reduction of 1.0 mM $[SVW_{11}O_{40}]^{3-}$ in DMF containing (a) 0.5 M [BMIM][PF_6] and (b) 0.5 M [Bu_4N][PF_6] at (from top to bottom) BDD, Pt, GC and Au electrodes with a scan rate of 0.1 V s^{-1}.

Please cite this article as: J. Li, et al., Influence of 1-butyl-3-methylimidazolium on the electron transfer kinetics associated with the [SVW11O40]3−/4− (VV/IV) and [SV..., Journal of Electroanalytical Chemistry (2016), http://dx.doi.org/10.1016/j.jelechem.2016.04.050

Table 1
DC cyclic voltammetric data derived from the reduction of 1.0 mM $[SVW_{11}O_{40}]^{3-}$ in DMF containing either 0.5 M [BMIM][PF_6] or [Bu_4N][PF_6] at BDD, Pt, GC and Au macrodisk electrodes with a scan rate of 0.1 V s^{-1}.

Electrode	E^0_V/V[a]	$(\Delta E_p)_V$/V[b]	E^0_W/V	$(\Delta E_p)_W$/V	ΔE^0/V[c]
			0.5 M [BMIM][PF_6]		
BDD	0.170	0.075	−1.215	0.093	1.385
Pt	0.170	0.065	−1.210	0.071	1.380
GC	0.170	0.062	−1.210	0.063	1.380
Au	0.170	0.062	−1.210	0.062	1.380
			0.5 M [Bu_4N][PF_6]		
BDD	0.100	0.076	−1.470	0.184	1.560
Pt	0.100	0.074	−1.465	0.191	1.565
GC	0.100	0.061	−1.460	0.066	1.570
Au	0.100	0.062	−1.470	0.071	1.560

[a] vs. $Fc^{0/+}$.
[b] ΔE_p is the peak-to-peak separation of the process.
[c] ΔE^0 is the difference in E^0_V and E^0_W.

−1.210 V (vs. $Fc^{0/+}$), respectively, with a separation (ΔE^0) of 1.38 V, while in DMF (0.5 M [Bu_4N][PF_6]), E^0_V and E^0_W are 0.100 V and −1.460 V, respectively, with a separation of 1.56 V. Since $[SVW_{11}O_{40}]^{3-}$ and its reduced forms are highly negatively charged, ion-pair formation between the POM and electrolyte cation (X^+) is expected to influence the thermodynamics of the overall electron transfer process. In the current case, the smaller $[BMIM]^+$ cation [27] induces a much stronger ion-pairing effect than $[Bu_4N]^+$, which results in considerably more positive E^0 values and a decreased potential gap between the $V^{V/IV}$ and $W^{VI/V}$ processes (i.e., smaller ΔE^0).

The E^0 and the peak-to-peak separation ΔE_p ($= E^{ox}_p - E^{red}_p$) data determined by DC cyclic voltammetry at all of the investigated electrode materials in DMF containing either 0.5 M [Bu_4N][PF_6] or [BMIM][PF_6] are summarized in Table 1. Interestingly, the ΔE_p values associated with the $W^{VI/V}$ process in DMF containing 0.5 M [BMIM][PF_6] are significantly smaller than those measured in DMF containing 0.5 M [Bu_4N][PF_6] at BDD, Pt and Au electrodes. Given that the R_u effect is comparable in the two systems (e.g., at Pt, R_u = 253 and 330 Ω with [BMIM][PF_6] and [Bu_4N][PF_6], respectively), a smaller ΔE_p is indicative of a larger k^0 value, as deduced using analysis based on the classical theoretical treatment of cyclic voltammetric *i*-*E* curves by Nicholson and Shain [28,29]. This finding indicates that the $W^{VI/V}$ process is more facile when [BMIM][PF_6] is the supporting electrolyte compared to [Bu_4N][PF_6], as will be quantitatively confirmed below. In addition, in some cases (e.g. in DMF containing 0.5 M [BMIM][PF_6] at the BDD electrode), significantly larger ΔE_p values are associated with the $W^{VI/V}$ process than for the $V^{V/IV}$ process, implying the identity of the metal centre also is significant in relation to the electrode kinetics.

3.2. Large amplitude FTAC voltammetry in DMF containing 0.5 M [BMIM][PF_6]

The k^0 values associated with the $V^{V/IV}$ (k^0_V) and $W^{VI/V}$ (k^0_W) processes in DMF containing 0.5 M [BMIM][PF_6] at BDD, Pt, GC and Au electrodes were determined by FTAC voltammetry using a sine wave perturbation (ΔE = 80 mV and f = 9.02 Hz or 34.01 Hz) and scanning the DC potential over the range where both the $V^{V/IV}$ and $W^{VI/V}$ reduction processes are present in the voltammogram. The parameters used in the simulations to define all aspects of the electron transfer process (i.e., E^0, k^0, α, A, R_u, C_{dl}) were derived as described in the Supporting Information and are provided in Table 2. Excellent agreement between simulated and experimental data obtained for the reduction of 1.0 mM $[SVW_{11}O_{40}]^{3-}$ is observed at all four electrode materials (see Figs. 3 to 6) when using the parameters provided in Table 2.

Shown in Fig. 3 is a simulation-experiment comparison obtained at the BDD electrode. Using an AC frequency of 9.02 Hz, k^0_V, α_V, k^0_W and α_W values were determined to be 0.04 cm s^{-1}, 0.57, 0.021 cm s^{-1} and 0.53, respectively. At a Pt electrode (see Fig. 4), the k^0_V value is too fast to measure at a frequency of 9.02 Hz (i.e., $k^0_V \geq 0.2$ cm s^{-1}, since a k^0 value of 0.2 cm s^{-1} produces a peak current that is 90% of the simulated reversible value under these conditions, which is arbitrarily defined as the upper limit of detection). Consequently, a higher frequency (f = 34.01 Hz) AC perturbation was used to shorten the time scale of the measurement so that a higher kinetic sensitivity could be achieved. Under these conditions, k^0_V, α_V, k^0_W and α_W at a Pt electrode were estimated to be 0.13 cm s^{-1}, 0.55, 0.07 cm s^{-1} and 0.60, respectively. At a GC electrode (see Fig. 5), the k^0_V value is still too fast to be determined when using a frequency of 34.01 Hz. In principle, an even higher frequency could be used to achieve a higher kinetic sensitivity, thereby allowing k^0_V to be measured. Unfortunately, as the measured current is frequency dependent and increases with increasing frequency, the iR_u effect was found to become very significant at higher frequencies. On the basis of data obtained at 34.01 Hz, k^0_V is defined as ≥0.40 cm s^{-1}. Nevertheless, the $W^{VI/V}$ process was found to be far from reversible at a frequency of 34.01 Hz, and accordingly, k^0_W and α_W were determined to be 0.08 cm s^{-1} and 0.50, respectively. Finally, at an Au electrode (see Fig. 6), a frequency of 34.01 Hz was used to measure k^0_V and k^0_W values of 0.16 and 0.18 cm s^{-1}, respectively. α_V and α_W were assumed to be 0.50 under these conditions (the voltmmetric characteristic were found to be insensitive to this parameter for these near-reversible processes).

FTAC voltammetric data were also acquired with a lower concentration of $[SVW_{11}O_{40}]^{3-}$, 0.20 mM, in order to lessen the iR_u effect. The results obtained at BDD, Pt, GC and Au electrodes in DMF containing 0.5 M [BMIM][PF_6] at the lower concentration are also summarized in Table 2. Comparisons of experimental and simulated data are presented in Figs.

Table 2
Electrode kinetic parameters derived for the $[SVW_{11}O_{40}]^{3-/4-/5-}$ processes in DMF containing $[SVW_{11}O_{40}]^{3-}$ and 0.5 M [BMIM][PF_6].[a]

Electrode	C (mM)	E^0_V (V)[b]	E^0_W (V)[b]	R_u (Ω)	C_{dl} (c_0, c_1, c_2, c_3, c_4) (μF cm^{-2})	k^0_V (cm s^{-1})	α_V	k^0_W (cm s^{-1})	α_W
BDD	1.0	0.170	−1.210	250	12.0, 0, 0, 0, 0	0.04	0.57[c]	0.021	0.53[c]
	0.20	0.170	−1.210	244	15.4, 2.2, −3.4, −3.1, −0.5	0.05	0.70[c]	0.02	0.50[c]
Pt	1.0	0.170	−1.210	253	18.0, 0, 0, 0, 0	0.13	0.55[c]	0.07	0.60[c]
	0.20	0.170	−1.210	260	13.0, −2.45, −0.28, 1.46, 0.8	0.13	0.50[d]	0.06	0.50[c]
GC	1.0	0.170	−1.210	273	37.0, 5.8, 3.2, −3.5, −1.3	≥0.4	0.50[d]	0.08	0.50[c]
	0.20	0.170	−1.210	293	32.8, 10.9, 6.7, −10.6, −5.1	≥0.2	0.50[d]	0.06	0.50[a]
Au	1.0	0.170	−1.210	246	23.9, −7.2, 0.5, 5.1, 2.5	0.16	0.50[d]	0.18	0.50[d]
	0.20	0.170	−1.210	273	20.0, 0.3, 1.8, 1.6, −0.8	0.18	0.50[d]	0.18	0.50[d]

[a] Other parameters used in the simulations are: ΔE = 80 mV, D ($[SVW_{11}O_{40}]^{3-}$) = D ($[SVW_{11}O_{40}]^{4-}$) = D ($[SVW_{11}O_{40}]^{5-}$) = 2.0×10^{-6} cm^2 s^{-1}, T = 295 K and scan rate = 0.138 V s^{-1}. The electrode areas are 8.14×10^{-3} cm^2, 7.71×10^{-3} cm^2, 7.45×10^{-3} cm^2 and 7.85×10^{-3} cm^2 for BDD, Pt, GC and Au electrodes, respectively. The frequencies are 34.01 Hz for the studies with GC (in the presence of 1.0 mM $[SVW_{11}O_{40}]^{3-}$), Pt and Au electrodes, and 9.02 Hz for the studies with GC (in the presence of 0.20 mM $[SVW_{11}O_{40}]^{3-}$) and BDD electrodes.
[b] vs. $Fc^{0/+}$.
[c] Calculated.
[d] Assumed.

Please cite this article as: J. Li, et al., Influence of 1-butyl-3-methylimidazolium on the electron transfer kinetics associated with the [SVW11O40]3−/4− (VV/IV) and [SV..., Journal of Electroanalytical Chemistry (2016), http://dx.doi.org/10.1016/j.jelechem.2016.04.050

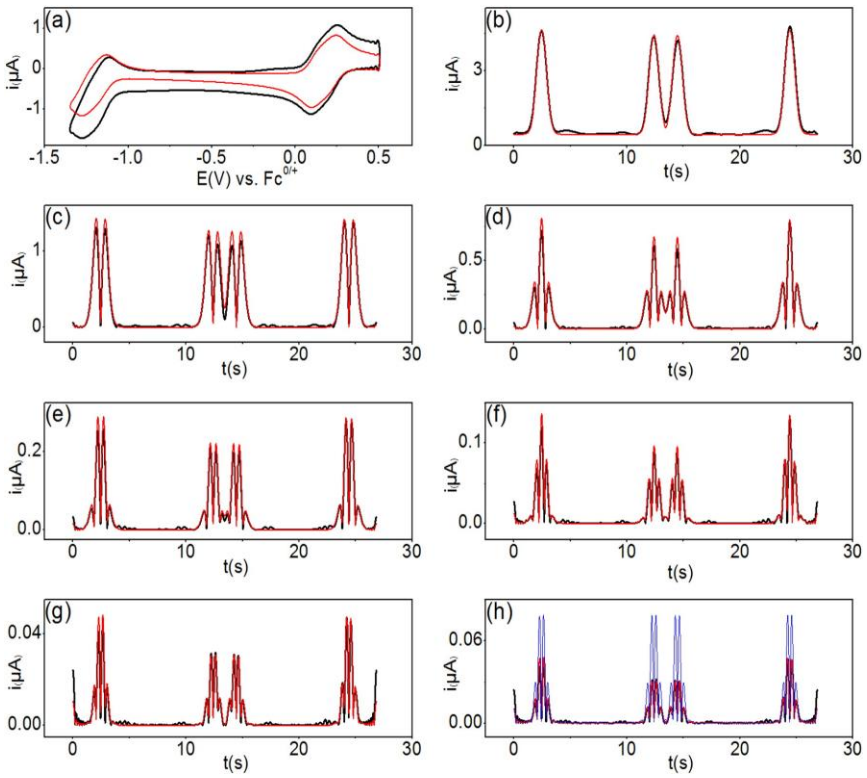

Fig. 3. Comparison of simulated (—) and experimental (–) FTAC voltammetric data obtained for the $V^{IV/V}$ and $W^{VI/V}$ processes in DMF containing 1.0 mM $[SVW_{11}O_{40}]^{3-}$ and 0.5 M [BMIM][PF_6] at a BDD electrode with $\Delta E = 80$ mV, $f = 9.02$ Hz and $\nu = 0.138$ V s^{-1}. (a) aperiodic DC component, (b–g) 1st to 6th AC harmonic components, and (h) simulated 6th harmonic component for the $V^{V/IV}$ process for the reversible case (—). To obtain the simulated data, $k^0_V = 0.04$ cm s^{-1}, $\alpha_V = 0.57$, $k^0_W = 0.021$ cm s^{-1} and $\alpha_W = 0.53$ were used. Other parameters used in the simulations are provided in Table 2.

S1 to S4 of the Supporting information. As expected, since the iR_u drop has been correctly accommodated in all simulations, the determined k^0 values are essentially independent of the $[SVW_{11}O_{40}]^{3-}$ concentration. The concentration-independent k^0 values also imply adsorption of the $[SVW_{11}O_{40}]^{3-/4-/5-}$ species is not occurring to any significant extent under the investigated conditions. It should be noted that the capacitance coefficients reported in Table 2 show a slight frequency dependence, which implies that the simple RC circuit model used to model this term is not strictly valid [30]. In practice, the capacitance coefficients were determined individually for each data set to achieve an excellent simulation-experiment agreements of the background at all frequencies studied.

Table 3 contains the kinetic parameters associated with the $[SVW_{11}O_{40}]^{3-/4-/5-}$ processes in DMF containing 0.5 M [BMIM][PF_6] as the supporting electrolyte along with those reported previously in DMF containing 0.5 M [Bu_4N][PF_6] [14]. As highlighted in our previous study [14], the k^0_W values at BDD, Pt and Au electrodes could not be determined by full comparison of experimental and simulated data obtained by large amplitude FTAC voltammetry due to complexities associated with the $W^{VI/V}$ process at these electrodes. Therefore, the kinetics of the $W^{VI/V}$ process at these electrodes are now estimated by simply comparing the peak-to-peak separations from the experimental cyclic voltammograms with those obtained by simulation using the DigiElch digital simulation software, taking into account the effect of R_u. These approximate k^0_W values are also included in Table 3.

Data in Table 3 clearly reveal that changing the electrolyte from [BMIM][PF_6] to [Bu_4N][PF_6] enhances the kinetics of the $[SVW_{11}O_{40}]^{3-/4-/5-}$ processes. For instance, when [BMIM][PF_6] is the supporting electrolyte, k^0_V was found to be a factor of 2 to 4 greater at BDD, Pt and Au electrodes; in the GC electrode case k^0_V was too large to be measured in either electrolyte. The $W^{VI/V}$ process was found to be even more sensitive to the supporting electrolyte cation, with k^0_W being approximately 25-fold, 10-fold and 100-fold higher at the BDD, Au and Pt electrodes, respectively, when $[BMIM]^+$ is used instead of $[Bu_4N]^+$. Interestingly, the electrode kinetics of $W^{VI/V}$ process was found to be relatively insensitive to the supporting electrolyte cation at GC, with k^0_W values of 0.08 and 0.10 cm s^{-1} in DMF containing [BMIM][PF_6] and [Bu_4N][PF_6], respectively.

Since $[SVW_{11}O_{40}]^{3-}$ and its reduced forms are highly negatively charged, ion-pair formation between the POM and electrolyte cation (X^+) are expected to influence the kinetics of the overall electron transfer reaction through the square reaction scheme described in the reaction scheme given in Eq. (3) below [31,32].

$$\begin{array}{ccc} A + e^- & \rightleftharpoons & B \quad (E_1^0, k_1^0) \\ K_1 \Big\updownarrow X^+ & & X^+ \Big\updownarrow K_2 \\ XA^+ + e^- & \rightleftharpoons & XB^+ \quad (E_2^0, k_2^0) \end{array} \tag{3}$$

In the treatment above, the symbols A and B are used instead of $[SVW_{11}O_{40}]^{3-}$ and $[SVW_{11}O_{40}]^{4-}$, $K_1 = \frac{[X^+][A]}{[XA^+]}$ and $K_2 = \frac{[X^+][B]}{[XB^+]}$ are the

Please cite this article as: J. Li, et al., Influence of 1-butyl-3-methylimidazolium on the electron transfer kinetics associated with the [SVW11O40]3−/4− (VV/IV) and [SV..., Journal of Electroanalytical Chemistry (2016), http://dx.doi.org/10.1016/j.jelechem.2016.04.050

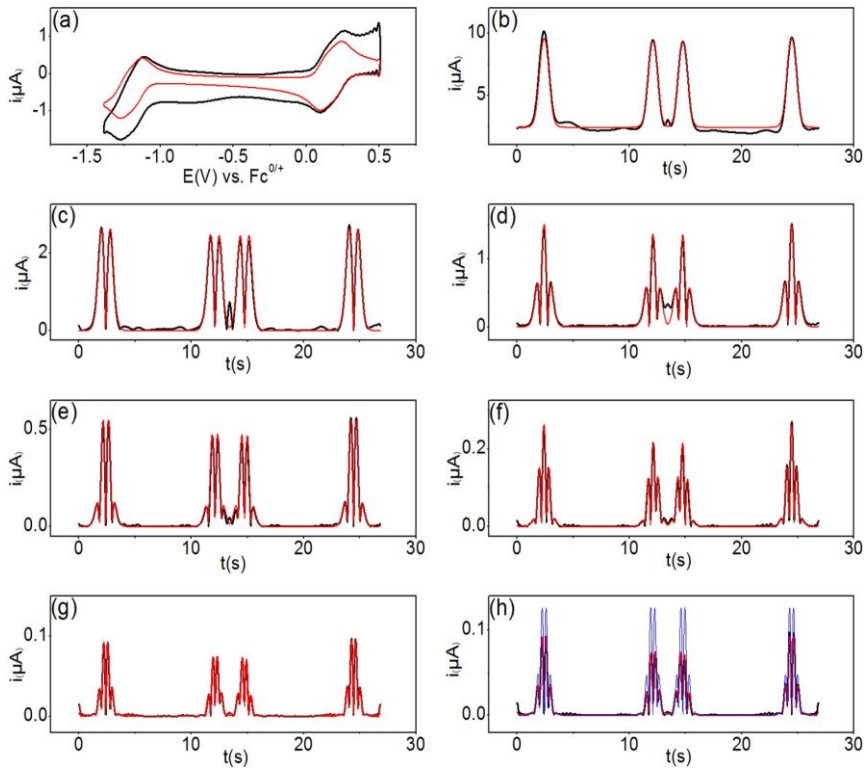

Fig. 4. Comparison of simulated (—) and experimental (—) FTAC voltammetric data obtained for the $V^{IV/V}$ and $W^{VI/V}$ processes in DMF containing 1.0 mM $[SVW_{11}O_{40}]^{3-}$ and 0.5 M [BMIM][PF_6] at a Pt electrode with $\Delta E = 80$ mV, $f = 34.01$ Hz and $\nu = 0.137$ V s^{-1}. (a) aperiodic DC component, (b–g) 1st to 6th AC harmonic components, and (h) simulated 6th harmonic component for the $V^{V/IV}$ process for the reversible case (—). To obtain the simulated data, $k^0_V = 0.13$ cm s^{-1}, $\alpha_V = 0.55$, $k^0_W = 0.07$ cm s^{-1} and $\alpha_W = 0.60$ were used. Other parameters used in the simulations are provided in Table 2.

equilibrium constants for the ion-pairing reactions involving either the oxidised or the reduced forms, E^0_1 and E^0_2 are the relevant formal potentials and; k^0_1 and k^0_2 are the formal electron transfer rate constants at E^0_1 and E^0_2, respectively. It has been shown that the voltammetric responses associated with this process is identical to a simple one-electron transfer process if the ion pairing reactions are reversible on the voltammetric timescale. The $k^0_{apparent}$ value associated with this process is a function of k^0_1, k^0_2, K_1, K_2 and $[X^+]$ [13]. The dependence of k^0 on cation identity (Li^+, Na^+, K^+ and NH_4^+) observed in a previous study [13] was attributed to this square reaction scheme. However, this cannot explain the electrode material dependence of the k^0 values or the dramatically different trends observed for the k^0_V and k^0_W values when changing the electrolyte, since the effect of the ion pairing is electrode material independent, and should be similar for both the $V^{V/IV}$ and $W^{VI/V}$ processes since K_1 and K_2 values associated with each process are not expected to differ significantly.

Another factor considered to explain the cation dependence of k^0 is adsorption of $[SVW_{11}O_{40}]^{3-}$, $[SVW_{11}O_{40}]^{4-}$ or $[SVW_{11}O_{40}]^{5-}$, which would more likely be electrode-material dependent. However, this phenomenon is expected to be concentration dependent, whereas nearly identical k^0_V and k^0_W values are obtained at the two different $[SVW_{11}O_{40}]^{3-}$ concentrations used, as previously mentioned. Furthermore, excellent agreement between the experimental and simulated data over all harmonics based on a simple model of electron transfer indicates that specific adsorption is not a significant factor.

Differences in the double layer is a possible cause of the large difference in k^0_V and k^0_W values [33]. For example, if it assumed that the point of zero charge (PZC) is independent of the supporting electrolyte and positive of the $W^{VI/V}$ process, the fact that E^0_W is cation dependent (i.e., −1.21 and −1.46 V for $[BMIM]^+$ and $[Bu_4N]^+$, respectively) means that the apparent k^0 is predicted to be larger in [BMIM][PF_6] compared to [Bu_4N][PF_6] if the double layer effect is significant. However, in the absence of knowledge of the PZC for each electrode material and the IL electrolyte dependence, discussion of the impact of the double layer effect is necessarily tentative.

The site of electron transfer may be assumed be at a plane coincident with the outer Helmholtz plane (OHP); the plane of closest approach for a non-specifically adsorbed molecules. Qualitatively, the cation dependence of k^0 can be explained on the basis of the variation of the location of the OHP. Since the length of $[BMIM]^+$ is 1.11 nm, which is smaller than the diameter of $[Bu_4N]^+$, 1.26 nm [34], the thickness of the inner part of the double layer would be expected to be smaller when using [BMIM][PF_6] as the supporting electrolyte. In addition, given the planar structure of the $[BMIM]^+$ cation [34] it is likely that the centre of charge of the cation can approach the electrode surface more closely than the spherical $[Bu_4N]^+$ ion. Thus, the larger k^0 values when using [BMIM][PF_6] as electrolyte may be attributable to a shift of the OHP (the site of electron transfer) to a region that is closer to the electrode surface. The $W^{VI/V}$ process is expected to be more sensitive to effects related to the size of the cation than to the $V^{V/IV}$ process because it occurs at very negative potential. Hence, the cation concentration in the double layer is expected to be very high in the $W^{VI/V}$ potential region. Changes induced in the apparent electron transfer kinetics with electrolyte ion size/structure have been reported by Evans and co-workers [35,36] in their investigation on the reduction of nitro compounds in aprotic organic media. In this case, the authors attributed the variation in k^0 to a double

Please cite this article as: J. Li, et al., Influence of 1-butyl-3-methylimidazolium on the electron transfer kinetics associated with the [SVW11O40]3−/4− (VV/IV) and [SV..., Journal of Electroanalytical Chemistry (2016), http://dx.doi.org/10.1016/j.jelechem.2016.04.050

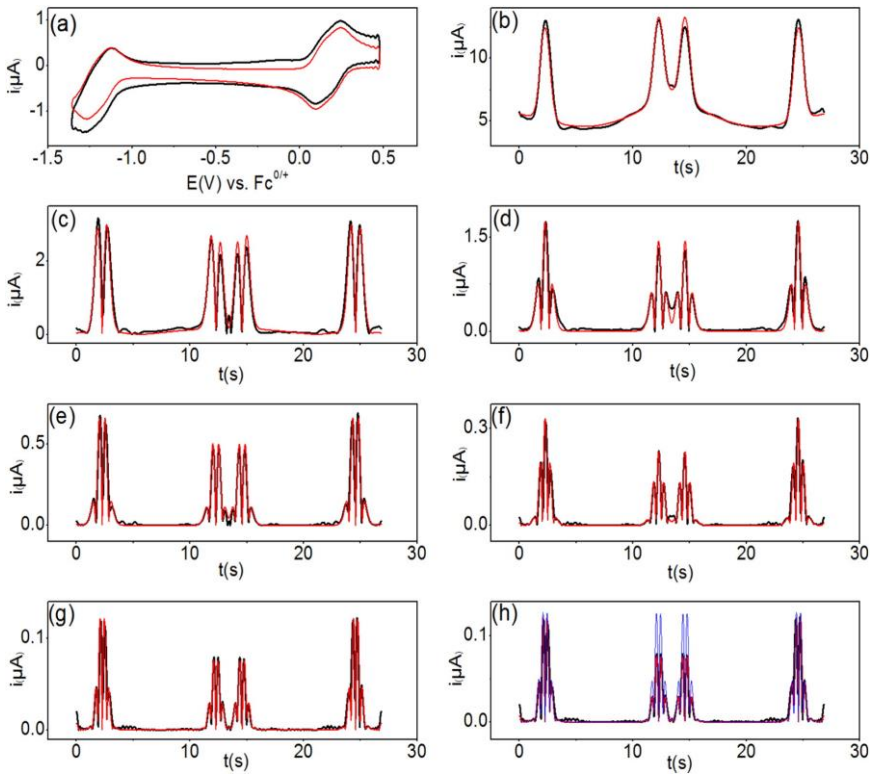

Fig. 5. Comparison of simulated (—) and experimental (–) FTAC voltammetric data obtained for the $V^{IV/V}$ and $W^{VI/V}$ processes in DMF containing 1.0 mM $[SVW_{11}O_{40}]^{3-}$ and 0.5 M [BMIM][PF_6] at a GC electrode with $\Delta E = 80$ mV, $f = 34.01$ Hz and $\nu = 0.137$ V s^{-1}. (a) aperiodic DC component, (b–g) 1st to 6th AC harmonic components, and (h) simulated 6th harmonic component for the $V^{V/IV}$ process for the reversible case (—). To obtain the simulated data, $k_V^0 \geq 0.40$ cm s^{-1}, $\alpha_V = 0.50$, $k_W^0 = 0.08$ cm s^{-1} and $\alpha_W = 0.50$ were used. Other parameters used in the simulations are provided in Table 2.

layer effect and a dependence of the distance of electron transfer on the nature of the electrolyte media.

Another possible explanation for the difference in k^0 values for the $V^{V/IV}$ and $W^{VI/V}$ processes as summarized in Table 2 is that the electron transfer reaction for former process is outer-sphere and the latter inner-sphere. For example, with the k_V^0 and k_W^0 values obtained in DMF containing 0.5 M [Bu_4N][PF_6], a much larger k_W^0 value was obtained at Au compared to Pt, while k_V^0 values were similar at both electrodes. For a nonadiabatic outer-sphere electron transfer reaction, electrode kinetics are expected to be electrode material dependent due to variation in the density of electronic states (DOS). This may explain why comparable k_V^0 values are obtained at Au and Pt electrodes, since their DOS values are similar (DOS (Pt) $= 1.46 \times 10^{23}$ cm^{-3} eV^{-1} [12] and DOS (Au) $= 1.7 \times 10^{22}$ cm^{-3} eV^{-1}) [12]. Clearly, the same dependence on electrode material does not apply for the $W^{VI/V}$ process. If the double layer is similar at these metallic electrodes, it is plausible that a different electrode material dependence occurs because the $W^{VI/V}$ process is inner-sphere rather than outer-sphere. This change in nature of the electron transfer process also could explain why k_W^0 is more sensitive to the cation type than k_V^0 at BDD, Pt and Au electrodes. In an inner-sphere reaction, the cation interacts with the electrode, thereby providing a 'ligand bridge' between the electrode and the anionic POM. Evidence for strong interaction between the POM and cation in solution is available from the strong cation dependence of the E_V^0, E_W^0 and ΔE^0 values. On this basis, the $[BMIM]^+$ ion may be expected to facilitate a more facile, inner-sphere electron transfer process ($W^{VI/V}$), due to its stronger interaction with the electrode surface and POM and a higher degree of electron delocalization associated with the imidazolium ring.

It is also interesting to note that the electrode kinetics of the $W^{VI/V}$ process at the GC electrode are almost independent of the cation type. As pointed out previously, surface functional groups present on a GC electrode may also play a critical role in electron transfer processes [14] and provide an alternative, kinetically facile inner-sphere electron transfer pathway which is independent of the cation type present in the double layer.

Finally, it is noted that the $V^{IV/V}$ process occurs at the sole V metal centre, while the $W^{VI/V}$ reduction may be delocalized over multiple (identical) metal centres.

4. Conclusions

The influence of the $[BMIM]^+$ cation on the electrode kinetics associated with the $[SVW_{11}O_{40}]^{3-/4-/5-}$ processes in DMF has been established at GC, BDD, Pt and Au electrodes using large amplitude FTAC voltammetry. The reversible potentials of the $V^{V/IV}$ and $W^{VI/V}$ processes are more positive, with the potential gap being smaller when [BMIM][PF_6] is used as the supporting electrolyte instead of [Bu_4N][PF_6]. These thermodynamic differences are attributable to ion-pairing effects between the POM and supporting electrolyte cation ($[BMIM]^+$ vs. $[Bu_4N]^+$). Changing the supporting electrolyte from [BMIM][PF_6] to [Bu_4N][PF_6] also increases k_V^0 2 to 4 fold at BDD, Pt and Au electrodes (k_V^0 is too fast to measure on GC in both cases). Even more significant increases of 10, 25 and 100-fold are found for the $W^{VI/V}$ process at Au, BDD and Pt electrodes, respectively when $[BMIM]^+$ is used, while this process was found to be insensitive to the identity of the cation at a GC electrode. Such distinct differences may be partially attributable to the

Please cite this article as: J. Li, et al., Influence of 1-butyl-3-methylimidazolium on the electron transfer kinetics associated with the [SVW11O40]3−/4− (VV/IV) and [SV..., Journal of Electroanalytical Chemistry (2016), http://dx.doi.org/10.1016/j.jelechem.2016.04.050

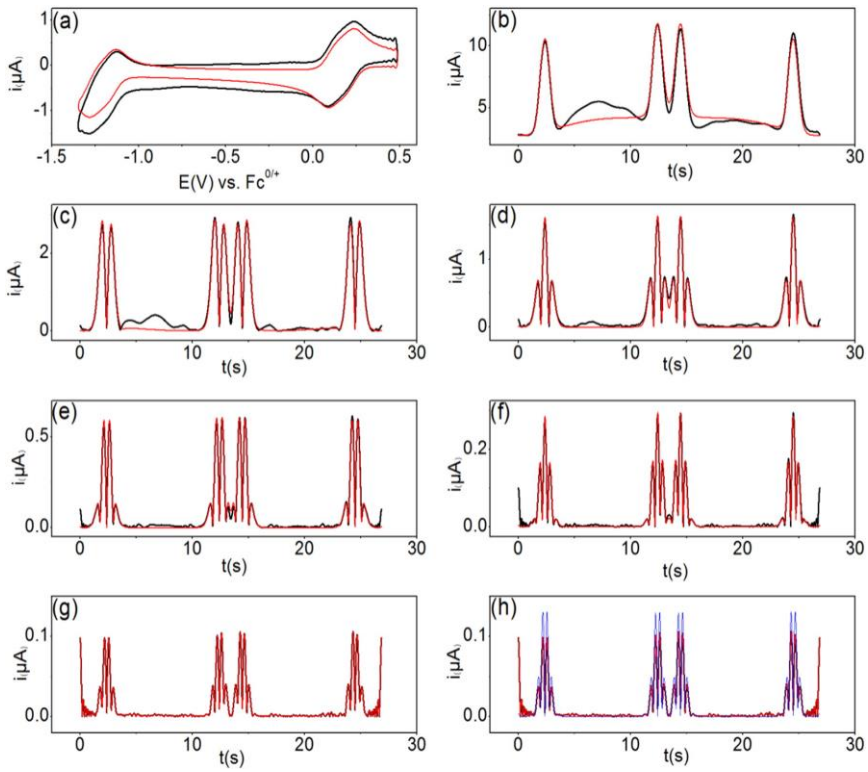

Fig. 6. Comparison of simulated (—) and experimental (–) FTAC voltammetric data obtained for the $V^{IV/V}$ and $W^{VI/V}$ processes in DMF containing 1.0 mM $[SVW_{11}O_{40}]^{3-}$ and 0.5 M [BMIM][PF_6] at an Au electrode with $\Delta E = 80$ mV, $f = 34.01$ Hz and $\nu = 0.137$ V s^{-1}. (a) aperiodic DC component, (b–g) 1st to 6th AC harmonic components, and (h) simulated 6th harmonic component for the $V^{V/IV}$ process for the reversible case (—). To obtain the simulated data, $k^0_V = 0.16$ cm s^{-1}, $\alpha_V = 0.50$, $k^0_W = 0.18$ cm s^{-1} and $\alpha_W = 0.50$ were used. Other parameters used in the simulations are provided in Table 2.

"double layer effect". However the strong electrolyte cation and electrode dependence imply that the $W^{VI/V}$ process is more likely to occur via an inner-sphere pathway, instead of an outer-sphere one which may occur for the $V^{IV/V}$ reaction.

Appendix A. Supplementary data

Details of experiments, simulations and data analysis. Figs. S1 to S4 provide a comparison of the simulated and experimental FTAC voltammograms obtained from 0.20 mM $[SVW_{11}O_{40}]^{3-}$ in DMF (0.5 M [BMIM][PF_6]) at BDD, Pt, GC and Au electrodes. Supplementary data associated with this article can be found in the online version, at doi:http://dx.doi.org/10.1016/j.jelechem.2016.04.050.

Table 3
Comparison of electrode kinetic parameters associated with the $[SVW_{11}O_{40}]^{3-/4-/5-}$ processes in DMF containing 0.5 M [Bu_4N][PF_6] or [BMIM][PF_6].

Electrode	[Bu_4N][PF_6]		[BMIM][PF_6]	
	k^0_V (cm s^{-1})[a]	k^0_W (cm s^{-1})	k^0_V (cm s^{-1})	k^0_W (cm s^{-1})
BDD	0.009	0.0008[b]	0.04	0.021
Pt	0.035	0.0007[b]	0.13	0.07
GC	≥0.50	0.10[a]	≥0.4	0.08
Au	0.08	0.02[b]	0.16	0.18

[a] Values are taken from reference [14].
[b] Estimated from ΔE_p using the DigiElch digital simulation software.

References

[1] D. Gatteschi, A. Caneschi, L. Pardi, R. Sessoli, Large clusters of metal ions: the transition from molecular to bulk magnets, Science 265 (1994) 1054–1058.
[2] E. Coronado, C.J. Gomez-Garcia, Polyoxometalate-based molecular materials, Chem. Rev. 98 (1998) 273–296.
[3] M. Pope, A. Müller, Polyoxometalate Chemistry from Topology via Self-Assembly to Applications, Springer Science & Business Media, 2001.
[4] C.L. Hill, C.M. Prosser-McCartha, Homogeneous catalysis by transition metal oxygen anion clusters, Coord. Chem. Rev. 143 (1995) 407–455.
[5] M. Sadakane, E. Steckhan, Electrochemical properties of polyoxometalates as electrocatalysts, Chem. Rev. 98 (1998) 219–238.
[6] C. Baffert, S.W. Feldberg, A.M. Bond, D.-L. Long, L. Cronin, pH-Dependence of the aqueous electrochemistry of the two-electron reduced α-$[Mo_{18}O_{54}(SO_3)]$ sulfite Dawson-like polyoxometalate anion derived from its triethanolammonium salt, Dalton Trans. (2007) 4599–4607.
[7] A.W. Mariotti, J. Xie, B.F. Abrahams, A.M. Bond, A.G. Wedd, Synthesis and voltammetry of $[Bmim]_4[\alpha\text{-}S_2W_{18}O_{62}]$ and related compounds: rapid precipitation and dissolution of reduced surface films, Inorg. Chem. 46 (2007) 2530–2540.
[8] S. Himeno, M. Takamoto, T. Ueda, Synthesis, characterisation and voltammetric study of a β-Keggin-type $[PW_{12}O_{40}]^{3-}$ complex, J. Electroanal. Chem. 465 (1999) 129–135.
[9] J. Zhang, A.M. Bond, D.R. MacFarlane, S.A. Forsyth, J.M. Pringle, A.W. Mariotti, A.F. Glowinski, A.G. Wedd, Voltammetric studies on the reduction of polyoxometalate anions in ionic liquids, Inorg. Chem. 44 (2005) 5123–5132.
[10] K.K. Kasem, Electrochemical behavior of sodium 12-tungstodicobaltoate in aqueous and mixed solvent electrolytes, Electrochim. Acta 41 (1996) 205–211.
[11] M. Takamoto, T. Ueda, S. Himeno, Solvation effect of Li^+ on the voltammetric properties of $[PW_{12}O_{40}]^{3-}$ in binary solvent mixtures, J. Electroanal. Chem. 521 (2002) 132–136.
[12] K. Bano, J. Zhang, A.M. Bond, P.R. Unwin, J.V. Macpherson, Diminished electron transfer kinetics for $[Ru(NH_3)_6]^{3+/2+}$, $[\alpha\text{-}SiW_{12}O_{40}]^{4-/5-}$ and $[\alpha\text{-}SiW_{12}O_{40}]^{5-/6-}$ processes at boron-doped diamond electrodes, J. Phys. Chem. C 119 (2015) 12464–12472.
[13] J. Li, A.M. Bond, J. Zhang, Probing electrolyte cation effects on the electron transfer kinetics of the $[\alpha\text{-}SiW_{12}O_{40}]^{4-/5-}$ and $[\alpha\text{-}SiW_{12}O_{40}]^{5-/6-}$ processes using a boron-doped diamond electrode, Electrochim. Acta 178 (2015) 631–637.

Please cite this article as: J. Li, et al., Influence of 1-butyl-3-methylimidazolium on the electron transfer kinetics associated with the [SVW11O40]3−/4− (VV/IV) and [SV..., Journal of Electroanalytical Chemistry (2016), http://dx.doi.org/10.1016/j.jelechem.2016.04.050

[14] J. Li, S.-X. Guo, C.L. Bentley, K. Bano, A.M. Bond, J. Zhang, T. Ueda, Electrode material dependence of the electron transfer kinetics associated with the $[SVW_{11}O_{40}]^{3-/4-}$ ($V^{V/IV}$) and $[SVW_{11}O_{40}]^{4-/5-}$ ($W^{VI/V}$) processes in dimethylformamide, Electrochim. Acta 201 (2016) 45–56.

[15] C.H. Bamford, C.F.H. Tipper, R.G. Compton, Electrode Kinetics: Principles and Methodology, vol. 26, Elsevier, 1986.

[16] J.-M. Savéant, Elements of Molecular and Biomolecular Electrochemistry: An Electrochemical Approach to Electron Transfer Chemistry, John Wiley & Sons, 2006.

[17] J. Zhang, A.M. Bond, Theoretical studies of large amplitude alternating current voltammetry for a reversible surface-confined electron transfer process coupled to a pseudo first-order electrocatalytic process, J. Electroanal. Chem. 600 (2007) 23–34.

[18] J. Zhang, S.-X. Guo, A.M. Bond, Discrimination and evaluation of the effects of uncompensated resistance and slow electrode kinetics from the higher harmonic components of a Fourier transformed large-amplitude alternating current voltammogram, Anal. Chem. 79 (2007) 2276–2288.

[19] A.M. Bond, N.W. Duffy, S.-X. Guo, J. Zhang, D. Elton, Changing the look of voltammetry, Anal. Chem. 77 (2005) 186 A–195 A.

[20] J. Zhang, S.-X. Guo, A.M. Bond, F. Marken, Large-amplitude Fourier transformed high-harmonic alternating current cyclic voltammetry: kinetic discrimination of interfering faradaic processes at glassy carbon and at boron-doped diamond electrodes, Anal. Chem. 76 (2004) 3619–3629.

[21] A.P. O'Mullane, J. Zhang, A. Brajter-Toth, A.M. Bond, Higher harmonic large-amplitude fourier transformed alternating current voltammetry: analytical attributes derived from studies of the oxidation of ferrocenemethanol and uric acid at a glassy carbon electrode, Anal. Chem. 80 (2008) 4614–4626.

[22] D.R. MacFarlane, M. Forsyth, P.C. Howlett, M. Kar, S. Passerini, J.M. Pringle, H. Ohno, M. Watanabe, F. Yan, W. Zheng, S. Zhang, J. Zhang, Ionic liquids and their solid-state analogues as materials for energy generation and storage, Nat. Rev. Mater. 1 (2016) 15005.

[23] J. Zhang, A.M. Bond, Practical considerations associated with voltammetric studies in room temperature ionic liquids, Analyst 130 (2005) 1132–1147.

[24] F. Endres, S.Z. El Abedin, Air and water stable ionic liquids in physical chemistry, Phys. Chem. Chem. Phys. 8 (2006) 2101–2116.

[25] M.C. Buzzeo, R.G. Evans, R.G. Compton, Non-haloaluminate room-temperature ionic liquids in electrochemistry — a review, ChemPhysChem 5 (2004) 1106–1120.

[26] T. Ueda, J.-i. Nambu, J. Lu, S.-X. Guo, Q. Li, J.F. Boas, L.L. Martin, A.M. Bond, Structurally characterised vanadium (V)-substituted Keggin-type heteropolysulfates $[SVM_{11}O_{40}]^{3-}$ (M = Mo, W): voltammetric and spectroscopic studies related to the V (V)/V (IV) redox couple, Dalton Trans. 43 (2014) 5462–5473.

[27] M.-H. Chiang, J.A. Dzielawa, M.L. Dietz, M.R. Antonio, Redox chemistry of the Keggin heteropolyoxotungstate anion in ionic liquids, J. Electroanal. Chem. 567 (2004) 77–84.

[28] R.S. Nicholson, Theory and application of cyclic voltammetry for measurement of electrode reaction kinetics, Anal. Chem. 37 (1965) 1351–1355.

[29] R.S. Nicholson, I. Shain, Theory of stationary electrode polarography. Single scan and cyclic methods applied to reversible, irreversible, and kinetic systems, Anal. Chem. 36 (1964) 706–723.

[30] K. Aoki, K. Hayashi, A frequency-dependent capacitance model and analysis of the ac impedance of conducting polyaniline films, J. Electroanal. Chem. 384 (1995) 31–37.

[31] S.-X. Guo, S.W. Feldberg, A.M. Bond, D.L. Callahan, P.J. Richardt, A.G. Wedd, Systematic approach to the quantitative voltammetric analysis of the Fe^{III}/Fe^{II} component of the $[\alpha_2\text{-}Fe(OH_2)P_2W_{17}O_{61}]^{7-/8-}$ reduction process in buffered and unbuffered aqueous media, J. Phys. Chem. B 109 (2005) 20641–20651.

[32] Y. Liu, S.-X. Guo, A.M. Bond, J. Zhang, Y.V. Geletii, C.L. Hill, Voltammetric determination of the reversible potentials for $[\{Ru_4O_4(OH)_2(H_2O)_4\}(\gamma\text{-}SiW_{10}O_{36})_2]^{10-}$ over the pH range of 2–12: electrolyte dependence and implications for water oxidation catalysis, Inorg. Chem. 52 (2013) 11986–11996.

[33] A.J. Bard, L.R. Faulkner, Electrochemical Methods: Fundamentals and Applications, second ed. Wiley and Sons, Hoboken, 2001.

[34] Y. Li, S. Roy, T. Ben, S. Xu, S. Qiu, Micropore engineering of carbonized porous aromatic framework (PAF-1) for supercapacitors application, Phys. Chem. Chem. Phys. 16 (2014) 12909–12917.

[35] D.H. Evans, One-electron and two-electron transfers in electrochemistry and homogeneous solution reactions, Chem. Rev. 108 (2008) 2113–2144.

[36] D.A. Corrigan, D.H. Evans, Cyclic voltammetric study of *tert*-nitrobutane reduction in acetonitrile at mercury and platinum electrodes: observation of a potential dependent electrochemical transfer coefficient and the influence of the electrolyte cation on the rate constant, J. Electroanal. Chem. 106 (1980) 287–304.

Please cite this article as: J. Li, et al., Influence of 1-butyl-3-methylimidazolium on the electron transfer kinetics associated with the [SVW11O40]3−/4− (VV/IV) and [SV..., Journal of Electroanalytical Chemistry (2016), http://dx.doi.org/10.1016/j.jelechem.2016.04.050

Supporting Information

Influence of 1-butyl-3-methylimidazolium on the Electron Transfer Kinetics Associated with the $[SVW_{11}O_{40}]^{3-/4-}$ ($V^{V/IV}$) and $[SVW_{11}O_{40}]^{4-/5-}$ ($W^{VI/V}$) Processes in Dimethylformamide

Jiezhen Li, Cameron L. Bentley, Alan M. Bond* and Jie Zhang*

School of Chemistry and ARC Centre of Excellence for Electromaterials Science, Monash University, Clayton, Victoria 3800, Australia

Tadaharu Ueda

Department of Applied Science, Faculty of Science, Kochi University, Kochi 780-8520, Japan

Corresponding authors: jie.zhang@monash.edu, alan.bond@monash.edu

Instrumentation and procedures. All electrochemical studies were carried out at 22 ± 2°C using a standard three electrode electrochemical cell. The working electrodes were platinum (Pt, nominal diameter = 1.0 mm), gold (Au, nominal diameter = 1.5 mm), glassy carbon (GC, nominal diameter = 1.0 mm) or BDD (constructed at the University of Warwick, UK, nominal diameter = 1.0 mm) [S1]. The BDD electrode was polycrystalline, hydrogen-terminated, degenerately doped above the metallic threshold, lapped to ~ nanometer roughness, and fabricated as described elsewhere [S2]. The electrochemically effective areas (A) of the macrodisk working electrodes were calculated from analysis of a plot of DC peak current versus the square root of scan rate for the oxidation of 1.0 mM Fc in CH_3CN (0.1 M $[Bu_4N][PF_6]$) using the Randles-Sevcik relationship and the known diffusion coefficient of 2.4×10^{-5} cm^2 s^{-1} for Fc under these conditions [S3].

$$i_p = 0.4463nFA\left(\frac{nFDv}{RT}\right)^{1/2}C \qquad \text{(S1)}$$

In eq. S1, i_p is the oxidation peak current, n is the number of electrons transerred (n = 1), C is the bulk concentration, D is the diffusion coefficient of Fc, T is the absolute temperature, R is the universal gas constant, F is Faraday's constant, A is the electrode area and v is the scan rate. The areas of the Pt, Au, GC and BDD macrodisk electrodes determined in this manner were 7.71×10^{-3} cm^2, 7.85×10^{-2} cm^2, 7.45×10^{-3} cm^2 and 8.14×10^{-3} cm^2, respectively.

Prior to each voltammetric experiment, the working electrode was polished with an aqueous 0.3 μm alumina slurry on a clean polishing cloth, rinsed with water, sonicated thoroughly in water to remove alumina, rinsed with acetone, and finally dried under nitrogen. Platinum wire was used as the auxiliary and reference electrodes. The potential of the Pt quasi-reference electrode was calibrated against the IUPAC recommended $Fc^{0/+}$ process [S4]. All electrolyte solutions were degassed with

N_2 for at least 5 min prior to experimentation, and a blanket of N_2 was maintained over the electrolytes while undertaking experiments.

DC cyclic voltammetric experiments were carried out using a CHI 760E electrochemical workstation (CH Instruments, Texas, USA). Large amplitude FTAC voltammetric experiments were undertaken with a home built instrument [S5] using an applied sine wave perturbation with an amplitude (ΔE) of 80 mV and frequency (f) of 9.02 Hz or 34.01 Hz, superimposed onto the DC potential ramp. After data collection, the total DC plus AC current was subjected to Fourier transformation to obtain the power spectrum. After selection of the frequency band of interest, inverse Fourier transformation was used to generate the required DC or AC harmonic components [S5-7].

Simulations and AC data analysis. For slow kinetics process, DigiElch software was used for the simulations. Simulations of FTAC voltammograms were carried out using the MECSim (Monash Electrochemistry Simulator, http://www.garethkennedy.net/MECSim.html) software. This Fortran package uses the expanding spatial grid formulation [S8] and is based on the mathematical approach derived by Rudolph [S9], with minor variations. The Butler-Volmer theory of electron transfer [S10] was used to describe the potential dependence of the electrode kinetics for the simple one-electron transfer reaction given in eq. S2.

$$O + e^- \rightleftharpoons R\ (E^0, k^0, \alpha) \qquad \text{(S2)}$$

where E^0 is the reversible potential. FTAC voltammetric data obtained from either experiment or simulation in the time domain were converted to the frequency domain to generate the power spectrum [S11, S12]. Six parameters E^0, k^0, α, D, R_u and C_{dl} (double layer capacitance) were determined in order to quantitatively define all aspects of the electrode processes. The R_u value was determined experimentally from

the *RC* time constant method available on the CHI potentiostat, E^0 was estimated from the midpoint of the reduction (E_p^{red}) and oxidation (E_p^{ox}) peak potentials in a DC cyclic voltammetric experiment and the *D* value of $[SVW_{11}O_{40}]^{3-}$ was calculated from the reduction peak measured at a GC electrode in DMF using the Randles-Sevcik relationship (see eq. S1) [S13]. The C_{dl} value was quantified from the background current in the fundamental harmonic component at potentials where faradaic current is absent. In order to define the potential dependence of C_{dl}, a non-linear capacitor model was used, as described elsewhere [S14]:

$$C_{dl}(t) = c_0 + c_1E(t) + c_2E^2(t) + c_3E^3(t) + c_4E^4(t) \qquad \text{(S3)}$$

In eq. S3, c_0, c_1, c_2, c_3, and c_4 are the coefficients that determine the degree of nonlinearity of the capacitor. Finally, k^0 and α values were determined by comparison of the experimental and simulated higher order AC harmonic component data.

As demonstrated in our previous study [S15], the impact of the cross redox reaction between $[SVW_{11}O_{40}]^{3-}$ and $[SVW_{11}O_{40}]^{5-}$ (eq. S4) on the voltammetric characteristics is insignificant under the conditions employed.

$$[SVW_{11}O_{40}]^{3-} + [SVW_{11}O_{40}]^{5-} \rightleftharpoons 2[SVW_{11}O_{40}]^{4-} \qquad \text{(S4)}$$

Consquently, the cross redox reaction does not need to be considered in simulations when determining the electrode kinetics of the $V^{IV/V}$ and $W^{VI/V}$ processes.

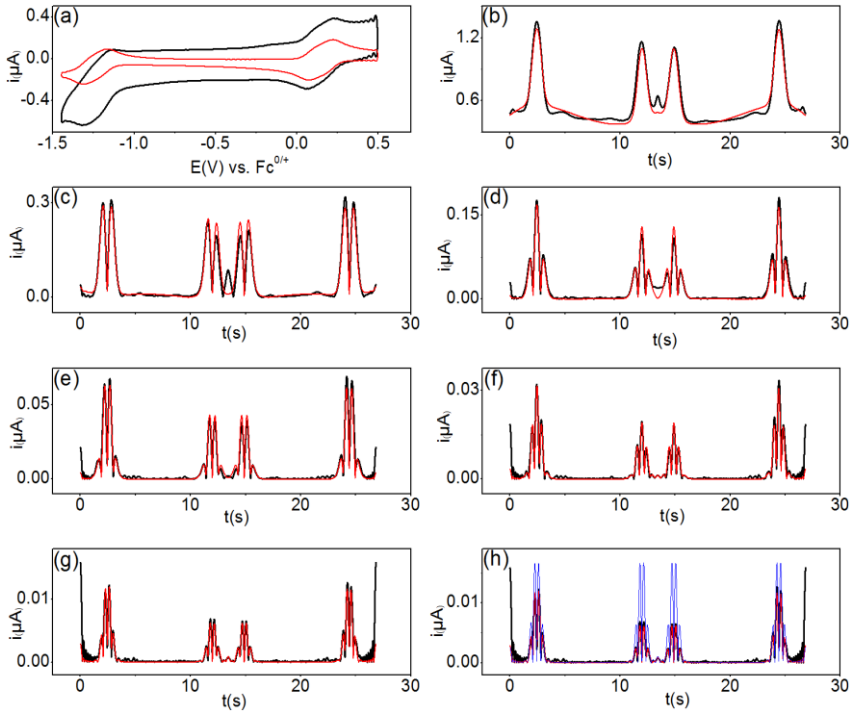

Figure S1. Comparison of simulated (—) and experimental (—) FTAC voltammetric data obtained for the $V^{IV/V}$ and $W^{VI/V}$ processes in DMF containing 0.20 mM $[SVW_{11}O_{40}]^{3-}$ and 0.5 M [BMIM][PF_6] at a BDD electrode with ΔE = 80 mV, f = 9.02 Hz and v = 0.145 V s^{-1}. (a) aperiodic DC component, (b-g) 1st to 6th AC harmonic components, and (h) simulated 6th harmonic component for the $V^{V/IV}$ process in a reversible case (—). To obtain the simulated data, k^0_V = 0.05 cm s^{-1}, α_V = 0.70, k^0_W = 0.02 cm s^{-1} and α_W = 0.50 were used. Other parameters used in the simulations are provided in Table 2.

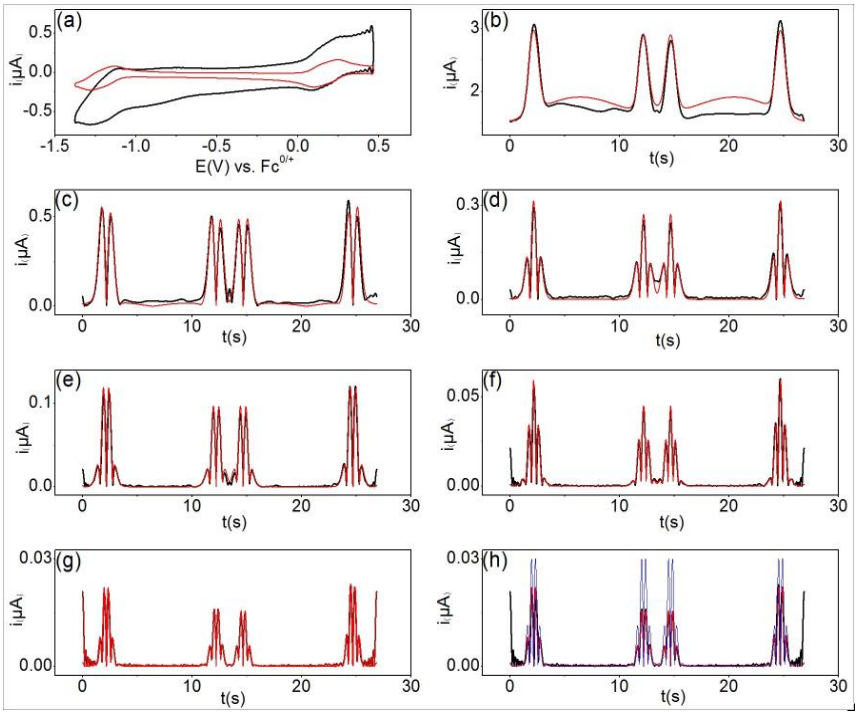

Figure S2. Comparison of simulated (—) and experimental (—) FTAC voltammetric data obtained for the $V^{IV/V}$ and $W^{VI/V}$ processes in DMF containing 0.20 mM $[SVW_{11}O_{40}]^{3-}$ and 0.5 M [BMIM][PF_6] at a Pt electrode with ΔE = 80 mV, f = 34.01 Hz and v = 0.137 V s^{-1}. (a) aperiodic DC component, (b-g) 1st to 6th AC harmonic components, and (h) simulated 6th harmonic component for the $V^{V/IV}$ process in a reversible case (—). To obtain the simulated data, ! ¦ = 0.13 cm s^{-1}, α_V = 0.50, ! ¦ = 0.06 cm s^{-1} and α_W = 0.50 were used. Other parameters used in the simulations are provided in Table 2.

! !

! S6

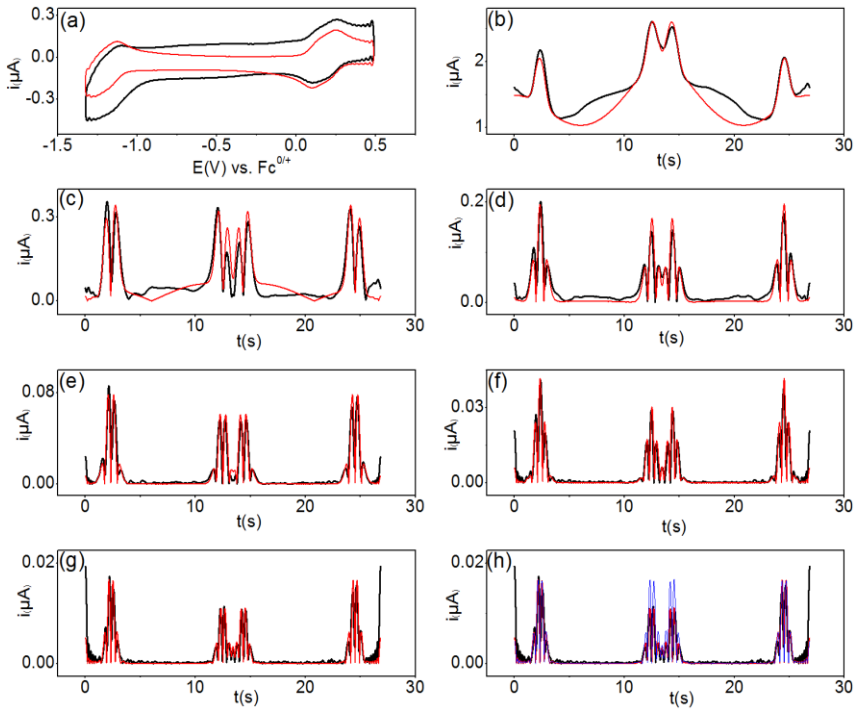

Figure S3. Comparison of simulated (—) and experimental (—) FTAC voltammetric data obtained for the $V^{IV/V}$ and $W^{VI/V}$ processes in DMF containing 0.20 mM $[SVW_{11}O_{40}]^{3-}$ and 0.5 M [BMIM][PF_6] at a GC electrode with ΔE = 80 mV, f = 9.02 Hz and v = 0.135 V s^{-1}. (a) aperiodic DC component, (b-g) 1st to 6th AC harmonic components, and (h) simulated 6th harmonic component for the $V^{V/IV}$ process in a reversible case (—). To obtain the simulated data, $k^0_V \geq 0.2$ cm s^{-1}, α_V = 0.50, k^0_W = 0.06 cm s^{-1} and α_W = 0.50 were used. Other parameters used in the simulations are provided in Table 2.

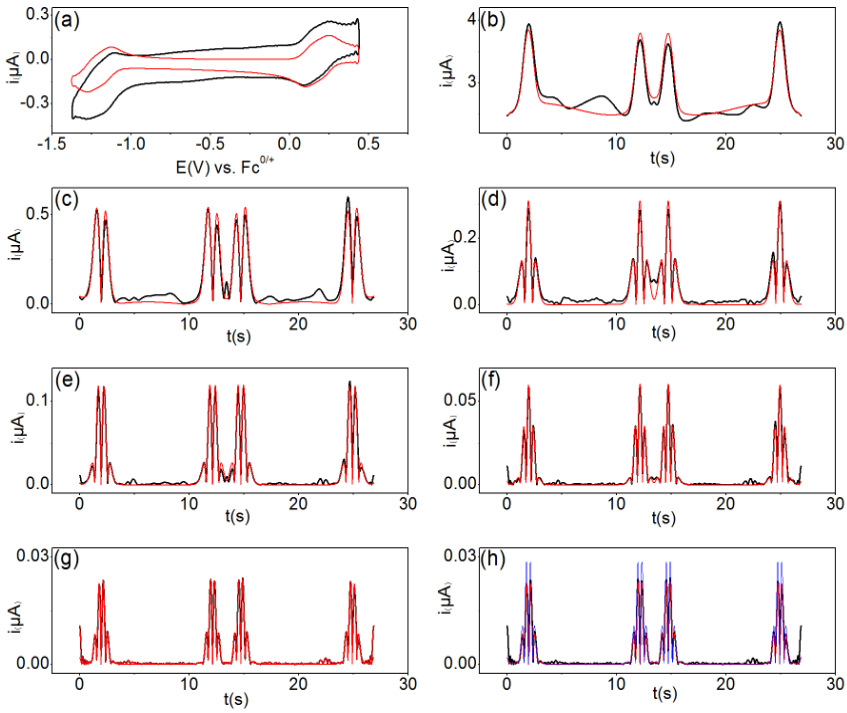

Figure S4. Comparison of simulated (—) and experimental (—) FTAC voltammetric data obtained for the $V^{IV/V}$ and $W^{VI/V}$ processes in DMF containing 0.20 mM $[SVW_{11}O_{40}]^{3-}$ and 0.5 M [BMIM][PF_6] at an Au electrode with ΔE = 80 mV, f = 34.01 Hz and v = 0.136 V s^{-1}. (a) aperiodic DC component, (b-g) 1st to 6th AC harmonic components, and (h) simulated 6th harmonic component for the $V^{V/IV}$ process in a reversible case (—). To obtain the simulated data, k^0_V = 0.18 cm s^{-1}, α_V = 0.50, k^0_W = 0.18 cm s^{-1} and α_W = 0.50 were used. Other parameters used in the simulations are provided in Table 2.

REFERENCES

[S1] K. Bano, J. Zhang, A.M. Bond, P.R. Unwin, J.V. Macpherson, Diminished Electron Transfer Kinetics for $[Ru(NH_3)_6]^{3+/2+}$, $[\alpha\text{-}SiW_{12}O_{40}]^{4-/5-}$ and $[\alpha\text{-}SiW_{12}O_{40}]^{5-/6-}$ Processes at Boron-Doped Diamond Electrodes, J. Phys. Chem. C 119 (2015) 12464-12472.
[S2] L. Hutton, M.E. Newton, P.R. Unwin, J.V. Macpherson, Amperometric oxygen sensor based on a platinum nanoparticle-modified polycrystalline boron doped diamond disk electrode, Anal. Chem. 81 (2008) 1023-1032.
[S3] J. Zhang, S.-X. Guo, A.M. Bond, Discrimination and evaluation of the effects of uncompensated resistance and slow electrode kinetics from the higher harmonic components of a Fourier transformed large-amplitude alternating current voltammogram, Anal. Chem. 79 (2007) 2276-2288.
[S4] G. Gritzner, J. Kuta, Recommendations on reporting electrode potentials in nonaqueous solvents (Recommendations 1983), Pure Appl. Chem. 56 (1984) 461-466.
[S5] A.M. Bond, N.W. Duffy, S.-X. Guo, J. Zhang, D. Elton, Changing the look of voltammetry, Anal. Chem. 77 (2005) 186 A-195 A.
[S6] S.-X. Guo, A.M. Bond, J. Zhang, Fourier Transformed Large Amplitude Alternating Current Voltammetry: Principles and Applications, Rev. Polarogr. 61 (2015) 21-32.
[S7] A.M. Bond, D. Elton, S.-X. Guo, G.F. Kennedy, E. Mashkina, A.N. Simonov, J. Zhang, An integrated instrumental and theoretical approach to quantitative electrode kinetic studies based on Large Amplitude Fourier Transformed ac Voltammetry: A mini-review, Electrochem. Commun. 57 (2015) 78-83.
[S8] S.W. Feldberg, Optimization of explicit finite-difference simulation of electrochemical phenomena utilizing an exponentially expanded space grid: Refinement of the Joslin-Pletcher algorithm, J. Electroanal. Chem. 127 (1981) 1-10.
[S9] M. Rudolph, A fast implicit finite difference algorithm for the digital simulation of electrochemical processes, J. Electroanal. Chem. 314 (1991) 13-22.
[S10] A.J. Bard, L.R. Faulkner, Electrochemical methods: fundamentals and applications, 2nd ed., Wiley and Sons, New York, 2001.
[S11] J. Zhang, S.-X. Guo, A.M. Bond, F. Marken, Large-amplitude Fourier transformed high-harmonic alternating current cyclic voltammetry: kinetic discrimination of interfering faradaic processes at glassy carbon and at boron-doped diamond electrodes, Anal. Chem. 76 (2004) 3619-3629.
[S12] A.A. Sher, A.M. Bond, D.J. Gavaghan, K. Harriman, S.W. Feldberg, N.W. Duffy, S.-X. Guo, J. Zhang, Resistance, capacitance, and electrode kinetic effects in fourier-transformed large-amplitude sinusoidal voltammetry: Emergence of powerful and intuitively obvious tools for recognition of patterns of behavior, Anal. Chem. 76 (2004) 6214-6228.
[S13] A.M. Bond, K. Bano, S. Adeel, L.L. Martin, J. Zhang, Fourier Transformed Large Amplitude AC Voltammetric Study of Tetrathiafulvalene (TTF): Electrode Kinetics of the $TTF^0/TTF^{\cdot+}$ and $TTF^{\cdot+}/TTF^{2+}$ Processes, ChemElectroChem 1 (2014) 99-107.
[S14] A.M. Bond, N.W. Duffy, D.M. Elton, B.D. Fleming, Characterization of nonlinear background components in voltammetry by use of large amplitude

periodic perturbations and Fourier transform analysis, Anal. Chem. 81 (2009) 8801-8808.
[S15] J. Li, S.-X. Guo, C.L. Bentley, K. Bano, A.M. Bond, J. Zhang, T. Ueda, Electrode Material Dependence of the Electron Transfer Kinetics Associated with the $[SVW_{11}O_{40}]^{3-/4-}$ ($V^{V/IV}$) and $[SVW_{11}O_{40}]^{4-/5-}$ ($W^{VI/V}$) Processes in Dimethylformamide, Electrochim. Acta, under revision.

Chapter 6

Electrolyte Cation Dependence of the Electron Transfer Kinetics Associated with the $[SVW_{11}O_{40}]^{3-/4-}$ ($V^{V/IV}$) and $[SVW_{11}O_{40}]^{4-/5-}$ ($W^{VI/V}$) Processes in Propylene Carbonate

Jiezhen Li[a], Cameron L. Bentley[b], Tadaharu Ueda[c], Alan M. Bond[a,*] and Jie Zhang[a,*]

[a]School of Chemistry and ARC Centre of Excellence for Electromaterials Science, Monash University, Clayton, Vic 3800, Australia

[b]Department of Chemistry, University of Warwick, Coventry, CV4 7AL, U.K.

[c]Department of Applied Science, Kochi University, Japan

Corresponding authors: jie.zhang@monash.edu, alan.bond@monash.edu

Abstract

Changing the supporting electrolyte cation from tetrabutylammonium to 1-butyl-3-methylimidazolium is known to significantly increase the apparent heterogeneous electron transfer rate constants (k^0 value at the formal reversible potential (E_F^0)) associated with the $[SVW_{11}O_{40}]^{3-/4-}$ ($V^{V/IV}$) and $[SVW_{11}O_{40}]^{4-/5-}$ ($W^{VI/V}$) processes in aprotic organic media. In this study, supporting electrolytes containing 7 different cations, namingly 1-ethyl-3-methylimidazolium ($[EMIM]^+$), 1-butyl-3-methylimidazolium ($[BMIM]^+$), 1-butyl-1-methylpyrrolidinium ($[Py_{14}]^+$), tetraethylammonium ($[TEA]^+$), tetrapropylammonium ($[TPA]^+$), tetrabutylammonium ($[TBA]^+$) and tetrahexylammonium ($[THA]^+$), have been investigated in order provide a systematic account of the influence of electrolyte cations on the rate of polyoxometalate (POM) electron transfer at a platinum disk electrode. Fourier transformed alternating current (FTAC) voltammetry has been used for the measurement of fast kinetics and DC cyclic voltammetry for slow processes. The new data reveal the formal reversible potentials and electron-transfer rate constants associated with the $V^{V/IV}$ (k_V^0) and $W^{VI/V}$ (k_W^0) processes correlate with the size of the supporting electrolyte cation. k_V^0 and k_W^0 values decrease in the order, $[EMIM]^+ > [BMIM]^+ > [Py_{14}]^+ \approx [TEA]^+ > [TPA]^+ > [TBA]^+ > [THA]^+$ for both processes. However, while k_V^0 decreases gently with increasing cation size (k^0 = 0.1 and 0.002 cm s^{-1} with $[EMIM]^+$ and $[THA]^+$ electrolyte cations, respectively), the decrease in k_W^0 is much more drastic (k^0 = 0.1 and 2×10^{-6} cm s^{-1} for $[EMIM]^+$ and $[THA]^+$, respectively). Possible explanations for the observed trends are discussed (*e.g.*, ion-pairing, viscosity, adsorption and the double-layer effect), with inhibition of electron-transfer by a blocking "film" of electrolyte cations considered likely to be the dominant factor, supported by a linear plot of $\ln(k^0)$ vs. $\ln(d)$

(where d is the estimated thickness of the adsorbed layer on the electrode surface) for both the $V^{V/IV}$ and $W^{VI/V}$ processes.

Introduction

It is of fundamental importance in electrochemistry to understand the factors that govern the rate of heterogeneous electron transfer. For an electrode reaction, this typically involves the transfer of charge (electrons) across an interface between a solid electrode and liquid electrolyte. It follows that the rate of electron transfer is governed by both the physicochemical properties of the electrode/electrolyte interface and the nature of the redox-active species. For an outer-sphere one electron transfer processes such as the reduction of $[Ru(NH_3)_6]^{3+}$ to $[Ru(NH_3)_6]^{2+}$ or the oxidation of ferrocene (Fc) to ferrenium cation (Fc^+), very similar electrochemical behavior is observed at Pt, Au, and carbon electrodes.[1, 2] However, the kinetics of the $Fe^{2+/3+}$ process, also considered to be an outer-sphere reaction in some studies, is much slower and differs markedly at these electrode materials.[3, 4]

The effects of the nature of the solvent (donor/acceptor or acid/base properties), supporting electrolyte and electrode material on electrode kinetics have been studied extensively.[5-12] For example, if the outer-shell contribution to the activation energy is the major factor governing the rate of electron transfer, the heterogeneous electron-transfer rate constant (k^0) exhibits a strong dependence on the properties of the solvent (dielectric constant).[13, 14] In addition, the rates of electrode reactions can be profoundly affected by the identity of the ions present in the supporting electrolyte[15-19]. For example, Peover and Davies[20] reported that the highly irreversible (kinetically sluggish) second step for reduction of 9,10-anthraquinone in

dimethylformamide (DMF) can be made reversible (kinetically facile) through the addition of alkali metal ions. This effect was attributed to interactions (ion-pairing) between the semiquinone anion and the alkali metal cations.

Polyoxometalates (POMs) are anionic oxoclusters containing early transition metals in high oxidation states. They are nano-sized and display a wide variety of compositions and structures. They exhibit a wide range of properties, which have led to proposed applications in diverse fields such as medicine, photochromic materials, solar energy, and so forth.[21-23] In particular, POMs can undergo fast, reversible and stepwise multielectron-transfer reactions without significant structural change, meaning they can be employed as catalysts for many redox reactions.[24-27] Furthermore, the properties of a POM, such as solubility, redox potential, and acidity can be finely-tuned by varying the constituent elements.[28]

The thermodynamic properties (formal reversible potentials, E_F^0) of POMs have been studied extensively.[28-30] For example, the electrochemical behaviour of $[Co_2W_{12}O_{42}]^{8-}$ was found to be highly solvent dependent.[31] The reversible potentials associated with these W-based redox centres shift negatively in a 50% mixed solvent aqueous electrolyte of dimethylformamide/water, acetonitrile/water or acetone/water compared to a pure aqueous electrolyte solution, while in dioxane/water mixtures, the processes shifted positively. The acidity of the media (proton availability) also influences the thermodynamic properties of POMs. Thus, while $[PMo_{12}O_{40}]^{3-}$ undergoes successive one-electron transfer processes in acetonitrile, the addition of acid causes a substantial change in reversible potential, so that when a high concentration is present, overall two-electron processes are detected.[32]

The kinetic properties (standard electron transfer rate constant, k^0 at E_F^0, and electron transfer coefficient, α) of POMs remain much less explored than the

thermodynamic ones. Recently, we have reported a series of studies on the electrode kinetics of POMs.[33-36] In aqueous media, the k^0 values of the Keggin-type silicon tungstate POMs, $[SiW_{12}O_{40}]^{4-}$ and $[SiW_{12}O_{40}]^{5-}$, were found to be electrode material dependent.[33, 34] Much slower rate constants were found with boron-doped diamond (BDD) electrode compared to use of glassy carbon (GC) as the electrode material.[33] The effect of the electrolyte cation (Li^+, Na^+, K^+ and NH_4^+) on the electrode kinetics of these processes has also been studied[34]. In organic media (dimethylformamide) containing supporting electrolyte, the electrode kinetics associated with the $[SVW_{11}O_{40}]^{3-/4-/5-}$ processes are strongly dependent on the electrode material as well as the ionic strength.[35] In our most recent study, we showed that changing the electrolyte cation from tetrabutylammonium to 1-butyl-3-methylimidazolium can significantly increase the electron-transfer kinetics of the $[SVW_{11}O_{40}]^{3-/4-/5-}$ processes at Pt, Au and BDD electrodes. We attributed this and other trends obvious to double layer effects and the nature of the electron-transfer processes (outer-sphere for the $V^{V/IV}$ reaction vs. inner-sphere for the $W^{VI/V}$ one).[36]

In the present study, our previous work is expanded systematically to provide a general account of the influence of electrolyte cations on the rate of POM electron transfer, using the $[SVW_{11}O_{40}]^{3-/4-/5-}$ reductive reactions as exemplar processes. The structure of $[SVW_{11}O_{40}]^{3-}$[37] shown in Figure 1 shows the location of the V and W metal constituents. $[SVW_{11}O_{40}]^{3-}$ exhibits three well-defined one-electron reduction processes in molecular solvent (electrolyte) media.[37] The two initial processes, which are the focus for the current study, correspond to the reduction of V^V to V^{IV} (Eq. 1) and W^{VI} to W^V (Eq. 2).

$$[SV^{V}W_{11}^{VI}O_{40}]^{3-} + e^- \rightleftharpoons [SV^{IV}W_{11}^{VI}O_{40}]^{4-} \qquad (1)$$

$$[SV^{IV}W_{11}^{VI}O_{40}]^{4-} + e^- \rightleftharpoons [SV^{IV}W^{V}W_{10}^{VI}O_{40}]^{5-} \qquad (2)$$

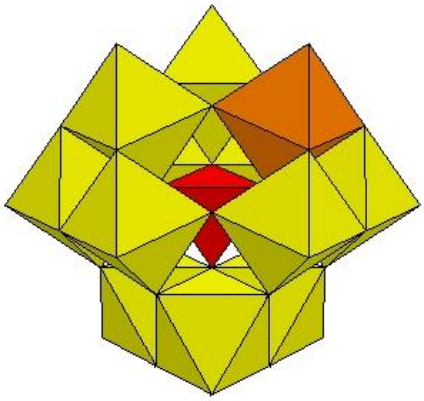

Figure 1. The structure of $[SVW_{11}O_{40}]^{3-}$. Color code: S (red), V (orange), W (yellow).[37]

Seven different electrolyte cations were used in this study, including imidazolium and tetraalkylammonium based cations (structures shown in Scheme 1). Salts containing large singly-charged cations such as tetraalkylammonium ions are commonly used for investigations in dipolar aprotic solvents due to their relatively high solubility and weak tendency to form ion associates with anions in these systems. However, a number of studies has been reported which demonstrate that the electrode kinetics of can depend on the nature (size or structural symmetry) of the tetraalkylammonium cations.[38-41] For example, the rate constants (k^0 values) of a series of organic molecules have been shown to decrease with increase in the size of the alkyl group.[38] The solvent chosen in this study is propylene carbonate (PC), which has a high dielectric constant (64.9 at 25°C[42]), reducing the influence of ion pairing effects. Supporting electrolytes were added at a concentration of 0.5 M to provide a well-defined double layer. As is the case in our previous study, fast electrode kinetics were measured using large-amplitude Fourier-transformed alternating current (FTAC) voltammetry, which exhibits superior kinetic sensitivity in comparison with the conventional dc voltammetry[43] and slow

processes were quantified by DC cyclic voltammetry using DigiElch digital simulation software package.

Scheme 1. Names, abbreviations and structures of the electrolyte cations used in this study.

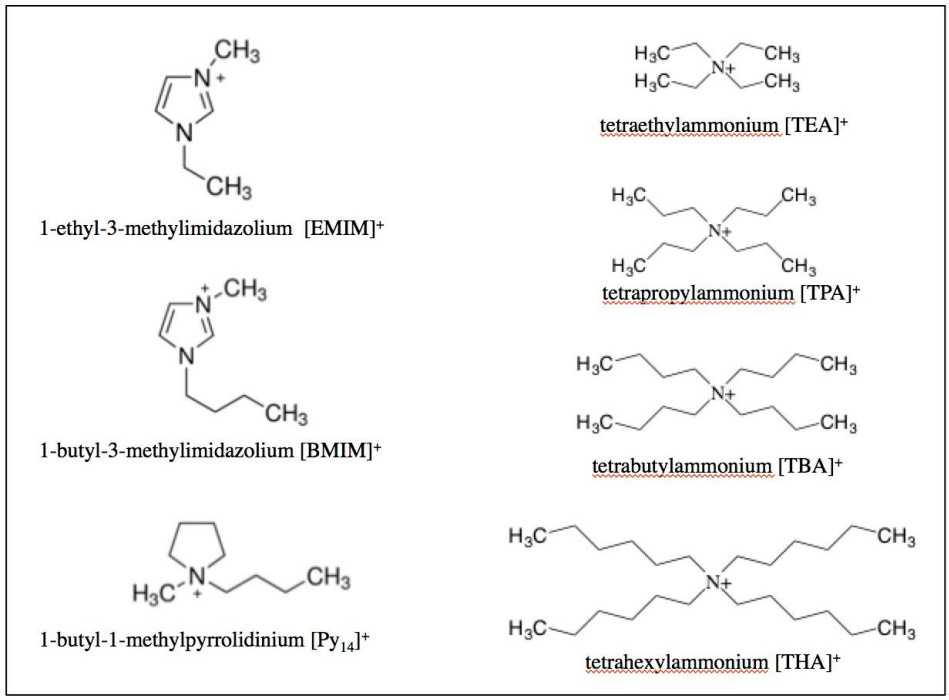

Experimental Section

Chemicals. Propylene carbonate (PC, 99.7%, Sigma-Aldrich), acetonitrile (CH_3CN, 97%, Sigma-Aldrich), ethanol (96%, Merck), 1-ethyl-3-methylimidazolium tetrafluoroborate ([EMIM][BF_4], 98%, Sigma-Aldrich), 1-butyl-3-methylimidazolium tetrafluoroborate ([BMIM][BF_4], 99%, IoLiTec), 1-butyl-3-methylimidazolium hexafluorophosphate ([BMIM][PF_6], 99%, IoLiTec), 1-butyl-1-methylpyrrolidinium tetrafluoroborate ([Py_{14}][BF_4], 99%, IoLiTec), tetraethylammonium tetrafluoroborate ([TEA][BF_4], 99%, Sigma-Aldrich), tetrabutylammonium hexafluorophosphate ([TBA][PF_6], 99%, Sigma-Aldrich) and tetrahexylammonium perchlorate ([THA][ClO_4], 99%, Sigma-Aldrich) were used as received from the manufacturer.

Ferrocene (Fc, Sigma-Aldrich, ≥ 98 %) was recrystallized from *n*-pentane (Merck) prior to use. Tetrapropylammonium tetrafluoroborate ([TPA][BF_4]) was prepared by a metathesis reaction between sodium tetrafluoroborate (Na[BF_4], Sigma-Aldrich) and tetrapropylammonium bromide ([TPA]Br, Sigma-Aldrich) in CH_3CN.

All electrochemical studies were carried out at 22 ± 2 °C using a standard three electrode electrochemical cell. Viscosity was measured using the falling ball method with an Anton Paar automated microviscometer (AMVn). The working electrode was platinum (Pt, nominal diameter = 1.0 mm) or glassy carbon (GC, nominal diameter = 1.0 mm). Platinum wire was used for the auxiliary and reference electrodes. Other experimental details are as reported elsewhere[36] and are summarized in the Supporting Information.

Results and Discussions

DC Cyclic Voltammetric Characterization of the $V^{V/IV}$ and $W^{VI/V}$ Processes. The $[SVW_{11}O_{40}]^{3-/4-}$ ($V^{V/IV}$) and $[SVW_{11}O_{40}]^{4-/5-}$ ($W^{VI/V}$) processes were initially characterized by DC cyclic voltammetry at a Pt electrode. Verification of the first process as reduction of V^V to V^{IV} and the second more negative one to reduction of W^{VI} to W^V is given in reference.[37] Figure 2 shows a comparison of the DC cyclic voltammograms obtained from 1.0 mM $[SVW_{11}O_{40}]^{3-}$ in PC containing 0.5 M electrolytes outlined in Scheme 1, at a scan rate (ν) of 0.1 V s^{-1}. Clearly, the formal reversible potentials (E_F^0) of the $V^{V/IV}$ and $W^{VI/V}$ processes, E_V^0 and E_W^0, are dependent upon the nature of the electrolyte. Slightly more positive E_V^0 and E_W^0 values are observed from [EMIM][BF_4] (0.316 V and -1.085 V, respectively) compared to [BMIM][BF_4] (0.306 V and -1.093 V, respectively). A larger variation is observed when using tetraalkylammonium cation as the cation constituent of the supporting

electrolyte, with E_V^0 and E_W^0 shifting towards more negative potentials in the order of $[Py_{14}]^+ \approx [TEA]^+ > [TPA]^+ > [TBA]^+ > [THA]^+$. The negative shift in the E_F^0 values, as well as the increased potential gap separating the $V^{V/IV}$ and $W^{VI/V}$ processes (ΔE_F^0) is attributed to increasingly strong interactions between the electrolyte cation and the reduced form of the POM (*e.g.*, $[SVW_{11}O_{40}]^{4-}$) compared to the oxidized form of the POM (*e.g.*, $[SVW_{11}O_{40}]^{3-}$). It should be noted that because $[SVW_{11}O_{40}]^{3-/4-/5-}$ are all highly negatively charged species, the identity of the anion (*e.g.*, $[BF_4]^-$ vs. $[PF_6]^-$ vs. $[ClO_4]^-$) is not expected to influence electrochemical behavior as confirmed by the fact that negligible differences in both reversible potentials and peak-to-peak separations was detected when using either [BMIM][BF_4] or [BMIM][PF_6] as the supporting electrolyte.

Table 1. DC cyclic voltammetric data derived at 22 ± 2 °C from the reduction of 1.0 mM $[SVW_{11}O_{40}]^{3-}$ in PC (0.5 M electrolyte) at a Pt macrodisk (diameter = 1.0 mm) electrode with a scan rate of 0.1 V s^{-1}.

Electrolyte	E_V^0(V)	$(\Delta E_p)_V$(V)	E_W^0(V)	$(\Delta E_p)_W$(V)	ΔE_F^0(V)
[EMIM][BF_4]	0.316	63	-1.085	65	1.400
[BMIM][BF_4]	0.306	67	-1.093	66	1.399
[BMIM][PF_6]	0.303	66	-1.090	68	1.393
[Py_{14}][BF_4]	0.333	76	-1.079	75	1.412
[TEA][BF_4]	0.342	79	-1.079	67	1.421
[TPA][BF_4]	0.309	82	-1.182	303	1.491
[TBA][PF_6]	0.254	88	-1.260	520	1.514
[THA][ClO_4]	0.214	110	-1.355	745	1.569

Another clearly evident feature is the electrolyte dependence of the DC voltammetric peak-to-peak separations, ΔE_p (= E_p^{Ox} - E_p^{Red}). Both $V^{V/IV}$ and $W^{VI/V}$ processes display similar trends in ΔE_p in the order $[EMIM]^+ \approx [BMIM]^+ > [Py_{14}]^+ \approx [TEA]^+ > [TPA]^+ > [TBA]^+ > [THA]^+$. Notable, ΔE_p values associated with the $V^{V/IV}$

process changes gradually, with the lowest and highest values being 63 and 110 mV for $[EMIM]^+$ and $[THA]^+$, respectively, whereas, in the case of the $W^{VI/V}$ process, ΔE_p changes significantly when changing the electrolyte cation from $[TEA]^+$ to $[TPA]^+$, $[TBA]^+$ and $[THA]^+$, with values of 67, 303, 520 and 745 mV, respectively. Even after considering differences in the uncompensated resistance (R_u) (*e.g.*, R_u = 415 and 1153 Ω with $[EMIM]^+$ and $[THA]^+$, respectively), a smaller ΔE_p reflects a larger k^0 value, as described in the classical theoretical treatment of dc cyclic voltammetric *I-E* curves by Nicholson and Shain.[44] This indicates that the kinetics of the $V^{V/IV}$ and $W^{VI/V}$ processes are electrolyte cation dependent in PC, as noted in other media.[36] Moreover, the kinetics of the $W^{VI/V}$ process appear to be more sensitive to the nature of electrolyte compared to the $V^{V/IV}$ one.

Full details of the E_F^0 and ΔE_p values associated with the $V^{V/IV}$ and $W^{VI/V}$ processes in the different electrolyte media at a Pt electrode, along with the separation between the E_F^0 values associated with the two processes (ΔE_F^0) are provided in Table 1. Finally, diffusion coefficients (*D*) calculated from the Randles-Sevcik relationship[35] based on the peak current associated with the reversible $V^{V/IV}$ process at a GC macrodisk electrode,[36] are included in Table 2. Interestingly, the value of *D* decreases by about 70% when changing the electrolyte cation from $[EMIM]^+$ to $[THA]^+$. The diffusion coefficient is governed by the Stokes-Einstein relationship[45],

$$D = \frac{k_B T}{6\pi\eta a} \tag{8}$$

where k_B is the Boltzmann constant, η is the viscosity of the medium and a is the hydrodynamic radius of the diffusing particle. Clearly, according to this equation, the value of *D* depends on the viscosity of the media as well as the size of the ion paired $[SVW_{11}O_{40}]^{3-}$. If it is assumed that the size term (a) is independent on the nature of

electrolyte, the D value of each electrolyte medium is expected to be inversely proportional to η values of corresponding media and the produced $[D \cdot \eta]$ is expected to be constant. However, there is no such relationship between D and η values as shown in Table 2. On this basis, both the size of the ion paired $[SVW_{11}O_{40}]^{3-}$ and viscosity are believed to contribute to difference in D values.

Table 2. Summary of the D values for the reduction of 1.0 mM $[SVW_{11}O_{40}]^{3-}$ in PC (0.5 M electrolyte) at a Pt macrodisk (diameter = 1.0 mm) electrode.

Electrolyte	η (cP)	D ($\times 10^6$ cm^2 s^{-1})	$[D \cdot \eta]$ ($\times 10^{13}$ m kg s^{-2})
$[EMIM][BF_4]$	3.07	1.3	4.0
$[BMIM][BF_4]$	3.21	1.1	3.5
$[Py_{14}][BF_4]$	3.44	0.93	3.2
$[TEA][BF_4]$	3.12	0.93	2.9
$[TPA][BF_4]$	3.58	0.77	2.8
$[TBA][PF_6]$	3.90	0.60	2.3
$[THA][ClO_4]$	4.98	0.42	2.1

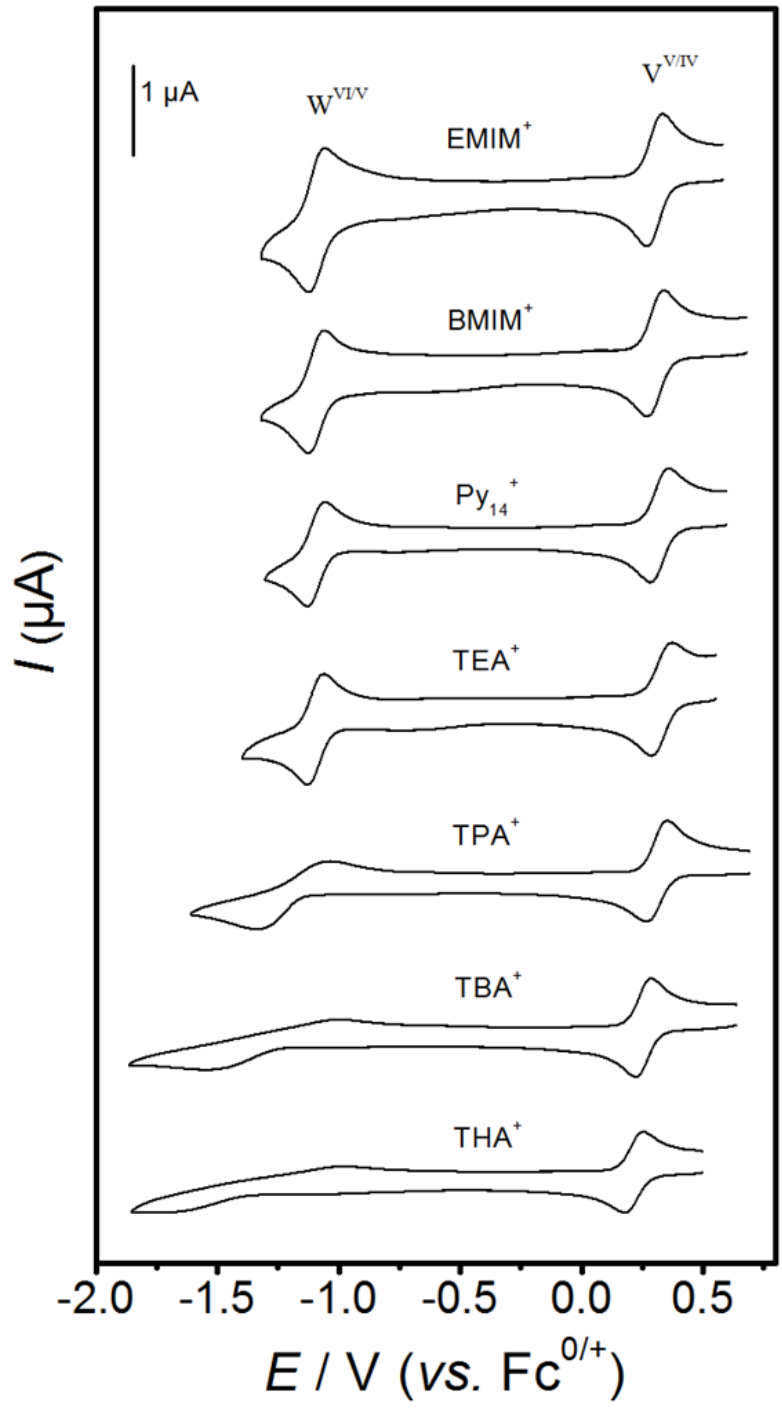

Figure 2. Dc cyclic voltammograms obtained at a Pt macrodisk electrode (v = 0.1 V s^{-1}) from the reduction of $[SVW_{11}O_{40}]^{3-}$ in PC containing 0.5 M electrolyte with constituent cations (from top to bottom) $[EMIM]^+$, $[BMIM]^+$, $[Py_{14}]^+$, $[TEA]^+$, $[TPA]^+$, $[TBA]^+$ and $[THA]^+$.

Determination of k^0 for fast processes by FTAC Voltammetry and slow ones by DC cyclic voltammetry. The k^0 values associated with the $V^{V/IV}$ (k_V^0) and $W^{VI/V}$ (k_W^0) processes in PC containing 0.5 M electrolyte were determined at a Pt macrodisk electrode by FTAC voltammetry using a sine wave perturbation (ΔE = 80 mV and f = 9.02 Hz or 27.01 Hz) and scanning the DC potential over the range where both the $V^{V/IV}$ and $W^{VI/V}$ reduction processes are present in the voltammogram. The parameters used in the simulations to define the electron transfer process, E^0, k^0, α, electrode area (A), R_u and double-layer capactitance (C_{dl}), were derived using the Bulter-Volmer model of electron transfer as described in the Supporting Information and are provided in Table 1 and 3. Since the electrode kinetics of the $V^{V/IV}$ and $W^{VI/V}$ processes in PC containing [EMIM][BF_4] and [BMIM][BF_4] are essentially reversible with a frequency of 9.02 Hz, a higher frequency (f = 27.01 Hz) AC perturbation was used to shorten the time scale of the measurement so that adequate kinetic sensitivity was avaliable. A representative FTAC voltammogram (f = 27.01 Hz) obtained in PC containing [EMIM][BF_4] as the supporting electrolyte is shown in Figure 3. For the other four electrolytes (see Table 1), the $V^{V/IV}$ and $W^{VI/V}$ processes were found to be far from reversible allowing the lower frequency of 9 Hz to be used to quantify the electrode kinetics. A representative FTAC voltammogram (f = 9.02 Hz) obtained in PC containing [TPA][BF_4] as the supporting electrolyte is shown in Figure 4.

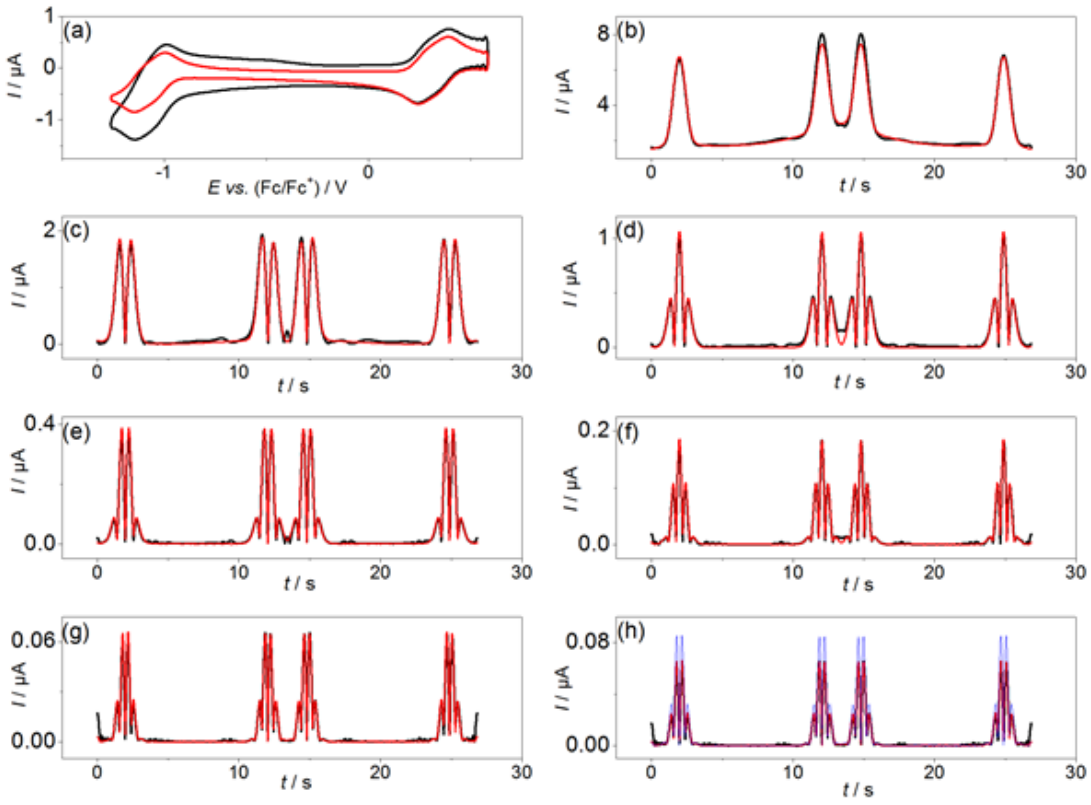

Figure 3. Comparison of simulated (—) and experimental (—) FTAC voltammetric data obtained for the $V^{IV/V}$ and $W^{VI/V}$ processes in PC containing 1.0 mM $[SVW_{11}O_{40}]^{3-}$ and 0.5 M [EMIM][BF_4] at a 1 mm diameter Pt macrodisk electrode with T = 295 K, ΔE = 80 mV, f = 27.01 Hz and v = 0.137 V s^{-1}. (a) aperiodic DC component, (b–g) 1st to 6th AC harmonic components, and (h) simulated 6th harmonic component for the reversible case (—). Simulated kinetic data was obtained with k_V^0 = 0.10 cm s^{-1}, α_V = 0.50, k_W^0 = 0.10 cm s^{-1} and α_W = 0.50. Other parameters are defined in the text.

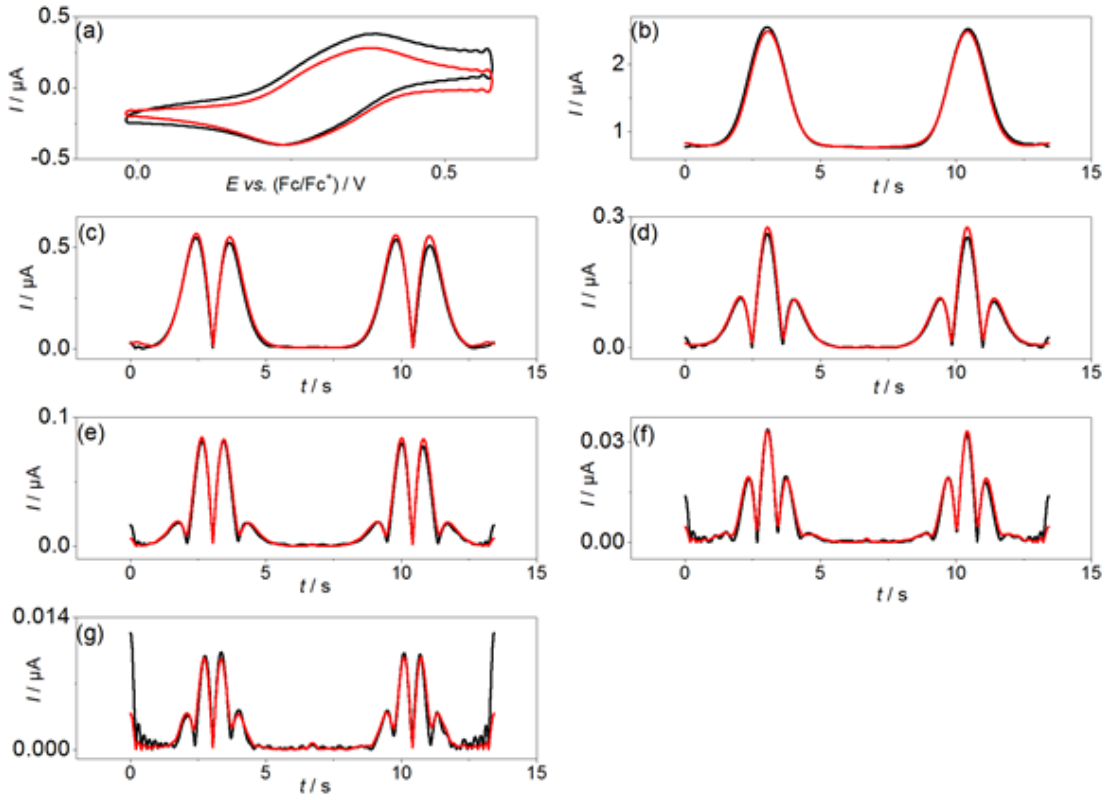

Figure 4. Comparison of simulated (—) and experimental (—) FTAC voltammetric data obtained for the $V^{IV/V}$ process in PC containing 1.0 mM $[SVW_{11}O_{40}]^{3-}$ and 0.5 M [TPA][BF_4] at a 1 mm diameter Pt electrode with T = 295 K, ΔE = 80 mV, f = 9.02 Hz and v = 0.089 V s^{-1}. (a) aperiodic DC component, (b–g) 1st to 6th AC harmonic components. Simulated kinetic data was obtained with k_V^0 = 0.0075 cm s^{-1}, α_V = 0.5 were used. Other parameters are defined in the text.

Figure 3 provides a simulation-experiment comparison for the $V^{V/IV}$ and $W^{VI/V}$ processes in PC containing 0.5 M [EMIM][BF_4]. In the 6th harmonic component, both processes can be treated as quasi-reversible rather than reversible on this timescale (see Figure 3h), since the current magnitude for this harmonic is significantly smaller than predicted for a reversible process (blue curve). Excellent agreement between the simulated and experimental data was achieved for all harmonic components with k_V^0 and k_W^0 both estimated to be 0.10 cm s^{-1}. α was reasonally assumed to be 0.50 in all simulations in accordance with the highly symmetric shapes of all AC harmonics.

Since the electrode kinetics of the $W^{VI/V}$ process when using [TPA][BF_4], [TBA][PF_4] and [THA][ClO_4] as the electrolyte are so slow, higher order harmonic components are almost absent, only the narrowed potential range associated with the $V^{V/IV}$ process was quantified by FTACV under these conditions. The FTAC voltammogram (f = 9.02 Hz) obtained for the $V^{V/IV}$ process in PC containing 0.5 M [TPA][BF_4] is shown in Figure 4. Excellent agreement between the simulated and experimental data was achieved using the measured A, D, C and R_u values to give a k_V^0 value of 0.0075 cm s^{-1}. For the $W^{VI/V}$ process, it should be noted that when using [TPA][BF_4], [TBA][PF_4] and [THA][ClO_4] as the electrolyte, the DC cyclic voltammograms obtained from the first cycling scan give larger peak-to-peak separations than those obtained from the following ones. Furthermore, the shapes of the reduction and oxidation peaks are not fitted perfectly with simulated ones obtained based on Butler-Volmer theory (Figure S1(a)). For slow electrode kinetics such as the $W^{VI/V}$ process, the differences between Butler-Volmer theory and Marcus-Hush theory in simulation are expected to be distinguishable. Better fitting was found when comparing the experimental data and simulated one based on Marcus-Hush theory (Figure S1(b)). However, a large deviation between experimental and simulated data

still exists. All the discussions above indicate there are complexities associated with the $W^{VI/V}$ process when using [TPA][BF_4], [TBA][PF_4] and [THA][ClO_4] as the electrolyte. Therefore, in this study the electrode kinetics of this process were estimated by comparing the peak-to-peak separations of the experimental DC cyclic voltammograms obtained from the first cycling scan with those obtained by DigiElch digital simulation based on Butler-Volmer theory, taking into account the effect of uncompensated resistance (R_u). A k^0_W value of 1.2×10^{-4} cm s^{-1} was estimated when using [THA][ClO_4] as the electrolyte. The heterogeneous electron transfer kinetics of the $V^{V/IV}$ and $W^{VI/V}$ processes were measured in PC with the 7 different electrolytes outlined in Scheme 1; the FTAC voltammetric data obtained for $[BMIM]^+$, $[Py_{14}]^+$, $[TEA]^+$, $[TBA]^+$ and $[THA]^+$ are included in the Supporting Information (see Figures S2 to S6) and the measured k^0 values are summarized in Table 3.

FTAC voltammetric data were also acquired with a lower bulk concentration of 0.20 mM $[SVW_{11}O_{40}]^{3-}$ in order to lessen the influence of the IR_u drop. The results obtained at a Pt macrodisk electrode in PC (0.5 M electrolyte) at this lower bulk concentration are also summarized in Table 3. Comparisons of experimental and simulated data are presented in Figures S7 to S13 in the Supporting Information. As expected, since the IR_u drop has been correctly accommodated for in all simulations, the determined k^0 values are essentially independent of the $[SVW_{11}O_{40}]^{3-}$ concentration. This concentration independence also implies that the contribution from specific adsorption is not significant.

The data summarized in Table 3 reveal that k^0_V and k^0_W are both affected by the nature of the supporting electrolyte, with increasing size of the electrolyte cation causing a decrease in the measured value. For example, for the $V^{V/IV}$ process, k^0 decreases by approximately three orders of magnitude when the electrolyte cation is

changed from $[EMIM]^+$ to $[THA]^+$. As discussed previously,[36] the length of the imidazolium based cations ($[EMIM]^+$ and $[BMIM]^+$) are similar to the diameter of ammonium based cations ($[TPA]^+$ or $[TBA]^+$). However, the planar structure of imidazolium based-cation is thought to cause its preferred orientation to be parallel rather than perpendicular to the electrode surface. With this in mind, we can conclude that the k_V^0 values are dependent on the size of the electrolyte cation, decreasing in the order; $[EMIM]^+ > [BMIM]^+ > [Py_{14}]^+ \approx [TEA]^+ > [TPA]^+ > [TBA]^+ > [THA]^+$. The same trend in k^0 is also observed for the $W^{VI/V}$ process, however with a more significant decrease (approximately two orders of magnitude) from $[TEA]^+$ to $[TPA]^+$, namely, $[EMIM]^+ > [BMIM]^+ > [Py_{14}]^+ \approx [TEA]^+ >> [TPA]^+ > [TBA]^+ > [THA]^+$. It should be noted that the impact of the thermodynamically favourable cross redox reaction between $[SVW_{11}O_{40}]^{3-}$ and $[SVW_{11}O_{40}]^{5-}$ on the voltametric characteristics is insignificant, as demonstrated in a previous study.[35]

Table 3. Electrode kinetic parameters derived at a 1 mm dimeter Pt macrodisk electrode for the $[SVW_{11}O_{40}]^{3-/4-/5-}$ processes in PC (0.5 M electrolyte).

Electrolyte	C (mM)	R_u[a] (Ω)	C_{dl}[a] (c_0, c_1, c_2, c_3, c_4) (μF cm^{-2})	E_V^0 (V)	k_V^0 (cm s^{-1})	E_W^0 (V)	k_W^0 (cm s^{-1})
[EMIM][BF_4]	1.0	415	16.1, -2.1, -5.3, -4.9, -1.1	0.316	0.10	-1.085	0.10
	0.20	430	13.2, 1.5, 6.1, 4.8, 1.4		0.10		0.10
[BMIM][BF_4]	1.0	535	20.9, 0.2, -4.0, -4.3, -1.2	0.306	0.040	-1.093	0.038
	0.20	515	14.6, 1.0, -1.5, -3.6, -1.3		0.050		0.045
[Py_{14}][BF_4]	1.0	470	28.5, 0.5, -4.5,-3.7, -0.9	0.333	0.016	-1.079	0.016
	0.20	502	14.3, 0.7, 0.2, -0.1, -0.1		0.018		0.017
[TEA][BF_4]	1.0	550	31.2, -2.8, -16.9, -14.6, -3.9	0.342	0.015	-1.079	0.020
	0.20	543	16.0, 1.11, -2.9, -4.3, -1.4		0.012		0.020
[TPA][BF_4]	1.0	530	21.5, -0.6, 8.2, 28.8, 24.5	0.309	0.0075	-1.182	1.2×10^{-4} [b]
	0.20	630	13.4, 0.6, -0.2, 8.0, 12.3		0.0085		c
[TBA][PF_6]	1.0	730	22.0, -0.5, 10.1, 7.3, -12.4	0.254	0.0040	-1.260	1.2×10^{-5} [b]
	0.20	750	12.4, 1.1, -4.1, 7.0, 19.5		0.0033		c
[THA][ClO_4]	1.0	1330	12.0, -0.5, 10.1, 7.2, -12.4	0.214	0.0018	-1.355	1.7×10^{-6} [b]
	0.20	1270	13.9, 2.4, 0.6, -3.1, -1.1		0.0016		c

[a] See supporting information for detailed measurement.
[b] Estimated from ΔE_p values obtained from DC cyclic voltammetry.
[c] No well-defined process observed at this lower concentration.
[d] FTACV simulations were obtained assuming $\alpha = 0.50$.

The solvent chosen in this study, PC, has a relatively high dielectric constant (64.9 at 25 °C[42]), which is expected to minimise the extent of ion pairing. For example, a measurable amount of ion pairing between the electrolyte cation and nitromesitylene radicals has been reported in acetonitrile and dimethylformamide[46] (with dielectric constants of 36 and 36.7, respectively), while negligible ion pairing between the same anion radical and the electrolyte cation has been suggested in PC.[47] Nevertheless, owing to the high negative charge of POM anions, the occurrence of electrolyte cation-POM ion pairing in the present study is expected (the electrolyte

cation dependence of the E^0 values (see Table 3) implies that ion pairing is significant). In this case, the electrode kinetics have been measured at apparent formal potentials (E^0_{app}) rather than formal potential E^0_{F}, so k^0 should be more appropriately considered as an apparent rate constant (k^0_{app}). In this situation, the kinetics of the overall electron transfer reaction scheme can be described by the square reaction given in Eq. 3,

$$\begin{array}{ccc} \mathrm{A} + \mathrm{e}^- & \rightleftharpoons & \mathrm{B} \quad (E_1{}^0, k_1{}^0) \\ K_1 \Big\| \; \mathrm{X}^+ & & \mathrm{X}^+ \; \Big\| K_2 \\ \mathrm{XA}^+ + \mathrm{e}^- & \rightleftharpoons & \mathrm{XB}^+ \quad (E_2{}^0, k_2{}^0) \end{array} \qquad (3)$$

In this scheme, the symbols A and B are used to represent $[SVW_{11}O_{40}]^{3-}$ and $[SVW_{11}O_{40}]^{4-}$, respectively so that $K_1 = \frac{[\mathrm{X}^+][\mathrm{A}]}{[\mathrm{XA}^+]}$ and $K_2 = \frac{[\mathrm{X}^+][\mathrm{B}]}{[\mathrm{XB}^+]}$ are the equilibrium constants for the ion-pairing reactions involving either the oxidised or the reduced forms, $E_1{}^0$ and $E_2{}^0$ are the relevant formal potentials and; $k_1{}^0$ and $k_2{}^0$ are the formal electron transfer rate constants at $E_1{}^0$ and $E_2{}^0$, respectively. It can be shown that the voltammetric responses associated with this process are identical to a simple one-electron transfer process in Eq. 4 if the ion pairing reactions are reversible on the voltammetric timescale.

$$\mathrm{A}' + \mathrm{e}^- \rightleftharpoons \mathrm{B}' \quad (k_{\mathrm{app}}{}^0, \alpha_{\mathrm{app}}, E_{\mathrm{app}}{}^0) \qquad (4)$$

where

$$k_{\mathrm{app}}{}^0 = \frac{k_1{}^0(K_2/K_1)^{\alpha_{app}} + k_2{}^0([\mathrm{X}^+]/K_1)}{[1 + ([\mathrm{X}^+]/K_1)]^{1-\alpha_{\mathrm{app}}}[(K_2/K_1) + ([\mathrm{X}^+]/K_1)]^{\alpha_{\mathrm{app}}}} \qquad (5)$$

Since a higher charge density is associated with the species B, K_2 is expected to be smaller than K_1. It is also reasonable to assume that both K_1 and K_2 are smaller than unity due to relatively strong association between highly charged POMs and electrolyte cations. Consequently, the relationships $K_2/K_1 \ll [X^+]/K_1$ and ${k_1}^0(K_2/K_1)^{1/2} \ll {k_2}^0([X^+]/K_1)$ are expected to be valid under the experimental conditions employed as noted in other studies.[48, 49] On this basis, Eq. 5 can be simplified to give Eq. 6 with α_{app} taken to be 0.5,

$$ {k_{app}}^0 = \frac{{k_1}^0(K_2/K_1)^{1/2} + {k_2}^0([X^+]/K_1)}{[1+([X^+]/K_1)]^{1/2}[(K_2/K_1)+([X^+]/K_1)]^{1/2}} \approx \frac{{k_2}^0([X^+]/K_1)^{1/2}}{[1+([X^+]/K_1)]^{1/2}} $$

$$ = \frac{{k_2}^0}{[1+(K_1/[X^+])]^{1/2}} \qquad (6) $$

As the size of the cation increase ($[TEA]^+ > [TPA]^+ > [TBA]^+ > [THA]^+$), the ion pairs formation become weaker and K_1 is expected to increase. Assuming ${k_2}^0$ is insensitive to the identity of the electrolyte cation, ${k_{app}}^0$ is therefore predicted to decrease in the order of $[TEA]^+ > [TPA]^+ > [TBA]^+ > [THA]^+$.

The apparent formal potentials E^0_{app} is also a function of E^0_1, K_1, K_2 and $[X^+]$ [49]

$$ (F/RT)(E^0_{app} - E^0_1) = \ln\left[\frac{1+([X^+]/K_1)}{1+([X^+]/K_2)}\right] \qquad (7) $$

Rearrangement gives

$$ (F/RT)(E^0_{app} - E^0_1) = \ln\left(\frac{K_2+[X^+]}{K_1+[X^+]} \cdot \frac{K_1}{K_2}\right) \qquad (8) $$

As K_1 and K_2 are much smaller than 1, it is reasonable to assume $\frac{K_2+[X^+]}{K_1+[X^+]} \approx 1$. Therefore,

$$ (F/RT)(E^0_{app} - E^0_1) \approx \ln\left(\frac{K_1}{K_2}\right) \qquad (9) $$

When the electrolyte cation is small, ion pair formation is stronger, and the difference between K_1 and K_2 is larger than that when using a larger cation. Since K_1 is expected to be larger than K_2 as explained above, the values of $\ln(\frac{K_1}{K_2})$ are predicted to increase with the size of electrolyte cation which decrease in the order $[THA]^+ < [TBA]^+ < [TPA]^+ < [TEA]^+$. Consequently, on the basis of Eq. (9), we can deduce that E^0_{app} values are expected to follow the order $[THA]^+ < [TBA]^+ < [TPA]^+ < [TEA]^+$. Figure 5 provides a plot of k^0_{app} values associated with the $V^{V/IV}$ and $W^{VI/V}$ processes as a function of their formal reversible potential, which indeed confirms k^0_V and k^0_W values decrease, and the E^0_V and E^0_W shift towards more negative potentials as the size of electrolyte cations increase as predicted. However, ion pairing cannot be the sole reason for the electrolyte cation dependence of the k^0 values, as this does not account for the dramatically different k^0_V and k^0_W dependence on supporting electrolyte.

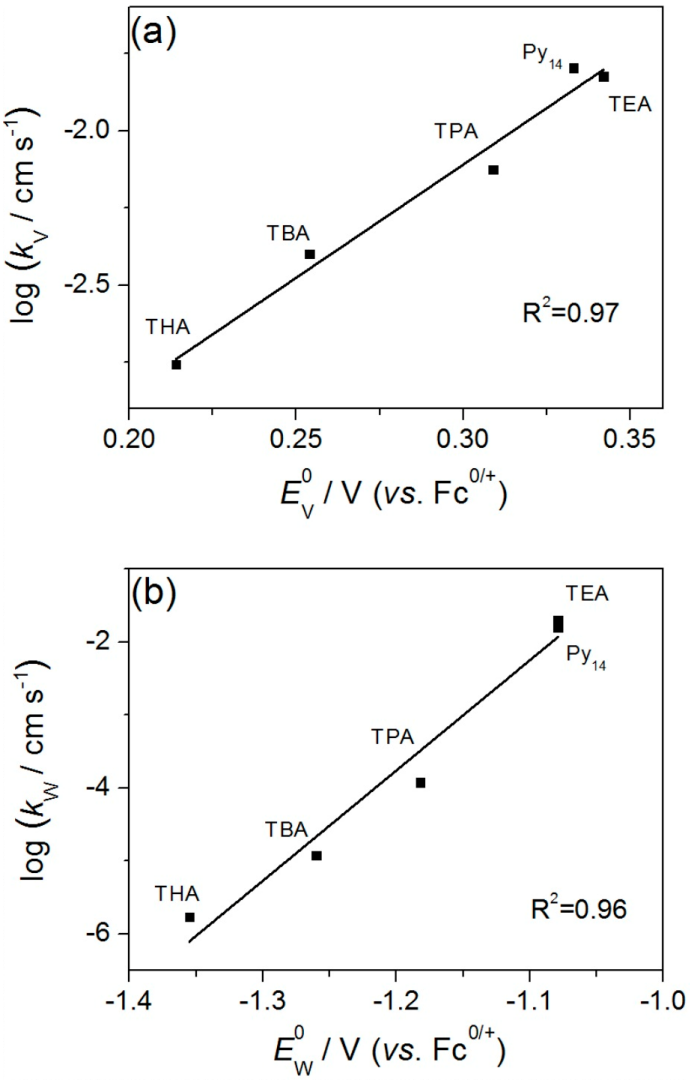

Figure 5. Plots of the logarithm of k^0 for the (a) $V^{V/IV}$ and (b) $W^{VI/V}$ processes *vs*. formal reversible potential in PC containing 0.5 M electrolyte.

In the Marcus Theory of electron transfer, the heterogeneous rate constant associated with a simple outer sphere electrode process is inverse proportional to the activation Gibbs energy, ΔG^*.[14] The total activation energy ΔG^* can be divided into inner ΔG_i^* and outer ΔG_o^* components of the reorganization energies. The inner component of reorganization energy reflects the bonds between the centered metal and the ligands. The outer component of reorganization energy corresponds to the interaction of the complex with the molecules or ions in the medium. Considering the

structure of the POM remains similar after electron transfer, it is reasonable to assume that ΔG_o^* makes a dominanth contribution. On this basis, the k^0 values are expected to descrease with increase in the viscosity of the solvent (electrolyte), which is the case for both k_V^0 and k_W^0 when the electrolyte cation is changed from $[TEA]^+$ to $[THA]^+$. However, the viscosity of PC containing 0.5 M [TEA][BF_4] is only 1.5 times smaller than that containing 0.5 M [THA][ClO_4], while the k_V^0 values decrease approximately by a factor of 10 and k_W^0 values decrease more significantly (approximately four orders of magnitude). Therefore, the contribution from media change in viscosity are not the major factor.

Significant electrolyte cation dependence of the k^0 values also may arise from specific adsorption of $[SVW_{11}O_{40}]^{3-}$, $[SVW_{11}O_{40}]^{4-}$ and/or $[SVW_{11}O_{40}]^{5-}$. However, since the k_V^0 and k_W^0 values found at the two $[SVW_{11}O_{40}]^{3-}$ concentrations (1 mM and 0.2 mM) are almost identical, a specific adsorption effect is unlikely, as this is expected to give rise to concentration dependence.

In general, if it is assumed that the reaction plane is coincident with the outer Helmholtz plane, the electrolyte cation dependence of k^0 may be consequence of the double layer effect.[50] However, as highlighted in previous studies, it appears that the double layer effect alone cannot account for the magnitude of the electrolyte cation size effect observed herein. Gamber, et al.[51] found that at negative potentials, tetraalkylammonium cations are adsorbed at a mercury electrode/electrolyte interface in acetonitrile, with the extent of adsorption becoming more extensive with increasing length of the constituent alkyl chain of the cation. Evans, et al.[52] studied the inhibiting effect of large tetraalkylammonium cations on the electrode kinetics for a wide variety of electrode reactions. In their study, these authors showed that the k^0 values became smaller when $[THA]^+$ replaced $[TEA]^+$ as the electrolyte cation. This suggested that at

negative potentials, the electrode is extensively covered with adsorbed tetraalkylammonium cations and thereforek^0 electrolyte dependence was explained in terms of blockage of electron transfer by the concentrated "film" of tetraalkylammonium cations.

It has been well established that adsorbed layers on the electrode/electrolyte interface can impede electron transfer.[50, 53-55] When electron tunneling occurs from an electrode which is covered by an adsorbed layer to a redox active species in the solution phase, the standard rate constant is proportional to thickness of adsorbed layer:[47]

$$k^0 = k^{0\prime} e^{-\beta d} \qquad (10)$$

where $k^{0'}$ is the standard rate constant for the uncovered electrode, β is the tunneling parameter and d is the thickness of the "film". Simply, it can be assumed that $d = 2r_+$ (the diameter of the electrolyte cation). However, since the alkyl arms of the larger tetraalkylammonium cations (n ≥ 3) can bend under the influence of an electric field, the charge center at the nitrogen atom is able to approach the surface at a distance of 0.37 nm.[47] This necessitate the introduction of correction factor to the thickness of the "film" for the larger tetraalkylammonium cations:[47]

$$d = 2r_+ \qquad n \leq 3 \qquad (11)$$

$$d = r_+ + 0.37 \qquad n \leq 3 \qquad (12)$$

Table 4 shows the crystallographic radius (r_+) and the calculated thickness of the coverage (d) for each of the tetraalkylammonium cations. A plot of $\ln k_0$ measured in PC solutions containing the range tetraalkylammonium cations used versus d (calculated using Eqs. 11 and 12) is shown in Figure 6. Reasonable linear correlations (r^2 = 0.99 and 0.98 for $V^{V/IV}$ and $W^{VI/V}$ processes, respectively) are obtained for both the $V^{V/IV}$ and $W^{VI/V}$ processes. The slopes of the plots, which are equivalent to β (see Eq.

10), are found to be 13.3 nm^{-1} for the $V^{V/IV}$ process and 58.9 nm^{-1} for the $W^{VI/V}$ process, which suggests the latter has a higher barrier height.[47] Lipkowski et al.,[53] who studied the electrode kinetics of redox processes at mercury electrodes coated with monolayers of quinolone, iso-quinoline and 3-methyl-iso-quinoline found that the monolayers existed as concentrated liquid-like films or compact solid-like films depending on the magnitude of the electrode potential. While the former has a significant inhibitive effect, the latter can decelerate the electrode reaction much more effectively, by up to 6-7 orders of magnitude. On this basis, the results in our study can be attribute in part to inhibiting effect of adsorbed tetraalkylammonium cations on the electrode surface that form a blocking layer which reduces the probability of electron transfer through the layer; the thickness of the layer increases with the size of electrolyte cation. In the potential region where the $V^{V/IV}$ process occurs (close to the potential of zero charge, pzc), the monolayer acts as a liquid-like film, and as a result, the k_V^0 values decrease gently with an increase in the electrolyte cation size. For the $W^{VI/V}$ process, which appears in a much more negative potential region (significantly negative of the pzc), the monolayer becomes more compact and acts as a solid-like film, particularly when using the larger tetraalkylammonium cations. Consequently, a more significant drop in k_W^0 is observed when changing the electrolyte cation from $[TEA]^+$ to $[TPA]^+$, $[TBA]^+$ and $[THA]^+$.

Although the dimensions of $[EMIM]^+$ and $[BMIM]^+$ are known, it is problematic to estimate the thickness of the layer for these two cations, since the centre of charge is able to approach the electrode surface at a closer distance than spherical ammonium cations, due to their planar structure. For this reason, k^0 data for these two cations are not included in the plot shown in Figure 6. However, it is important to note that comparison of these k^0 values also reveals a decrease with increase in the length of the

alkyl chain (see Table 3). Furthermore, given that the structure of $[Py_{14}]^+$ is similar to that of $[TEA]^+$, in terms of the length of the alkyl groups, comparable k^0 values are expected when using these two cations, as observed experimentally (k_V^0 = 0.016 cm s^{-1}, k_W^0 = 0.016 cm s^{-1} with $[Py_{14}]^+$ and k_V^0 = 0.015 cm s^{-1}, k_W^0 = 0.02 cm s^{-1} with $[TEA]^+$).

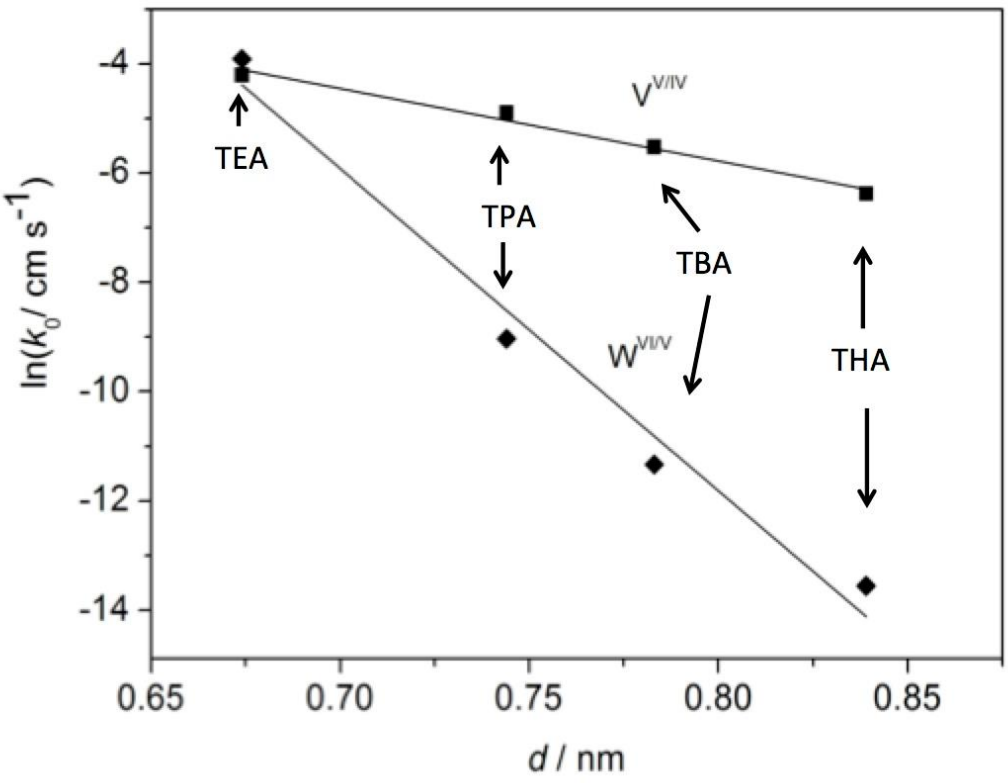

Figure 6. Plot of the natural logarithm of k^0 for the $V^{V/IV}$ (■) and $W^{VI/V}$ (◆) processes measured at a Pt electrode in the presence of designated tetraalkylammonium cations versus the thickness of the coverage (*d*), calculated from the crystallographic radius of the relative cations (see Eqs. 11 and 12).

Table 4. Cation Crystallographic radii (r_+) and calculated thickness of the coverage (d) of the tetraalkylammonium cations employed in this study.

Electrolyte	Cation crystallographic radius r_+ (nm)[56]	Thickness of the coverage d (nm)
[TEA][BF_4]	0.337	0.674
[TPA][BF_4]	0.372	0.744
[TBA][PF_6]	0.413	0.783
[THA][ClO_4]	0.469	0.839

Conclusions

The heterogeneous electron transfer kinetics associated with the $[SVW_{11}O_{40}]^{3-/4-/5-}$ processes at a platinum electrode have been investigated in PC containing seven different supporting electrolyte cations using large amplitude FTAC voltammetry to quantify very fast kinetics and DC cyclic voltammetry for slow kinetics. The formal reversible potentials and electron-transfer rate constants associated with the $V^{V/IV}$ and $W^{VI/V}$ processes were found to correlate with the size of the supporting electrolyte cation. k^0 values decrease in the order, $[EMIM]^+ > [BMIM]^+ > [Py_{14}]^+ \approx [TEA]^+ > [TPA]^+ > [TBA]^+ > [THA]^+$ for both processes even though they occur at very different potentials, and while k_V^0 decreases more gently with increasing cation size, changing by approximately three orders of magnitude, the decrease in k_W^0 is more drastic, changing by approximately five orders of magnitude from $[EMIM]^+$ to $[THA]^+$. Possible explanations for the electrolyte cation depedence were considered (*e.g.*, ion-pairing, viscosity, adsorption and the double-layer effect), with inhibition of electron-transfer by a blocking "film" of electrolyte cations being proposed as the dominant factor, supported by the linear plot of $\ln(k^0)$ vs. $\ln(d)$ for both the $V^{V/IV}$ and $W^{VI/V}$ electron transfer processes. The nature of the cation "film" is thought to change from

liquid-like (moderately inhibiting) in the potential region where the $V^{V/IV}$ process occurs, to solid-like (strongly inhibiting) in the potential region where the $W^{VI/V}$ process occurs, thereby explaining the different sensitivities of the respective processes to the nature of the supporting electrolyte cations.

References

[1] J. Velmurugan, P. Sun, M.V. Mirkin, Scanning electrochemical microscopy with gold nanotips: the effect of electrode material on electron transfer rates, The Journal of Physical Chemistry C, 113 (2008) 459-464.
[2] R.K. Jaworski, R.L. McCreery, Laser activation of carbon microdisk electrodes: Surface oxide effects on $Ru(NH_3)_6^{3+/2+}$ kinetics, Journal of Electroanalytical Chemistry, 369 (1994) 175-181.
[3] Z. Samec, J. Weber, The effect of the double layer on the rate of the Fe^{3+}/Fe^{2+} reaction on a platinum electrode and the contemporary electron transfer theory, Journal of Electroanalytical Chemistry and Interfacial Electrochemistry, 77 (1977) 163-180.
[4] C.A. McDermott, K.R. Kneten, R.L. McCreery, Electron Transfer Kinetics of Aquated $Fe^{3+/2+}$, $Eu^{3+/2+}$ and $V^{3+/2+}$ at Carbon Electrodes Inner Sphere Catalysis by Surface Oxides, Journal of The Electrochemical Society, 140 (1993) 2593-2599.
[5] S. Sahami, M.J. Weaver, Solvent effects on the kinetics of simple electrochemical reactions: Part I. Comparison of the behavior of Co (III)/(II) trisethylenediamine and ammine couples with the predictions of dielectric conitnuum theory, Journal of Electroanalytical Chemistry and Interfacial Electrochemistry, 124 (1981) 35-51.
[6] A. Kapturkiewicz, B. Behr, Solvent effect on electrode reaction kinetics of transition metal salene complexes, Journal of electroanalytical chemistry and interfacial electrochemistry, 179 (1984) 187-199.
[7] G.E. McManis, M.N. Golovin, M.J. Weaver, Role of solvent reorganization dynamics in electron-transfer processes. Anomalous kinetic behavior in alcohol solvents, The Journal of Physical Chemistry, 90 (1986) 6563-6570.
[8] K. Hsueh, E. Gonzalez, S. Srinivasan, Electrolyte effects on oxygen reduction kinetics at platinum: a rotating ring-disc electrode analysis, Electrochimica Acta, 28 (1983) 691-697.
[9] C. Beriet, D. Pletcher, A microelectrode study of the mechanism and kinetics of the ferro/ferricyanide couple in aqueous media: The influence of the electrolyte and its concentration, Journal of Electroanalytical Chemistry, 361 (1993) 93-101.
[10] S.K. Cook, B.R. Horrocks, Heterogeneous Electron-Transfer Rates for the Reduction of Viologen Derivatives at Platinum and Bismuth Electrodes in Acetonitrile, ChemElectroChem, DOI (2016).
[11] T. Iwasita, W. Schmickler, J. Schultze, The influence of metal adatoms deposited at underpotential on the kinetics of an outer-sphere redox reaction, Journal of electroanalytical chemistry and interfacial electrochemistry, 194 (1985) 355-359.
[12] T. Iwasita, W. Schmickler, J. Schultze, The influence of the metal on the kinetics of outer sphere redox reactions, Berichte der Bunsengesellschaft für physikalische Chemie, 89 (1985) 138-142.

[13] M.J. Weaver, T. Gennett, Influence of solvent reorientation dynamics upon the kinetics of some electron-exchange reactions, Chemical physics letters, 113 (1985) 213-218.
[14] C. Lagrost, L. Preda, E. Volanschi, P. Hapiot, Heterogeneous electron-transfer kinetics of nitro compounds in room-temperature ionic liquids, Journal of Electroanalytical Chemistry, 585 (2005) 1-7.
[15] M.D. Ryan, D.H. Evans, Effect of metal ions on the electrochemical reduction of benzil in non-aqueous solvents, Journal of Electroanalytical Chemistry and Interfacial Electrochemistry, 67 (1976) 333-357.
[16] M. Ryan, D.H. Evans, Effect of Sodium Ions on the Electrochemical Reduction of Diethyl Fumarate in Dimethylsulfoxide and Acetonitrile, Journal of The Electrochemical Society, DOI (1974).
[17] M.J. Hazelrigg, A.J. Bard, Electrohydrodimerization Reactions IV. A Study of the Effect of Alkali Metal Ions on the Hydrodimerization of Several 1, 2-Diactivated Olefins in DMF Solutions by Chronoamperometry and Chronocoulometry, Journal of The Electrochemical Society, 122 (1975) 211-220.
[18] W. Fawcett, A. Lasia, The influence of ion pairing on the electroreduction of nitromesitylene in aprotic solvents. 2. Kinetic aspects, The Journal of Physical Chemistry, 82 (1978) 1114-1121.
[19] R. Andreu, J.J. Calvente, W.R. Fawcett, M. Molero, Role of ion pairing in double-layer effects at self-assembled monolayers containing a simple redox couple, The Journal of Physical Chemistry B, 101 (1997) 2884-2894.
[20] M. Peover, J. Davies, The influence of ion-association on the polarography of quinones in dimethylformamide, Journal of Electroanalytical Chemistry (1959), 6 (1963) 46-53.
[21] M.T. Pope, A. Müller, Polyoxometalate chemistry: an old field with new dimensions in several disciplines, Angewandte Chemie International Edition in English, 30 (1991) 34-48.
[22] D.-L. Long, E. Burkholder, L. Cronin, Polyoxometalate clusters, nanostructures and materials: from self assembly to designer materials and devices, Chemical Society Reviews, 36 (2007) 105-121.
[23] P. Special, issue: L. Cronin and A. Müller (guest eds.), Chem. Soc. Rev, 41 (2012) 7325-7648.
[24] M.V. Vasylyev, R. Neumann, New heterogeneous polyoxometalate based mesoporous catalysts for hydrogen peroxide mediated oxidation reactions, Journal of the American Chemical Society, 126 (2004) 884-890.
[25] K. Kamata, K. Yonehara, Y. Sumida, K. Yamaguchi, S. Hikichi, N. Mizuno, Efficient epoxidation of olefins with≥ 99% selectivity and use of hydrogen peroxide, Science, 300 (2003) 964-966.
[26] H. Lü, J. Gao, Z. Jiang, F. Jing, Y. Yang, G. Wang, C. Li, Ultra-deep desulfurization of diesel by selective oxidation with $[C_{18}H_{37}N(CH_3)_3]_4[H_2NaPW_{10}O_{36}]$ catalyst assembled in emulsion droplets, Journal of Catalysis, 239 (2006) 369-375.
[27] C.L. Hill, Progress and challenges in polyoxometalate-based catalysis and catalytic materials chemistry, Journal of Molecular Catalysis A: Chemical, 262 (2007) 2-6.
[28] M. Sadakane, E. Steckhan, Electrochemical properties of polyoxometalates as electrocatalysts, Chemical Reviews, 98 (1998) 219-238.
[29] M. Zhou, L.-p. Guo, F.-y. Lin, H.-x. Liu, Electrochemistry and electrocatalysis of polyoxometalate-ordered mesoporous carbon modified electrode, Analytica chimica acta, 587 (2007) 124-131.

[30] Z. Han, Y. Zhao, J. Peng, Y. Feng, J. Yin, Q. Liu, The electrochemical behavior of Keggin polyoxometalate modified by tricyclic, aromatic entity, Electroanalysis, 17 (2005) 1097-1102.
[31] K.K. Kasem, Electrochemical behavior of sodium 12-tungstodicobaltoate in aqueous and mixed solvent electrolytes, Electrochimica acta, 41 (1996) 205-211.
[32] K. Maeda, S. Himeno, T. Osakai, A. Saito, T. Hori, A voltammetric study of Keggin-type heteropolymolybdate anions, Journal of Electroanalytical Chemistry, 364 (1994) 149-154.
[33] K. Bano, J. Zhang, A.M. Bond, P.R. Unwin, J.V. Macpherson, Diminished Electron Transfer Kinetics for $[Ru(NH_3)_6]^{3+/2+}$, $[\alpha\text{-}SiW_{12}O_{40}]^{4-/5-}$ and $[\alpha\text{-}SiW_{12}O_{40}]^{5-/6-}$ Processes at Boron-Doped Diamond Electrodes, The Journal of Physical Chemistry C, 119 (2015) 12464-12472.
[34] J. Li, A.M. Bond, J. Zhang, Probing Electrolyte Cation Effects on the Electron Transfer Kinetics of the $[\alpha\text{-}SiW_{12}O_{40}]^{4-/5-}$ and $[\alpha\text{-}SiW_{12}O_{40}]^{5-/6-}$ Processes using a Boron-Doped Diamond Electrode, Electrochimica Acta, 178 (2015) 631-637.
[35] J. Li, S.-X. Guo, C.L. Bentley, K. Bano, A.M. Bond, J. Zhang, T. Ueda, Electrode Material Dependence of the Electron Transfer Kinetics Associated with the $[SVW_{11}O_{40}]^{3-/4-}$ ($V^{V/IV}$) and $[SVW_{11}O_{40}]^{4-/5-}$ ($W^{VI/V}$) Processes in Dimethylformamide, Electrochimica Acta, 201 (2016) 45-56.
[36] J. Li, C.L. Bentley, A.M. Bond, J. Zhang, T. Ueda, Influence of 1-butyl-3-methylimidazolium on the electron transfer kinetics associated with the $[SVW_{11}O_{40}]^{3-/4-}$ ($V^{V/IV}$) and $[SVW_{11}O_{40}]^{4-/5-}$ ($W^{VI/V}$) processes in dimethylformamide, Journal of Electroanalytical Chemistry, DOI (2016).
[37] T. Ueda, J.-i. Nambu, J. Lu, S.-X. Guo, Q. Li, J.F. Boas, L.L. Martin, A.M. Bond, Structurally characterised vanadium (v)-substituted Keggin-type heteropolysulfates $[SVM_{11}O_{40}]^{3-}$ (M= Mo, W): voltammetric and spectroscopic studies related to the V (v)/V (iv) redox couple, Dalton Transactions, 43 (2014) 5462-5473.
[38] A. Baranski, W. Fawcett, Medium effects in the electroreduction of cyanobenzenes, Journal of Electroanalytical Chemistry and Interfacial Electrochemistry, 100 (1979) 185-196.
[39] D.A. Corrigan, D.H. Evans, Cyclic voltammetric study of tert-nitrobutane reduction in acetonitrile at mercury and platinum electrodes: Observation of a potential dependent electrochemical transfer coefficient and the influence of the electrolyte cation on the rate constant, Journal of Electroanalytical Chemistry and Interfacial Electrochemistry, 106 (1980) 287-304.
[40] C. Rüssel, W. Jaenicke, Heterogeneous electron transfer to quinones in aprotic solvents: Part II. The dependence on solvent and supporting electrolyte, Journal of electroanalytical chemistry and interfacial electrochemistry, 180 (1984) 205-217.
[41] A. Kapturkiewicz, M. Opałło, Medium effect in the electroreduction of nitromesitylene, Journal of electroanalytical chemistry and interfacial electrochemistry, 185 (1985) 15-28.
[42] J. Barthel, F. Feuerlein, Dielectric properties of propylene carbonate and propylene carbonate solutions, Journal of solution chemistry, 13 (1984) 393-417.
[43] A.M. Bond, D. Elton, S.-X. Guo, G.F. Kennedy, E. Mashkina, A.N. Simonov, J. Zhang, An integrated instrumental and theoretical approach to quantitative electrode kinetic studies based on large amplitude Fourier transformed ac voltammetry: A mini review, Electrochemistry Communications, 57 (2015) 78-83.
[44] R.S. Nicholson, Theory and Application of Cyclic Voltammetry for Measurement of Electrode Reaction Kinetics, Analytical Chemistry, 37 (1965) 1351-1355.

[45] C.C. Miller, The Stokes-Einstein Law for diffusion in solution, Proceedings of the Royal Society of London. Series A, Containing Papers of a Mathematical and Physical Character, 106 (1924) 724-749.
[46] B. Chauhan, W. Fawcett, A. Lasia, The influence of ion pairing on the electroreduction of nitromesitylene in aprotic solvents. 1. Thermodynamic aspects, The Journal of Physical Chemistry, 81 (1977) 1476-1481.
[47] W.R. Fawcett, M. Fedurco, M. Opallo, The inhibiting effects of tetraalkylammonium cations on simple heterogeneous electron transfer reactions in polar aprotic solvents, The Journal of Physical Chemistry, 96 (1992) 9959-9964.
[48] Y. Liu, S.-X. Guo, A.M. Bond, J. Zhang, Y.V. Geletii, C.L. Hill, Voltammetric Determination of the Reversible Potentials for $[\{Ru_4O_4(OH)_2(H_2O)_4\}(\gamma\text{-}SiW_{10}O_{36})_2]^{10-}$ over the pH Range of 2–12: Electrolyte Dependence and Implications for Water Oxidation Catalysis, Inorganic chemistry, 52 (2013) 11986-11996.
[49] S.-X. Guo, S.W. Feldberg, A.M. Bond, D.L. Callahan, P.J. Richardt, A.G. Wedd, Systematic Approach to the Quantitative Voltammetric Analysis of the FeIII/FeII Component of the $[\alpha_2\text{-}Fe(OH_2)P_2W_{17}O_{61}]^{7-/8-}$ Reduction Process in Buffered and Unbuffered Aqueous Media, The Journal of Physical Chemistry B, 109 (2005) 20641-20651.
[50] D.H. Evans, A.G. Gilicinski, Comparison of heterogeneous and homogeneous electron-transfer rates for some nitroalkanes and diketones, The Journal of Physical Chemistry, 96 (1992) 2528-2533.
[51] R. Gambert, H. Baumgärtel, The influence of cations on the interface between the mercury electrode and non-aqueous CH_3CN, Journal of electroanalytical chemistry and interfacial electrochemistry, 183 (1985) 315-328.
[52] R.A. Petersen, D.H. Evans, Heterogeneous electron transfer kinetics for a variety of organic electrode reactions at the mercury-acetonitrile interface using either tetraethylammonium perchlorate or tetraheptylammonium perchlorate electrolyte, Journal of electroanalytical chemistry and interfacial electrochemistry, 222 (1987) 129-150.
[53] J. Lipkowski, C. Buess-Herman, J. Lambert, L. Gierst, Mechanism of electron transfer through monomolecular films of neutral organic species adsorbed at an electrode surface, Journal of electroanalytical chemistry and interfacial electrochemistry, 202 (1986) 169-189.
[54] C. Miller, P. Cuendet, M. Graetzel, Adsorbed. omega.-hydroxy thiol monolayers on gold electrodes: evidence for electron tunneling to redox species in solution, The Journal of Physical Chemistry, 95 (1991) 877-886.
[55] H.O. Finklea, D.D. Hanshew, Electron-transfer kinetics in organized thiol monolayers with attached pentaammine (pyridine) ruthenium redox centers, Journal of the American Chemical Society, 114 (1992) 3173-3181.
[56] Y. Marcus, J. Chipperfield, Ionic solvation: Wiley-Interscience, Chichester, 1985 (ISBN 0-471-90756-1). viii+ 306 pp. Price£ 42.00, Elsevier, 1986.

Supporting Information

Electrolyte Cation Dependence of the Electron Transfer Kinetics Associated with the $[SVW_{11}O_{40}]^{3-/4-}$ ($V^{V/IV}$) and $[SVW_{11}O_{40}]^{4-/5-}$ ($W^{VI/V}$) Processes in Propylene Carbonate

Jiezhen Li[a], Cameron L. Bentley[b], Tadaharu Ueda[c], Alan M. Bond[a,*] and Jie Zhang[a,*]

[a]School of Chemistry and ARC Centre of Excellence for Electromaterials Science, Monash University, Clayton, Vic 3800, Australia

[b]Department of Chemistry, University of Warwick, Coventry, CV4 7AL, U.K.

[c]Department of Applied Science, Kochi University, Japan

Corresponding authors: jie.zhang@monash.edu, alan.bond@monash.edu

Instrumentation and procedures. The electrochemically effective areas (*A*) of the macrodisk working electrodes were calculated from analysis of a plot of DC peak current versus the square root of scan rate for the oxidation of 1.0 mM Fc in CH_3CN (0.1 M $[Bu_4N][PF_6]$) using the Randles-Sevcik relationship and the known diffusion coefficient of 2.4×10^{-5} cm^2 s^{-1} for Fc under these conditions.[1]

$$i_p = 0.4463nFA(\frac{nFDv}{RT})^{1/2}C \qquad \text{(S1)}$$

In eq. S1, i_p is the oxidation peak current, n is the number of electrons transerred (n = 1), C is the bulk concentration, D is the diffusion coefficient of Fc, T is the absolute temperature, R is the universal gas constant, F is Faraday's constant, A is the electrode area and v is the scan rate. The areas of the Pt and GC amacrodisk electrodes determined in this manner were 7.71×10^{-3} cm^2 and 7.45×10^{-3} cm^2, respectively.

Prior to each voltammetric experiment, the working electrode was polished with an aqueous 0.3 μm alumina slurry on a clean polishing cloth, rinsed with water, sonicated thoroughly in water to remove alumina, rinsed with acetone, and finally dried under nitrogen. Platinum wire was used as the auxiliary and reference electrodes. The potential of the Pt quasi-reference electrode was calibrated against the IUPAC recommended $Fc^{0/+}$ process.[2] All electrolyte solutions were degassed with N_2 for at least 5 min prior to commencing voltametric experimentation, and a blanket of N_2 was maintained over the solvent (electrolyte) medium while undertaking experiments.

DC cyclic voltammetric experiments were carried out using a CHI 760E electrochemical workstation (CH Instruments, Texas, USA). Large amplitude FTAC voltammetric experiments were undertaken with a home built instrument[3] using an applied sine wave perturbation with an amplitude (ΔE) of 80 mV and frequency (f) of 9.02 Hz or 27.01 Hz, superimposed onto the DC potential ramp. After data collection,

the total DC plus AC current was subjected to Fourier transformation (FT) to obtain the power spectrum. After selection of the frequency band of interest, inverse Fourier transformation (i-FT) was used to generate the required DC or AC harmonic components.[3-5]

DC and AC Simulations and AC data analysis. For slow kinetics, DigiSim software was used for the DC simulations. Simulations of FTAC voltammograms were carried out using the MECSim (Monash Electrochemistry Simulator, http://www.garethkennedy.net/MECSim.html) software.[6] This Fortran package uses the expanding spatial grid formulation[7] and is based on the mathematical approach derived by Rudolph,[8] with minor variations. The Butler-Volmer theory of electron transfer[9] was used to describe the potential dependence of the electrode kinetics for the simple one-electron transfer reaction given in eq. S2.

$$O + e^- \rightleftharpoons R\ (E^0, k^0, \alpha) \qquad \text{(S2)}$$

where E^0 is the reversible potential. FTAC voltammetric data obtained from either experiment or simulation in the time domain were converted to the frequency domain to generate the power spectrum followed by use of the i-FT algorithm to resolve the aperiodic DC component and AC harmonic and display these response in the time domain.[10-11] Six parameters E^0, k^0, α, D, R_u and C_{dl} (double layer capacitance) were determined in order to quantitatively define all aspects of the electrode processes. The R_u value was determined experimentally from the *RC* time constant method available on the CHI potentiostat, E^0 was estimated from the midpoint of the reduction (E_p^{red}) and oxidation (E_p^{ox}) peak potentials in a DC cyclic voltammetric experiment and the D value of $[SVW_{11}O_{40}]^{3-}$ was calculated from the reduction peak measured at a GC electrode in PC using the Randles-Sevcik relationship (see eq. S1).[12] The C_{dl} value was

quantified from the background current in the fundamental harmonic component at potentials where faradaic current is absent. In order to define the potential dependence of C_{dl}, a non-linear capacitor model was used, as described elsewhere:[13]

$$C_{dl}(t) = c_0 + c_1E(t) + c_2E^2(t) + c_3E^3(t) + c_4E^4(t) \qquad \text{(S3)}$$

In eq. S3, c_0, c_1, c_2, c_3, and c_4 are the coefficients that determine the degree of nonlinearity of the capacitor. Finally, k^0 and α values were determined by comparison of the experimental and simulated higher order AC harmonic component data.

As demonstrated by simulation,[14] the impact of the cross redox reaction between $[SVW_{11}O_{40}]^{3-}$ and $[SVW_{11}O_{40}]^{5-}$ (eq. S4) on the voltammetric characteristics is insignificant under the conditions employed.

$$[SVW_{11}O_{40}]^{3-} + [SVW_{11}O_{40}]^{5-} \rightleftharpoons 2[SVW_{11}O_{40}]^{4-} \qquad \text{(S4)}$$

Consquently, the cross redox reaction was not needed included in simulations when determining the electrode kinetics of the $V^{IV/V}$ and $W^{VI/V}$ processes.

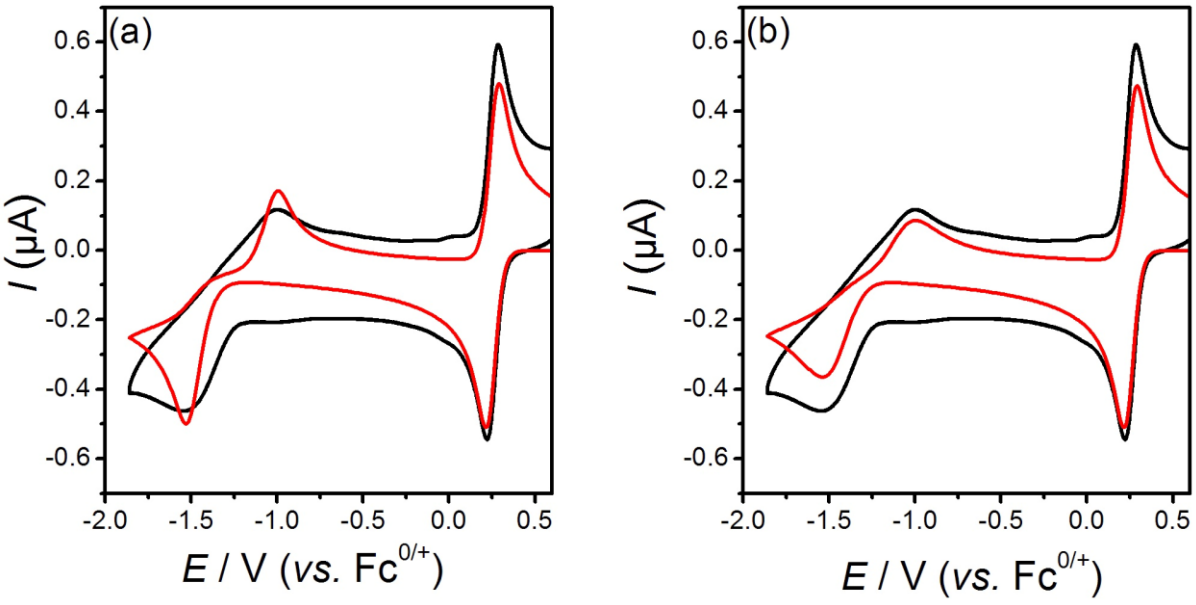

Figure S1. Comparison of simulated (—) and experimental (—) cyclic voltammograms obtained for the $V^{IV/V}$ and $W^{VI/V}$ processes in PC containing 1.0 mM $[SVW_{11}O_{40}]^{3-}$ and 0.5 M [TBA][PF_6] at a 1 mm diameter Pt macrodisk based on (a) Butler-Volmer theory and (b) Marcus-Hush theory. The simulation parameters are as follows: A = 7.71 × 10^{-3} cm^2, D = 6 × 10^{-7} cm^2 s^{-1}, R_u = 750 Ω, T = 296 K, k_V^0 = 0.0040 cm s^{-1}, α_V = 0.5. For (a) Butler-Volmer theory, k_W^0 = 1.2 × 10^{-5} cm s^{-1}, α_W = 0.50. For (b) Marcus-Hush theory, k_W^0 = 2.8 × 10^{-5} cm s^{-1}, λ = 0.30.

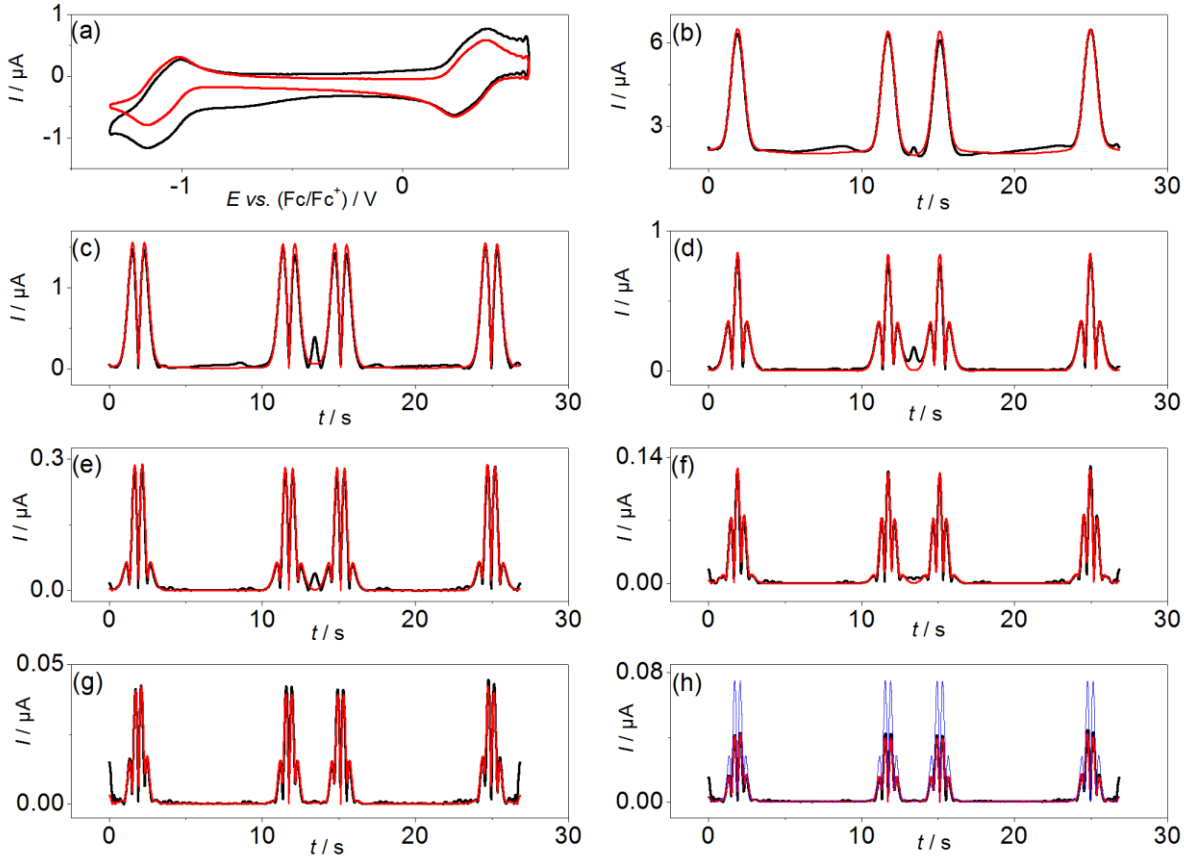

Figure S2. Comparison of simulated (—) and experimental (—) FTAC voltammetric data obtained for the $V^{IV/V}$ and $W^{VI/V}$ processes in PC containing 1.0 mM $[SVW_{11}O_{40}]^{3-}$ and 0.5 M [BMIM][BF_4] at a 1 mm diameter Pt macrodisk electrode with T = 295 K, ΔE = 80 mV, f = 27.01 Hz and v = 0.142 V s^{-1}. (a) aperiodic DC component, (b–g) 1st to 6th AC harmonic components, and (h) simulated 6th harmonic component for the reversible case (—). To obtain the simulated data, k_V^0 = 0.04 cm s^{-1}, α_V = 0.5, k_W^0 = 0.038 cm s^{-1} and α_W = 0.5 were used.

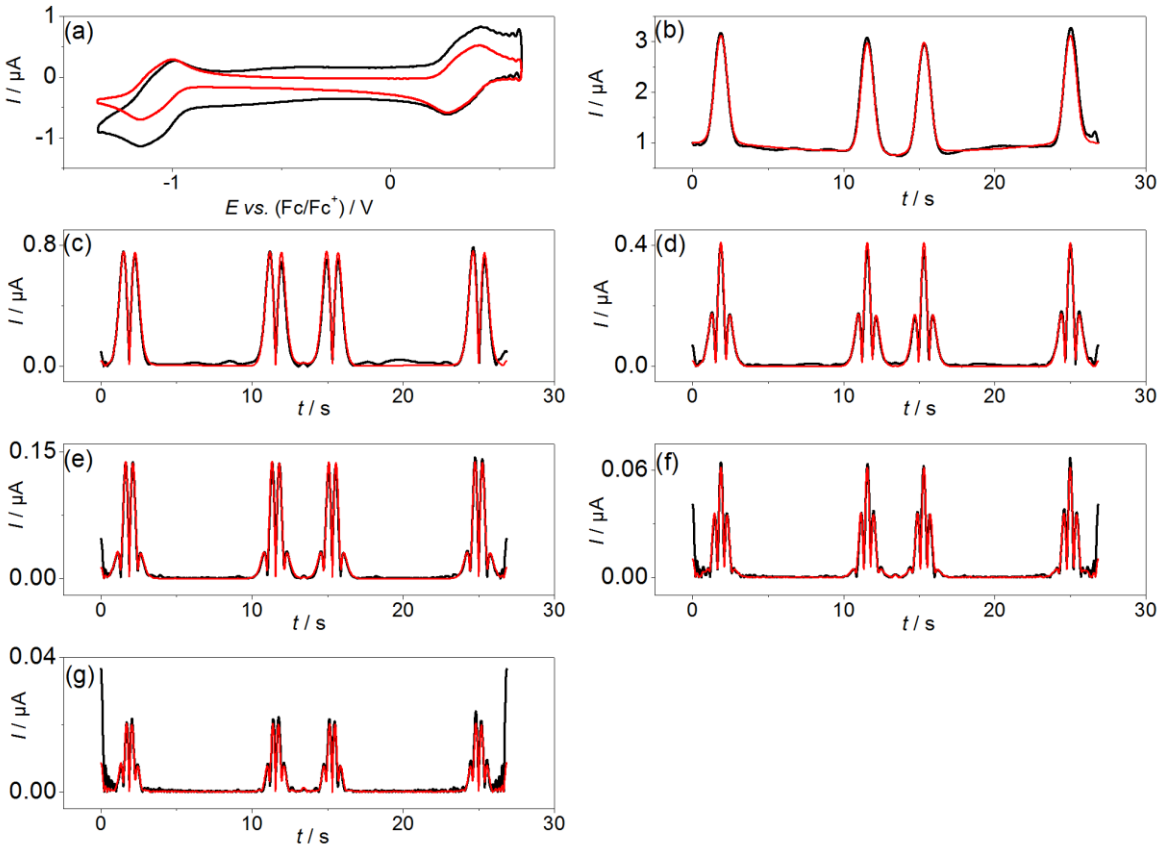

Figure S3. Comparison of simulated (—) and experimental (—) FTAC voltammetric data obtained for the $V^{IV/V}$ and $W^{VI/V}$ processes in PC containing 1.0 mM $[SVW_{11}O_{40}]^{3-}$ and 0.5 M $[Py_{14}][BF_4]$ at a 1 mm diameter Pt macrodisk electrode with T = 295 K, ΔE = 80 mV, f = 9.02 Hz and v = 0.145 V s^{-1}. (a) aperiodic DC component, (b–g) 1st to 6th AC harmonic components. To obtain the simulated data, k_V^0 = 0.016 cm s^{-1}, α_V = 0.5, k_W^0 = 0.016 cm s^{-1} and α_W = 0.5 were used.

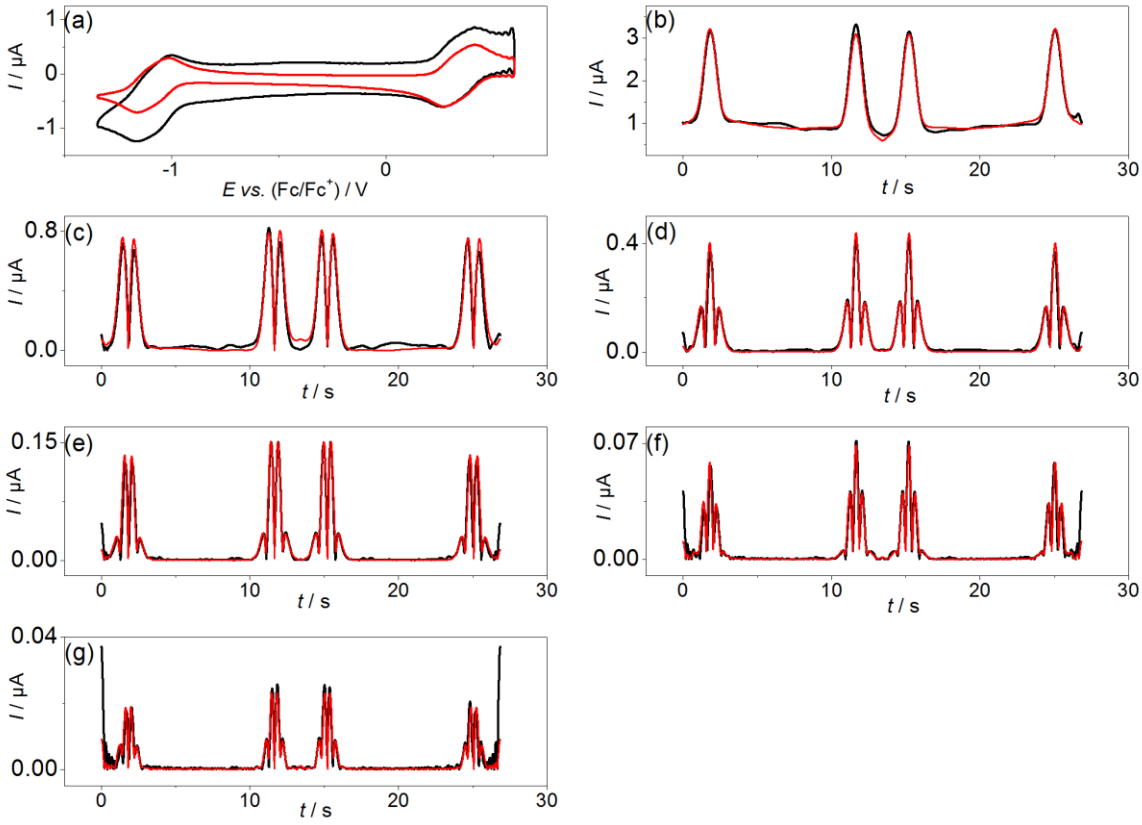

Figure S4. Comparison of simulated (—) and experimental (—) FTAC voltammetric data obtained for the $V^{IV/V}$ and $W^{VI/V}$ processes in PC containing 1.0 mM $[SVW_{11}O_{40}]^{3-}$ and 0.5 M [TEA][BF_4] at a 1 mm diameter Pt macrodisk electrode with T = 295 K, ΔE = 80 mV, f = 9.02 Hz and v = 0.145 V s^{-1}. (a) aperiodic DC component, (b–g) 1st to 6th AC harmonic components. To obtain the simulated data, k^0_V = 0.15 cm s^{-1}, α_V = 0.5, k^0_W = 0.02 cm s^{-1} and α_W = 0.5 were used.

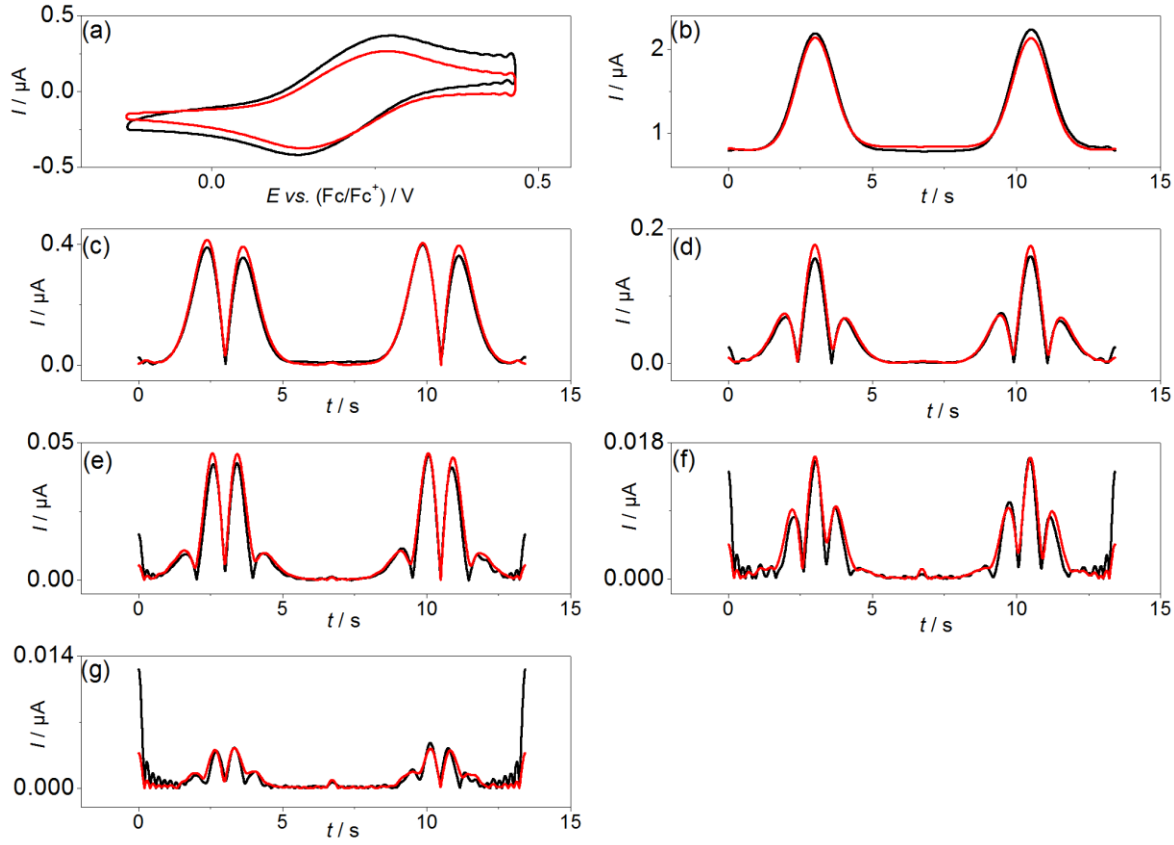

Figure S5. Comparison of simulated (—) and experimental (—) FTAC voltammetric data obtained for the $V^{IV/V}$ and $W^{VI/V}$ processes in PC containing 1.0 mM $[SVW_{11}O_{40}]^{3-}$ and 0.5 M [TBA][PF_6] at a 1 mm diameter Pt macrodisk electrode with T = 295 K, ΔE = 80 mV, f = 9.02 Hz and v = 0.089 V s^{-1}. (a) aperiodic DC component, (b–g) 1st to 6th AC harmonic components. To obtain the simulated data, k_V^0 = 0.004 cm s^{-1}, α_V = 0.5 were used.

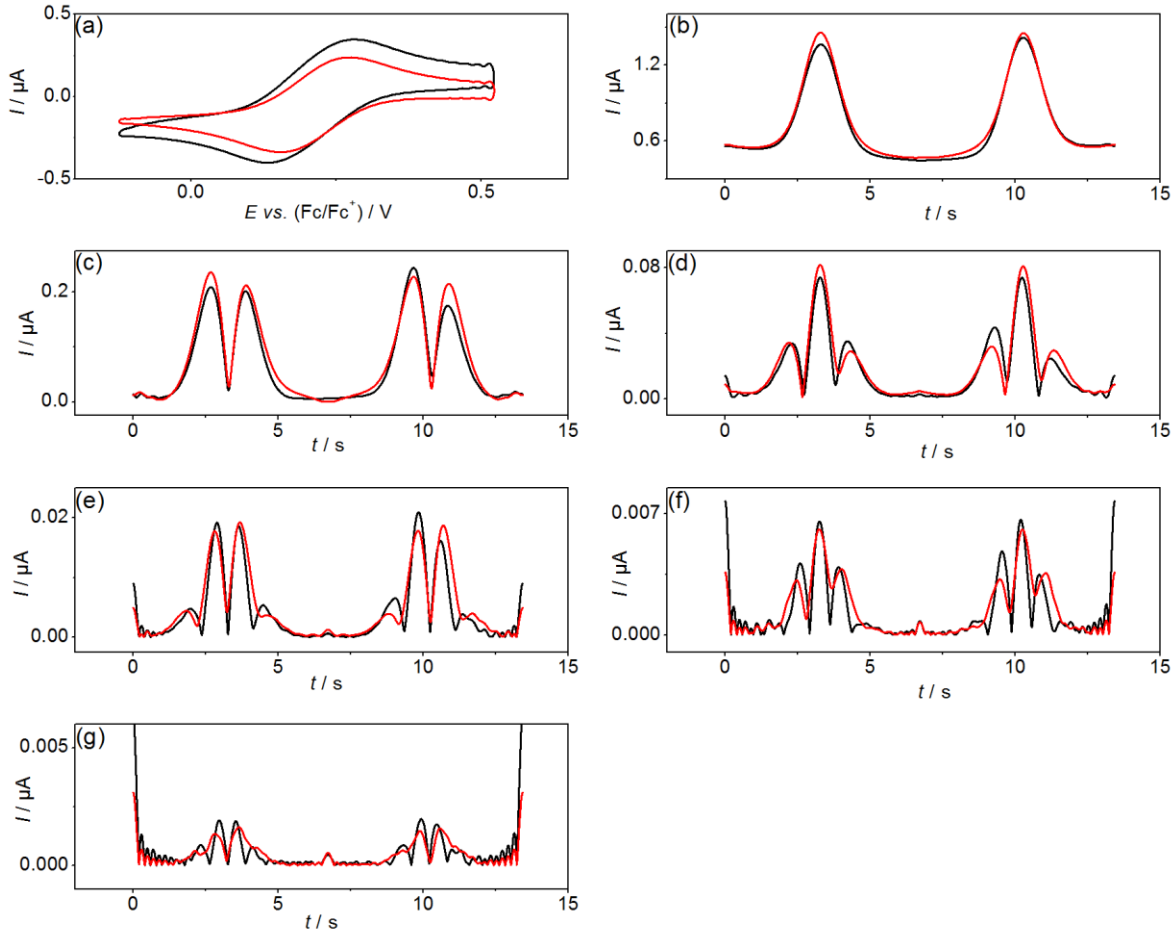

Figure S6. Comparison of simulated (—) and experimental (—) FTAC voltammetric data obtained for the $V^{IV/V}$ and $W^{VI/V}$ processes in PC containing 1.0 mM $[SVW_{11}O_{40}]^{3-}$ and 0.5 M [THA][ClO_4] at a 1 mm diameter Pt macrodisk electrode with T = 295 K, ΔE = 80 mV, f = 9.02 Hz and v = 0.097 V s^{-1}. (a) aperiodic DC component, (b–g) 1st to 6th AC harmonic components. To obtain the simulated data, k_V^0 = 0.00175 cm s^{-1}, α_V = 0.5 were used.

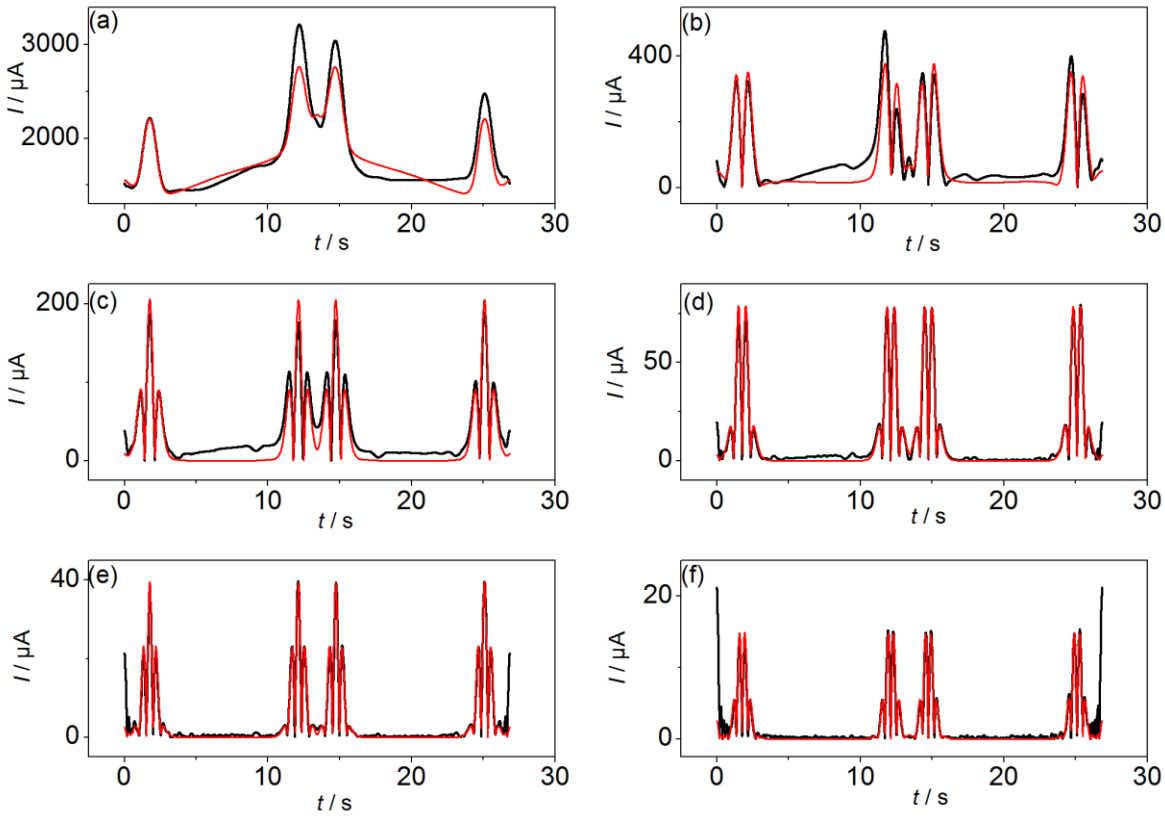

Figure S7. Comparison of simulated (—) and experimental (—) FTAC voltammetric data obtained for the $V^{IV/V}$ and $W^{VI/V}$ processes in PC containing 0.20 mM $[SVW_{11}O_{40}]^{3-}$ and 0.5 M [EMIM][BF_4] at a 1 mm diameter Pt macrodisk electrode with T = 295 K, ΔE = 80 mV, f = 27.01 Hz and v = 0.134 V s^{-1}. (a) aperiodic DC component, (b–g) 1st to 6th AC harmonic components. To obtain the simulated data, k_V^0 = 0.1 cm s^{-1}, α_V = 0.5, k_W^0 = 0.1 cm s^{-1} and α_W = 0.5 were used.

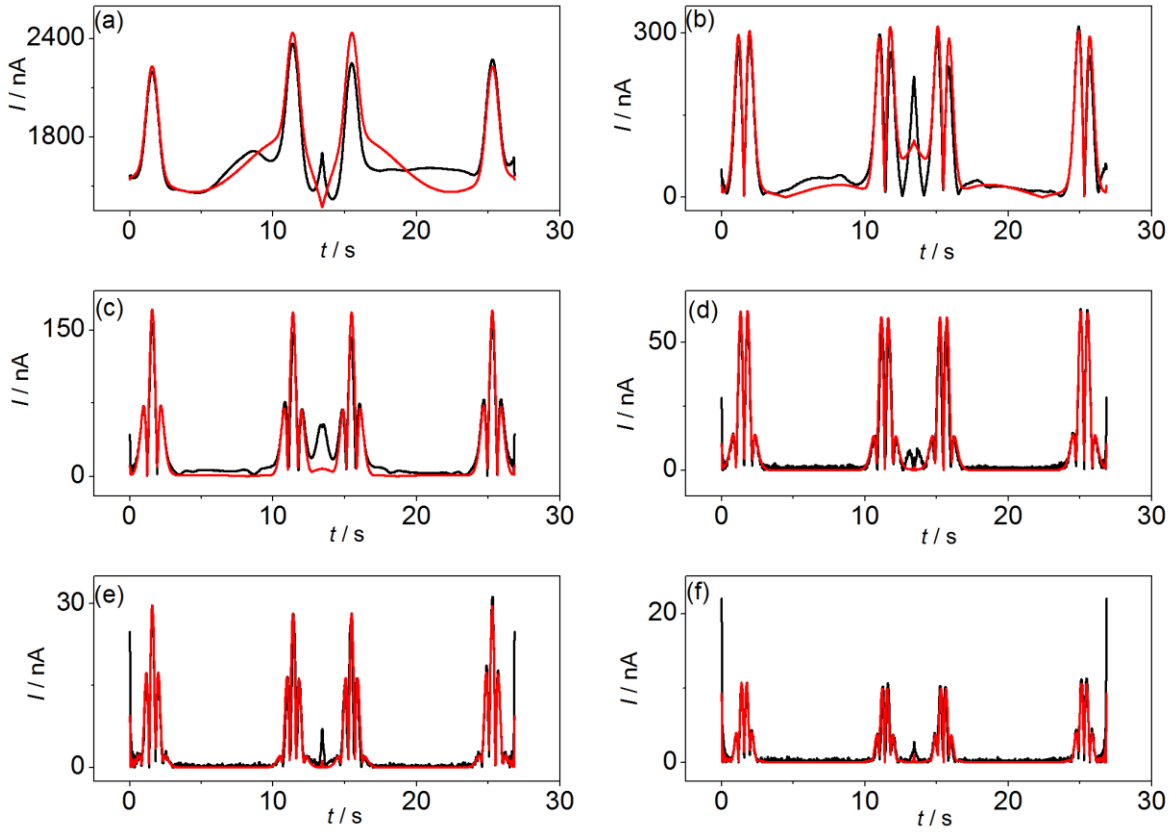

Figure S8. Comparison of simulated (—) and experimental (—) FTAC voltammetric data obtained for the $V^{IV/V}$ and $W^{VI/V}$ processes in PC containing 0.20 mM $[SVW_{11}O_{40}]^{3-}$ and 0.5 M [BMIM][BF_4] at a 1 mm diameter Pt macrodisk electrode with T = 295 K, ΔE = 80 mV, f = 27.01 Hz and v = 0.142 V s^{-1}. (a) aperiodic DC component, (b–g) 1st to 6th AC harmonic components. To obtain the simulated data, k^0_V = 0.05 cm s^{-1}, α_V = 0.5, k^0_W = 0.045 cm s^{-1} and α_W = 0.5 were used.

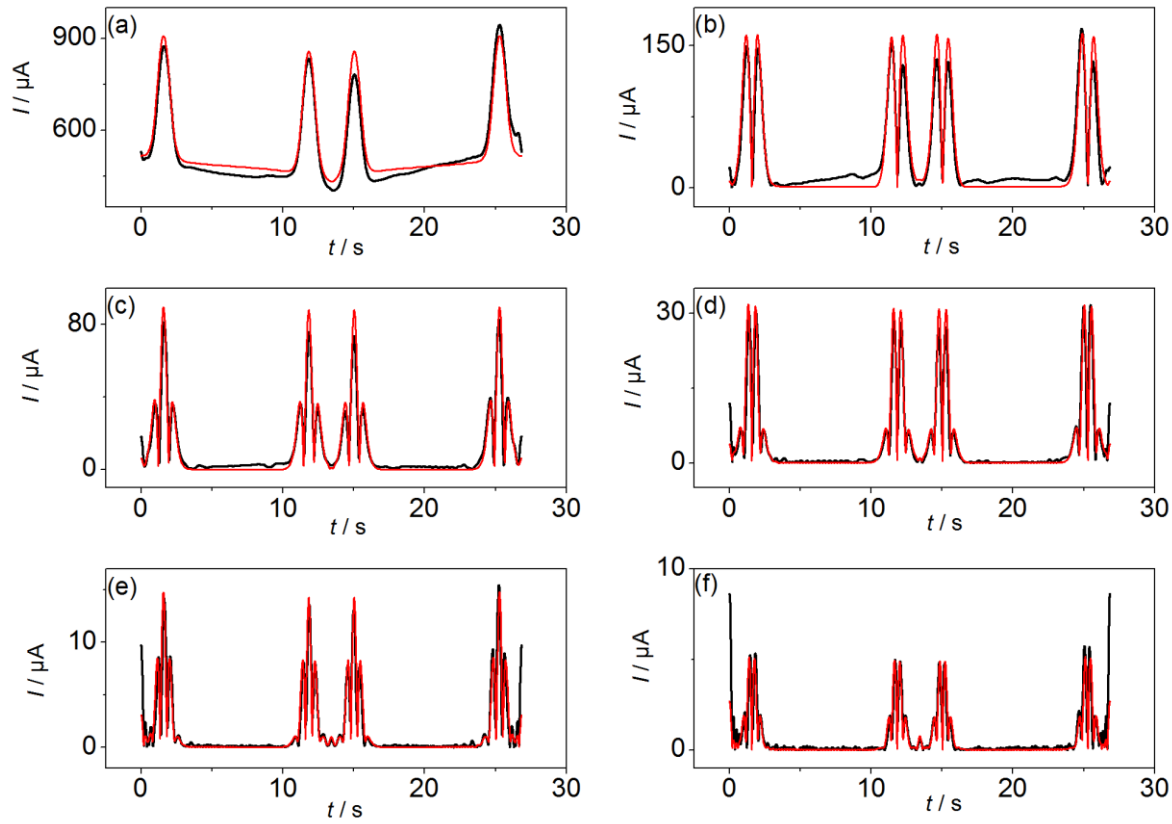

Figure S9. Comparison of simulated (—) and experimental (—) FTAC voltammetric data obtained for the $V^{IV/V}$ and $W^{VI/V}$ processes in PC containing 0.20 mM $[SVW_{11}O_{40}]^{3-}$ and 0.5 M $[Py_{14}][BF_4]$ at a 1 mm diameter Pt macrodisk electrode with T = 295 K, ΔE = 80 mV, f = 9.02 Hz and v = 0.137 V s^{-1}. (a) aperiodic DC component, (b–g) 1st to 6th AC harmonic components. To obtain the simulated data, k^0_V = 0.018 cm s^{-1}, α_V = 0.5, k^0_W = 0.017 cm s^{-1} and α_W = 0.5 were used.

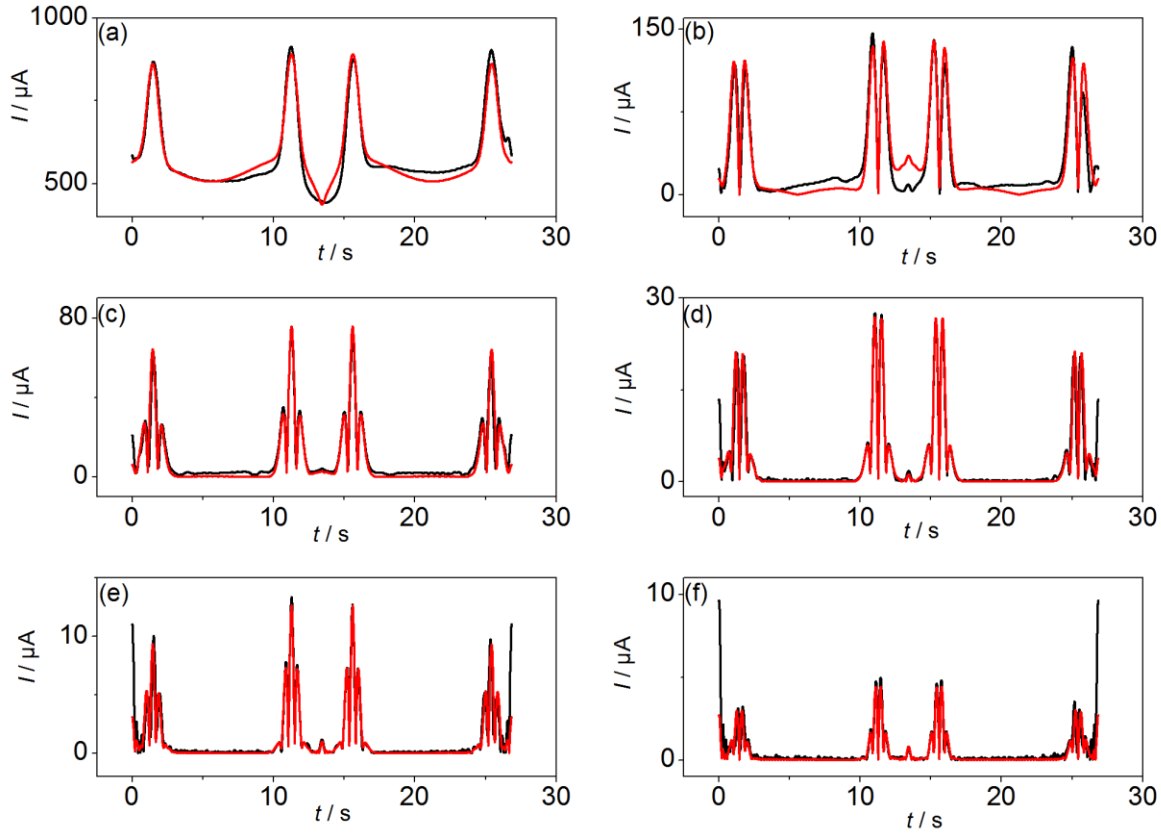

Figure S10. Comparison of simulated (—) and experimental (—) FTAC voltammetric data obtained for the $V^{IV/V}$ and $W^{VI/V}$ processes in PC containing 0.20 mM $[SVW_{11}O_{40}]^{3-}$ and 0.5 M [TEA][BF_4] at a 1 mm diameter Pt macrodisk electrode with T = 295 K, ΔE = 80 mV, f = 9.02 Hz and v = 0.145 V s^{-1}. (a) aperiodic DC component, (b–g) 1st to 6th AC harmonic components. To obtain the simulated data, k_V^0 = 0.012 cm s^{-1}, α_V = 0.5, k_W^0 = 0.02 cm s^{-1} and α_W = 0.5 were used.

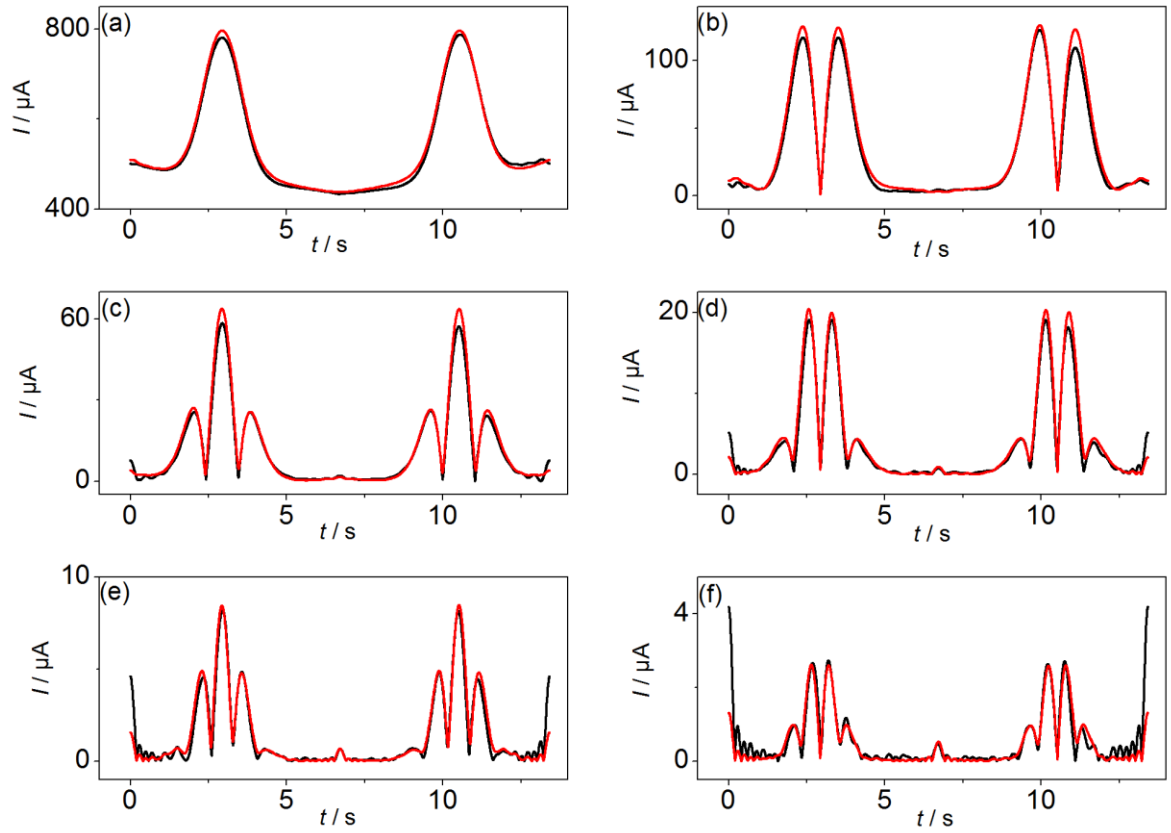

Figure S11. Comparison of simulated (—) and experimental (—) FTAC voltammetric data obtained for the $V^{IV/V}$ and $W^{VI/V}$ processes in PC containing 0.20 mM $[SVW_{11}O_{40}]^{3-}$ and 0.5 M [TPA][BF_4] at a 1 mm diameter Pt macrodisk electrode with T = 295 K, ΔE = 80 mV, f = 9.02 Hz and v = 0.097 V s^{-1}. (a) aperiodic DC component, (b–g) 1st to 6th AC harmonic components. To obtain the simulated data, k_V^0 = 0.0085 cm s^{-1}, α_V = 0.5 were used.

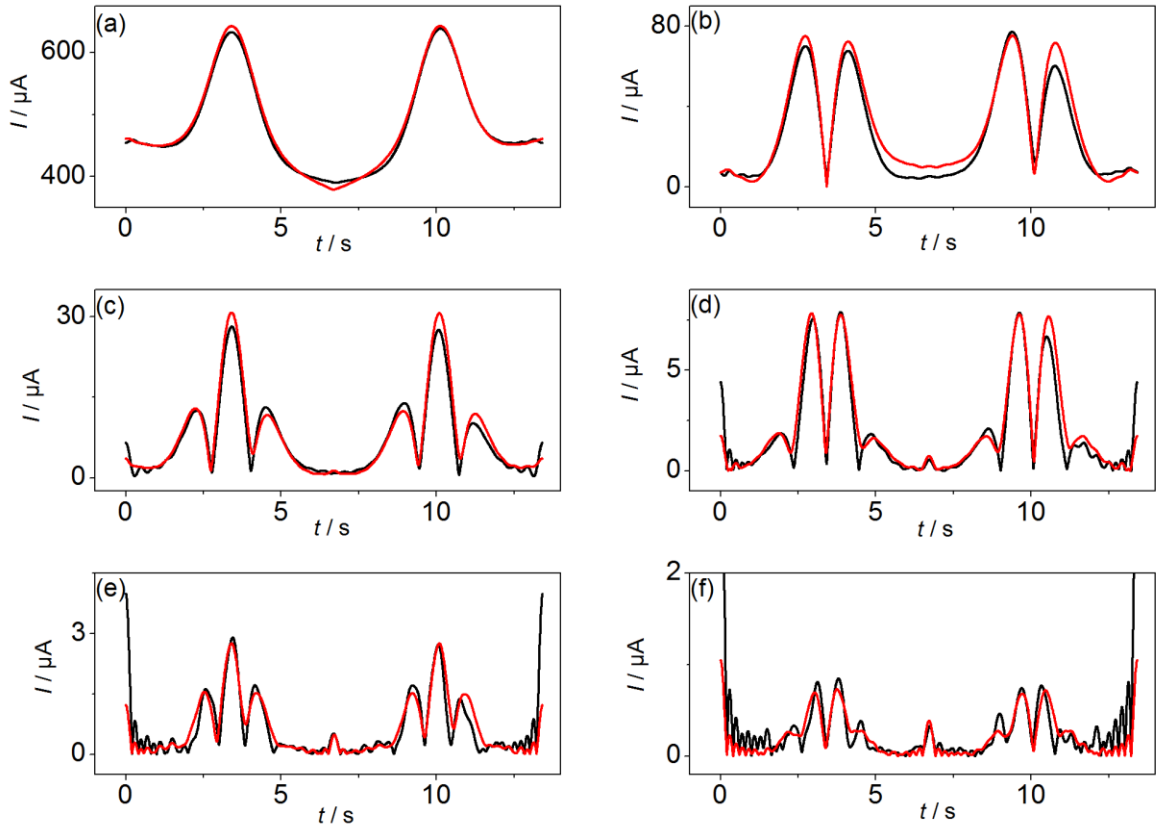

Figure S12. Comparison of simulated (—) and experimental (—) FTAC voltammetric data obtained for the $V^{IV/V}$ and $W^{VI/V}$ processes in PC containing 0.20 mM $[SVW_{11}O_{40}]^{3-}$ and 0.5 M [TBA][PF_4] at a 1 mm diameter Pt macrodisk electrode with T = 295 K, ΔE = 80 mV, f = 9.02 Hz and v = 0.082 V s^{-1}. (a) aperiodic DC component, (b–g) 1st to 6th AC harmonic components. To obtain the simulated data, k_V^0 = 0.0033 cm s^{-1}, α_V = 0.5 were used.

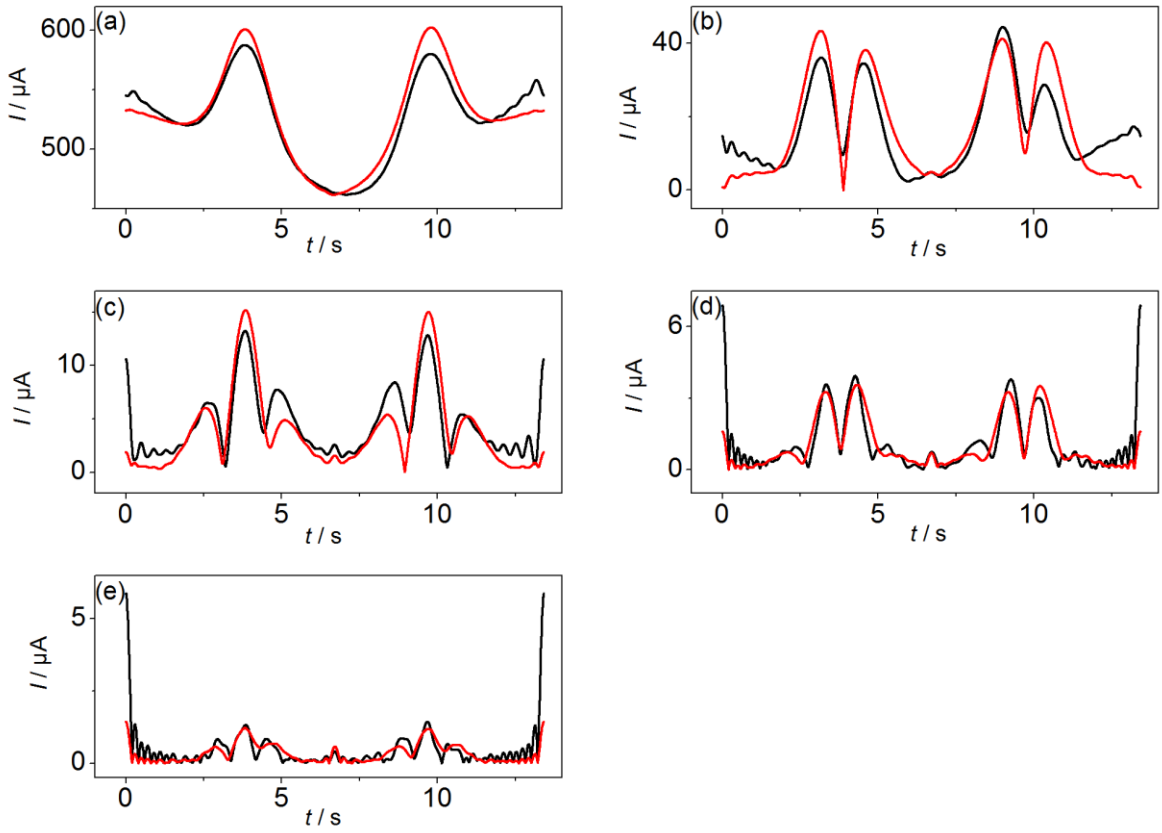

Figure S13. Comparison of simulated (—) and experimental (—) FTAC voltammetric data obtained for the $V^{IV/V}$ and $W^{VI/V}$ processes in PC containing 0.20 mM $[SVW_{11}O_{40}]^{3-}$ and 0.5 M [THA][ClO_4] at a 1 mm diameter Pt macrodisk electrode with T = 295 K, ΔE = 80 mV, f = 9.02 Hz and v = 0.082 V s^{-1}. (a) aperiodic DC component, (b–g) 1st to 6th AC harmonic components. To obtain the simulated data, k_V^0 = 0.0016 cm s^{-1}, α_V = 0.5 were used.

REFERENCES

1. Zhang, J.; Guo, S.-X.; Bond, A. M., Discrimination and evaluation of the effects of uncompensated resistance and slow electrode kinetics from the higher harmonic components of a Fourier transformed large-amplitude alternating current voltammogram. *Anal. Chem.* **2007,** *79* (6), 2276-2288.
2. Gritzner, G.; Kuta, J., Recommendations on reporting electrode potentials in nonaqueous solvents (Recommendations 1983). *Pure Appl. Chem.* **1984,** *56* (4), 461-466.
3. Bond, A. M.; Duffy, N. W.; Guo, S.-X.; Zhang, J.; Elton, D., Changing the look of voltammetry. *Analytical chemistry* **2005,** *77* (9), 186 A-195 A.
4. Si-Xuan, G.; Alan M, B.; Jie, Z., Fourier Transformed Large Amplitude Alternating Current Voltammetry: Principles and Applications. *Review of Polarography* **2015,** *61* (1), 21-32.
5. Bond, A. M.; Elton, D.; Guo, S.-X.; Kennedy, G. F.; Mashkina, E.; Simonov, A. N.; Zhang, J., An integrated instrumental and theoretical approach to quantitative electrode kinetic studies based on Large Amplitude Fourier Transformed ac Voltammetry: A mini-review. *Electrochem. Commun.* **2015**.
6. Kennedy, G. F.; Bond, A. M.; Simonov, A. N., Modelling ac voltammetry with MECSim: facilitating simulation–experiment comparisons. *Current Opinion in Electrochemistry* **2017**.
7. Feldberg, S. W., Optimization of explicit finite-difference simulation of electrochemical phenomena utilizing an exponentially expanded space grid: Refinement of the Joslin-Pletcher algorithm. *Journal of Electroanalytical Chemistry and Interfacial Electrochemistry* **1981,** *127* (1), 1-10.
8. Rudolph, M., A fast implicit finite difference algorithm for the digital simulation of electrochemical processes. *Journal of electroanalytical chemistry and interfacial electrochemistry* **1991,** *314* (1), 13-22.
9. Bard, A. J.; Faulkner, L. R., Fundamentals and applications. *Electrochemical Methods, 2nd ed.; Wiley: New York* **2001**.
10. Zhang, J.; Guo, S.-X.; Bond, A. M.; Marken, F., Large-amplitude Fourier transformed high-harmonic alternating current cyclic voltammetry: kinetic discrimination of interfering faradaic processes at glassy carbon and at boron-doped diamond electrodes. *Analytical chemistry* **2004,** *76* (13), 3619-3629.
11. Sher, A. A.; Bond, A. M.; Gavaghan, D. J.; Harriman, K.; Feldberg, S. W.; Duffy, N. W.; Guo, S.-X.; Zhang, J., Resistance, capacitance, and electrode kinetic effects in fourier-transformed large-amplitude sinusoidal voltammetry: Emergence of powerful and intuitively obvious tools for recognition of patterns of behavior. *Anal. Chem.* **2004,** *76* (21), 6214-6228.
12. Bond, A. M.; Bano, K.; Adeel, S.; Martin, L. L.; Zhang, J., Fourier‐Transformed Large‐Amplitude AC Voltammetric Study of Tetrathiafulvalene (TTF): Electrode Kinetics of the $TTF^{0}/TTF^{\cdot+}$ and $TTF^{\cdot+}/TTF^{2+}$ Processes. *ChemElectroChem* **2014,** *1* (1), 99-107.
13. Bond, A. M.; Duffy, N. W.; Elton, D. M.; Fleming, B. D., Characterization of nonlinear background components in voltammetry by use of large amplitude

periodic perturbations and Fourier transform analysis. *Analytical chemistry* **2009,** *81* (21), 8801-8808.

14. Li, J.; Guo, S. X.; Bentley, C. L.; Bano, K.; Bond, A. M.; Zhang, J.; T., U., Electrode Material Dependence of the Electron Transfer Kinetics Associated with the $[SVW_{11}O_{40}]^{3-/4-}$ (VV/IV) and $[SVW_{11}O_{40}]^{4-/5-}$ (WVI/V) Processes in Dimethylformamide. *Accepted by Electrochimica Acta* **2016**.

Chapter 7

A Systematic Study of the Kinetic and Thermodynamic Properties of the Fe^{III}/Fe^{II} Electron Transfer Process at Glassy Carbon and Boron-Doped Diamond Electrodes

Electrochimica Acta 249 (2017) 421–430

Contents lists available at ScienceDirect

Electrochimica Acta

journal homepage: www.elsevier.com/locate/electacta

A Systematic Study of the Mass Transport, Kinetic and Thermodynamic Properties of the $Fe^{III/II}$ Process at Glassy Carbon and Boron-Doped Diamond Electrodes

Mingyue Lin[a,c,d,1], Jiezhen Li[a,1], Dawei Pan[c], Alan M. Bond[a,b,*], Jie Zhang[a,b,*]

[a] School of Chemistry, Monash University, Clayton, Victoria 3800, Australia
[b] ARC Centre of Excellence for Electromaterials Science, Monash University, Clayton, Vic 3800, Australia
[c] Key Laboratory of Coastal Environmental Processes and Ecological Remediation, Yantai Institute of Coastal Zone Research (YIC), Chinese Academy of Sciences (CAS), Shandong Provincial Key Laboratory of Coastal Environmental Processes, YICCAS, Yantai, Shandong 264003, PR China
[d] University of Chinese Academy of Sciences, Beijing 100049, PR China

ARTICLE INFO

Article history:
Received 8 July 2017
Accepted 25 July 2017
Available online 26 July 2017

Keywords:
$Fe^{III/II}$ process
electron transfer kinetics
Fourier transformed alternating current voltammetry
medium effect
electrode heterogeneity

ABSTRACT

The heterogeneous electron transfer kinetics (k^0 values), mass transport and thermodynamic properties (E^0 values) associated with the $Fe^{III/II}$ process have been determined in aqueous solutions containing 0.1 M HCl, $HClO_4$, bis(trifluoromethanesulfonyl)imide ($HNTf_2$) or 0.05 M silicotungstic acid ($H_4[\alpha\text{-}SiW_{12}O_{40}]$) supporting electrolytes. The diffusion coefficient (D) values for Fe^{III} and Fe^{II} are dependent on the radius of the electrolyte anion and follow the order $D(SiW_{12}O_{40}^{4-}) < D(NTf_2^-) < D(ClO_4^-) < D(Cl^-)$. The k^0 values are found to be smaller at boron doped diamond (BDD) electrodes than glassy carbon (GC) electrodes, and influenced by the ion-pairing between electrolyte anions and Fe^{III} and Fe^{II}. Based on the formal potential value, $HNTf_2$ is found to be a more innocent electrolyte than commonly used $HClO_4$ with regard to determine the true k^0 values of the outer-sphere $[Fe(H_2O)_6]^{3+/2+}$ process. Fourier transformed large amplitude alternating current voltammetry, which provides favorable signal to background ratio, was used to determine k^0 values associated with the $Fe^{III/II}$ process in $H_4[\alpha\text{-}SiW_{12}O_{40}]$ and $HNTf_2$ electrolyte media at GC electrodes and probe the implications of the heterogeneity of the BDD electrode surface on the electrode kinetic determination in $H_4[\alpha\text{-}SiW_{12}O_{40}]$ electrolyte media.

1. Introduction

In an electrolyte medium containing a poorly coordinating supporting electrolyte anion, such as perchlorate, the ferric/ferrous redox reaction is reported to follow a slow uncomplicated single-step, outer-sphere heterogeneous electron transfer (HET) mechanism: [1]

$$[Fe(H_2O)_6]^{3+} + e^- = [Fe(H_2O)_6]^{2+} \quad (1)$$

Although both the reactant and product have an octahedral geometry, they differ in the Fe-O bond lengths (2.21 Å for Fe (II) and 2.05 Å for Fe (III)) [2]. Based on the Marcus theory for HET, significant changes in structure lead to a high activation energy for electron tunneling resulting in sluggish electrode kinetics.

In solutions containing a chloride salt as the supporting electrolyte, this anion coordinates with Fe^{III} and Fe^{II} and changes the redox reaction to the $[Fe(Cl)_6]^{3-/4-}$ rather than $[Fe(H_2O)_6]^{3+/2+}$ process. Consequently, to determine the heterogeneous charge transfer rate constant (k^0 values) for the $[Fe(H_2O)_6]^{3+/2+}$ process, perchloric acid ($HClO_4$) has been commonly used as the supporting electrolyte [3]. Early studies on the $[Fe(H_2O)_6]^{3+/2+}$ process using platinum and gold electrodes in $HClO_4$ solutions reported reasonably fast kinetics with k^0 lying in the range of 10^{-3} to 10^{-2} cm s^{-1} [4,5]. Later it was found that these k^0 values were enhanced by the catalytic effect of trace anion impurities [6]. The catalytic effect of chloride was firstly reported by Gerischer [7]. He found that the exchange current density for the reaction in sulfuric acid solutions increased by adding a small amount of chloride (~4 ppm). This catalytic effect was attributed to chloride adsorption on the electrode, either modifying the double layer structure or acting as a "bridging-ligand". When Weber [6] applied a rigorous purification procedure, much smaller k^0 values of 9×10^{-6} and 5×10^{-5} cm s^{-1} were obtained for the $[Fe(H_2O)_6]^{3+/2+}$ process on platinum and gold electrodes, respectively.

* Corresponding authors.
E-mail addresses: alan.bond@monash.edu (A.M. Bond), jie.zhang@monash.edu (J. Zhang).
[1] Both authors contributed equally to this work.

http://dx.doi.org/10.1016/j.electacta.2017.07.155
0013-4686/

Even though the perchlorate anion is stable, it can be electrochemically reduced to chloride, hence introducing trace concentrations of this anion [8]. In an endeavor to further explore the nature of the outer-sphere electron transfer kinetics associated with the $[Fe(H_2O)_6]^{3+/2+}$ electrode process, highly pure, electrochemically stable electrolytes containing even more innocent electrolyte anions than ClO_4^- should be of interest. Bis(trifluoromethanesulfonyl)imide (NTf_2^-) (structure given in Fig. 1) is an anion present in a class of widely used ionic liquids [9,10] that has an even lower charge density and coordinating propensity than ClO_4^- [11,12], which makes it an interesting alternative for use in studies of the electrode kinetics of the $[Fe(H_2O)_6]^{3+/2+}$ process.

Carbon based electrode materials also have commonly been used for the investigation of the $[Fe(H_2O)_6]^{3+/2+}$ process [13]. However, McCreery, et al. have shown that the $[Fe(H_2O)_6]^{3+/2+}$ process is very sensitive to the presence of C=O groups present on the surface of glassy carbon (GC) electrodes which can function as an inner sphere bridge between $[Fe(H_2O)_6]^{3+}$ or $[Fe(H_2O)_6]^{2+}$ and the electrode surface [14–16]. Boron doped diamond (BDD) electrodes also have been used to study the electrode kinetics of the $[Fe(H_2O)_6]^{3+/2+}$ process. BDD is more inert to surface adsorption than GC [17], although sp^2 impurity sites containing carbon-oxygen functional groups are often present on the BDD electrode surface [18] and can affect the k^0 value for the $[Fe(H_2O)_6]^{3+/2+}$ process [19–21]. Depending on the dopant concentration, BDD electrode can behave as a wide-gap semiconductor or a semi-metal [22]. In a BDD electrode, micrometer-sized grains/crystallites of sp^3-bonded carbon incorporated with different surface boron dopant level result in heterogeneity [23] which is often neglected in kinetic analysis due to complicated analysis requirements. Limitations in the ability to electrochemically identify kinetic dispersion is also a problem.

To determine k^0 values, a wide variety of electrochemical techniques have been used. If the k^0 values are sufficiently low, they can be determined accurately by direct current (DC) cyclic voltammetry using a macrodisc electrode at a moderate scan rate [24,25] and using the theory of Nicholson [26]. A major disadvantages of using Nicholson's method is that it does not take into account the effect of uncompensated resistance (R_u) which is often not negligible. As pointed out by Nicholson [27], the uncompensated resistance and slow kinetics give rise to similar effects on voltammetric characteristics such as peak shape and peak separation. As a consequence, omission of R_u will lead to an underestimation of k^0. The limitation can be overcome by comparing the entire experimental voltammogram to the theoretically predicted one obtained from numerical simulation which takes R_u into account [28]. To measure fast HET rates by cyclic voltammetry, in principle a high scan rate can be used to shorten the timescale of measurements. However, under these conditions, the effect of both R_u and the double layer charging current become more significant making it more difficult to determine electrode kinetics accurately [29]. To minimize the drawbacks of DC cyclic voltammetry, techniques such as scanning electrochemical microscopy SECM [30], microelectrode voltammetry [31] and Fourier transformed alternating current (FTAC) voltammetry [32] may be used. FTAC voltammetry, used in this study, is an attractive option since the nonlinear harmonic components resulting from a large amplitude ac perturbation can be used and are essentially devoid background charging current and are highly sensitive to the kinetics of heterogeneous electron transfer processes [33–36].

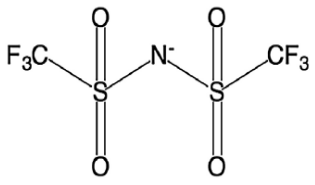

Fig. 1. Structure of NTF_2-.

In this study, $HNTf_2$ as well as hydrochloric acid (HCl), perchloric acid ($HClO_4$) and silicotungstic acid ($H_4[\alpha\text{-}SiW_{12}O_{40}]$ are used as supporting electrolytes to investigate the influence of electrolyte anions on the rate of the $Fe^{III/II}$ HET process. DC and FTAC voltammetry are employed to quantify the electrode kinetics, mass transport and thermodynamics of the process. GC as well as BDD electrodes [37–39] are used for measurement of k^0 values. Use of a high quality BDD electrode allows the influence of the sp^2 impurity on the electrode kinetics of $Fe^{III/II}$ process to be minimized. However, the impact of electrode heterogeneity at a BDD electrode needs to be considered. Other commonly used electrodes, such as Pt and Au, were not chosen for this study due to the formation of oxide layers in the potential region where the $Fe^{III/II}$ process occurs [40].

2. Experimental Section

2.1. Chemicals

All chemicals used were of reagent grade quality or better. Iron (III) perchlorate hydrate (Sigma-Aldrich, impurities $<0.005\%$ chloride), Iron(II) perchlorate hydrate (Sigma-Aldrich, 98%), perchloric acid ($HClO_4$, Merck, 70-72%), hydrochloric acid (HCl, Ajax Finechem, 32%), silicotungstic acid ($H_4[\alpha\text{-}SiW_{12}O_{40}]$, Sigma-Aldrich, 98%), bis(trifluoromethanesulfonyl)imide ($HNTf_2$, Io-Li-Tec, 80 wt% in water), were used as provided by the manufacturer. The concentration of impurity Cl^- in $HNTf_2$ was determined by ICP-MS (Perkin Elmer NexION 350) and shown to below the detection limit of 1.3×10^{-7} M. All aqueous electrolyte solutions were prepared with high purity deionized water. The concentrations of Fe^{III} and Fe^{II} were determined by ICP-OES (Perkin Elmer Optima 8000).

2.2. Instrumentation and Procedures

DC cyclic voltammetric experiments were undertaken with a CHI 760E electrochemical workstation (CH Instruments, USA) in a conventional three-electrode cell configuration. The working electrodes were GC (glassy carbon electrode, diameter = 3.0 mm, CH Instruments, USA) or BDD (boron-doped diamond electrode, diameter = 3.0 mm, Windsor Scientific, UK). A mercury/mercurous sulfate reference electrode (MSE, CH Instruments, USA) was used instead of the more commonly used silver/silver chloride or calomel ones to avoid chloride contamination. A platinum wire was employed as the counter electrode. Large amplitude FTAC voltammetric experiments were undertaken with a homemade instrument [35]. Simulations of DC cyclic voltammograms were undertaken with a commercial software package (Digisim 3.0, BASi Int.), while the FTAC voltammetric data were simulated with MECSim (Monash Electrochemistry Simulator) software (http://www.garethkennedy.net/MECSim.html). Either the Butler-Volmer model or the Marcus-Hash model for electron transfer was used in simulations. pH values were measured with a SevenCompact™ pH/Ion Meter S220 (Thomas Scientific). All electrochemical measurements were carried out at the room temperature (23 ± 2 °C) in solutions deoxygenated by purging solution with nitrogen gas. The parameters presented in tables represent the average values of three experiments and those parameters used in simulations can be found in the corresponding captions.

The GC and BDD electrodes were polished with an aqueous alumina slurry (0.3 μm) and washed extensively with water. The polished GC electrode was then sonicated in water for about 1 min before being placed into the electrochemical cell. Viscosity was measured with an Anton Paar Automated Micro Viscometer (AMVn). SEM images were acquired with a FEI Nova NanoSEM 450 FEG SEM. The R_u (uncompensated resistence) value was determined experimentally from the *RC* time constant method available with the CHI potentiostat

2.3. Theory

For a simple one-electron transfer process taking place in solution

$$O + e^- \rightleftharpoons R \quad (E_f^0) \tag{2}$$

where E_f^0 is the formal potential and k^0 is the standard electrochemical rate constant. According to Bulter-Volmer (BV) model [41], the reduction and oxidation rate constants (k_{red}, k_{ox}) are functions of k^0, the transfer coefficient (α) and the applied potential (E) with respect to E_f^0, as in equations (3) and (4)

$$k_{red}^{BV} = k^0 e^{-\alpha\eta} \tag{3}$$

$$k_{ox}^{BV} = k^0 e^{(1-\alpha)\eta} \tag{4}$$

where $\eta = F\left(E - E_f^0\right)/RT$, F is the Faraday constant, R is the universal gas constant and T is the absolute temperature. An alternative approach to describe the kinetics of electron transfer process in a microscopic way is known as the Marcus-Hush (MH) model. From this model, the rate constants are functions of three parameters k^0, η and the reorganization energy (λ): [42]

$$k_{red}^{MH} = k^0 e^{-\eta/2} \frac{I(\eta, \lambda^*)}{I(0, \lambda^*)} \tag{5}$$

$$k_{ox}^{MH} = k^0 e^{\eta/2} \frac{I(\eta, \lambda^*)}{I(0, \lambda^*)} \tag{6}$$

where λ^* is dimensionless reorganization energy, defined as $\lambda^* = \lambda F/RT$ and $I(\eta, \lambda^*)$ is an integral of the form:

$$I(\eta, \lambda^*) = \int_{-\infty}^{\infty} \frac{\exp\left[\frac{-(\varepsilon-\eta)^2}{4\lambda^*}\right]}{2\cosh(\varepsilon/2)} d\varepsilon \tag{7}$$

in which ε (eV) is an integration variable. $I(\eta, \lambda^*)$ values can be computed numerically using the trapezium rule.

In this study, the least-squares correlation (LS) is also reported to quantify the agreement between experimental and simulated data and is given by eq. (8) for DC and AC voltammetric data,

$$LS = 1 - \sqrt{\frac{\sum_{i=1}^{N}\left(f^{exp}(x_i) - f^{sim}(x_i)\right)^2}{\sum_{i=1}^{N} f^{exp}(x_i)^2}} \tag{8}$$

where $f^{exp}(x_i)$ and $f^{sim}(x_i)$ are the experiment and simulated functions of data, respectively and N is the number of data points. Comparisons of simulated and experimental data were undertaken in triplicate (n = 3).

3. Results and Discussion

3.1. Investigation of electrolyte anion effects by DC voltammetry

DC voltammetric studies of the reduction of 1.0 mM Fe^{III} were initially undertaken in aqueous electrolyte solutions containing 1.0 mM Fe^{III} and 0.1 M $HNTf_2$, $HClO_4$, HCl or 0.05 M $H_4[\alpha\text{-}SiW_{12}O_{40}]$. A comparison of DC cyclic voltammograms obtained at GC and BDD electrodes with a scan rate of 100 mV s^{-1} is shown in Fig. 2. Comparison with simulated data also provided in this figure, allowed the required thermodynamic, kinetic and mass transport parameters to be estimated with their values summarized in Table 1. For a process which is reversible or close to reversible, the midpoint potential (average of oxidation and reduction peak potentials) is often taken as a good approximation of the formal potential, E_f^0 [33] and the diffusion coefficient (D) value can be determined from the peak current using Randles-Sevcik equation when the effect of the uncompensated resistance is not significant [43]. However, since the electrode kinetics of the $Fe^{III/II}$ process is slow, these options are not available. Therefore E_f^0 and D values as

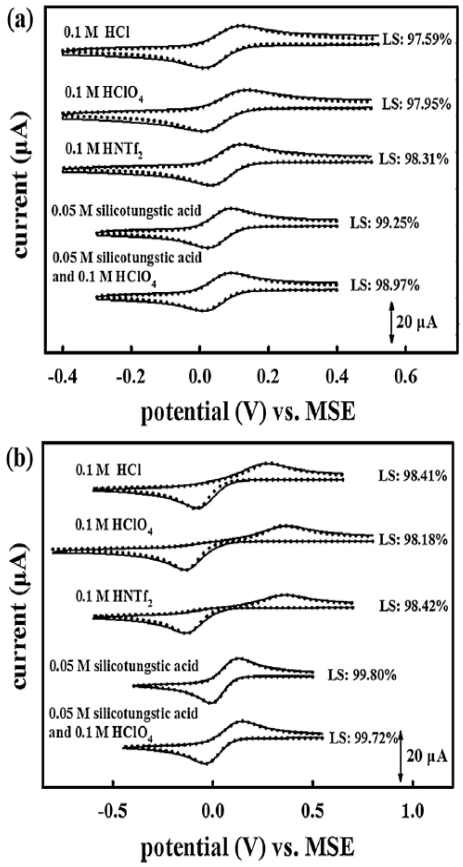

Fig. 2. A comparison of the simulated (dotted line) and experimental (solid line) DC voltammetric data obtained from the reduction of 1.0 mM Fe^{III} in designated electrolytes at (a) a GC electrode and (b) a BDD electrode with a scan rate of 100 mV s^{-1}. LS refers to analysis obtained by least squares fitting. Other parameters used in the simulations are provided in Table S1.

Table 1
Electrode kinetic, thermodynamic and mass transport parameters derived from comparison of simulated and experimental DC cyclic voltammetric data for the reduction of 1.0 mM Fe^{III} in 5 electrolytes at GC and BDD electrodes with a scan rate of 100 mV s^{-1} ($n = 3$).

Electrolyte	Electrode	ΔE_p (mV)	k^0 (cm s^{-1})[a]	E_f^0 (mV)[a]	D (cm^2 s^{-1})[a]	α[a]
HCl	GC	111 ± 5	(4.8 ± 0.5) × 10^{-3}	60 ± 2	(5.3 ± 0.2) × 10^{-6}	0.65 ± 0.05
	BDD	378 ± 27	(2.5 ± 0.3) × 10^{-4}	60 ± 3	(5.3 ± 0.2) × 10^{-6}	0.60 ± 0.02
$HClO_4$	GC	130 ± 10	(3.0 ± 0.5) × 10^{-3}	65 ± 2	(5.2 ± 0.2) × 10^{-6}	0.60 ± 0.04
	BDD	517 ± 15	(7.0 ± 1) × 10^{-5}	64 ± 2	(5.2 ± 0.2) × 10^{-6}	0.60 ± 0.01
$HNTf_2$	GC	117 ± 5	(3.7 ± 0.5) × 10^{-3}	75 ± 2	(4.9 ± 0.2) × 10^{-6}	0.60 ± 0.1
	BDD	493 ± 5	(8.0 ± 1) × 10^{-5}	74 ± 3	(4.9 ± 0.2) × 10^{-6}	0.56 ± 0.02
$H_4[\alpha\text{-}SiW_{12}O_{40}]$	GC	67 ± 3	(2.8 ± 0.5) × 10^{-2}	47 ± 2	(4.0 ± 0.2) × 10^{-6}	0.55 ± 0.09
	BDD	140 ± 5	(2.2 ± 0.2) × 10^{-3}	46 ± 3	(4.0 ± 0.2) × 10^{-6}	0.55 ± 0.09
$H_4[\alpha\text{-}SiW_{12}O_{40}]$ + $HClO_4$	GC	78 ± 5	(7.0 ± 0.2) × 10^{-3}	51 ± 2	(4.1 ± 0.1) × 10^{-6}	0.55 ± 0.08
	BDD	190 ± 7	(1.2 ± 0.1) × 10^{-3}	50 ± 2	(4.1 ± 0.1) × 10^{-6}	0.56 ± 0.09

[a] Values obtained from comparison of experimental and simulated data.

well as k^0 and α parameters were also obtained by comparison of experimental and simulated data.

To further validate the accuracy of the measured k^0 and E_f^0 values from the reduction of 1.0 mM Fe^{III}, these parameters were also derived from oxidation of 1.0 mM Fe^{II} (Fig. S1 and Table S2). For an uncomplicated electron transfer reaction, k^0 and E_f^0 values should be independent on the valent state of the iron species present in bulk solution [44]. Similar k^0 and E_f^0 values were obtained for reduction of Fe^{III} and oxidation of Fe^{II} as expected if the reaction is a simple one-electron transfer process and consistent with predictions based on the Butler-Volmer relationship.

In the absence of supporting electrolyte other than that provided by the Fe^{III} salt, the value of E_f^0 was measured to be 83 mV *vs.* MSE. As shown in Table 1, E_f^0 becomes less positive in the presence of added supporting electrolyte and is dependent on the identities of the electrolyte anion, lying in the order $[SiW_{12}O_{40}]^{4-} > Cl^- > ClO_4^- > NTf_2^-$. The value of E_f^0 in $HNTf_2$ (75 mV *vs.* MSE) is close to the value of 83 mV in the absence of electrolyte, which implies that $HNTf_2$ is the most innocent of the electrolytes used with respect to the $[Fe(H_2O)_6]^{3+/2+}$ process. As noted in the Introduction, Cl^- acts as a ligand bridge to Fe^{III}, which enhances the electrode kinetics of the $[Fe(H_2O)_6]^{3+/2+}$ process [3]. Thus, as expected, the k^0 value in HCl is larger than in NTf_2^- or ClO_4^- containing electrolytes. Interestingly, the most negative E_f^0 and largest k^0 values were found with $[\alpha\text{-}SiW_{12}O_{40}]^{4-}$ as the electrolyte anion, which is attributed to a strong electrostatic attraction between $[\alpha\text{-}SiW_{12}O_{40}]^{4-}$ and Fe^{III}. Additionally, it is noted that the E_f^0 and k^0 values in the mixed $HClO_4$ and $H_4[\alpha\text{-}SiW_{12}O_{40}]$ electrolyte are similar to that found with $H_4[\alpha\text{-}SiW_{12}O_{40}]$ only electrolyte, which suggests that ion-pairing effect derived from $H_4[\alpha\text{-}SiW_{12}O_{40}]$ is substantial.

The origin of the anion effect on the electrode kinetics could be a double layer effect. It is reasonable to assume the $Fe^{III/II}$ process occurs at potentials positive of the potential of zero charge (PZC) [6,45] since E_f^0 is about 700 mV *vs.* NHE. When NTf_2^- and ClO_4^- are used as electrolyte anions, their interactions with Fe^{III} and Fe^{II} are weak, although Fe^{III} is reported to form a 1:1 complex with ClO_4^- [46]. Thus, the positively charged Fe^{III} complex ($Fe(H_2O)_6^{3+}$) will be repelled from the positively charged electrode surface due to the double layer effect. Coordination of Cl^- generates negatively charged $[Fe(Cl)_6]^{3-}$ and $[Fe(Cl)_6]^{4-}$, respectively. Thus, on the basis of the double layer argument, the larger k^0 values found when using Cl^- as the electrolyte anion may be attributable to the attraction of negatively charged chloride complex to the positively charged electrode surface in addition to the ligand bridge effect. Analogously, the increase in k^0 values when $[\alpha\text{-}SiW_{12}O_{40}]^{4-}$ is used as electrolyte anion can be explained by lowering of the positively charge by strong interaction of their anions with Fe^{III} and Fe^{II} (evidenced by a more negative E_f^0 value compared to Cl^-).

Another possible explanation for the electrolyte dependence of k^0 values is ion pairing. A simple square-scheme mechanism that takes into account the contribution from ion pairing has been proposed [47]:

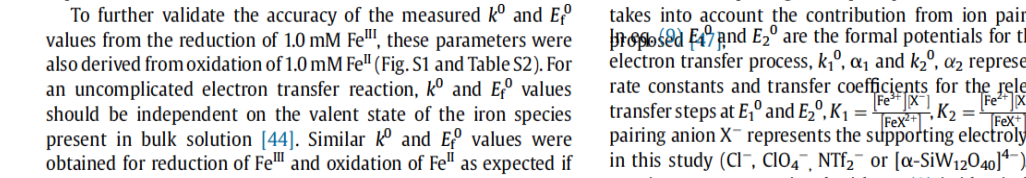

In eq. (9) E_1^0 and E_2^0 are the formal potentials for the designated electron transfer process, k_1^0, α_1 and k_2^0, α_2 represent the formal rate constants and transfer coefficients for the relevant electron transfer steps at E_1^0 and E_2^0, $K_1 = \frac{[Fe^{2+}][X^-]}{[FeX^{2+}]}$, $K_2 = \frac{[Fe^{2+}][X^-]}{[FeX^{+}]}$ and the ion-pairing anion X^- represents the supporting electrolyte anion used in this study (Cl^-, ClO_4^-, NTf_2^- or $[\alpha\text{-}SiW_{12}O_{40}]^{4-}$). The voltammetric response associated with eq. (9) is identical to that for a simple one-electron transfer process (eq. (10)) if the ion pairing reactions are reversible on the voltammetric timescale [48].

$$A' + e^- \rightleftharpoons B' \ (k_{app}^0, \alpha_{app}) \qquad (10)$$

If K_1 and K_2 are both large (*e.g.* HCl or $[\alpha\text{-}SiW_{12}O_{40}]^{4-}$ electrolyte), the $Fe^{III/II}X^-$ pathway is dominant and k_{app}^0 is close to k_2^0. If K_1 and K_2 are both small, the $Fe^{III/II}$ pathway is dominant and k_{app}^0 is close to k_1^0. In general, the k_{app}^0 value measured is a function of k_1^0, k_2^0, K_1, K_2 and $[X^-]$ [49], which leads to the prediction of an electrolyte anion dependence of k_{app}^0.

Evidence for the interaction between Fe^{III} and/or Fe^{II} and the electrolyte anion is provided by the anion dependence of the D values. As shown in Table 1 and Table S1, D values for Fe^{III} and Fe^{II} derived from analysis of cyclic voltammetric data obtained at GC and BDD electrodes follow the order ($H_4[\alpha\text{-}SiW_{12}O_{40}]$ + $HClO_4$) ≈ $H_4[\alpha\text{-}SiW_{12}O_{40}] < HNTf_2 < HClO_4 < HCl$.

The Stokes-Einstein equation [50], is given in eq. (11).

$$D = \frac{k_B T}{6\pi\mu r} \qquad (11)$$

where, k_B is the Boltzmann constant, μ is the solvent viscosity, and r is the radius of the diffusing particle. Thus, D values are predicted to depend on the viscosity of the media as well as the radius of the ion-paired species. Viscosity values are summarized in Table 2 and do not vary significantly, so the r parameter is assumed to be the major factor leading to electrolyte dependent D values. From eq. (11), $[D{\cdot}\mu]$ is inversely proportional to r. Interestingly, the $[D{\cdot}\mu]$ product values obtained in HCl, $HClO_4$ and $HNTf_2$ are similar ($\sim 5.1 \times 10^{-13}$ m kg s^{-2}), but much smaller than that found with $H_4[\alpha\text{-}SiW_{12}O_{40}]$ as the electrolyte ($\sim 4.1 \times 10^{-13}$ m kg s^{-2}). This is attributed to strong ion pairing between $[\alpha\text{-}SiW_{12}O_{40}]^{4-}$ and Fe^{III} and noting that the radius of $[\alpha\text{-}SiW_{12}O_{40}]^{4-}$ (~1 nm [51]) is much larger than that of Cl^-, ClO_4^- or NTf_2^- (181 pm [52], 236 pm [53] and 262 pm [54], respectively). Moreover, a larger $[D{\cdot}\mu]$ value is found in the absence of added supporting electrolyte as would be expected since ion pairing is now minimal.

Table 2
Values of viscosity and $D_{Fe^{III}}$ obtained in present of supporting electrolyte.

Electrolyte	μ (cP)	$D_{Fe^{III}}$ ($\times 10^6$ cm^2 s^{-1})[a]	[$D\cdot\mu$] ($\times 10^{13}$ m kg s^{-2})
HCl	0.984	5.3 ± 0.2	5.2
$HClO_4$	0.972	5.2 ± 0.2	5.1
$HNTF_2$	1.01	4.9 ± 0.2	5.0
$H_4[\alpha\text{-}SiW_{12}O_{40}]$	1.03	4.0 ± 0.2	4.1
$H_4[\alpha\text{-}SiW_{12}O_{40}]$ + $HClO_4$	1.04	4.1 ± 0.1	4.2
H_2O	0.974	6.0[b]	5.8

[a] Determined voltemmtricly by reduction of 1.0 mM Fe^{III} in relevant electrolytes.
[b] Ref. [55].

3.2. Determination of k^0 at a GC electrode using FTAC voltammetry

The k^0 value for the $Fe^{III/II}$ process at a GC electrode was also determined using the kinetically sensitive FTAC voltammetry. A comparison of experimental and simulated FTAC voltammetric data for the $Fe^{III/II}$ process with $H_4[\alpha\text{-}SiW_{12}O_{40}]$ and $HNTf_2$ as the supporting electrolyte at a GC electrode is shown in Figs. 3 and 4 and parameters derived from these simulation-experiment comparisons exercises are provide in Table S3 ($Fe^{II/III}$ data are shown in Figs. S2, S3 and Table S3). As summarized in Table 3, k^0 values at the GC electrode obtained from FTAC voltammetry and DC cyclic voltammetry are comparable.

3.3. Impact of heterogeneity of the BDD electrode surface by FTAC voltammetry

With the FTAC voltammetric technique, the AC harmonic current magnitudes become too small to measure in the higher order harmonics if k^0 values are too low. Data suitable for FTAC voltammetric experiment and simulation comparisons were therefore only available with $H_4[\alpha\text{-}SiW_{12}O_{40}]$ at the BDD electrode. FTAC voltammetric experiment *vs.* simulation comparisons were therefore undertaken for the $Fe^{III/II}$ process with $H_4[\alpha\text{-}SiW_{12}O_{40}]$ as the supporting electrolyte at a BDD electrode. With this electrolyte, reasonable agreement between theory and experiment was obtained for the $Fe^{III/II}$ (Fig. 5) and $Fe^{II/III}$ (Fig. S4) processes for the fundamental harmonic under low frequency conditions of 2.94 Hz and 2.92 Hz and use of slow DC scan rates of 13.04 and 15.83 mV s^{-1}, respectively, where k^0 values were determined to be

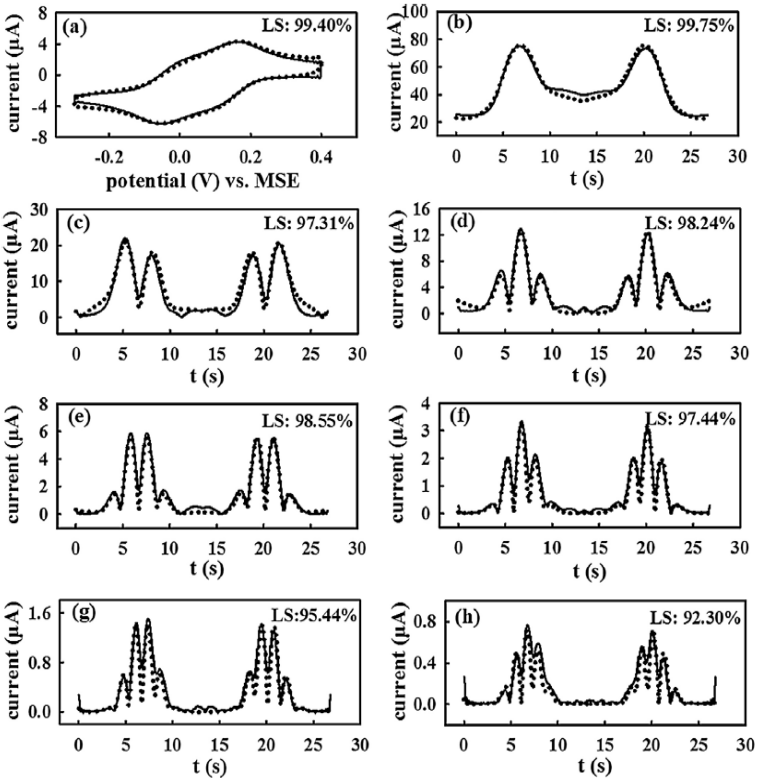

Fig. 3. A comparison of simulated (dotted line) and experimental (solid line) FTAC voltammograms obtained from the reduction of 1.0 mM Fe^{III} in 0.05 M $H_4[\alpha\text{-}SiW_{12}O_{40}]$ at a GC electrode with ν = 52.15 mV s^{-1} f = 7.93 Hz and ΔE = 120 mV. (a) aperiodic DC component, (b-h) 1st-7th AC harmonic components. LS refers to analysis obtained by least squares fitting. Other parameters used in the simulations are: A (area) = 0.071 cm^2, R_u = 50 Ω, C_{dl} (c_0, c_1, c_2, c_3, c_4) = (1.06×10^{-4}, -3.18×10^{-5}, -1.70×10^{-4}, 3.56×10^{-5}, 3.64×10^{-4}) μF cm^{-2}, $D_{Fe^{III}} = D_{Fe^{II}} = 3.9\times10^{-6}$ cm^2 s^{-1}, E_f^0 = 52 mV, $k^0 = 2.8\times10^{-2}$ cm s^{-1}, α = 0.55 and T (temperature) = 296 K. See Supporting Information for definition of C_{dl}.

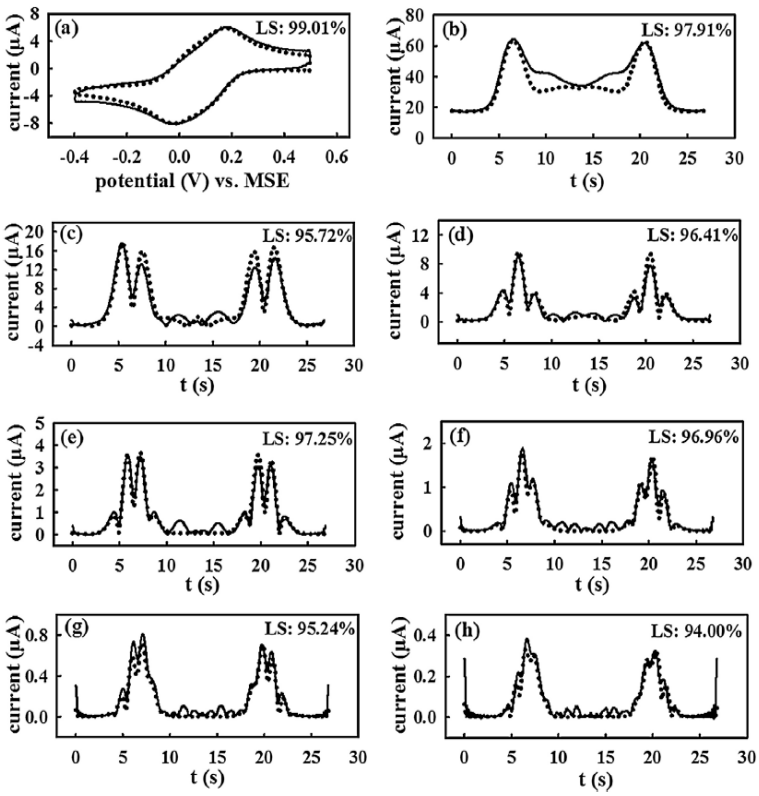

Fig. 4. A comparison of simulated (dotted line) and experimental (solid line) FTAC voltammograms obtained from the reduction of 1.0 mM Fe^{III} in 0.1 M $HNTf_2$ at a GC electrode with $v = 67.06\,mV\,s^{-1}$, $f = 7.79\,Hz$ and $\Delta E = 120\,mV$. (a) aperiodic DC component, (b–h) 1st–7th AC harmonic components. LS refers to analysis obtained by least squares fitting. Other parameters used in the simulations are: $A = 0.071\,cm^2$, $R_u = 40\,\Omega$, C_{dl} (c_0, c_1, c_2, c_3, c_4) = (6.07×10^{-5}, -4.77×10^{-5}, 2.22×10^{-4}, 7.17×10^{-5}, -6.76×10^{-5}) $\mu F\,cm^{-2}$, $D_{Fe^{III}} = D_{Fe^{II}} = 5.3 \times 10^{-6}\,cm^2\,s^{-1}$, $E_f^0 = 75\,mV$, $k^0 = 5.0 \times 10^{-}\,cm\,s^{-1}$, $\alpha = 0.57$ and $T = 296\,K$.

Table 3
Comparison of k^0 values obtained by DC and FTAC voltammetry from the reduction of 1.0 mM Fe^{III} and oxidation of 1.0 mM Fe^{II} in 0.05 M $H_4[\alpha\text{-}SiW_{12}O_{40}]$ or 0.1 M $HNTf_2$ with a GC electrode ($n = 3$).

Electrolyte	$Fe^{III/II}$ process at GC		$Fe^{II/III}$ process at GC	
	k^0_{DC} ($cm\,s^{-1}$)[a]	k^0_{AC} ($cm\,s^{-1}$)[b]	k^0_{DC} ($cm\,s^{-1}$)[a]	k^0_{AC} ($cm\,s^{-1}$)[b]
$H_4[\alpha\text{-}SiW_{12}O_{40}]$	$(2.8 \pm 0.5) \times 10^{-2}$	$(2.8 \pm 0.3) \times 10^{-2}$	$(2.0 \pm 0.5) \times 10^{-2}$	$(2.2 \pm 0.2) \times 10^{-2}$
$HNTf_2$	$(3.7 \pm 0.5) \times 10^{-3}$	$(5.1 \pm 0.2) \times 10^{-3}$	$(3.5 \pm 0.7) \times 10^{-3}$	$(4.6 \pm 0.4) \times 10^{-3}$

Notes: the estimated upper limit of $k^0 = 0.3\,cm\,s^{-1}$ at GC (the simulated peak currents are 90% of that predicted for a reversible process).
[a] Determined by DC voltammetry.
[b] Determined by FTAC voltammetry.

$(2.4 \pm 0.5) \times 10^{-3}$ and $(2.4 \pm 0.2) \times 10^{-3}\,cm\,s^{-1}$, respectively. These values are similar to those found with the DC method of $(2.2 \pm 0.2) \times 10^{-3}$ and $(2.6 \pm 0.2) \times 10^{-3}\,cm\,s^{-1}$, respectively. However, the fit to the higher harmonics was significantly poorer with use of the same parameters.

An increasing level of discrepancy between experimental and simulated data was also observed in BDD electrode with the higher order harmonics when using higher frequencies. Comparison exercises using higher frequencies are displayed for the reduction of Fe^{III} (Fig. S5) and oxidation of Fe^{II} (Fig. S6). Parameters derived from these simulation-experiment comparison exercises are provided in Tables 4 and S4. The aperiodic DC components of $Fe^{III/II}$ redox couples in $H_4[\alpha\text{-}SiW_{12}O_{40}]$ at BDD electrode are well matched to the simulated data, but not the higher order AC harmonic components using theory obtained based on Bulter-Volmer model of electron transfer [56]. In fact the data implies that the k^0 value is harmonic dependent, which is not possible leading to the conclusion that the reaction is more complex than assumed in the model.

Studies with a higher concentration (1.0 mM) of Fe^{III} or Fe^{II} led to similar deviations between experimental and simulated data for $Fe^{III/II}$ (Fig. S7(A)) and $Fe^{II/III}$ (Fig. S8(A)) as found with the 0.20 mM concentration. This result implies that the observed discrepancy is not due to a concentration dependent adsorption effect. The fact that the same set of parameters (except concentration) can be used to achieve optimal theory-experiment agreement in two analyte concentrations also confirms that (1) the effect of uncompensated resistance has been accurately accounted for and (2) the absence of second or higher order reactions.

Another factor that could explain the deviation is the choice of Butler-Volmer model in the simulations rather than the physically more meaningful Marcus-Hush model. Differences between

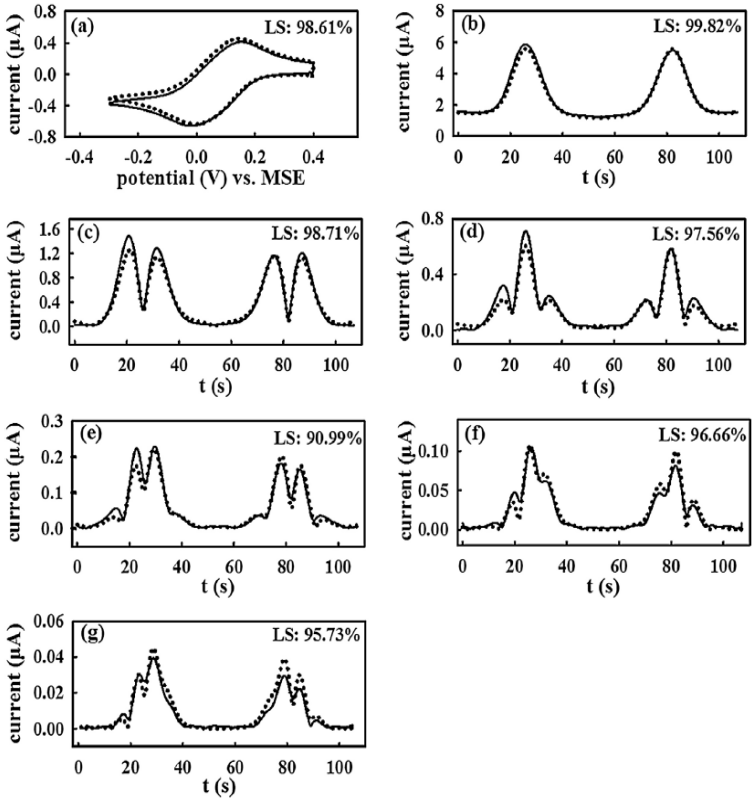

Fig. 5. Comparison of simulated (dotted line) and experimental (solid line) FTAC voltammograms obtained from the reduction of 0.20 mM Fe^{III} in 0.05 M $H_4[\alpha\text{-}SiW_{12}O_{40}]$ at a BDD electrode with $f = 2.94$ Hz, $\Delta E = 120$ mV and $v = 13.04$ mV s^{-1} with simulations being based on Bulter-Volmer theory. (a) aperiodic DC component, (b-g) 1st-6th AC harmonic components. LS refers to analysis obtained by least squares fitting. Other parameters used in the simulations are: $A = 0.071$ cm^2, $R_u = 10\,\Omega$, C_{dl} (c_0, c_1, c_2, c_3, c_4) = (9.55×10^{-6}, 2.20×10^{-6}, -8.42×10^{-6}, -3.99×10^{-6}, 2.53×10^{-5}) uF cm^{-2}, $D_{Fe^{III}} = D_{Fe^{II}} = 4.3 \times 10^{-6}$ cm^2 s^{-1}, $E_f^0 = 50$ mV, $k^0 = 2.3 \times 10^{-3}$ cm s^{-1}, $\alpha = 0.55$ and $T = 296$ K.

Table 4
Parameters derived from comparison of AC voltammetric experimental and simulated data based on the Butler-Volmer model for the reduction of 0.20 mM Fe^{III} at a BDD electrode in 0.05 M $H_4[\alpha\text{-}SiW_{12}O_{40}]$ at designated frequencies and scan rates. ($n = 3$).

f (Hz)	v (mV s^{-1})	C_{dl} (c_0, c_1, c_2, c_3, c_4) (μF cm^{-2})	R_u (Ω)	k^0 (cm s^{-1})	E_f^0 (mV)	D (cm^2 s^{-1})	α
2.94	13.04	9.55, 2.20, −8.42, −3.99, 25.3	10 ± 2	$(2.4 \pm 0.5) \times 10^{-3}$	47 ± 3	$(4.4 \pm 0.1) \times 10^{-6}$	0.55 ± 0.05
4.92	26.08	8.63, 1.52, −1.39, −1.58, 4.23	19 ± 3	$(2.3 \pm 0.2) \times 10^{-3}$	49 ± 2	$(4.2 \pm 0.2) \times 10^{-6}$	0.55 ± 0.05
7.93	52.15	7.82, 1.40, −1.85, −1.44, 4.74	15 ± 5	$(2.2 \pm 0.2) \times 10^{-3}$	49 ± 1	$(4.2 \pm 0.1) \times 10^{-6}$	0.56 ± 0.05
9.02	52.15	8.14, 1.55, −1.37, −1.43, 3.33	20 ± 3	$(2.3 \pm 0.3) \times 10^{-3}$	49 ± 2	$(4.1 \pm 0.2) \times 10^{-6}$	0.56 ± 0.05
45.0	40.98	7.22, 1.40, −1.72, −1.44, 4.74	15 ± 3	$(2.1 \pm 0.3) \times 10^{-3}$	50 ± 1	$(4.1 \pm 0.1) \times 10^{-6}$	0.58 ± 0.05

Butler-Volmer and Marcus-Hush theory in simulations are expected when the electron transfer kinetics are slow [43,57,58] such as applies to the $Fe^{III/II}$ process. However, when Marcus-Hush theory [59,60] was used to simulate the experimental data, as shown in Fig. S7(B) and S8(B), differences between experimental and simulated data become even larger. The reason for the failure of both theories will be discussed below.

Ion-pairing between Fe^{III} or Fe^{II} and electrolyte anion are expected to influence the voltammetric responses via a square reaction scheme as noted above [49]. However, the harmonic dependence is only found at BDD electrode, whereas the effect of ion-pairing should be electrode material independent. Therefore, the deviation between experimental and simulated data at BDD electrode due to the neglect of ion-pairing in the simulation is ruled out.

BDD is a heterogeneous electrode with distinctly different regions of ~10 μm dimension containing different levels of boron doping, as shown in a SEM image of the BDD electrode surface (Fig. 6). This heterogeneity can give rise to kinetic dispersion if the diffusion layers do not fully overlap [61–63]. The lighter and darker areas correspond to less-doped and more-doped regions, respectively. On a long measurement timescale (low frequency, low order harmonic), the diffusion layers $(\sim(Dt)^{1/2}$ where t is the measurement timescale) associated with the two regions may fully overlap. In this case, the voltammetric response is dominated by the region with faster kinetics. On a short measurement timescale (high frequency, high order harmonic), overlapping of the diffusion layers is more restricted so the voltammetric response represents a combination from two or more regions (kinetic dispersion). Under these conditions, a frequency/harmonic (*i.e.* timescale) dependent response may be expected since the extent of diffusion layer

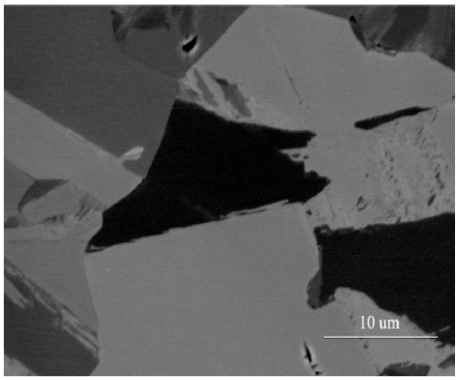

Fig. 6. A SEM image of the BDD electrode surface.

overlap is timescale dependent. To test this hypothesis, results of FTAC voltammograms were simulated based on either linear or radial diffusion models for a 10 μm radii electrode. The radii matches the size of the more highly doped grain (*i.e.* high HET activity regions) on BDD electrode [64]. The following parameters were used in these simulations: $v = 13\ mV\ s^{-1}$, c (concentration) = 0.20 mM, $D_{ox\ (oxidised\ form)} = D_{red\ (reduced\ form)} = 5 \times 10^{-6}\ cm^2\ s^{-1}$, $E_f^0 = 0.0\ V$, $T = 298.2\ K$, $\Delta E = 80\ mV$ and $f = 3$ Hz, 9 Hz or 45 Hz, which resemble those used in the experimental studies. The electron transfer process is assumed to be reversible so that the effect of mass transport can be investigated without the complications from kinetic factors. This simulation therefore allows mass transfer differences associated with linear and radial diffusion to be probed. Fig. S9 provides comparisons of simulated AC harmonic components derived from linear and radial diffusion models. At long timescale (low frequency, low harmonics), the peak currents derived from radial diffusion model are larger than those based on linear diffusion. The radial diffusion model contains a time dependent radial term plus a contribution from planar diffusion. At a short measurement timescale (high frequency, high harmonics), the contribution from radial diffusion becomes less significant, as does the difference in mass transfer between the two models. Clearly, with a 10 μm electrode, unless radial diffusion is negligible, apparent frequency and harmonic dependent k^0 values would be obtained. This feature is readily revealed by comparing the peak current ratios (I_{linear}/I_{radial}) for each AC harmonic derived from the radial and planar diffusion models. As shown in Table S5, the I_{linear}/I_{radial} ratios approach unity with high frequency and higher order harmonics. A similar outcome with respect to this ratio should apply to the time dependence or overlap of different domains in a heterogeneous electrode, but the theory for these scenarios is not yet available and will be very complex. However, it is concluded that the heterogeneity of the BDD electrode surface is a likely reason as theories based on neither the Butler-Volmer nor Marcus-Hush models are fully applicable in our study since both are based on the assumption of a homogeneous electrode surface.

In principle, the influence of electrode heterogeneity on k^0 values for the $Fe^{III/II}$ process, postulated to be detected under FTAC voltammetric conditions at BDD electrode, also should emerge in DC cyclic voltammetric studies undertaken at variable scan rate. However, this requires a series of experiments where variation in apperent k^0 (due to the surface sensitivity of the kinetically slow $Fe^{III/II}$ process), double layer capacitance and R_u values can be expected. A major advantage of using FTAC voltammetry is that widely varying time scale data devoid of charging current can be obtained from a single experiment so variability in measurement conditions can be eliminated. This feature facilitates detection of electrode heterogeneity or other forms of non-ideality on k^0 values.

4. Conclusions

The impact of electrolyte anions on the thermodynamics, kinetics and mass transfer properties associated with $Fe^{III/II}$ process at GC and BDD electrodes has been investigated by DC and FTAC voltammetry. The electrolyte anion NTf_2^- with a very low charge density may provide a more innocent electrolyte anion than ClO_4^- and optimal conditions needed for measurement of an intrinsically slow outer-sphere HET process. The D values also depend on the electrolyte anion identity and contributions from ion-pairing, and follow the order, $H_4[\alpha\text{-}SiW_{12}O_{40}] + HClO_4 \approx H_4[\alpha\text{-}SiW_{12}O_{40}] < HNTf_2 < HClO_4 < HCl$. Excellent agreement between theory and experiment is achieved for the $Fe^{III/II}$ process at GC and BDD electrodes using DC cyclic voltammetry with a scan rate of $100\ mV\ s^{-1}$. The E_f^0 and k^0 values associated with the $Fe^{III/II}$ process are also dependent on the identity of the electrolyte anion. k^0 values follow the order, $H_4[\alpha\text{-}SiW_{12}O_{40}] > HCl > HClO_4 \approx HNTf_2$. Possible explanations for the trends are considered based on the ion-pairing and double-layer effects. k^0 values determined by FTAC voltammetry for the moderately fast electron transfer reaction found at a GC electrode with $H_4[\alpha\text{-}SiW_{12}O_{40}]$ and $HNTf_2$ as the electrolyte are in good agreement with DC cyclic voltammetric data. However, with a BDD electrode, the apparent k^0 values are Fe^{III} concentration independent, but display frequency and scan rate dependence which suggests that the simulation model based on Butler-Volmer theory for electron transfer and linear diffusion is not fully correct. The FTAC voltammetric data suggest that heterogeneity of the BDD electrode surface is a probable cause of variation in k^0 values, as detected by SECM [63].

Acknowledgments

M.L. gratefully acknowledges financial support from a joint PhD Training Program supported by University of Chinese Academy of Sciences. J.L. gratefully acknowledges Monash University for provision of postgraduate publication award support. The authors thank the Australian Research Council for financial support through the award of a Discovery grant. The authors also express their appreciation for use of facilities within the Monash Centre for Electron Microscopy.

Appendix A. Supplementary data

Supplementary data associated with this article can be found, in the online version, at http://dx.doi.org/10.1016/j.electacta.2017.07.155.

References

[1] W. Schmickler, E. Santos, Interfacial electrochemistry, Springer Science & Business Media, 2010.
[2] R.G. Compton, C.E. Banks, Understanding voltammetry, World Scientific (2011).
[3] H. Bochmann, W. Vielstich, On the reaction rate of the Fe^{3+}/Fe^{2+} redox couple in sulfate solution, Electrochimica acta 33 (1988) 805–809.
[4] N. Tanaka, R. Tamamushi, Kinetic parameters of electrode reactions, Electrochimica Acta 9 (1964) 963–989.
[5] R. Tamamushi, Kinetic parameters of electrode reactions of metallic compounds, Butterworths, (1975) .
[6] J. Weber, Z. Samec, V. Mareček, The effect of anion adsorption on the kinetics of the Fe^{3+}/Fe^{2+} reaction on Pt and Au electrodes in $HClO_4$, Journal of Electroanalytical Chemistry and Interfacial Electrochemistry 89 (1978) 271–288.
[7] H. Gerischer, The exchange current density at the equilibrium potential at electrodes with a potential-determining process, Z. Elektrochem 54 (1950) 362.

[8] G.M. Brown, The reduction of chlorate and perchlorate ions at an active titanium electrode, Journal of electroanalytical chemistry and interfacial electrochemistry 198 (1986) 319–330.
[9] S. Rivera-Rubero, S. Baldelli, Surface characterization of 1-butyl-3-methylimidazolium Br^-, I^-, PF_6^-, BF_4^-,$(CF_3SO_2)_2N^-$, SCN^-, $CH_3SO_3^-$, $CH_3SO_4^-$, and $(CN)_2N^-$ ionic liquids by sum frequency generation, The Journal of Physical Chemistry B 110 (2006) 4756–4765.
[10] T. Welton, Room-temperature ionic liquids. Solvents for synthesis and catalysis, Chemical reviews 99 (1999) 2071–2084.
[11] M. Freemantle, An introduction to ionic liquids, Royal Society of chemistry (2010).
[12] A. Lewandowski, I. Stępniak, Relative molar Gibbs energies of cation transfer from a molecular liquid to ionic liquids at 298.15K, Physical Chemistry Chemical Physics 5 (2003) 4215–4218.
[13] B.D.B. Aaronson, C.-H. Chen, H. Li, M.T.M. Koper, S.C.S. Lai, P.R. Unwin, Pseudo-Single-Crystal Electrochemistry on Polycrystalline Electrodes: Visualizing Activity at Grains and Grain Boundaries on Platinum for the Fe^{3+}/Fe^{2+} Redox Reaction, J. Am. Chem. Soc. 135 (2013) 3873–3880.
[14] P. Chen, R.L. McCreery, Control of electron transfer kinetics at glassy carbon electrodes by specific surface modification, Analytical Chemistry 68 (1996) 3958–3965.
[15] P. Chen, M.A. Fryling, R.L. McCreery, Electron transfer kinetics at modified carbon electrode surfaces: the role of specific surface sites, Analytical Chemistry 67 (1995) 3115–3122.
[16] T.-C. Kuo, R.L. McCreery, Surface chemistry and electron-transfer kinetics of hydrogen-modified glassy carbon electrodes, Analytical Chemistry 71 (1999) 1553–1560.
[17] M.A.Q. Alfaro, S. Ferro, C.A. Martínez-Huitle, Y.M. Vong, Boron doped diamond electrode for the wastewater treatment, Journal of the Brazilian Chemical Society 17 (2006) 227–236.
[18] T. Yano, E. Popa, D. Tryk, K. Hashimoto, A. Fujishima, Electrochemical Behavior of Highly Conductive Boron-Doped Diamond Electrodes for Oxygen Reduction in Acid Solution, Journal of The Electrochemical Society 146 (1999) 1081–1087.
[19] M.C. Granger, M. Witek, J. Xu, J. Wang, M. Hupert, A. Hanks, M.D. Koppang, J.E. Butler, G. Lucazeau, M. Mermoux, Standard electrochemical behavior of high-quality, boron-doped polycrystalline diamond thin-film electrodes, Analytical Chemistry 72 (2000) 3793–3804.
[20] J.A. Bennett, J. Wang, Y. Show, G.M. Swain, Effect of sp2-bonded nondiamond carbon impurity on the response of boron-doped polycrystalline diamond thin-film electrodes, Journal of The Electrochemical Society 151 (2004) E306–E313.
[21] S. Wang, V.M. Swope, J.E. Butler, T. Feygelson, G.M. Swain, The structural and electrochemical properties of boron-doped nanocrystalline diamond thin-film electrodes grown from Ar-rich and H 2-rich source gases, Diamond and Related Materials 18 (2009) 669–677.
[22] Y.V. Pleskov, Synthetic diamond in electrochemistry, Russian chemical reviews 68 (1999) 381–392.
[23] N.R. Wilson, S.L. Clewes, M.E. Newton, P.R. Unwin, J.V. Macpherson, Impact of grain-dependent boron uptake on the electrochemical and electrical properties of polycrystalline boron doped diamond electrodes, The Journal of Physical Chemistry B 110 (2006) 5639–5646.
[24] D.K. Gosser, Cyclic voltammetry: simulation and analysis of reaction mechanisms, VCH, New York, 1993.
[25] K. Oldham, J. Myland, Fundamentals of electrochemical science, Elsevier, 2012.
[26] R.S. Nicholson, Theory and Application of Cyclic Voltammetry for Measurement of Electrode Reaction Kinetics, Analytical Chemistry 37 (1965) 1351–1355.
[27] R.S. Nicholson, Some examples of the numerical solution of nonlinear integral equations, Analytical Chemistry 37 (1965) 667–671.
[28] S.W. Feldberg, Effect of uncompensated resistance on the cyclic voltammetric response of an electrochemically reversible surface-attached redox couple: Uniform current and potential across the electrode surface, Journal of Electroanalytical Chemistry 624 (2008) 45–51.
[29] C.G. Zoski, Handbook of electrochemistry, Elsevier, 2006.
[30] M.V. Mirkin, T.C. Richards, A.J. Bard, Scanning electrochemical microscopy. 20. Steady-state measurements of the fast heterogeneous kinetics in the ferrocene/acetonitrile system, Journal of Physical Chemistry 97 (1993) 7672–7672.
[31] P. Sun, M.V. Mirkin, Kinetics of electron-transfer reactions at nanoelectrodes, Analytical chemistry 78 (2006) 6526–6534.
[32] S.-X. Guo, A.M. Bond, J. Zhang, Fourier Transformed Large Amplitude Alternating Current Voltammetry: Principles and Applications, Review of Polarography 61 (2015) 21–32.
[33] G. Si-Xuan, B. Alan M, Z. Jie, Fourier Transformed Large Amplitude Alternating Current Voltammetry: Principles and Applications, Review of Polarography 61 (2015) 21–32.
[34] J. Zhang, A.M. Bond, Theoretical studies of large amplitude alternating current voltammetry for a reversible surface-confined electron transfer process coupled to a pseudo first-order electrocatalytic process, Journal of Electroanalytical Chemistry 600 (2007) 23–34.
[35] A.M. Bond, N.W. Duffy, S.-X. Guo, J. Zhang, D. Elton, Changing the look of voltammetry, Analytical chemistry (2005) 186A-195A.
[36] A.P. O'Mullane, J. Zhang, A. Brajter-Toth, A.M. Bond, Higher harmonic large-amplitude fourier transformed alternating current voltammetry: analytical attributes derived from studies of the oxidation of ferrocenemethanol and uric acid at a glassy carbon electrode, Analytical chemistry 80 (2008) 4614–4626.
[37] L.A. Hutton, J.G. Iacobini, E. Bitziou, R.B. Channon, M.E. Newton, J.V. Macpherson, Examination of the factors affecting the electrochemical performance of oxygen-terminated polycrystalline boron-doped diamond electrodes, Analytical chemistry 85 (2013) 7230–7240.
[38] L.A. Hutton, M.E. Newton, P.R. Unwin, J.V. Macpherson, Factors controlling stripping voltammetry of lead at polycrystalline boron doped diamond electrodes: new insights from high-resolution microscopy, Analytical chemistry 83 (2011) 735–745.
[39] A.N. Patel, S. -y. Tan, T.S. Miller, J.V. Macpherson, P.R. Unwin, Comparison and reappraisal of carbon electrodes for the voltammetric detection of dopamine, Analytical chemistry 85 (2013) 11755–11764.
[40] B.D. Aaronson, C.-H. Chen, H. Li, M.T. Koper, S.C. Lai, P.R. Unwin, Pseudo-single-crystal electrochemistry on polycrystalline electrodes: Visualizing activity at grains and grain boundaries on platinum for the Fe^{3+}/Fe^{2+} redox reaction, Journal of the American Chemical Society 135 (2013) 3873–3880.
[41] A.J. Bard, L.R. Faulkner, Fundamentals and applications, Electrochemical Methods 2 (2001).
[42] S.W. Feldberg, Implications of Marcus- Hush Theory for Steady-State Heterogeneous Electron Transfer at an Inlaid Disk Electrode, Analytical chemistry 82 (2010) 5176–5183.
[43] B. LRFAJ, Electrochemical methods: fundamentals and applications, Wiley, New York, 2001.
[44] K. Bano, A. Nafady, J. Zhang, A.M. Bond, Electrode Kinetics Associated with Tetracyanoquinodimethane (TCNQ), $TCNQ^{\cdot}$, and $TCNQ^{2-}$ Redox Chemistry in Acetonitrile As Determined by Analysis of Higher Harmonic Components Derived from Fourier Transformed Large Amplitude ac Voltammetry, The Journal of Physical Chemistry C 115 (2011) 24153–24163.
[45] Z. Samec, Ultraslow kinetics of the ferric/ferrous electron transfer reaction on Au (110) electrode in perchloric acid solutions, Journal of The Electrochemical Society 146 (1999) 3349–3356.
[46] A.E. Martell, R. Smith, Critical Stability Constants, Vols. 1–6, Plenum Press, New York, 1975 (1974) 1977.
[47] D.H. Evans, Solution electron-transfer reactions in organic and organometallic electrochemistry, Chemical Reviews 90 (1990) 739–751.
[48] S.-X. Guo, S.W. Feldberg, A.M. Bond, D.L. Callahan, P.J. Richardt, A.G. Wedd, Systematic Approach to the Quantitative Voltammetric Analysis of the Fe^{III}/Fe^{II} Component of the $[\alpha_2\text{-}Fe(OH_2)P_2W_{17}O_{61}]^{7-/8-}$ Reduction Process in Buffered and Unbuffered Aqueous Media, The Journal of Physical Chemistry B 109 (2005) 20641–20651.
[49] J. Li, A.M. Bond, J. Zhang, Probing Electrolyte Cation Effects on the Electron Transfer Kinetics of the $[\alpha\text{-}SiW_{12}O_{40}]^{4-/5-}$ and $[\alpha\text{-}SiW_{12}O_{40}]^{5-/6-}$ Processes using a Boron-Doped Diamond Electrode, Electrochimica Acta 178 (2015) 631–637.
[50] C.C. Miller, The Stokes-Einstein law for diffusion in solution, Proceedings of the Royal Society of London. Series A, Containing Papers of a Mathematical and Physical Character 106 (1924) 724–749.
[51] K. Bano, J. Zhang, A.M. Bond, P.R. Unwin, J.V. Macpherson, Diminished Electron Transfer Kinetics for $[Ru(NH_3)_6]^{3+/2+}$, $[\alpha\text{-}SiW_{12}O_{40}]^{4-/5-}$ and $[\alpha\text{-}SiW_{12}O_{40}]^{5-/6-}$ Processes at Boron-Doped Diamond Electrodes, The Journal of Physical Chemistry C 119 (2015) 12464–12472.
[52] W.M. Haynes, CRC handbook of chemistry and physics, CRC press, 2014.
[53] T. Kondo, M. Okamura, K. Uosaki, Anion effect on the electrochemical characteristics of a gold electrode modified with a self-assembled monolayer of ferrocenylhexanethiol in aqueous and dichloromethane solutions, Journal of Organometallic Chemistry 637 (2001) 841–844.
[54] J. Vitorino, J.P. Leal, M.E. Minas da Piedade, Gas-Phase Affinity Scales for Typical Ionic Liquid Moieties Determined by using Cooks'Kinetic Method, ChemPhysChem 16 (2015) 1969–1977.
[55] H.V. Lide, CRC handbook of thermophysical and thermochemical data, Crc Press, 1994.
[56] H.V. Patten, K.E. Meadows, L.A. Hutton, J.G. Iacobini, D. Battistel, K. McKelvey, A.W. Colburn, M.E. Newton, J.V. Macpherson, P.R. Unwin, Electrochemical Mapping Reveals Direct Correlation between Heterogeneous Electron-Transfer Kinetics and Local Density of States in Diamond Electrodes, Angewandte Chemie International Edition 51 (2012) 7002–7006.
[57] T.J. Davies, B.A. Brookes, A.C. Fisher, K. Yunus, S.J. Wilkins, P.R. Greene, J.D. Wadhawan, R.G. Compton, A computational and experimental study of the cyclic voltammetry response of partially blocked electrodes. Part II: Randomly distributed and overlapping blocking systems, The Journal of Physical Chemistry B 107 (2003) 6431–6444.
[58] Y. Wang, E. Laborda, M.C. Henstridge, F. Martinez-Ortiz, A. Molina, R.G. Compton, The use of differential pulse voltammetries to discriminate between the Butler?Volmer and the simple Marcus–Hush models for heterogeneous electron transfer: The electro-reduction of europium (III) in aqueous solution, Journal of Electroanalytical Chemistry 668 (2012) 7–12.
[59] R.A. Marcus, On the theory of oxidation-reduction reactions involving electron transfer, I, The Journal of Chemical Physics 24 (1956) 966–978.
[60] R.A. Marcus, Electron transfer reactions in chemistry. Theory and experiment, Reviews of Modern Physics 65 (1993) 599.
[61] J. Xu, M.C. Granger, Q. Chen, J.W. Strojek, T.E. Lister, G.M. Swain, Peer reviewed: boron-doped diamond thin-film electrodes, Analytical Chemistry 69 (1997) 591A–597A.

[62] L. Hutton, M.E. Newton, P.R. Unwin, J.V. Macpherson, Amperometric oxygen sensor based on a platinum nanoparticle-modified polycrystalline boron doped diamond disk electrode, Analytical chemistry 81 (2008) 1023–1032.
[63] H.V. Patten, S.C. Lai, J.V. Macpherson, P.R. Unwin, Active sites for outer-sphere, inner-sphere, and complex multistage electrochemical reactions at polycrystalline boron-doped diamond electrodes (pBDD) revealed with scanning electrochemical cell microscopy (SECCM), Analytical chemistry 84 (2012) 5427–5432.
[64] J. Zhang, S.-X. Guo, A.M. Bond, F. Marken, Large-amplitude Fourier transformed high-harmonic alternating current cyclic voltammetry: kinetic discrimination of interfering faradaic processes at glassy carbon and at boron-doped diamond electrodes, Analytical chemistry 76 (2004) 3619–3629.

Supporting Information

A Systematic Study of the Mass Transport, Kinetic and Thermodynamic Properties of the $Fe^{III/II}$ Process at Glassy Carbon and Boron-Doped Diamond Electrodes

Mingyue Lin,[a,c,d,1] Jiezhen Li,[a,1] Dawei Pan,[c] Alan M. Bond[a,b,*] and Jie Zhang[a,b,*]

[a]School of Chemistry, Monash University, Clayton, Victoria 3800, Australia

[b]ARC Centre of Excellence for Electromaterials Science, Monash University, Clayton, Vic 3800, Australia

[c]Key Laboratory of Coastal Environmental Processes and Ecological Remediation, Yantai Institute of Coastal Zone Research (YIC), Chinese Academy of Sciences (CAS); Shandong Provincial Key Laboratory of Coastal Environmental Processes, YICCAS, Yantai Shandong 264003, P. R. China

[d]University of Chinese Academy of Sciences, Beijing 100049, P. R. China

[1]Both authors contributed equally to this work.

*Corresponding authors

E-mail addresses: alan.bond@monash.edu; jie.zhang@monash.edu

Supplementary Note

The C_{dl} value was quantified from the background current in the fundamental harmonic component at potentials where faradaic current is absent. In order to define the potential dependence of C_{dl}, a non-linear capacitor model was used, as described elsewhere [S1]:

$$C_{dl}(t) = c_0 + c_1E(t) + c_2E^2(t) + c_3E^3(t) + c_4E^4(t) \qquad \text{(S1)}$$

In eq. S1, c_0, c_1, c_2, c_3, and c_4 are the coefficients that determine the degree of nonlinearity of the capacitor.

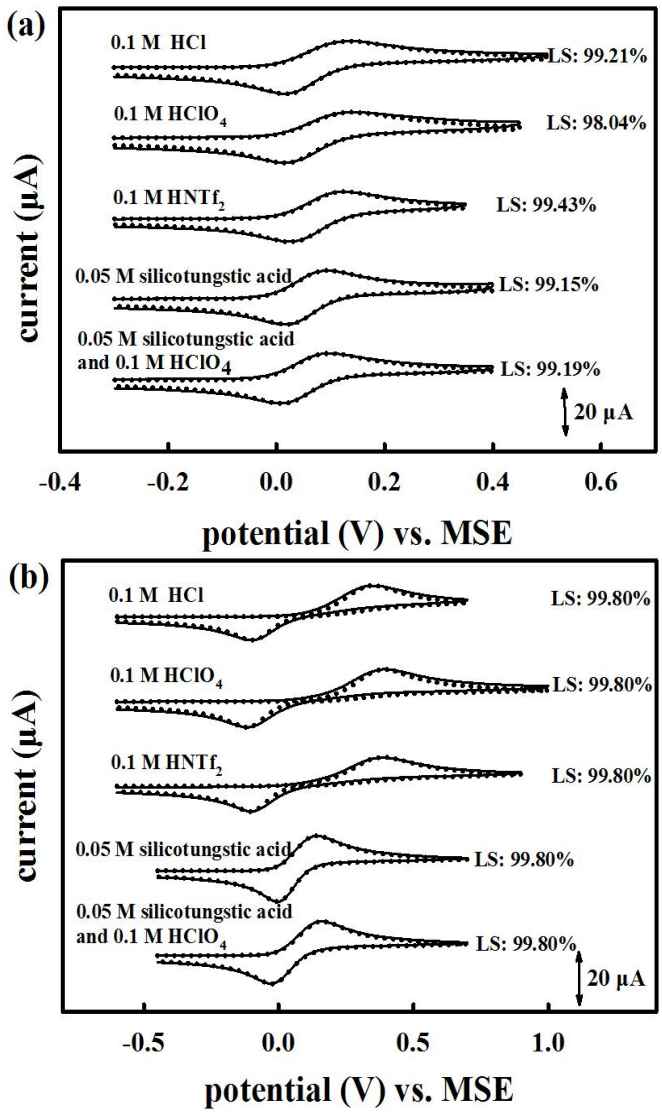

Fig.S1. A comparison of simulated (dotted line) and experimental (solid line) DC voltammetric data for the oxidation of 1.0 mM Fe^{II} in designated electrolytes at (a) a GC electrode and (b) a BDD electrode. v = 100 mV s^{-1}. LS refers to results analysis obtained by least squares fitting. Other parameters used in these simulations are provided in Table S2.

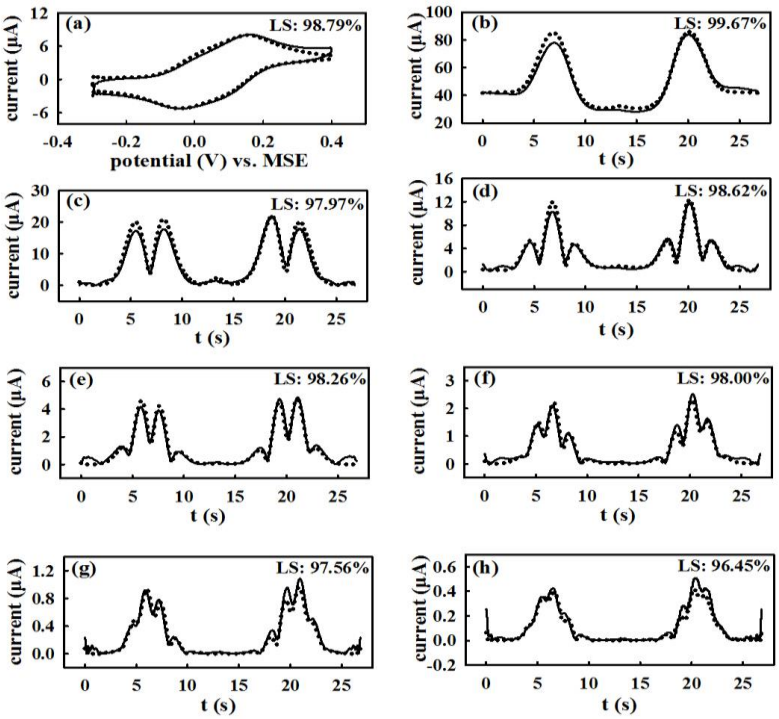

Fig.S2. A comparison of simulated (dotted line) and experimental (solid line) FTAC voltammograms for the oxidation of 1.0 mM Fe^{II} with 0.05 M $H_4[\alpha\text{-}SiW_{12}O_{40}]$ as the supporting electrolyte at a GC electrode. v = 52.15 mV s^{-1}, f = 8.31 Hz and ΔE = 120 mV. (a) aperiodic DC component, (b-h) 1^{st}-7^{th} AC harmonic components. LS refers to analysis obtained by least squares fitting. Other parameters used in the simulation are: A = 0.071 cm^2, R_u = 40 Ω, C_{dl} values are given in Table S3, $D_{Fe}^{III} = D_{Fe}^{II} = 6.5 \times 10^{-6}$ cm^2 s^{-1}, E_f^0 = 55 mV, $k^0 = 2.2 \times 10^{-2}$, α = 0.55 and T = 296 K.

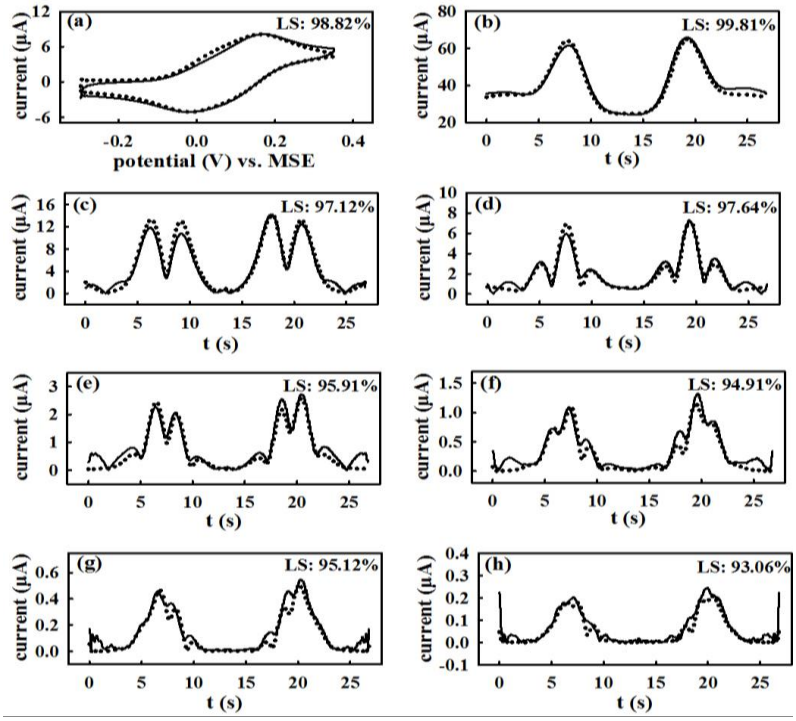

Fig.S3. A comparison of simulated (dotted line) and experimental (solid line) FTAC voltammograms for the oxidation of 1.0 mM Fe^{II} with 0.1 M $HNTf_2$ as the electrolyte at a GC electrode. v = 48.43 mV s^{-1}, f = 8.42 Hz and ΔE = 120 mV. (a) aperiodic DC component, (b-h) 1^{st}-7^{th} AC harmonic components. LS refers to analysis obtained by least squares fitting. Other parameters used in the simulation are: A = 0.071 cm^2, R_u = 40 Ω, C_{dl} values are given in Table S3, $D_{Fe^{III}} = D_{Fe^{II}} = 6.0 \times 10^{-6}$ cm^2 s^{-1}, E_f^0 = 70 mV, $k^0 = 5.0 \times 10^{-3}$, α = 0.55 and T = 296 K.

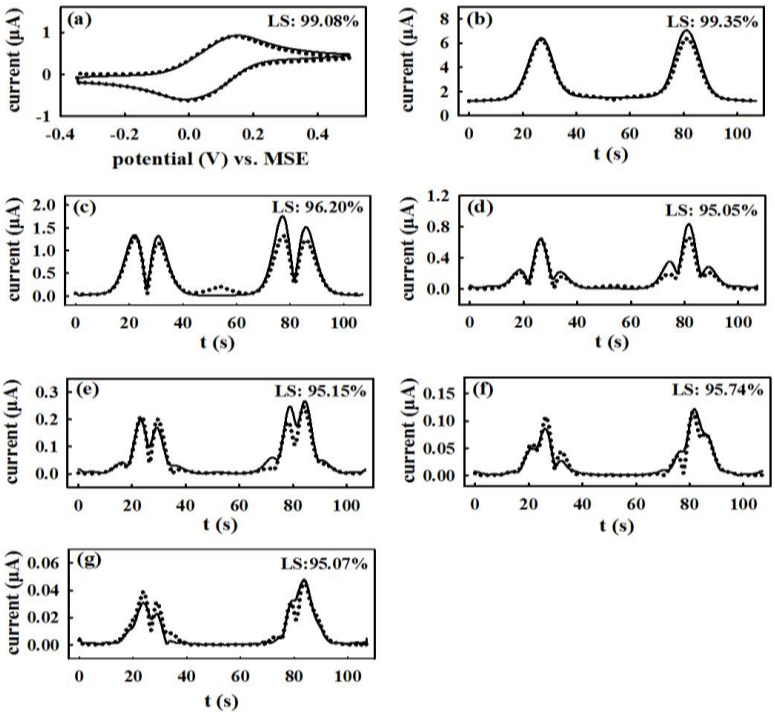

Fig.S4. A comparison of simulated (dotted line) and experimental (solid line) FTAC voltammograms for the oxidation of 0.20 mM Fe^{II} with 0.05 M $H_4[\alpha\text{-}SiW_{12}O_{40}]$ as electrolyte at a BDD electrode based on Bulter-Volmer theory. f = 2.92 Hz, v = 15.83 mV s^{-1} and ΔE = 120 mV. (a) aperiodic DC component, (b-g) 1^{st}-6^{th} AC harmonic components. LS refers to analysis obtained by least squares fitting. Other parameters used in the simulation are: A = 0.071 cm^2, R_u = 20 Ω, C_{dl} values are given in Table S4, $D_{Fe^{III}} = D_{Fe^{II}} = 6.6 \times 10^{-6}$ cm^2 s^{-1}, E_f^0 = 64 mV, $k^0 = 2.4 \times 10^{-3}$, α = 0.55 and T = 296 K.

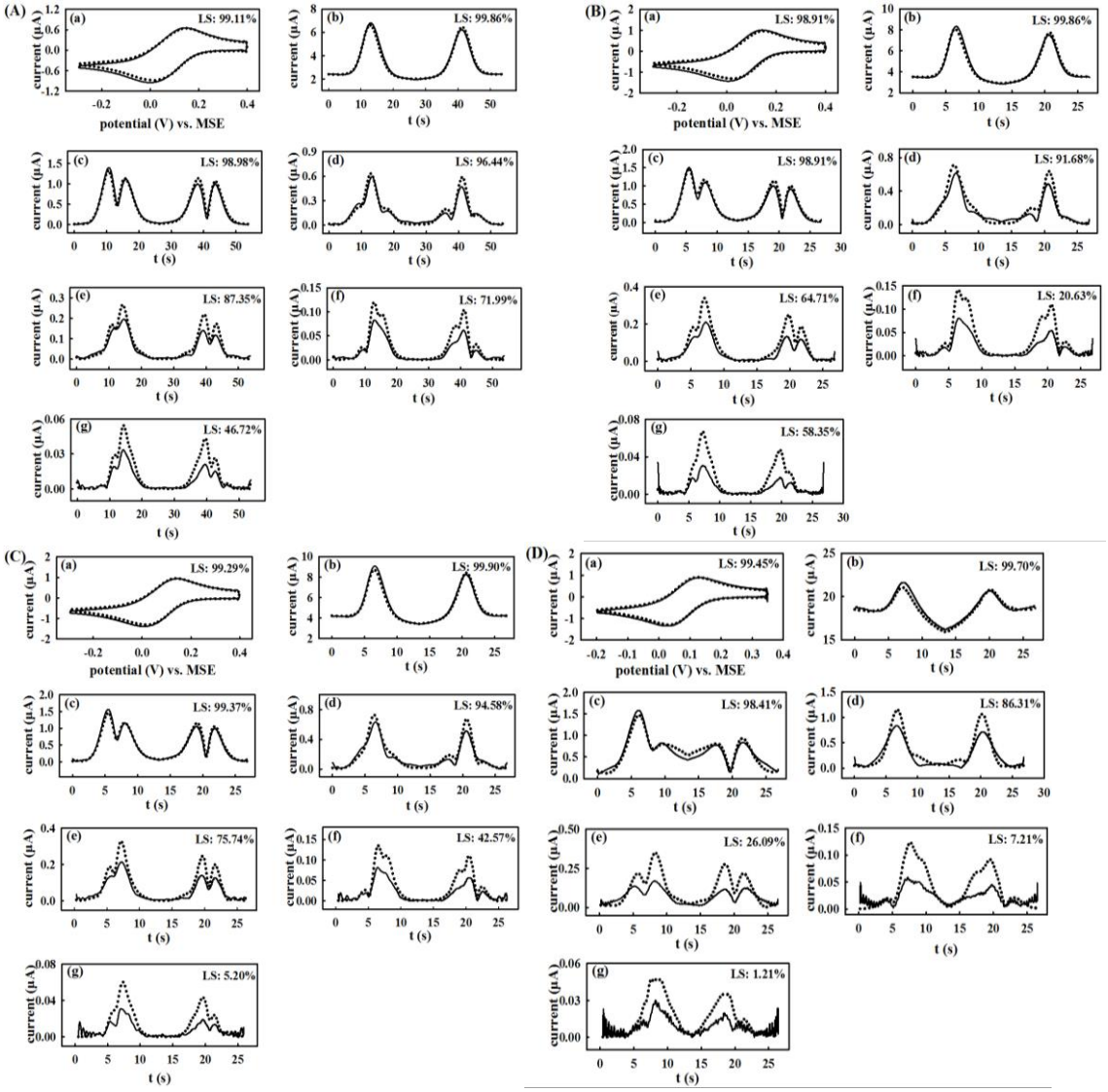

Fig.S5. A comparison of simulated (dotted line) data base on Bulter-Volmer theory and experimental (solid line) FTAC voltammograms for the reduction of 0.20 mM Fe^{III} in 0.05 M $H_4[\alpha\text{-}SiW_{12}O_{40}]$ at a BDD electrode with designated frequencies and scan rates. ΔE = 120 mV. (A) f = 4.92 Hz, v = 26.08 mV s^{-1}; (B) f = 7.93 Hz, v = 52.15 mV s^{-1}. (C) f = 9.02 Hz, v = 52.15 mV s^{-1}; (D) f = 45.00 Hz, v = 40.98 mV s^{-1}. (a) aperiodic DC component, (b-g) 1^{st}-6^{th} AC harmonic components. LS refers to analysis obtained by least squares fitting. For further details of other parameters used in the simulation are given in Table S6.

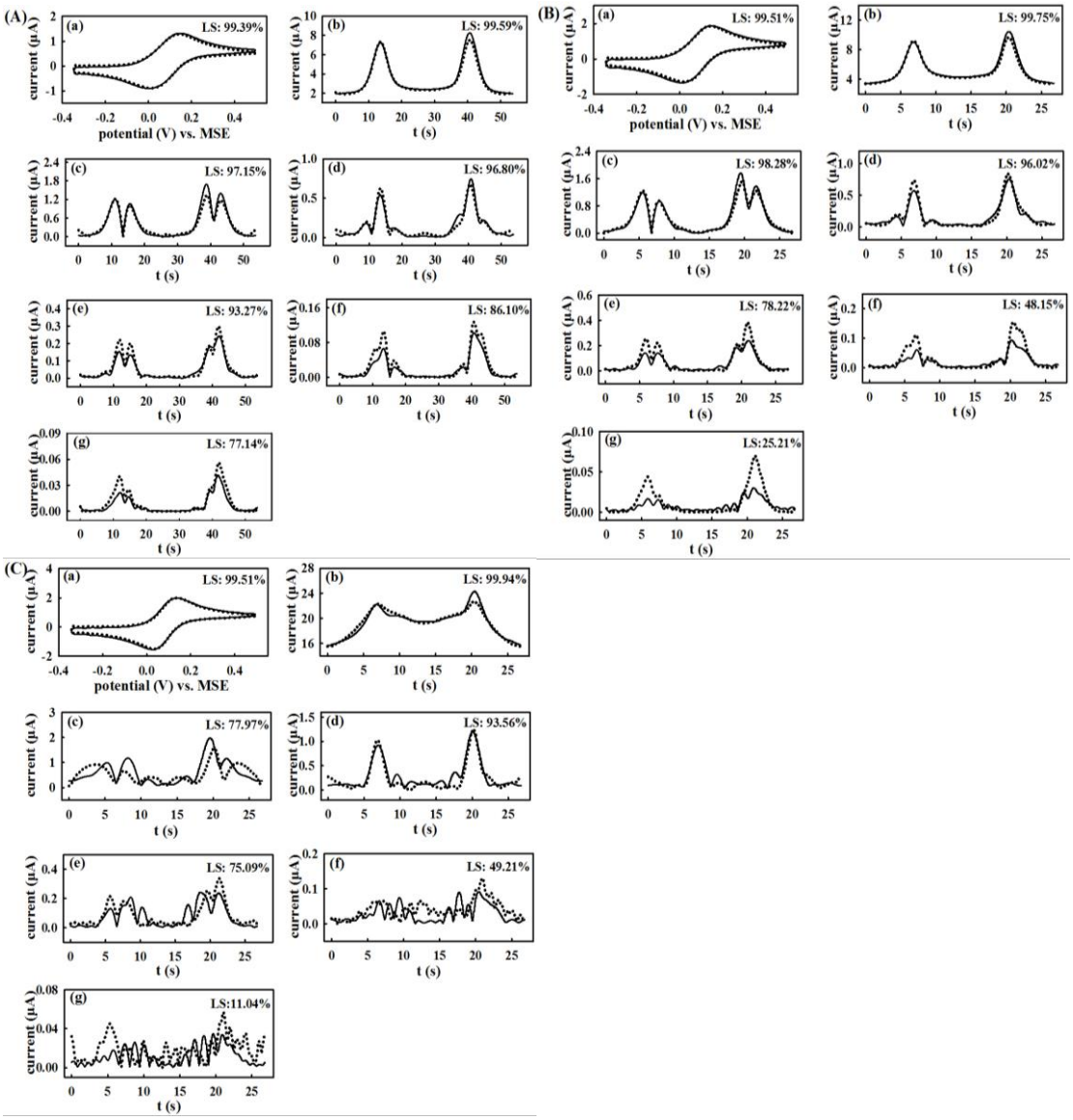

Fig.S6. A comparison of simulated (dotted line) and experimental (solid line) FTAC voltammograms for the oxidation of 0.20 mM Fe^{II} with 0.05 M $H_4[\alpha\text{-}SiW_{12}O_{40}]$ as electrolyte at a BDD electrode with different frequencies and scan rates based on Bulter-Volmer theory. (A) f = 4.94 Hz, v = 31.66 mV s^{-1}; (B) f = 9.02 Hz, v = 63.33 mV s^{-1}; (C) f = 45 Hz, v = 63.33 mV s^{-1}. (a) aperiodic DC component, (b-g) 1^{st}-6^{th} AC harmonic components. ΔE = 120 mV. LS refers to results analysis obtained by least squares fitting. Other parameters used in these simulations are: A = 0.071 cm^2, R_u = 20 Ω, C_{dl} values are given in Table S4, $D_{Fe^{III}} = D_{Fe^{II}} = 6.6 \times 10^{-6}$ cm^2 s^{-1}, E_f^0 = 65 mV, T = 296 K, (A) $k^0 = 2.3 \times 10^{-3}$, α = 0.56, (B) $k^0 = 2.4 \times 10^{-3}$, α = 0.57 and (C) $k^0 = 1.9 \times 10^{-3}$, α = 0.59.

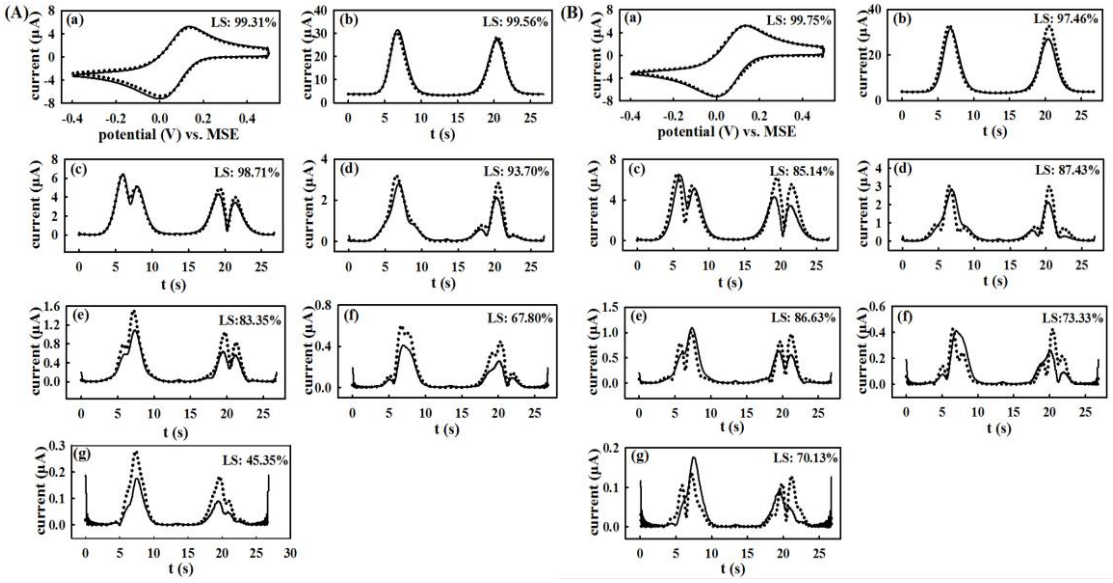

Fig.S7. A comparison of simulated (dotted line) and experimental (solid line) FTAC voltammograms for the reduction of 1.0 mM Fe^{III} with 0.05 M $H_4[\alpha\text{-}SiW_{12}O_{40}]$ as electrolyte at a BDD electrode. Simulations are based on (A) Bulter-Volmer theory and (B) Marcus-Hush theory. (a) aperiodic DC component, (b-g) 1^{st}-6^{th} AC harmonic components. v = 67.06 mV s^{-1}, f = 7.93 Hz and ΔE = 120 mV. LS refers to analysis obtained by least squares fitting. Other parameters used in these simulations are: A = 0.071 cm^2, R_u = 10 Ω, D_{Fe}^{III} = D_{Fe}^{II} = 4.0 × 10^{-6} cm^2 s^{-1}, C_{dl} (c_0, c_1, c_2, c_3, c_4) = (9.17, 5.92, -3.05, 1.29, 5.00) μF cm^{-2}, T = 296 K, (A) E_f^0 = 55 mV, k^0 = 2.0 × 10^{-3}, α = 0.59 and (B) E_f^0 = 68 mV, k^0 = 2.3 × 10^{-3}, λ = 1 eV.

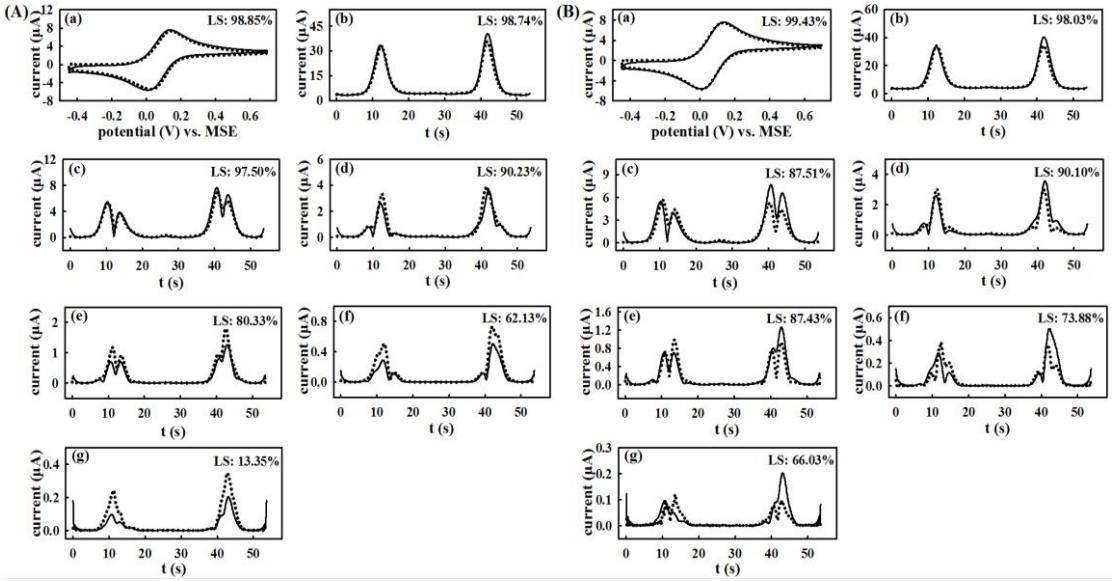

Fig.S8. A comparison of simulated (dotted line) and experimental (solid line) FTAC voltammograms for the oxidation of 1.0 mM Fe^{II} with 0.05 M $H_4[\alpha\text{-}SiW_{12}O_{40}]$ as electrolyte at a BDD electrode. Simulations are based on (A) Bulter-Volmer theory and (B) Marcus-Hush theory. (a) aperiodic DC component, (b-g) 1^{st}-6^{th} AC harmonic components. v = 42.84 mV s^{-1}, f = 8.29 Hz and ΔE = 120 mV. LS refers to analysis obtained by least squares fitting. Other parameters used in these simulations are: A = 0.071 cm^2, R_u = 10 Ω, C_{dl} (c_0, c_1, c_2, c_3, c_4) = (9.36, 2.28, -3.70, -3.82, 7.05) μF cm^{-2}, $D_{Fe}^{III} = D_{Fe}^{II} = 6.5 \times 10^{-6}$ cm^2 s^{-1}, T = 296 K, (A) E_f^0 = 63 mV, $k^0 = 2.1 \times 10^{-3}$, α = 0.62 and (B) E^0 = 69 mV, $k^0 = 2.0 \times 10^{-3}$, λ = 1 eV.

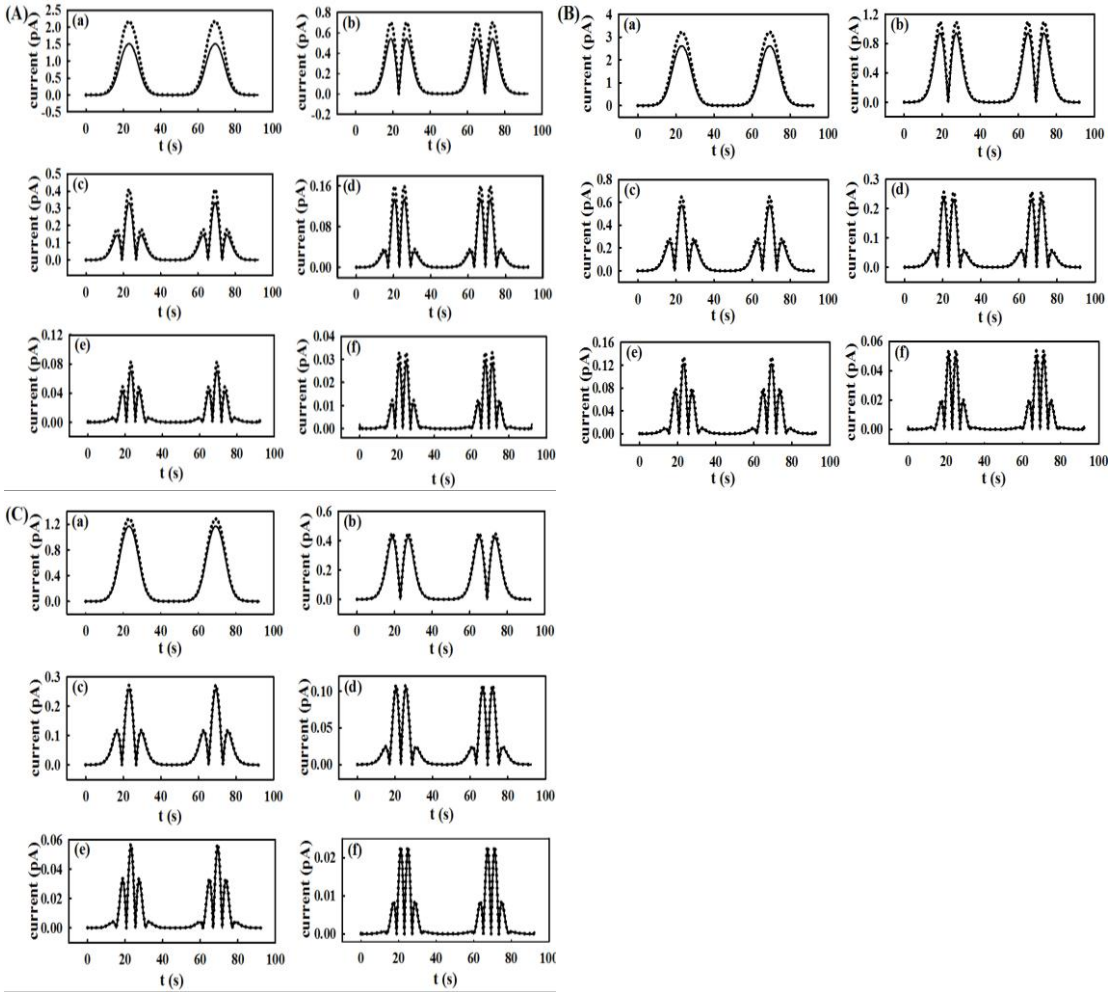

Fig.S9. A comparison of simulated FTAC voltammograms based on linear diffusion (solid line) and radial diffusion (dotted line) for a reversible one-electron-reduction process. Simulation parameters are as follows: v = 0.013 V s^{-1}, c = 0.20 mM, A = 3.14 × 10^{-6} cm^2, D_{ox} = D_{red} = 5 × 10^{-6} cm^2 s^{-1}, E_f^0 = 0 V, α = 0.50, T = 298.2 K, ΔE = 80 mV and f = (A) 3 Hz (B) 9Hz and (C) 45Hz. (a-f) 1^{st}-6^{th} AC harmonic components.

Table S1

Typical parameters[a] used to simulate the DC cyclic voltammetric data for reduction of 1.0 mM Fe^{III} in the designated electrolyte solutions at GC and BDD electrodes with a scan rate of 100 mV s^{-1}. Simulations are based on Bulter-Volmer theory.

Electrolyte	Electrode	E_f^0 (mV)	R_u (Ω)	C_{dl} (μF cm^{-2})	D (cm^2 s^{-1})	k^0 (cm s^{-1})	α
HCl	GC	58	50	6	5.3×10^{-6}	4.8×10^{-3}	0.65
	BDD	68	10	0	5.2×10^{-6}	2.8×10^{-4}	0.59
$HClO_4$	GC	65	50	8	5.2×10^{-6}	3.0×10^{-3}	0.61
	BDD	63	100	0	5.2×10^{-6}	7.2×10^{-5}	0.60
$HNTf_2$	GC	68	50	3	4.9×10^{-6}	7.0×10^{-3}	0.63
	BDD	80	20	0	4.9×10^{-6}	3.2×10^{-4}	0.55
$H_4[\alpha\text{-}SiW_{12}O_{40}]$	GC	45	50	5	4.0×10^{-6}	2.8×10^{-2}	0.55
	BDD	48	20	0	4.0×10^{-6}	2.4×10^{-3}	0.55
$H_4[\alpha\text{-}SiW_{12}O_{40}]$ and $HClO_4$	GC	50	60	5	4.0×10^{-6}	7.2×10^{-3}	0.56
	BDD	42	20	0	4.0×10^{-6}	1.3×10^{-3}	0.56

[a]Other parameters used in simulations are $A_{GC} = A_{BDD} = 0.071$ cm^2, $T = 296$ K.

Table S2

Typical parameters[a] used to simulate the DC cyclic voltammetric data for oxidation of 1.0 mM Fe^{II} in the designated electrolyte solutions at GC and BDD electrodes with a scan rate of 100 mV s^{-1}. Simulations are based on Bulter-Volmer theory.

Electrolyte	Electrode	E_f^0 (mV)	R_u (Ω)	C_{dl} (μF cm^{-2})	D (cm^2 s^{-1})	k^0 (cm s^{-1})	α
HCl	GC	73	30	6	7.5×10^{-6}	4.0×10^{-3}	0.65
	BDD	88	20	0	6.9×10^{-6}	1.2×10^{-4}	0.60
$HClO_4$	GC	65	40	7	7.1×10^{-6}	3.3×10^{-3}	0.65
	BDD	93	40	0	7.2×10^{-6}	7.0×10^{-5}	0.60
$HNTf_2$	GC	78	50	5	6.7×10^{-6}	5.3×10^{-3}	0.60
	BDD	78	20	0	6.7×10^{-6}	9.5×10^{-4}	0.65
$H_4[\alpha\text{-}SiW_{12}O_{40}]$	GC	61	30	7	6.6×10^{-6}	1.2×10^{-2}	0.61
	BDD	66	20	0	6.6×10^{-6}	2.4×10^{-3}	0.59
$H_4[\alpha\text{-}SiW_{12}O_{40}]$ and $HClO_4$	GC	58	50	5	6.2×10^{-6}	7.2×10^{-3}	0.64
	BDD	64	10	0	6.5×10^{-6}	1.4×10^{-3}	0.56

[a]Other parameters used in simulations are $A_{GC} = A_{BDD} = 0.071 cm^2$, T =296 K.

Table S3

Parameters[a] derived from comparisons of simulated and experimental AC voltammetric data for the reduction of 1.0 mM Fe^{III} and the oxidation of 1.0 mM Fe^{II} with 0.05 M $H_4[\alpha\text{-}SiW_{12}O_{40}]$ or 0.1 M $HNTf_2$ as the electrolyte at a GC electrode (n = 3). Simulations are based on Bulter-Volmer theory.

Species	electrolyte	C_{dl} ($\mu F\ cm^{-2}$)	R_u (Ω)	k^0 ($cm\ s^{-1}$)	E_f^0 (mV)	D ($cm^2\ s^{-1}$)	α
Fe^{3+}	$H_4[\alpha\text{-}SiW_{12}O_{40}]$	106, -31.8, -170, 35.6, 364	50 ± 2	$(2.8 \pm 0.3) \times 10^{-2}$	64 ± 2	$(3.9\pm 0.3) \times 10^{-6}$	0.55 ± 0.05
	$HNTf_2$	60.7, -47.7, 22.2, 71.7, -67.6,	43 ± 3	$(5.1 \pm 0.2) \times 10^{-3}$	65 ± 1	$(5.3\pm 0.2) \times 10^{-6}$	0.57 ± 0.02
Fe^{2+}	$H_4[\alpha\text{-}SiW_{12}O_{40}]$	86.5, -37.6, -30.3, 81.2, 65.5	43 ± 2	$(2.2 \pm 0.2) \times 10^{-2}$	65 ± 2	$(6.5\pm 0.1) \times 10^{-6}$	0.55 ± 0.05
	$HNTf_2$	72.4, -40.2, -14.7, 109, -11.7	40 ± 2	$(4.6 \pm 0.4) \times 10^{-3}$	65 ± 2	$(6.6\pm 0.2) \times 10^{-6}$	0.55 ± 0.05

[a]Other parameters used in simulations are: f = 8.31 Hz, v = 67.06 mV s^{-1}, ΔE = 120 mV, A_{GC} = 0.071 cm^2 and T =296 K.

Table S4

Parameters[a] derived from comparisons of simulated and experimental AC voltammetric data for the oxidation of 0.20 mM Fe^{II} at a BDD electrodes with 0.05 M $H_4[\alpha\text{-}SiW_{12}O_{40}]$ as the electrolyte using designated frequencies and scan rates. (n = 3)

f (Hz)	v ($mV\ s^{-1}$)	C_{dl} ($\mu F\ cm^{-2}$)	R_u (Ω)	k^0 ($cm\ s^{-1}$)	E_f^0 (mV)	D ($cm^2\ s^{-1}$)	α
2.92	15.83	9.28, 2.67, 1.47, -3.34, -8.60	20 ± 4	$(2.4 \pm 0.2) \times 10^{-3}$	64 ± 2	$(6.5 \pm 0.3) \times 10^{-6}$	0.55 ± 0.05
4.94	31.66	9.4, 4.0, -6.8, -12.0, 21.4	25 ± 3	$(2.4 \pm 0.1) \times 10^{-3}$	65 ± 1	$(6.5 \pm 0.5) \times 10^{-6}$	0.56 ± 0.05
9.02	63.33	8.78, 2.34, -3.18, -3.95, 6.91	18 ± 5	$(2.3 \pm 0.2) \times 10^{-3}$	64 ± 2	$(6.5 \pm 0.1) \times 10^{-6}$	0.57 ± 0.05
45.00	63.33	8.3, 2.34, -3.6, -3.95, 6.91	30 ± 2	$(2.1 \pm 0.2) \times 10^{-3}$	64 ± 2	$(6.6 \pm 0.1) \times 10^{-6}$	0.59 ± 0.05

[a]Other parameters used in simulations are: ΔE = 120 mV, A_{BDD} = 0.071 cm^2 and T = 296 K.

Table S5
Peak current ratio (I_{linear}/I_{radial}) derived by simulation for one electron reduction process with mass transport by linear or radial diffusion models in 1st to 6th AC harmonics at 3 frequencies. Parameters used in simulations are provided in text.

f	I_{linear}/I_{radial}					
	1st	2nd	3rd	4th	5th	6th
3 Hz	69.41%	77.46%	81.23%	83.50%	85.18%	86.40%
9 Hz	81.12%	85.99%	88.39%	90.10%	91.19%	91.94%
45 Hz	90.96%	93.16%	94.86%	95.36%	95.67%	95.76%

Table S6
Parameters[a] used to simulate AC cyclic voltammetric data for the reduction of 0.2 mM Fe^{III} at a BDD electrode with 0.05 M $H_4[\alpha\text{-}SiW_{12}O_{40}]$ as the supporting electrolyte using designated frequencies and scan rates.

f (Hz)	v (mV s^{-1})	C_{dl} (μF cm^{-2})	R_u (Ω)	k^0 (cm s^{-1})	E_f^0 (mV)	D (cm^2 s^{-1})	α
4.92	26.08	8.63, 1.52, -1.39, -1.58, 4.23	20	2.2×10^{-3}	51	4.0×10^{-6}	0.55
7.93	52.15	7.82, 1.40, -1.85, -1.44, 4.74	18	2.2×10^{-3}	50	4.1×10^{-6}	0.56
9.02	52.15	8.14, 1.55, -1.37, -1.43, 3.33	20	2.2×10^{-3}	50	4.0×10^{-6}	0.56
45.00	40.98	7.22, 1.40, -1.72, -1.44, 4.74	15	2.1×10^{-3}	49	4.0×10^{-6}	0.58

[a]Other parameters used in simulations are: ΔE = 120 mV, A_{BDD} = 0.071 cm^2 and T =296 K.

Reference

[S1] A.M. Bond, N.W. Duffy, D.M. Elton, B.D. Fleming, Characterization of nonlinear background components in voltammetry by use of large amplitude periodic perturbations and Fourier transform analysis, Anal. Chem. 81 (2009) 8801-8808.

Chapter 8

Conclusions and Future Work

8.1 Conclusions

The field of polyoxometalates (POMs) has attracted great attention in both academia and industry in the past two decades. They are discrete nanometer-sized oxide clusters of molybdenum, tungsten and other transition metals in high oxidation states. Applications of POMs in a range of areas include medicine, capacitor, solar energy, sensor, catalysis, etc. Most of the reported applications are focus on catalysis. Numbers of electrochemical studies associated with POMs are reported, however, quantitative studies of heterogeneous electron transfer kinetics at an electrode/electrolyte interface are relatively rare, which limits our knowledge on fundamental aspect of electron transfer associated with POMs. To this end, the work presented here aim to reveal the electrode kinetics properties of POMs.

Dual-frequency method has been developed to increase the reliability of determination of k^0 value near reversible limit in FTAC voltammetry. By applying two different frequencies simultaneously, two sets of data are obtained in a single experiment. The low frequency, which is in a time scale where the target process is reversible, is used as an internal standard to calibrated the parameters C, D, A and R_u. Then the new calibrated values are used to determine k^0 value in the high frequency data set which is in a time scale where the target process is quasi-reversible. This method can reduce the systematic error in k^0 determination from uncertainties in the parameters C, D, A and R_u. By using this method, k^0 values of 0.28 and 0.11 cm s^{-1}

were calculated for the $Fc^{0/+}$ process in the ionic liquids 1-ethyl-3-methylimidazolium bis-(trifluoromethanesulfonyl)imide and 1-butyl-3-methylimidazoliumbis(trifluoromethanesulfonyl)imide, respectively. In principle, a designer waveform with any combination of sine waves can be employed in this method, as long as the target process is reversible in the low frequency but quasi-reversible in the high frequency.

Even using kinetically sensitive FTAC voltammetry, the electrode kinetics associated with $[a\text{-}SiW_{12}O_{40}]^{4-/5-}$ and $[a\text{-}SiW_{12}O_{40}]^{5-/6-}$ in aqueous media are still very fast and close to reversible limit at GC electrode. It is shown that much slower kinetics are found at BDD electrode for these two processes. Therefore, BDD electrode is suited to quantitative study the electrolyte cation effect on the electrode kinetics of POM. The electron transfer kinetics for $[a\text{-}SiW_{12}O_{40}]^{4-/5-}$ and $[a\text{-}SiW_{12}O_{40}]^{5-/6-}$ are dependent on the electrolyte cation identity, increasing in the order of $LiNO_3$ < $NaNO_3$ < KNO_3 < NH_4NO_3. This order is attributed to a decrease in the strength of ion-pairing between electrolyte cations and POMs, which follows the order $NH_4^+ < K^+ < Na^+ < Li^+$, due to an increase in the hydration sphere of the electrolyte cations.

Then the electrode kinetics study of POM is changed to organic media. In DMF containing [TBA][PF_6], the electrode kinetics associated with the $[SVW_{11}O_{40}]^{3-/4-/5-}$ processes have been quantified at GC, BDD, Pt and Au electrodes using FTAC voltammetry. For the $V^{V/IV}$ process, excellent fits between simulated and experimental FTAC voltammetric data show that the k^0 values are electrode material dependent increasing in the order BDD < Pt ≈ Au < GC when the supporting electrolyte concentration is 0.1 M. By changing the supporting electrolyte concentration from 0.1 to 0.5 M, the electrode kinetics of the $V^{V/IV}$ process increases at GC electrode, while at BDD, Pt, Au electrodes, they decrease to different degrees. For the $W^{VI/V}$ process, at all

electrode materials except GC, generally poor simulation-experiment fits are achieved, preventing the data from being analysed quantitatively by FTAC voltammetry, indicating that additional complexities are associated with this process at BDD, Pt and Au electrodes. By changing the supporting electrolyte concentration from 0.1 to 0.5 M also resulted in an increase in the electrode kinetics of the $W^{VI/V}$ process. All these findings suggest that the electrode materials dependence of the k^0 values are not fully correlate with their DOS values. Other factors such as potential dependent double layer effects and functional groups on a GC electrode surface may also play critical roles.

Significant difference are found on the electrode kinetics associated with the $[SVW_{11}O_{40}]^{3-/4-/5-}$ processes in DMF when using $[BMIM]^+$ as supporting electrolyte cation instead of $[Bu_4N]^+$. The reversible potential of the $V^{V/IV}$ and $W^{VI/V}$ processes become more positive and the potential gap becomes smaller due to a stronger ion-pairing between POM and $[BMIM]^+$. 2 to 4 fold of increments are observed for the electrode kinetics of $V^{V/IV}$ process at BDD, Pt and Au electrodes by changing the supporting electrolyte from $[Bu_4N][PF_6]$ to $[BMIM][PF_6]$ (k^0 values are too fast to measure on GC electrode). Even more significant increases of 10, 25 and 100-fold are found for the $W^{VI/V}$ process at Au, BDD and electrodes, respectively, while this process was found to be insensitive to the identity of the cation at a GC electrode. Double layer effect may contribute to the observed difference of k^0 values when changing the supporting electrolyte cation. However, such strong electrolyte cation and electrode dependence imply that the $W^{VI/V}$ process is more likely to occur via an inner-sphere pathway, instead of an outer-sphere one which may occur for the $V^{IV/V}$ reaction.

8.2 Future work

In the following section, three topics are proposed and deserve further study.

In chapter 2, a dual frequency strategy was applied to investigate electrode kinetics of $Fc^{0/+}$ process in ionic liquids using a platinum microelecytrode (nominal diameter = 50 μm). In theory, when the D value of a redox species is 2.0×10^{-5} cm^2 s^{-1}, the upper limit of the dual frequency method for k^0 values determination can be as high as 7 to 10 cm s^{-1}, which is the range of the reported k^0 values for $Fc^{0/+}$ process in acetonitrile. With the advantage of duel frequency method, the kinetics property of $Fc^{0/+}$ process in acetonitrile can be probed at a macro electrode (*i.e.* diameter = 1 mm) accurately, which is very challenging for other techniques since a micro or even nanoelectrode was usually used for fast kinetics study. Such measurement can be also applied for ferrocenemethanol ($FcCH_2OH$) redox process in aqueous solution at a macro electrode.

In 2010, Khenkin and et al.[1] firstly reported that photochemical reduction of carbon dioxide could be catalyzed by a Ruthenium-Substituted polyoxometalate. After that, however, there have been not many reports on the electrochemical reduction of CO_2 catalyzed by polyoxometalates. An optimal electrocatalyst should display a good thermodynamic match between the redox potential for the electron transfer reaction of the catalyst and the chemical reaction that is being catalyzed. It is interesting to investigate the electrocatalytic property of POMs for CO_2 reduction since POMs have several reversible redox processes in negative potential. It is also interesting to study the product distribution of CO_2 reduction catalyzed by POMs at different electrode materials since the electrode kinetics of POMs are electrode materials dependent as shown in the previous studies. This will be invaluable in gaining a better understanding on how the electrode kinetics of an active center affects the following electrocatalytic step.

Throughout the thesis, the kinetic properties of targeted redox processes were

determined by comparison of experimental and simulated data artificially. Therefore, the fitting of these two sets of data may not be the best fit and the k^0 values obtained from this "by-eye" method may also vary between different people. Ideally, the excises of comparison should be done by computer in order to improve the accuracy of the method. By scripting MECSim to run across ranges for several parameters, the best fit can be found automatically, which is challenging and interesting for the future work.